Heat Pump Systems with Vertical Ground Heat Exchangers and Uncovered Solar Thermal Collectors

Von der Fakultät für Architektur und Landschaft
der Gottfried Wilhelm Leibniz Universität Hannover
zur Erlangung des Grades
Doktor der Ingenieurwissenschaften
Dr.-Ing.
genehmigte Dissertation
von

Dipl.- Ing Erik Bertram
Geboren 10.08.1976 in Berlin

Februar 2015

Erster Gutachter: Prof. Dr.-Ing. Dirk Bohne

Zweiter Gutachter: Prof. Dr.-Ing. habil. Stephan Kabelac

Tag der Prüfung: 03. Dezember 2014

Acknowledgements

I am grateful to Dirk Bohne, professor for building technology at Leibniz University of Hannover, for mentoring this thesis and his trust in me that he showed by accepting me as an external doctoral candidate. Also, my sincere gratitude goes to Stephan Kabelac, professor at the Institute of thermodynamics at Leibniz University of Hannover, who gave valuable comments on many aspects of this thesis.

This thesis was mainly conducted at the Institute for Solar Energy Research Hameln (ISFH). I like to express my gratitude to Professor Rolf Brendel and especially Gunter Rockendorf at the ISFH who always supported my intention to write this dissertation and never doubted its successful outcome. Representative for the whole department my sincerest thanks goes to the working group "Thermal Energy systems": Jan Steinweg, Jens Glembin, Peter Pärisch, Rainer Tepe, Jonas Warmuth, Christoph Büttner, Oliver Mercker, Martin Stegmann, and Oliver Arnold. The mutual support in TRNSYS, and especially the component measurements of Peter Pärisch, have been a privileged starting point for the system simulations. I could always rely on the technical support from Wolfgang Wetzel, Henri Diekmann, and Maik Kirchner. Sebastian Föste and Federico Giovannetti gave important support and valuable survival tips in the wilderness of my doctorate process. For me, the persons and the working atmosphere at ISFH are exceptional. I am honestly grateful and want to thank all colleagues at ISFH for the very cooperative, productive and fruitful time we shared.

This dissertation was part of the research project GeoSolar-WP (EFRE, W2-8011 4860). The project was funded by the European Union and the Federal State of Lower Saxony, which I gratefully acknowledge.

In the course of this project my work was continuously stimulated through the exchange with other researchers and practitioners. Holger Jensen, Martin Duddek and Wolfgang Wirth (State Authority for Mining, Energy and Geology, LBEG) always encouraged me and confirmed the practical relevance of my work. Johannes Brugmann (Stiebel Eltron), and Markus Sommer (Lohr Consult) gave valuable insight from the perspective of real applications in systems and their planning. Phillip Oberdorfer and Ekkehard Holzbecher (University of Göttingen) contributed with hard data and general discussion on modelling around their detailed multi-

physics FEM model of a ground heat exchanger.

The work in the IEA SHC Task 44 / HPP ANNEX 38, led by Jean-Christoph Hadorn, must be highlighted because the international meetings had a remarkabley cooperative and open atmosphere. The “Task” also coined my understanding of good scientific practice and mutual beneficial exchange.

I deeply appreciate the opportunity to take part in the subtask working group “Modeling and Simulation”. The vivid scientific dialogue and cooperative work on system simulations and component modelling gave this thesis the right context. I worked and learned a lot about modelling of collectors, heat pumps, and complex systems from discussions with Michel Haller, Daniel Carbonell (SPF, Switzerland), Bengt Perers (DTU Denmark), Fabian Ochs (University of Innsbruck, Austria), Sarah Eicher, Mircea Bunea, Jaques Bony (Lesbat, Switzerland) Tomas Afjei and Ralph Dott (FHNW Switzerland), Werner Lerch and Andreas Heinz (TU Graz, Austria).

I also appreciate very much that Anja Loose (ITW Stuttgart, Germany), Jörn Ruschenburg, and Sebastian Herkel (Fraunhofer ISE, Germany) exchanged their valuable experience on solar assisted heat pump systems monitored. Bernard Thissen, (Energie Solaire, Switzerland) also provided great insights into uncovered solar thermal collectors and systems aspects from the manufacturer’s perspective. Likewise, my sincere thanks goes to Roberto Fedrizzi, Matteo D'Antoni and the whole solar thermal systems group at EURAC, Italy. Their invitation and strong support allowed me to include solar assisted air heat pumps to this thesis. This task and the people in it were a stroke of luck for my thesis and a real pleasure for me to work with.

Finally, science is just a small world within a much more complex universe. My family, my friends, Ruaidhri O’Bolguidhir, who had the questionable pleasure of proofreading large parts of this thesis, the Trillke, and of course Janika have been absolutely crucial for this thesis.

I would never have made it without you all.

Erik Bertram 30.01.2015

Abstract

Vertical ground heat exchanger and uncovered collectors are studied as a hybrid heat source in heat pump systems.

The effects are separated into over-seasonal effects and effects with an impact shorter than one year. Within one year the improvement due to solar thermal assistance is small. A defined temperature potential revealed a 5 K increase only due to the uncovered solar collector. Dynamic system simulations confirm that there is little improvement in efficiency as shown in numerical experiments. The system simulations adopt a reproducible simulation framework from SHC Task 44 / HPP Annex 38 of the International Energy Agency and modified and validated models for the vertical ground heat exchanger as well as the heat pump. Nevertheless, the small changes in temperature due to solar regeneration allow for 10-20% ground heat exchanger shortening.

This possible shortening increases significantly in the case of over-seasonal effects where an interference between multiple borehole heat exchangers occurs. It is correspondingly highly relevant in larger or adjacent systems. It is demonstrated in theoretical analysis and in case studies that solar regeneration eliminates the interference and correspondingly allows free scaling of systems with vertical ground heat exchangers.

Simple dimensioning rules have been derived that allow for collector dimensioning on a monthly data basis. Moreover, a method for vertical ground heat exchanger dimensioning is presented in the case of an even heat balance. The methods are successfully validated against data from measured systems and the dynamic system model. As a rule of thumb, around 1.1 m² uncovered collector per MWh of heat used suffices for solar regeneration of the vertical ground heat exchanger.

Key words:
Temperature potential, solar ground regeneration, dimensioning method for uncovered collector

Kurzfassung

Vertikale Erdwärmesonden und unabgedeckte Kollektoren wurden als hybride Wärmequelle in Wärmepumpensystemen untersucht.

Die Einflüsse werden in übersaisonale und einjährige Einflüsse aufgeteilt. Die Verbesserung innerhalb eines Jahres ist klein. Das definierte Temperaturpotential zeigte nur eine Temperaturverbesserung um 5 K durch den unabgedeckten Kollektor auf. Dynamische Systemsimulationen bestätigen den geringen Einfluss auf die Systemeffizienz in numerischen Experimenten. Die Systemsimulationen verwenden modifizierte und validierte Modelle für die vertikalen Erdwärmesonden und die Wärmepumpe und eine reproduzierbare Simulationsumgebung aus dem SHC Task 44 / HPP Annex 38 der Internationalen Energie Agentur. Dennoch erlaubt die solare Regeneration eine Kürzung der Erdwärmesonde um 10 -20%.

Die mögliche Kürzung steigt deutlich mit den Wechselwirkungen zwischen den Erdwärmesonden an und wird hochrelevant in größeren Anlagen und benachbarten Systemen. In theoretischen Untersuchungen und einigen Fallbeispielen wird gezeigt, dass die solare Regeneration die Wechselwirkungen aufhebt und dementsprechend eine freie Skalierung von Erdwärmesondenanlagen ermöglicht.

Einfache Dimensionierungsregeln wurden abgeleitet, die eine Kollektorauslegung auf monatlicher Datengrundlage ermöglichen. Die Methoden wurden anhand von Messdaten und dem dynamischen Systemmodell validiert. Darüber hinaus wird eine Methode zur Erdwärmesondendimensionierung im Fall einer ausgeglichenen Wärmebilanz vorgestellt. Die Methoden werden mit gemessenen Anlagendaten und dem dynamischen Systemmodell erfolgreich validiert. Als Faustformel reichen ungefähr 1.1 m² unabgedeckter Kollektor pro MWh Wärmebedarf, um einen vertikalen Erdreichwärmetauscher zu regenerieren.

Schlagworte:
Temperaturpotential, Solare Erdreichregeneration, Auslegungsverfahren für unabgedeckte Kollektoren

Table of Contents

Nomenclature

Symbols

A	Area, [m^2]
a_1, a_2	Loss coefficients for steady-state glazed collector model, [W m^{-2} K^{-1}, W $m^{-2}K^{-2}$]
b_1, b_2, b_u	Loss coefficients for steady-state unglazed collector model related to average collector temperature, [W $m^{-2}K^{-1}$, J m^{-3} K^{-1}, s m^{-1}]
c	Velocity, [m s^{-1}]
$c_{1\text{-}6}$	collector model loss coefficients related to inlet collector temperature, [-]
c_{eff}	Effective collector capacity, [kJ K^{-1}]
c_p	Heat capacity, [kJ kg^{-1} K^{-1}]
D	Diameter, [m]
d_0, d_1	Regression values for electric consumption correlation
E	Energy, [J, kWh]
ES	Eskilson time, [-]
E_{el}	Electric monthly energy consumption per living area, [kWh m^{-2} $month^{-1}$]
F_R	Heat removal factor of collector, [-]
g_{grav}	Acceleration of gravity, 9.86 [m s^{-2}]
G_g	Geothermal gradient, [K m^{-1}]
$G´, G_T´$	Irradiance in collector pane, [W m^{-2}]
$G´´$	Net irradiance in collector pane, [W m^{-2}]
G_{TC}	Monthly critical radiation level, [W m^{-2}]
$g()$	g-function, [-]
H	Depth of borehole heat exchanger, [m]
$\overline{H_T}$	Monthly average daily radiation in collector pane, [kWh d^{-1} m^{-2}]
h	Specific enthalpy, [kJ kg^{-1}]
k	Parameter for heat pump polynomial, [-]
L	Overall length of ground heat exchanger(s), [m]
L_{sky}	Incoming long wave radiation of sky, [W m^{-2}]
$\dot{m}$	Mass flow rate, [kg h^{-1}, kg s^{-1}]
p	Parameter for heat pump polynomial, [-]

P	Power, [W or kW]
$\dot{q}$	Specific heat flow rate per m borehole, [W m^{-1}]
$\dot{Q}$	Heat flow rate, [W or kW]
$\overline{Q_u}$	Monthly average daily useful energy yield, kWh d^{-1}
R	Thermal resistance, [K W^{-1}]
r	Radius, [m]
$R^{\#}$	Specific thermal resistance, [K m^{-1} W^{-1}]
R_b	Effective borehole resistance, [K W^{-1}]
$s_{d,DHW}$	Solar fraction only for domestic hot water, [-]
T	Temperature, [K or °C]
t	Time, [s]
UA	Overall heat transfer coefficient, [W K^{-1}, kW K^{-1}]
U_L	Loss coefficient of collector, [W m^{-2} K^{-1}]
z	Height, [m]

Greek symbols

α	Absorptance, [-]
α_g	Thermal diffusivity, [m^2 K^{-1}]
τ	Time interval or time constant, [s]
ϵ_{HP}	Exergetic or carnot efficiency, [-]
ϵ	Hemispheric emissivity (long wave >3μm) irradiation, [-]
λ	Heat conductivity of the ground, [W m^{-1} K^{-1}]
ρ	Density, [kg m^{-3}]
γ	Euler constant ~0.5772
σ	Stefan-Boltzmann constant 5.67, [10^{-8} W m^{-2} K^{-4}]
$(\tau\alpha)$	Effective transmittance-absorptance product of collector, [-]
$\bar{\Phi}$	Daily utilizability, [-]
η	Efficiency, [-]
η_0	Conversion coefficient of solar collector, [-]
ζ	Run-time coefficient, 0.33 of solar collector, [-]

Indices

*	Energy weighted quantity

‘	Heat load specific quantity
amb	Ambient air
Aux	Auxiliary
b	Borehole
BU	Back-up
bui	Building
Cold	Cold/evaporator side of the heat pump
coll	Solar thermal collector
cond	Heat pump condenser
conv	Convection
cov	Recovering
CU	Controller unit
DHW	Domestic hot water
down	Inertia effect respecting cooling of heat pump
eff	Effective
el	Electrical
evap	Heat pump evaporator
g	Ground
GHX	Vertical ground heat exchanger
hot	Hot/condenser side of the heat pump
HP	Heat pump
HS	Heat source
HX	Heat exchanger
in	Fluid inlet
k	Counting index for months
Low	Lower hysteresis value of differential controller
LW	Long wave radiation with wave lengths > 3µm
max	Maximum
Min	Minimum inlet temperature
n	Number
off	Heat pump is switched off
on	Heat pump is operating
out	Fluid outlet

p	periodic
peak	Peak load
pen	Penalty
Pre-pipe	Pre-pipe model extension
protect	Lower allowed minimum temperature for protection of the vertical ground heat exchanger
pulse	Heat pulse
PV	Photovoltaic
q	Heat flow rate
red	Reduced
s	Eskilson
SH	Space heating
shift	Shift in time to calculate restarting power of the heat pump
SHP	Solar and heat pump system
SPF	Seasonal performance factor
Side	Conduction at the rear side of collector
stag	Stagnation of solar collector
steady	Steady state conditions
UC	Uncovered collector
undis	Undisturbed ground conditions
up	Inertia effect respecting heating of heat pump
upper	Upper hysteresis value of differential controller
x	Ma**X**imum temperature potential of a hybrid heat source

Abbreviations and product names

ASHRAE	American Society of Heating, Refrigerating and Air-Conditioning Engineers
COMSOL	Comsol multiphysics
COP	Coefficient of performance
DHW	Domestic hot water
EED	Earth energy designer
FEM	Finite element method
GHX	(Vertical) ground heat exchanger
HP	Heat pump
HPP	Heat pump programme

IEA	International Energy Agency
IPCC	Intergovernmental Panel on Climate Change
ISFH	Institut für Solarenergieforschung Hameln
PVT	Photovoltaic Thermal
SD	Standard deviation
SHC	Solar heating and cooling programme
T44/A38	International Energy Agency Solar Heating and Cooling programme Task 44 / Heat Pump Programme Annex 38
TRNSYS	Transient System Simulation Tool
U-tube	U shaped vertical ground heat exchanger
VdZ	Vereinigung der deutschen Zentralheizungswirtschaft "Association of the german central heating industry"

1 Introduction

1.1 Motivation

The rapid reduction of global greenhouse gas emissions is a worldwide goal in order to reduce anthropogenic induced climate change [1]. The growing and major part, 56% of global anthropogenic greenhouse gas emissions, is caused by the usage of fossil fuels [2, p. 103]. Moreover, limited fossil fuel reserves and renewable energy sources are meeting an on-going increase in the energy demand [3, p. 29]. An obvious way to reduce emissions is therefore to replace fossil fuel with renewable sources and to improve energy efficiency.

In this context, heating in the building sector offers significant potential to reduce emissions from fossil fuels. A large part, 47% of the world's final energy consumption consists of heat [4, p. 8] and 50% of this heat is consumed in the building sector (52% in OECD countries) [4, p. 10].

The heat pump is a key component of the building sector, allowing for improved efficiency and making low-temperature heat sources accessible. This makes it possible to use heat from air, ground-water, rivers or the ground, which are otherwise not usable for space heating or domestic hot water preparation. In the vast majority electric compression heat pumps are used in the heating systems of buildings. Accordingly, heat pumps are generally used as an efficient way to generate heat and are in most cases driven by electricity.

The use of fuel, however, makes the heat pump a double edged component. Highly efficient heat pump systems driven by renewably generated electricity have an extremely low impact on the climate. Inefficient heat pump systems, using electricity that is generated from fossil fuels at low efficiencies, cause an ecological damage comparable to directly burned fossil fuels [2, p. 397].

The efficiency of the heat pump system increases with higher heat source temperatures which are determined by the heat source. A promising solution for high efficiencies is therefore the combination of heat sources that offer as a hybrid source higher temperatures as a single source. Possible natural heat sources are limited: air, water, solar or ground.

As one promising possible combination vertical ground heat exchangers with uncovered collectors are studied. The vertical ground heat exchangers are chosen because they provide high efficiencies in comparison to other heat sources [5, p. 17]. Uncovered

collectors are chosen because they provide solar energy at a low cost and offer high efficiencies at low temperature applications.

While this combination has been investigated in case studies and by monitoring, the theoretical limits of this combination are unknown and dimensioning rules are lacking. This thesis will attempt to close this gap of knowledge.

The idea for this thesis developed while conducting two research projects “UmSys” [6] and “BisolarWP” [7] with uncovered collector and vertical ground heat exchanger. In these projects the measurement data basis was gathered in three systems over several years. The first dynamic simulation studies already revealed some possible component model improvements for intermittent operation and higher source temperatures.

The thesis itself was founded as part of the research project “GeoSolar-WP” by the state of Lower Saxony and the European Union[1]. Here, new component models were developed, parameterised and validated for the heat pump and vertical ground heat exchanger. Component model development was conducted in parallel to this thesis and has been an excellent starting point for system simulations.

1.2 Scope

The combination of uncovered collectors with vertical heat exchangers is examined with the objective of quantifying and understanding the possible benefits of this hybrid heat source combination.

The effects are assessed though system efficiency, the seasonal performance factor, and the possible shortening of the ground heat exchanger. This includes the connection of this combination to a wider context as comparison to air source systems or solar only systems. Moreover, a theoretical analysis of the ground heat exchanger and the combined heat source is conducted to assess the potential of this heat source combination. Eventually, a design method will be derived.

The thesis has a clear focus on single family houses though higher heat loads and multiple adjacent single systems together are also discussed. The work does not include

- Seasonal storing of solar heat at high temperatures with vertical ground heat exchangers for seasonal storing such as Drake Landing [8], Neckarsulm or

[1] Hocheffiziente Wärmepumpensysteme mit Geo- und Solarthermie-Nutzung, Geo-Solar-WP, File number W2 – 80114860, Duration 01.09.2010 – 28.02.2014

Crailsheim [9].

- Effects of ground water flow for the ground heat exchanger
- Horizontal or other very shallow ground heat exchangers
- Cooling loads

While these aspects are not covered, they can to some extend be connected to the systems studied. For example cooling loads will have very comparable effects as solar regeneration.

1.3 Publication list

The main content of this thesis has not been published previously; otherwise this is clearly indicated and referred to. In the following list all publications are presented that have been produced during this thesis and are in context to it. The most relevant publications from before the starting date of this thesis in 2011 are also given.

Bertram, E., Glembin, J. and Scheuren, J.. *Unverglaste Metalldach-Sonnenkollektoren in Wärmeversorgungssystemen: Systemkonzepte und Auslegung*. Technical Report #21098. Deutsche Bundesstiftung Umwelt (DBU) 2008.

Bertram, E., Glembin, J., Scheuren, J. and Zienterra, G. *Soil regeneration by unglazed solar collectors in heat pump systems*. Johannesburg, South Africa, 2009.

Bertram, E., Stegmann, M., Scheuren, J. and Rockendorf, G., *Condensation Heat Gains on Unglazed Solar Collectors in Heat Pump Systems*. Proceedings of EuroSun 2010 International Conference on Solar Heating, Cooling and Buildings, Graz, Austria, 2010.

Bertram, E., Stegmann, M. and Rockendorf, G. *Heat Pump Systems with Borehole Heat Exchanger and Unglazed PVT-Collector*. Proceedings of ISES Solar World Congress 2011, Kassel. 1170–1179, 2011.

Bertram, E., Stegmann, M. and Rockendorf, G. 2011. *Solarthermie 2000plus: Solare Gebäudewärmeversorgung mit unverglasten photovoltaisch-thermischen Kollektoren, Erdsonden und Wärmepumpen für 100% Deckungsanteil*, Teilprojekt B: Wissenschaftliche Begleitung.

Bertram, E. and Tepe, R. *Wärmpumpensystem mit solarthermisch unterstützten Erdwärmesonden*. Proceedings of 2. VDI Fachkonferenz Wärmepumpen, Frankfurt a. M., Jun. 2011, 187–195. 2011.

Stegmann, M., Bertram, E., Rockendorf, G. and Janßen, S., *Model of an unglazed photovoltaic thermal collector based on standard test procedures*. Proceedings of ISES Solar World Congress, Kassel, Germany, 2011.

Stegmann, M., Bertram, E., Rockendorf, G. and Janßen, S. *Modell eines unverglasten photovoltaisch-thermischen Kollektors basierend auf genormten Prüfverfahren*. Proceedings 22. Symposium Thermische Solarenergie, Bad Staffelstein, Germany, 2012).

Pärisch, P., Warmuth, J., Bertram, E. and Tepe, R. *Experiments for combined solar and heat pump systems*. Proceedings of Eurosun 2012, Rijeka Croatia. (2012).

Bertram, E., Pärisch, P. and Tepe, R. *Impact of solar heat pump system concepts on seasonal performance - Simulation studies*. Proceedings of Eurosun 2012, Rijeka Croatia. (2012).

Haller, M.Y., Bertram, E., Dott, R., Afjei, T., Ochs, F. and Hadorn, J.-C. *Review of Component Models for the Simulation of Combined Solar and Heat Pump Heating Systems*. Energy Procedia. 30, (Jan. 2012), 611–622.

Bertram, E., Carbonell, D., Perers, B., Haller, M., Bunea, M. and Eicher, S. *Models of Sub-Components and Validation for the IEA SHC Task 44 / HPP Annex 38 (Final Draft Part B: Collector Models*. Technical Report # Report C2 Part B. International Energy Agency(to be published 2014).

Bertram, E., Glembin, J. and Rockendorf, G., *Unglazed PVT collectors as additional heat source in heat pump systems with borehole heat exchanger*. Energy Procedia. Volume 30, (2012), 414–423, 2012.

Pärisch, P., Malenkovich, I., Hartl, M., Bertram, E., Tepe, R. and Rockendorf, G. *Effizienz oder Effektivität? Kennzahlen für die Bewertung von Solar-Wärmepumpensystemen*. Proceedings 23. Symposium Thermische Solarenergie, Bad Staffelstein, Germany, 2013.

Bertram, E., Pärisch, P. and Tepe, R., *Solare Wärmepumpensysteme mit Erdwärmesonde Konzeptvergleich von Systemvarianten*. Proceedings of Symposium Thermische Solarenergie (Bad Staffelstein, Germany, 2013).

Bertram, E., Pärisch, P. and Tepe, R., *Solare Wärmepumpensysteme mit Erdwärmesonden-Konzeptvergleiche*. Proceedings 12. Internationales Anwenderforum Oberflächennahe Geothermie, Neumarkt i. d. Oberpfalz, Germany, 2013.

Bertram, E., Dott, R., Mojic, I., Lerch, W., Heinz, A., Haller, M.Y., Carbonell, D., Bunea, M., Winteler, C. and Ochs, F. 2013. *Annex G Summary reports for simulations with T44A38 boundary conditions* (Final Draft - Dec. 2013). Technical Report #Annex G to Report C3. IEA SHC / HP Programme. (to be published 2014).

Bertram, E. 2013 et. al. *Annex F to Report C3 of the IEA SHC Task 44 / HPP Annex 38 - Platform independence checks reported for T44A38*. Technical Report #Adaption for the IEA SHC & HPP T44/A38 Boundary Conditions of ISFH Simulations in TRNSYS (to be published 2014).

Bertram, E. et al. *Annex H to Report C3 of the IEA SHC Task 44 / HPP Annex 38 Summary reports for simulations with differing boundary conditions (Final Draft Dec. 2013)*. Technical Report #Annex G to Report C3. IEA SHC / HP Programme (to be published 2014).

Haller, M.Y., Bertram, E., Dott, R., Afjei, T., Ochs, F., Sunliang, S., Siren, K. and Hadorn, J.-Ch. *Models of Sub-Components and Validation for the IEA SHC Task 44 / HPP Annex 38 Part A: Summary (Final Draft Dec. 2013)*. Technical Report #Report C2 Part A. International Energy Agency. (to be published 2014)

Haller, M., Carbonell, D. and Bertram, E. Report C4 *Synthesis of System Simulation Results for the IEA SHC Task 44 / HPP Annex 38 (Draft 9th Dec. 2013)*. Technical Report #Report C4. IEA SHC / HP Programme (to be published 2014)

Pärisch, P., Mercker, O., Oberdorfer, P., Bertram, E., Tepe, R. and Rockendorf, G. *Short-term experiments with borehole heat exchangers and model validation in TRNSYS*. Renewable Energy, Volume 74, February 2015, Pages 471–477

Pärisch, P., Mercker, O., Warmuth, J., Tepe, R., Bertram, E. and Rockendorf, G. *Investigations and model validation of a ground-coupled heat pump for the*

combination with solar collectors. Applied Thermal Engineering. 62, 2 p. 375–381 (Jan. 2014).

Haller, M.Y., Carbonell, D., Mojic, I., Winteler, C., Bertam, E., Mircea, B., Lerch, W. and Ochs, F. *Solar and Heat Pump Systems - Summary of simulation results of the IEA SHC Task 44 / HPP Annex*, submitted to 11th International Energy Agency Heat Pump Conference, Montreal, Canada, 2014.

Bertram, E. *Solar assisted heat pump systems with ground heat exchanger– Simulation studies*. Energy Procedia, Volume 48, 2014, Pages 505-514, 2014.

2 Basics

2.1 Electrical Heat Pump

2.1.1 Working Principle

A heat pump converts or pumps heat from a low temperature level to heat at a higher temperature level. The process of heat transfer from a cold to a hot heat reservoir is possible only, if driven by an exergetic energy carrier, typically electricity or chemical energy.

Figure 2-1: Left: Compression heat pump at test facility at ISFH. Right: Glance into the inner parts of the heat pump: Black cylinder-compressor, silvery box behind the compressor-plate heat exchanger

Electric compression heat pumps are widespread in domestic applications. Their working principle is that of a left hand cycle process which runs through four process steps: (1) Compression, (2) Condensation, (3) Expansion, (4) Evaporation.

The heat pump's (coefficient of) performance COP is defined as the obtained heat flow rate $\dot{Q}_{Hot}$ per applied electric power P_{el}, [10, p. 576, Eq. 9.1]. For a reversible process the temperature levels on both sides of the heat pump determine the maximum COP. In such a theoretical, reversible working heat pump the exergetic efficiency ϵ_{HP} is 1. For real, non-reversible heat pumps ϵ_{HP} is smaller than 1. Eq. 2-1 is given for the hot side temperature T_{Hot} and the ambient temperature T_{amb}.

As a simplification it is assumed that the ambient air temperature T_{amb} equals the cold side temperature T_{cold}. Strictly speaking this is not true in combination with a ground

heat exchanger. In most times of the year there is a temperature difference between the ambient air and the ground and therefore also some exergy content in the low temperature heat from the ground. In other words, the relevant heat pump temperature T_{cold}, here assumed as the ground temperature, does not represent the theoretical equilibrium temperature of the ambient air.

$$COP = \frac{\dot{Q}_{Hot}}{P_{el}} \cdot \epsilon_{HP} = \frac{T_{Hot}}{T_{Hot} - T_{amb}} \cdot \epsilon_{HP} = \frac{T_{Hot}}{T_{Hot} - T_{cold}} \cdot \epsilon_{HP} \qquad \text{Eq. 2-1}$$

COP	*Coefficient of performance of the heat pump in* -
P_{el}	*Electric power in* W
$\dot{Q}_{Hot}$	*Hot side or condenser heat flow rate in* W
T_{Hot}	*Hot side or condenser temperature in* K
T_{amb}	*Ambient air temperature in* K
T_{cold}	*Cold side or evaporator temperature in* K
ϵ_{HP}	*Exergetic efficiency in* -

Heat pumps for domestic applications achieve today exergetic efficiencies of 0.4 to 0.5 [11, p. 378] and COPs of up to 5 [12, p. 10] for brine to water heat pumps at nominal space heating conditions. In short, the heat pump provides usable heat with very little electricity requirement and the market for heat pumps is rapidly growing. 1.5 million heat pumps were sold in Europe in 2012 [13, p. 3].

The heat pump is the core component and main energy consumer of the heating system in an increasing number of domestic heating systems. Eq. 2-1 presents 3 ways to improve the efficiency of a heat pump.

Firstly, the exergetic efficiency of the heat pump ϵ_{HP} can be improved. This results in heat pumps with higher COPs. Secondly, the hot side temperature T_{Hot} can be lowered, which is typically achieved with low temperature heat distribution systems e.g. floor heating systems. Thirdly, the cold side temperature T_{cold} can be increased. In principle, this can be done by using larger components, other heat sources, or a combination of two heat sources that leads to a higher source temperature.

All three measures will improve the system performance and reduce the electric consumption of the heat pump. Ignoring any one of the three limits the possible efficiency of the overall system.

2.1.2 Mathematical Model

The use of Eq. 2-1 for a heat pump modelling is very limited in the context of dynamic and transient system simulations.

In general, heat pump manufacturers provide COP data as a function of heat source and sink temperatures. This allows the heat pump's performance to be predicted in a conventional application range. The exergetic efficiency, however, is not constant for different temperature conditions and a simple extrapolation of the manufacturer data causes high uncertainty in simulations. The modelling of the heat pump in an extended temperature range, which occurs in combination with solar collector support on the heat source side, is normally unknown.

Moreover, heat pump operation in systems includes cycling losses. These cycling losses are caused by the thermal inertia of the heat pump and the energy required to raise the pressure. Both, effects reduce the power consumption determined under steady state conditions.

Furthermore, the simulations require a description of the heat pump's characteristic as a function of the inlet and outlet temperatures. This is in contrast to most heat pump descriptions, where the COP is a function of the average temperatures at the condenser T_{Hot} and the evaporator T_{cold}.

All three aspects are dealt with by employing the black box model from [14]. This model describes the thermal heat pump heat flow rate and the electrical consumption with the help of a biquadratic polynomial as a function of the normalized temperatures for the condenser outlet $T_{n,c}$ and evaporator inlet $T_{n,e}$, see Figure 2-2.

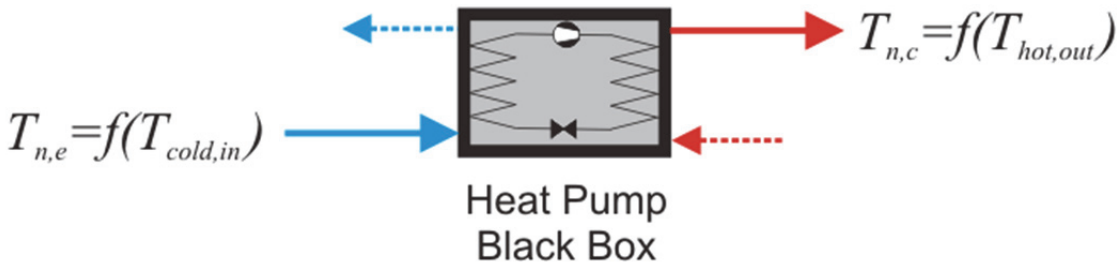

Figure 2-2: Heat pump black box model with temperature inputs for parameter fit of condenser heat flow rate and electrical compressor power, blue is the evaporator side of the heat pump and red the condenser side of the heat pump

The polynomials for the steady state heat flow rate of the condenser $\dot{Q}_{Hot,steady}$ are given by equation Eq. 2-2 and for the electrical compressor power $P_{com,steady}$ by equation Eq. 2-3. Both values are a function of the aforementioned normalized temperatures $T_{n,e}$ at the evaporator inlet and $T_{n,c}$ at the condenser outlet, which are attained according to Eq. 2-4. The equations' parameters required $p_{p,j}$ and $p_{q,j}$ are derived from measured data points by a numerical least-square fit. The evaporator heat

flow rate is calculated by a heat balance.

$$\dot{Q}_{Hot,steady} = \left(p'_{q,0} + p'_{q,1} \cdot T_{n,e} + p'_{q,2} \cdot T_{n,c}\right)^2 \quad \text{Eq. 2-2}$$

$$= p_{q,1} + p_{q,2} \cdot T_{n,e} + p_{q,3} \cdot T_{n,c} + p_{q,4} \cdot T_{n,e} \cdot T_{n,c} + p_{q,5} \cdot T_{n,e}^2 + p_{q,6} \cdot T_{n,c}^2$$

$$P_{com,steady} = \left(p'_{p,0} + p'_{p,1} \cdot T_{n,e} + p'_{p,2} \cdot T_{n,c}\right)^2 \quad \text{Eq. 2-3}$$

$$= p_{p,1} + p_{p,2} \cdot T_{n,e} + p_{p,3} \cdot T_{n,c} + p_{p,4} \cdot T_{n,e} \cdot T_{n,c} + p_{p,5} \cdot T_{n,e}^2 + p_{p,6} \cdot T_{n,c}^2$$

$$with \quad \text{Eq. 2-4}$$

$$T_{n,e} = \frac{T_{cold,in}}{273.15\ \mathrm{K}} + 1;\ T_{n,c} = \frac{T_{hot,out}}{273.15\ \mathrm{K}} + 1;\ [T_{cold,in}] = [T_{hot,out}] = °C$$

This model includes cycling losses. These are described as a simple system response function of first order (PT1) for the condenser heat flow rate $\dot{Q}_{cond}(t_{on})$ after the runtime t_{on}, compare Figure 2-3 and Eq. 2-5.

$$\dot{Q}_{hot}(t_{on}) = \dot{Q}_{hot,steady} \cdot \left(1 - e^{-\frac{t_{shift,up} + t_{on}}{\tau_{on}}}\right) \quad \text{Eq. 2-5}$$

$\dot{Q}_{hot}(t_{on})$	*Condenser heat flow rate at the time step t in* W
$\dot{Q}_{hot}$	*Condenser heat flow rate under nominal conditions in* W
$t_{shift,up}$	*Time shift for restarting from heat flow rate point* $Q_{cold,start}(t)$ *in* s
t_{on}	*Running time of heat pump since last start in* s
τ_{on}	*Time constant for heating of the heat pump in* s

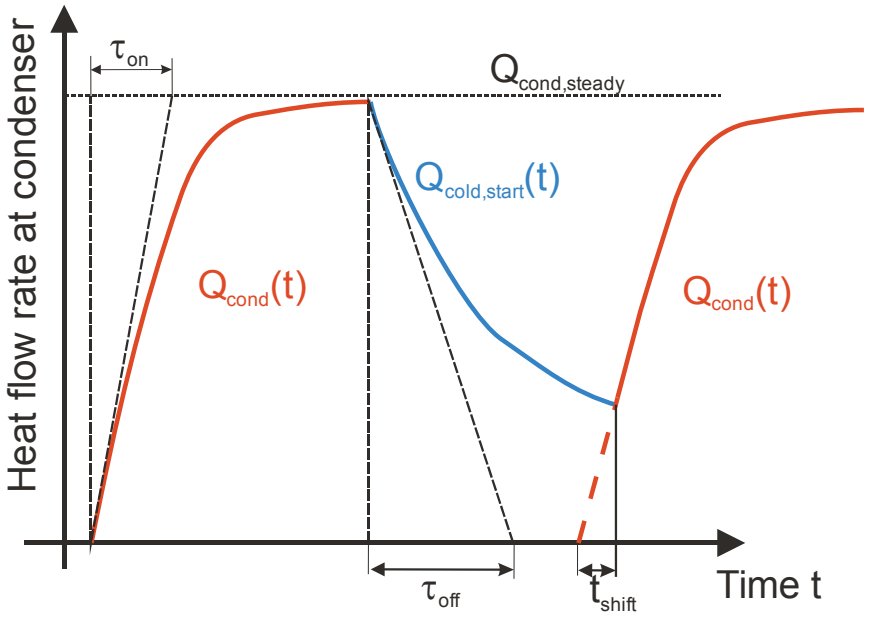

Figure 2-3: Condenser heat flow rate including cycling losses for heating and cooling. The marked time shift t_{shift} is given for the heating of the condenser heat flow rate in the second operating period.

Furthermore, the heat pump also has a cooling constant. In intermittent operation the heat pump does not have a cold restart. Instead, it benefits from previous operation. This inertia effect is respected by a condenser heat flow rate $\dot{Q}_{cold,start}(t_{off})$, from which the

heat pump is started. If the heat pump operation is stopped at the time *t* the $\dot{Q}_{cold,start}(t)$ exactly equals the condenser heat flow rate $\dot{Q}_{hot}(t)$. During standstill the heat pump exponentially loses its restarting heat flow rate $Q_{cold,start}(t)$.

$$\dot{Q}_{cold,start}(t_{off}) = \dot{Q}_{cond,steady} \cdot e^{-\frac{t_{shift,down}+t_{off}}{\tau_{off}}} \quad \text{Eq. 2-6}$$

$\dot{Q}_{cold,start}(t_{off})$ *Restarting heat flow rate of the heat pump after time* t_{off} W
$\dot{Q}_{cond,steady}$ *Condenser heat flow rate under nominal conditions in* W
$t_{shift,down}$ *Time shift for cooling down from point* $Q_{cond}(t)$ *in* s
t_{off} *Shut-off time of heat pump since last start in* s
τ_{off} *Time constant for cooling-down of the heat pump in* s

The effect of a starting point that is influenced by the previous operation is included for the heating and the cooling of the heat pump by the time shift t_{shift}. This time shift t_{shift} is used for the heating $t_{shift,up}$ and the cooling $t_{shift,down}$ of the heat pump. This represents the time, in which the heat pump reaches the power that is the starting heat flow rate for cooling or heating. This time shift t_{shift} is calculated once for each operation or shut-off period. In the case of a running heat pump the heating time shift is $t_{shift,up}$

$$t_{shift,up} = -\tau_{on} \ln\left(1 - \frac{\dot{Q}_{cold,start}}{\dot{Q}_{cond,steady}}\right) \quad \text{Eq. 2-7}$$

$\dot{Q}_{cold,start}$ *Restarting heat flow rate at starting of the heat pump in* W
$\dot{Q}_{cond,steady}$ *Condenser heat flow rate under nominal conditions in* W
$t_{shift,up}$ *Time shift for heating from power point* $Q_{cond}(t)$ *in* s
τ_{on} *Time constant for heating the heat pump in* s

In case of the heat pump shut-off the cooling time shift $t_{shift,down}$ is

$$t_{shift,down} = -\tau_{off} \ln\left(1 - \frac{\dot{Q}_{hot}}{\dot{Q}_{hot,steady}}\right) \quad \text{Eq. 2-8}$$

$\dot{Q}_{hot}$ *Condenser heat flow rate at shut-off of the heat pump in* W
$\dot{Q}_{hot,steady}$ *Condenser heat flow rate under nominal conditions in* W
$t_{shift,down}$ *Time shift for cooling from power point* $Q_{cond}(t)$ *in* s
τ_{off} *Time constant for cooling the heat pump in* s

2.1.3 Model Parameters

The heat pump can be described including cycling losses with the given correlations [14]. Even so, the equations require parameters that determine a particular heat pump. These modelling parameters have been derived from measurements by Pärisch [11].

The measured heat pump is a brine/water heat pump with a condenser heat flow rate of 7.8 kW at nominal conditions of 0°C evaporator inlet and 35°C condenser outlet

temperature. The refrigerant fluid applied is R410A. The heat pump comprises a scroll compressor and a thermostatic expansion valve.

The parameters for the heat pump compressor and condenser performance are obtained (Eq. 2-2 and Eq. 2-3) from measurements. These performance measurements have been conducted on the basis of the European standard EN 14511-3 [15] at constant mass flow rates. The measurement uncertainty is 1.87-3.66 % for the compressor power and 1.5 % for the heat flux. The mean relative deviation between measurement and the performance model derives to 0.64% for the condenser heat flow rate, -0.26% for the compressor power and 1.14% for the COP.

The maximum model deviation at particular operating points can be higher especially if mass flow rates are varied compared to the measurement conditions. Therefore, the heat pump mass flow rates are held constant in the simulations of this thesis. The mass flow rate is 900 kg h^{-1} at the condenser and 1900 kg h^{-1} at the evaporator. For these conditions the maximum model deviation at any operating point is always below 4% for the condenser heat flow rate, the electric compressor power and the COP.

It is emphasized that the measured temperature range at the evaporator has been extended to 25°C, which allows excellent assessment of the efficiency improvement induced by solar heat on the evaporator side. The parameters are the result of a least square fit to the measured steady state performance points, Table 2-1. Further information on the heat pump modelling is presented by Pärisch et. al. [11].

Table 2-1: Coefficients for the calculation of heat pump power of condenser and compressor according to model [14]

Coefficients thermal condenser power in kW					
$p_{q,1}$	$p_{q,2}$	$p_{q,3}$	$p_{q,4}$	$p_{q,5}$	$p_{q,6}$
-49.0716	83.5751	-13.4352	183.2230	-121.1532	-76.0657
Coefficients electrical compressor power in kW					
$p_{p,1}$	$p_{p,2}$	$p_{p,3}$	$p_{p,4}$	$p_{p,5}$	$p_{p,6}$
41.9710	-37.2937	-48.6282	-2.8270	19.5511	27.8347

The polynomial calculated and the COP measured are presented as a function of condenser temperature in Figure 2-4 and as a function of the evaporator temperature in Figure 2-5.

The polynomial has been determined with a maximum deviation for power of the compressor of 4.8% and of the condenser of 3.6%. The standard deviation for the thermal power of the polynomial at the condenser is 174 W and for electrical power at

the compressor is 46 W.

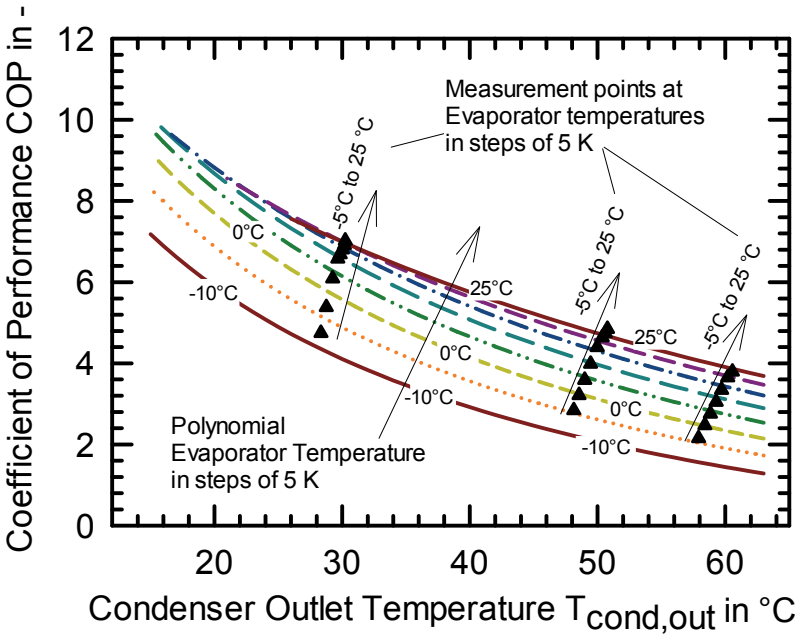

Figure 2-4: Coefficient of performance COP for the heat pump as a function of different condenser temperatures for the measured and polynomial values. The measured data points are given exactly for the condenser outlet temperature, but at approximate evaporator inlet temperatures (+/- 1 K).

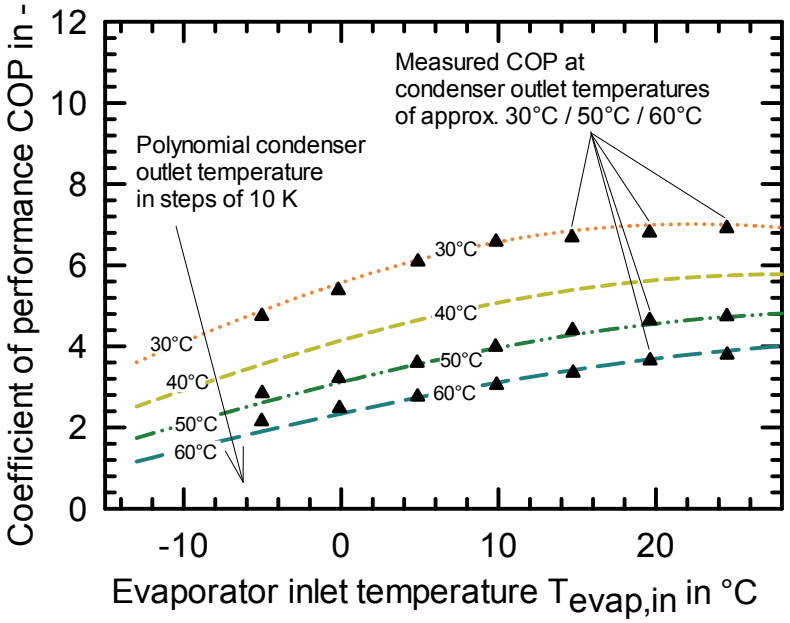

Figure 2-5: Coefficient of performance COP for the heat pump as a function of different evaporator temperatures for the measured and polynomial values. The measured data points are given exactly for the evaporator inlet temperatures, but at approximate condenser outlet temperatures (+/- 1 K).

Regrettably, the data points measured could not be determined at exactly identical conditions, but instead show a small drift. For instance, the condenser temperature at 30°C drifts from 28.3°C to 30.3°C for different evaporator temperatures, see Figure 2-4. This does not influence the quality of the fit, but can lead to overestimation of the inaccuracy of the fit in the figure. In other words, the measured points do not exactly

match the temperatures of the polynomial lines for two superimposed reasons: fitting error and the aforementioned temperature drift.

The model also requires the determination of the heating up and cooling down constants (Eq. 2-9 and Eq. 2-18). These parameters have also been measured. The heating constant τ_{on} is 30 s and the cooling constant τ_{off} is 80 s [16, p. 82 and 94]. The determination of these coefficients includes some uncertainty because the assumption of a first order function is a simplification of the heat pump. A heating constant of 20 s is proposed by Pärisch [11] for the same heat pump. While the influence within 10 s seems small, the given default values of 180 s do have a significant impact on results. It will be shown in a sensitivity analysis that this would result in a seasonal performance error of over 0.5, see Figure 5-24 in Sensitivity Analysis chapter 5.3.7.

To conclude, the measured time constants are also an important improvement for the quality of the simulation results. The constants and their determination will improve the simulation quality significantly, even if the first order function is a strong simplification. In contrast, the given default values of heating constants of 180 s appear to be inappropriate for brine/water heat pumps.

2.2 Vertical Ground Heat Exchanger

2.2.1 Working Principle

Vertical ground heat exchangers (GHX) are used as heat source for heat pumps. The heat exchangers are inserted into a vertically drilled borehole. The drilling of such a borehole is displayed in Figure 2-6.

Figure 2-6: Drilling of a borehole for a vertical ground heat exchanger at the experimental ground heat exchanger field at ISFH, Emmerthal

Vertical ground heat exchangers are categorised by their depth. In this thesis vertical ground heat exchangers are defined as heat exchangers with a depth of between 10 m and 400 m. This definition is in accordance with VDI 4640-2 [17, p. 15] and the nomenclature of [18]. Vertical ground heat exchangers are also called borehole heat exchangers VDI 4640-2 [17, p. 15] or vertical loop in North America [19]. Currently, ground source heat pumps have a decreasing market share of 34.5% in Europe (see [13, p. 9] Abb. 2) compared to air heat pumps, although absolute numbers are still high and 100.000 new systems per year were installed in Europe in 2011 and 2012 [13, p. 6].

Ground heat exchangers exist in numerous designs. The drilled holes are in most cases exactly vertical but can also be tilted (Geothermal radial drilling). The material between the actual heat exchanger and the ground can be water [20, p. 509] or in many cases cement filling material. The heat within the ground heat exchanger is transferred to the surface usually in closed loop pipes with forced fluid flow. In most cases the heat exchanger is a double U-tube of a polymeric pipe. Several other pipe designs are used in many sizes: single U-tube, coaxial ground heat exchanger, one central pipe with many satellite pipes, partly insulated pipes [21], pipes with large volumes that also use the heat exchanger as a cold storage volume [22]. Another possible method of heat transfer is a steel heat pipe as ground heat exchanger typically filled with CO_2 [23, p. 81] and working according to a heat pipe principle.

In this thesis the wide-spread solution of a polymeric pipe with double u-tube, Figure 2-7, and a cement filling material is investigated.

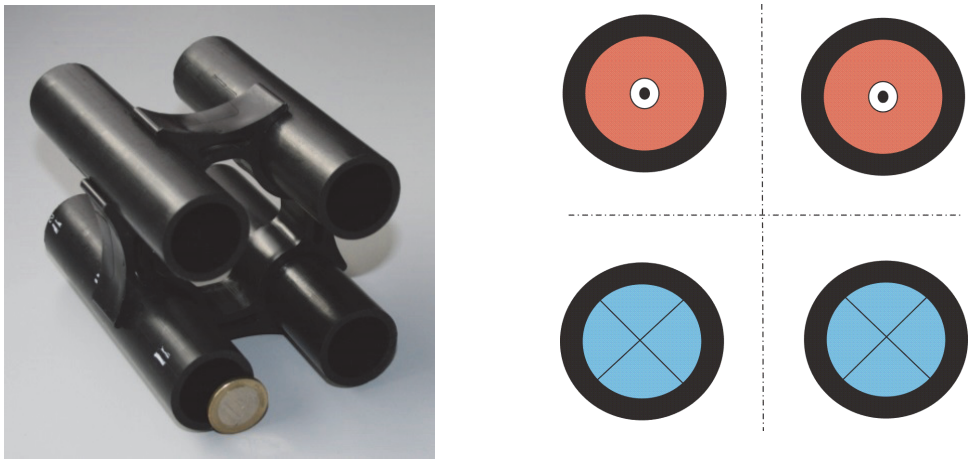

Figure 2-7: Left: Sample of a double U-tube ground heat exchanger with spacer. Right: A schematic cross cut through a double U-tube, red is upwards flow, blue is downwards flow

Vertical ground heat exchangers deliver a high temperature heat flux source for heat pumps compared to air or very surface near ground heat exchangers. A direct ground

water source is the only heat source that supplies higher and more stable source temperatures than vertical ground heat exchangers. Corresponding temperature trends are presented in a broad field test study ISE [24, p. 94] which measured over 100 different electrically driven heat pump systems between 2007 and 2010 in Germany.

Systems with vertical ground heat exchanger perform better than systems with other heat sources in this field test study and they achieve the highest seasonal performance of 3.94 [24, p. 72]. In comparison horizontal ground exchanger achieve a seasonal performance of 3.75 (p.72), ground water systems achieve 3.71 (p.59), and systems with air heat source reach 2.88 (p.56)[1].

Also the heat source temperatures are high. 41 systems with vertical ground heat exchangers (depths from 60 to 300 m) reveal an average source temperature of 7.1°C for their temperature outlet.

The question of the heat sources origin is essential to the understanding of the character of vertical ground heat exchangers. The heat flow at the heat exchangers surface is mainly perpendicular to the ground heat exchanger itself. There is, however, no ground heat source in radial direction. As a result, the radial heat transport process is strictly of heat capacity origin or from heat transfer of sources in vertical direction far below or above the ground heat exchanger. These natural heat sources in vertical direction are the geothermal heat flux from deep underground and the solar heat absorbed at the surface.[2]

These two heat sources refill the capacities around the ground heat exchanger under quasi-steady state conditions. In this case the annual heat flow to the ground capacity is equal to the heat extraction from the ground heat exchanger. The temperature regime in the ground takes decades to reach a steady state condition and can extend even deeper than the depth of the ground heat exchanger. The ratio between heat from geothermal heat flux and the surface is a function of depth and location specific parameters.

[1] The given seasonal performance factors correspond to the boundaries of SPF_{bSt} and are not comparable to seasonal performances presented later on SPF_{SHP+}.

[2] Huber and Pahud [25, p. 2] calculate a steady state example of a single ground heat exchanger of 100 m depth. They find that 85% of the heat is of solar origin coming from the surface and only 15% of the heat is coming from the geothermal flux from deep underground.

2.2.2 Minimum Inlet Temperature

Excessively low temperatures in the ground heat exchanger fluid can damage the ground heat exchanger, mainly the filling material. In case of a water filled borehole the polymeric pipes can also be damaged. This leads to a loss of the ground heat exchanger or a fracturing of the filling material. In extreme cases the fractured and water permeable filling material connects with otherwise separated ground water levels. Normally, legal limits are set for the inlet fluid temperature to avoid such effects.

In fact, such a temperature limit $T_{protect}$ for the vertical ground heat exchanger inlet is the crucial sizing parameter for vertical ground heat exchangers. Currently, the legal limits differ depending on location. In Germany the VDI 4640 is often referred to in legal frameworks and guidelines. This VDI 4640 defines a limit in relation to the undisturbed ground temperature weekly average +/-12 K and in peaks +/-18 K [17, p. 12]. The legal framework often demands frost free operation for example in [26, p. 16], [27, p. 24]. The frost protection relates in most cases to the averaged heat extraction and not to the peak load.

In fact, recent measurements show that the effective system permeability of the filling material is increased by frost cycles [28, p. 391]. Frost cycles in the filling material should therefore be avoided. This means a material dependant and constant temperature limit. An example for such constant limit is the temperature limit existing in Baden-Württemberg [29, p. 12]. Here, a temperature limit of -3°C, measured at the heat pump's outlet, is demanded to prevent freezing in the ground. A temperature drop of 3 K is assumed due to heat transfer and thermal gains of the connecting pipe. All things considered this -3°C limit seems a reasonable limit. It is therefore used in the simulations. Nevertheless, the current VDI guideline is in revision and new materials are developed and tested that might enhance the resilience of the filling material to frost cycling in the future.

In the system simulations the temperature limit permitted is -3°C at the heat pump outlet. A direct electric heat of 7 kW will supply the heating demand instead of the heat pump, if the borehole heat exchanger fluid inlet temperature T_{min} reaches this limit, see $T_{protect}$, Figure 2-8. The controller will hold this modus for at least 20 min, while the vertical ground heat exchanger is flushed every 10 min to check whether to switch back into the heat pump and ground heat exchanger modus. As a result, the vertical ground heat exchanger is protected from excessively cold temperatures. The temperature limit $T_{protect}$ can also be seen as the bivalence point of the system.

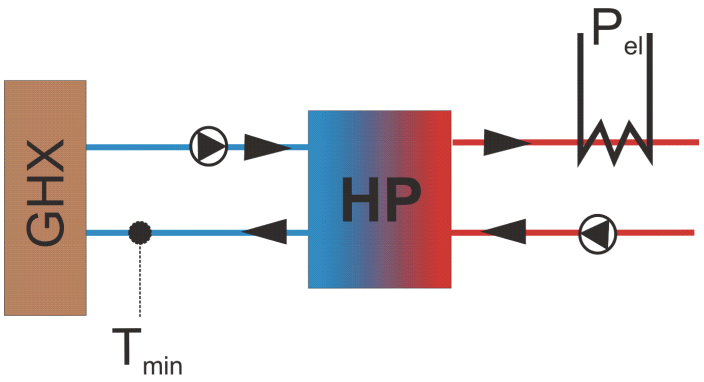

Figure 2-8: Heat pump and direct electric heater in the dynamic system simulation. The direct electric heater will replace the heat pump for some time, if the minimum temperature T_{min} falls below the allowed temperature limit $T_{protect}$

2.2.3 Mathematical Description

In a first-order approximation the vertical ground heat exchanger is an infinite line source in the ground. Analytic solutions for the temperature field as a function of the heat flow rate are given for example by [30, p. 193]. The solution, however, is a strong simplification and many influences on the heat transfer processes in the ground and within the ground heat exchanger are neglected. A picture of a ground heat exchanger before inserting into a borehole is displayed in Figure 2-9.

Figure 2-9: An approximate line source: 70 m of double U-tube ground heat exchanger just before inserting it into a borehole

In most cases the ground will not be homogenous and can furthermore be influenced by ground water flow. Freezing water causes very non-linear heat capacities in the ground.

Many more simplifications of a line source are evident in relation to the ground heat exchanger itself. Heat transfer along the line is not constant, the inner thermal inertia as fluid capacities are neglected and there are many interfering influences. Ground heat exchanger models are accordingly either very complex or very simplifying depending on the purpose of the model.

In fact, there is a variety of analytical, numerical and cross-over models implemented to even more software solutions.

The most detailed simulation models are generic multi-physic models, see for instance [31]. Here, the physical grade of detail can be defined freely in these generic models even though the software often gives limits in numerical stability, resolution and possible physical phenomena. Such detailed models, however, utilise as input files a constant heat load constraint.

In contrast, numerical models in system simulation are much more restricted. Here, the ground and the heat exchanger are defined within the limits of the model applied and its particular range of validity, for instance no ground water flow or only double U-tube configuration. Nevertheless, such models cover most applications as they are comparatively fast. This allows the accurate dynamic simulation of complete systems in small time steps and including the feedback of the heat load. Typical examples for these models and, correspondingly, implementations are SBM [32], EWS type 451 [33], DST type 557 [34]. Nonetheless, the more complicated system models in particular have weaknesses in the planning process since they still require extensive parameterisation and a deep knowledge of the particular model and its parameters.

Analytic models are comparatively simple but effective for most dimensioning tasks. These are also used in a variety of implementations e.g. Earth Energy Designer, EED [35], or the free software GEO-HAND^{light} [36] or EWS [37] which is an example of a crossover model, where a numerical model of the heat exchanger and the near ground are combined with an analytical far ground model.

The most popular analytical model is a finite line source solution of Eskilson [20], which assumes a finite line source in homogenous ground conditions and a uniform heat extraction from the borehole. This model simplifies the transient conduction in the ground to a time dependant thermal resistance $R_q(t)$. The temperature change in the ground at the outer surface of the ground heat exchanger $T_{r_{GHX}}(t)$ is calculated as a step response function of a heat flow rate $\dot{q}$ extracted over a time t, see Eq. 2-9 to Eq. 2-11 from [20], Eq. 10 & Eq. 11.

$$T_{r_{GHX}}(t) = T_{g,undis} - \dot{q} \cdot R_q^{\#}(t) \qquad \text{Eq. 2-9}$$

$$= T_{g,undis} - \frac{\dot{q}}{2 \cdot \pi \cdot \lambda} \cdot g\left(\frac{t}{t_s}, \frac{r_{GHX}}{H}\right)$$

$T_{r_{GHX}}(t)$ *Temperature at the outer rim of the borehole in* °C
$T_{g,undis}$ *Undisturbed ground temperature in* °C
$\dot{q}$ *Constant extraction heat pulse over the time t per m GHX in* W m^{-1}
$R_q^{\#}(t)$ *Time dependant resistance of the ground in* K m^{-1} W^{-1}

t *Time of heat pulse* $\dot{q}$ *in* s
λ *Heat conductivity of the ground in* W m^{-1} K^{-1}
$g\left(\frac{t}{t_s}, \frac{r_{GHX}}{H}\right)$ *Dimensionless G-function (ground resistance) in* –
r_{GHX} *Borehole radius in* m
H *Depth of borehole heat exchanger in* m

The undisturbed ground temperature $T_{g,undis}$ *as* Eq. 2-10

$$T_{g,undis} = \overline{T_{amb}} + 0.5 \cdot H \cdot G_g$$

$\overline{T_{amb}}$ *Average ambient temperature at the surface in* °C
G_g *Geothermal gradient in* K m^{-1}

Eq. 2-11

The Eskilson time t_s *in s is defined as*

$$t_s = \frac{H^2}{9 \cdot \alpha_g} = \frac{H^2 \rho\, c_p}{9 \cdot \lambda}$$

α_g *Temperature diffusivity of the ground in* m^2 s^{-1}

Superimposing positive and negative heat flow rates this equation allows the calculation of the temperature response in the ground of any train of heat pulses.

The difficulty with this equation lies in the determination of the dimensionless g-function. In the simplest case of a single ground heat exchanger analytic solutions can be found. Yet, the solution includes integrating an error function, so graphical and simpler calculation methods are quite popular and also demonstrated in the following. Eskilson gives a numerically calculated solution [38, p. 25] and more graphical solutions for many configurations [38, pp. 199–225]. Alternatively, ground heat exchanger fields can be calculated as superimposed single ground heat exchangers [39] and also demonstrated in [18, p. 18]. Analytical solutions are presented for average or middle temperatures [39, p. 194].

The g-function is not valid for “short” heat pulses. Approximations are given for pulses of characteristic length. The lower limit as $\frac{5 \cdot r_{GHX}^2}{\alpha} < t$, which is characteristically 2-3 h.

In times between $\frac{5 \cdot r_{GHX}^2}{\alpha} < t < 0.1\, t_s$ the g-function has an asymptote, see Eq. 2-12. Typical Eskilson times t_s (defined in Eq. 2-9) for 100 m ground heat exchangers range between 20-40 years.

$$g(t) = \ln\left(\frac{\sqrt{4\alpha_g t}}{r_{GHX}^2}\right) - \frac{\gamma}{2}$$ Eq. 2-12

γ Euler constant ~0.5772

For larger ground times Huber [40, p. 18] proposes a useful solution that is a simple polynomial fit. The polynomial is fitted to the graphical solution using 5 supporting points ($x=\ln(t/t_s)$ =-4/-2/0/2/3).

Such a fit is made for the values of Figure 2-10 and presented in Eq. 2-13.

$$g(t) = 0.0001814\,x^4 - 0.00015648\,x^3 - 0.04013054\,x^2 + 0.22081296\,x + 6.28915577\,x + 0.000181 \qquad \text{Eq. 2-13}$$

This solution is valid for $\ln\left(\frac{t}{ts}\right) = x \in [-4; 3]$.

For extremely long times $t > 10t_s$ the second, steady state asymptote is given by Eskilson according to Eq. 2-13.

$$g(t) = \ln\left(\frac{H}{2\,r_{GHX}}\right) \qquad \text{Eq. 2-14}$$

A graphical solution of the g-function and the long and short term asymptote are displayed in Figure 2-10.

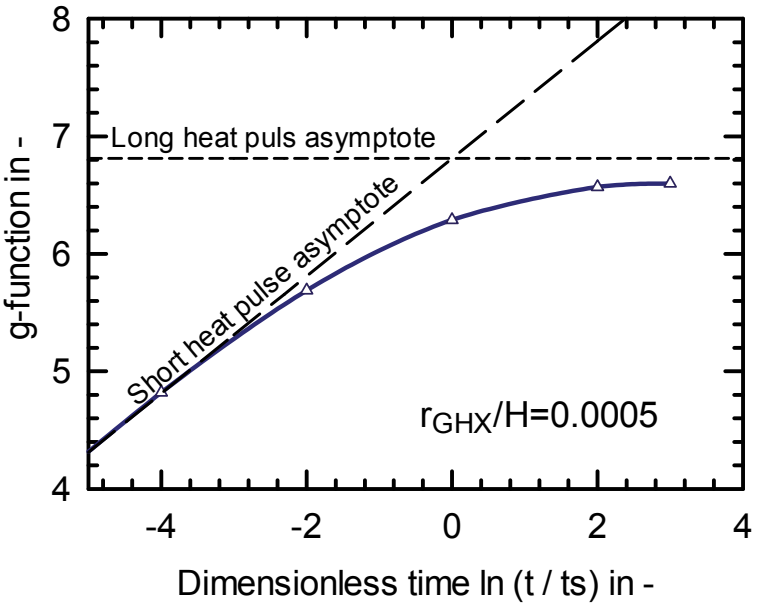

Figure 2-10: g-function for single ground heat exchanger and the asymptotes for short and infinitely long heat pulses. The g-function is valid for $r_{GHX}/H=0.0005$, the asymptotes are calculated (Eq. 2-12 and Eq. 2-14). The short time asymptote validity is given ln(0.1)=-2.3. The long pulse asymptote validity is ln(10)=2.3. The g-function is taken from literature [38, p. 25].

Strictly speaking the g-functions are only valid for a particular relation of borehole radius and depth, in Figure 2-10 and nearly every other graphical display of g-functions this ratio is $\frac{r_{GHX}}{H} = 0.0005$. G-functions for other radii r^*_{GHX} can be calculated with Eq. 2-15, [20] Eq. (12).

$$g\left(\frac{t}{t_s},\frac{r^*_{GHX}}{H}\right) = g\left(\frac{t}{t_s},\frac{r_{GHX}}{H}\right) - \ln(\frac{r^*_{GHX}}{r_{GHX}})$$ Eq. 2-15

2.2.4 Dimensioning of the Ground heat exchanger length

The dimensioning limit for the ground heat exchanger is the permitted minimum temperature T_{min} of the fluid at the ground heat exchanger inlet, compare chapter 2.2.2. Defining an effective borehole resistance R_b the average fluid temperature T_{fluid} is calculated from the ground temperature. Using Eq. 2-9 derives Eq. 2-16

$$T_{fluid}(t) = T_{g,undis} - \dot{q} \cdot R^{\#}_q(t) - \dot{q} \cdot R^{\#}_b$$ Eq. 2-16

$T_{fluid}(t)$ *Average fluid temperature in* °C
R_b *Effective borehole resistance in* m K W^{-1}
$\dot{q}$ *Constant extraction heat pulse over the time t per m GHX in* W m^{-1}
$R^{\#}_q(t)$ *Time dependant resistance of the ground in* K m W^{-1}

The effective borehole resistance $R^{\#}_b$ is defined as the thermal resistance between the average fluid and ground temperature according to Eq. 2-17. The average fluid temperature is the arithmetic average between in- and outlet fluid temperature $\frac{T_{fluid,in}+T_{fluid,out}}{2}$ of the ground heat exchanger. The average ground temperature $T_{r_{GHX}}(t)$ represents the temperature at the contact surface between the ground and the filling material of the ground heat exchanger averaged across the length of the complete ground heat exchanger.

$$R^{\#}_b = (T_{r_{GHX}}(t) - \frac{T_{fluid,in} + T_{fluid,out}}{2}) \cdot \frac{1}{\dot{q}}$$ Eq. 2-17

Typical values of the thermal resistances $R^{\#}_b$ in the field range between 0.05 and 0.1 K m W^{-1} [41, p. 53]. Detailed information about the calculation can be found in [42], laboratory measurements reach $R^{\#}_b$ values as low as 0.01 K m W^{-1} in [43, p. 46].

Strictly speaking Eq. 2-17 will allow the calculation of every fluid temperature, including the minimum $T_{fluid,min}$, in the course of the year, if all heat pulses are known and superimposed.

The calculation of every heat pump pulse would, however, only be possible in form of a numeric simulation and not be applicable to a comprehensive analytical calculation. Instead three heat pulses are used that characterise the heat extraction in the course of the year and calculate the minimum fluid temperature $T_{fluid,min}$. These three characteristic heat pulses allow the clear connection between a particular heat extraction

and the corresponding temperature answer of the ground.

This simplification assumes that the minimum fluid temperature occurs simultaneously with the heat extraction maximum. Theoretically, earlier heat extractions can result in a fluid temperature minimum that does not appear simultaneously but after the heat extraction maximum. However, in most applications the heat extraction and temperature will peak simultaneously.

The three heat extractions are, in this simplified case, an over-seasonal long term pulse $\dot{q}_{g,lt}$ a seasonal term $\dot{q}_{g,p}$ and a peak load $\dot{q}_{g,peak}$. To each heat pulse corresponds a time step and a ground resistance for long term influences· $R^{\#}_{g,lt}$, a monthly or periodical resistance $R^{\#}_{g,p}$, and a peak load resistance $R^{\#}_{g,peak}$, Eq. 2-18 and Eq. 2-19. A network of the thermal resistances is presented in Figure 2-11.

$$T_{fluid,min} = T_{g,undis} - \dot{q}_{g,lt} \cdot R^{\#}_{g,lt} - \dot{q}_{g,p} \cdot R^{\#}_{g,p} - \dot{q}_{g,peak} \cdot R^{\#}_{g,peak} - \dot{q}_{GHX} \cdot R^{\#}_{b} \qquad \text{Eq. 2-18}$$

Simple conversion derives the ground heat exchanger length required, Eq. 2-19:

$$L = -\frac{\dot{Q}_{g,lt} \cdot R^{\#}_{g,lt} + \dot{Q}_{g,p} \cdot R^{\#}_{g,p} + \dot{Q}_{g,peak} \cdot R^{\#}_{g,peak} + \dot{Q}_{GHX} \cdot R^{\#}_{b}}{T_{fluid,min} - T_{g,undis}} \qquad \text{Eq. 2-19}$$

With $\frac{\dot{Q}_{g,xx}}{L} = \dot{q}_{g,xx}$

$\dot{Q}_{g,xx}$ *Overall ground heat extraction during period XX in* W
L *Required overall length of ground heat exchanger(s) in* m

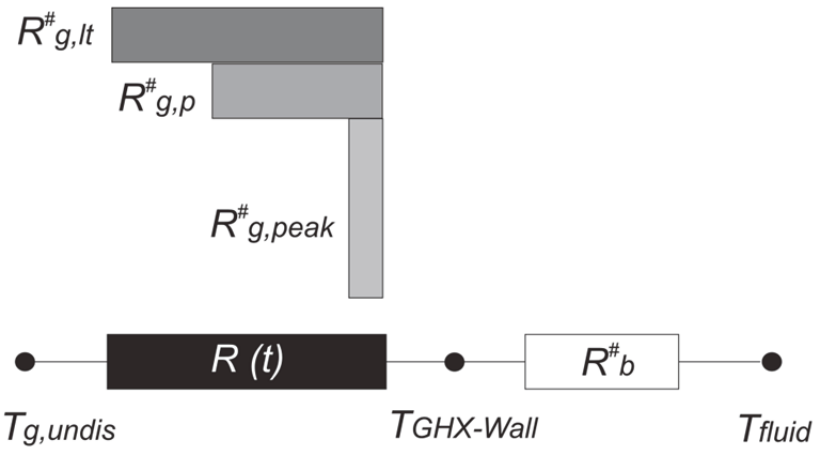

Figure 2-11: Thermal resistance network represents the ground and borehole resistance according to Eq. 2-16. The resistance R(t) is replaced by the simplifying approach of three parallel resistances · $R^{\#}_{g,lt}, R^{\#}_{g,p}, R^{\#}_{g,peak}$ for dimensioning calculations

A decisive question is the view on the duration and the size of these three characteristic heat pulses.

The analytical approach, which is used for development of dimensioning rules in this thesis, is presented by Eskilson [20, p. 522]. Here, the three heat flow rates in the ground are superimposed and merged. This means that the actual peak load in the ground is reduced by the heat flow rates that are already respected by the periodic and over-seasonal heat flow, Eq. 2-16 and Figure 2-18. The heat flow rates result from the assumption that the minimum temperature occurs also during the maximum heat flow rate $\dot{q}_{GHX}$.

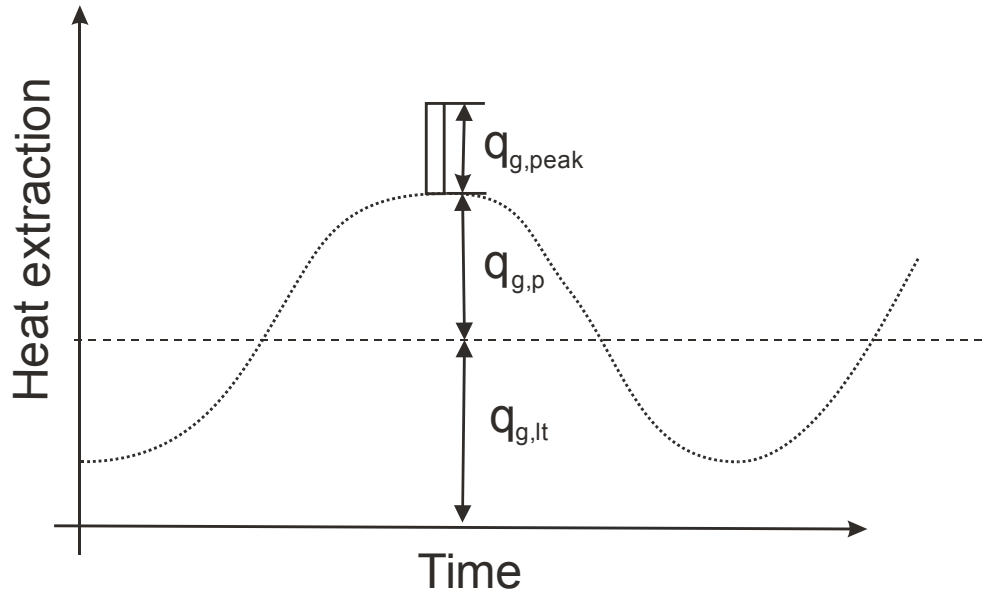

Figure 2-12: Heat flow rate distribution in the course of the year and superposing heat flow rates for the ground response calculation according to Eskilson [20, p. 522]

$$\dot{q}_{GHX} = \dot{q}_{g,lt} + \dot{q}_{g,p} + \dot{q}_{g,peak} \qquad \text{Eq. 2-20}$$

Eskilson [20] gives solutions for the heat loads, while characteristic times for heat extractions are not proposed. For the peak load time t_{peak} derives from Eq. 2-9 and Eq. 2-12 the peak load resistance $R^{\#}_{peak}$, Eq. 2-21.

$$R^{\#}_{peak} = \frac{1}{2 \cdot \lambda \cdot \pi} \cdot \left(\ln\left(\frac{\sqrt{4 \cdot \alpha_g \cdot t_{peak}}}{r_{GHX}} \right) - \frac{\gamma}{2} \right) \qquad \text{Eq. 2-21}$$

The periodical resistance $R^{\#}_{g,p}$ is calculated not as a peak load response but as the answer to a periodic forcing function, Eq. 2-22. An alternative approach for fully regenerated ground heat exchangers will be presented in section 7.2.1.

$$R_{g,p}^{\#} = \frac{1}{2 \cdot \lambda \cdot \pi} \cdot \sqrt{\left(\ln\left(\frac{2 \cdot \sqrt{\frac{\alpha_g \cdot t_p}{2 \cdot \pi}}}{r_{GHX}} \right) - \gamma \right)^2 + \frac{\pi^2}{16}} \qquad \text{Eq. 2-22}$$

The over-seasonal resistance $R_{g,lt}^{\#}$ depends on the $t_{g,lt}$, the operation time of the system, and the g-function. The time $t_{g,lt}$ should be set according to the maximum possible time of operation. The resistance $R_{g,lt}^{\#}$ can then be determined from the corresponding g-function for the particular borehole configuration and a particular relative borehole distance *B/H*.

$$R_{g,lt}^{\#} = \frac{1}{2 \cdot \lambda \cdot \pi} \cdot g\left(\frac{t_{g,lt}}{t_s}, \frac{r_{BHX}}{H}, \frac{B}{H}\right) \qquad \text{Eq. 2-23}$$

B *Borehole distance in* m

Eventually, the minimum temperature Eq. 2-18 and ground heat exchanger length Eq. 2-19 can be calculated knowing the resistances and characteristic heat flow rates.

Note that a similar but different calculation approach is used in North America. This approach gives a solution according to Eq. 2-19 for the necessary ground heat exchanger length. The three characteristic resistances, however, are calculated for constant time frames of 10 years, 1 month and 6 hours. The three heat loads are calculated from the heat flow rate in the corresponding period. In contrast to the Eskilson approach, the heat loads do not add up to the overall heat flow rate at the borehole resistance, compare Eq. 2-20. The calculation approach is explained in [44, p. 15] and a spread sheet calculation of ASHRAE is provided in [45]. This method is likely to overestimate the ground heat exchanger length necessary.

2.2.5 Separation in Solar Long-term and Short-term Effects

The characterisation of different heat flow rates long-term, seasonal and peak load presented in Eq. 2-18 is tremendously instructive. It is, moreover, the key to the systematic examination of the contingent of solar energy interacting with the ground heat exchanger.

The influence of additional solar energy is separated into 4 different effects, Figure 2-13.

1. The direct, instantaneous supply of solar energy to the evaporator or a source storage tank. This reduces the heat demand from the ground heat exchanger.
2. The solar heat delivered shortly before or simultaneously to the peak load to the

ground heat exchanger.

3. Solar energy can affect the ground in a seasonal or monthly time frame.
4. Solar energy changes the overall seasonal demand from the ground because the annual net heat extraction is changed.

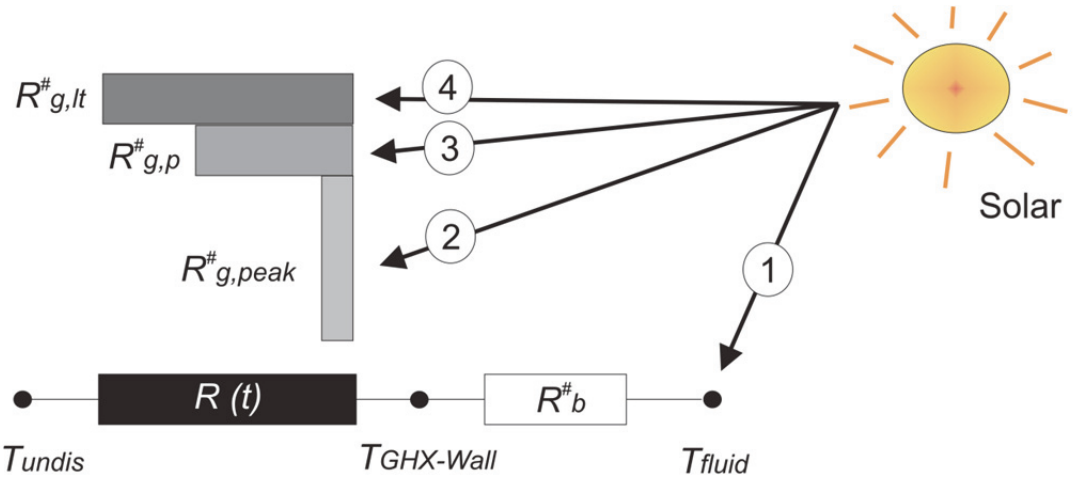

Figure 2-13: Possible interactions between solar energy and the ground heat exchanger. The possible heat flow rates: 1- Solar yield directly to the evaporator 2- Short term storage effects of solar energy relevant for the peak load (hours, days) 3- Solar energy influence on a seasonal basis changing the periodic load (months) 4 – Over-seasonal influence of solar energy

In real applications all four influences are felt. For instance the heat flow rates on short term or monthly basis at the same time reduce the annual heat extraction. This means they also influence the long term behaviour. In essence, the impact of solar energy on the ground is separated and discussed in two time frames: The seasonal (1-3) and the over-seasonal time frame (4).

2.2.6 Long-term influence of Solar Regeneration

The over-seasonal temperature difference $\Delta T_{g,lt}$ between undisturbed ground temperature and the temperature at the contact surface between ground heat exchanger and its surrounding ground can easily be calculated by Eq. 2-9. For the detailed discussion of this temperature drop the equation is split in two factors, see Eq. 2-24.

$$\Delta T_{g,lt} = \dot{q}_{g,lt} \cdot R^{\#}_{g,lt} = \frac{\dot{Q}_{g,lt}}{2 \cdot \lambda \cdot \pi \cdot L} \cdot g\left(\frac{t_{g,lt}}{t_s}, \frac{r_{GHX}}{H}, \frac{B}{H}\right), \quad \text{with } t_s = \frac{H^2 \rho \, c_p}{9 \cdot \lambda} \qquad \text{Eq. 2-24}$$

The first factor $\frac{\dot{Q}_{g,lt}}{2 \cdot \lambda \cdot \pi \cdot L}$ ·represents the ground conditions and the specific annual heat extraction. The second factor, the g-function $g\left(\frac{t_{g,lt}}{t_s}, \frac{r_{GHX}}{H}, \frac{B}{H}\right)$, represents the dimensionless ground heat exchanger field dependency on geometry, ground properties

and time.

The equation clearly demonstrates that no over-seasonal temperature development occurs for solar regeneration because in this case the long term heat extraction $\dot{Q}_{g,lt}$ becomes zero. Furthermore, this general statement applies independently of the ground properties, time and geometric distribution of the ground heat exchangers.

Nonetheless, in the course of the year there is a temperature drop in the ground around the ground heat exchanger which arises from heat extraction in time frames shorter than one year. In fact, in the course of the year the annual heat balance of the ground heat exchanger is most of the time imbalanced and not zero. In effect, a seasonal temperature response results in the ground. This remaining temperature drop can also be calculated with Eq. 2-24 but it should be kept in mind that the characteristic time $t_{g,lt}$ within the g-function is always shorter than one year due to the yearly regenerated ground.

The discussion of imbalanced ground heat exchangers is much more complex in contrast to the regenerated ground heat exchangers. The over-seasonal heat flow rate $\dot{Q}_{g,lt}$ is larger than zero. Correspondingly, many constraints influence the temperature difference $\Delta T_{g,lt}$. The properties of the ground, the specific annual heat extraction, and the geometry have an impact on the time dependant development of this temperature difference. In addition, the dimensionless description is not well suited to gain an understanding of the possible temperature range. Nonetheless, the comparison of imbalanced ground heat exchangers is crucial to assess the benefits of balanced solar regenerated ones.

For this reason, the general g-functions are discussed for a group of equivalent systems in different sizes. Two assumptions are made to obtain a group of such equivalent but differently sized systems. Firstly, a particular example case is defined, a family house with one ground heat exchanger of 100 m length. Secondly, it is assumed that the larger systems investigated have the same ground heat exchanger length, depth, ground properties and specific heat extraction rate compared to the single family house but a *n* times larger number of ground heat exchangers. In other words, these bigger systems consist of *n* adjacent single family houses with *n* ground heat exchangers under identical conditions or one large, single building but with an equivalent load file *n* times larger.

The values for the single family reference builidng represent a well-insulated single family house with 140 m² living area in Strasbourg. The overall heat extraction from the ground is 7.2 MWh a^{-1} and the ground heat exchanger has a depth of 100 m. Therefore,

the specific annual heat extraction $\frac{\dot{Q}_{g,lt}}{L}$ is 72 kWh a^{-1} m^{-1}. This is comparable small. The current dimensioning guideline VDI-4640 allows up to 100-150 kWh a^{-1} m^{-1} for single family houses [17, p. 16]. All these values and ground properties applied correspond to the later frequently used reference system simulation for a single family house, see chapter 4.

These values change Eq. 2-24 to Eq. 2-25.

$$\Delta T_{g,lt} = \frac{7.164\ \text{MWh}}{8760\ \text{h} \cdot 100\ \text{m} \cdot 2 \cdot 2\frac{\text{W}}{\text{mK}} \cdot \pi} \cdot g\left(\frac{t_{g,lt}}{t_s}, \frac{r_{GHX}}{H}, \frac{B}{H}\right) \qquad \text{Eq. 2-25}$$

$$\Delta T_{g,lt} = 0.651 \cdot g\left(\frac{t_{g,lt}}{t_s}, \frac{r_{GHX}}{H}, \frac{B}{H}\right)$$

$$With\ \frac{r_{GHX}}{H} = 0.005;\ t_s = 35.3\ \text{years} = 1111 \cdot 10^6\ \text{sec.};\ H = 100\ \text{m}$$

As a result, the temperature drop $\Delta T_{g,lt}$ depends only on the shape of the g-function and the elapsed time for the investigated reference case and all equivalent and up scaled systems with the same specific annual heat extraction rate. Assuming *n* identical houses with *n* single 100 m ground heat exchanger reveals the same solution but a different g-function g_n due to the ground heat exchangers' interference. This procedure allows easy comparison of the long-term temperature development between systems of different size.

Figure 2-14 displays the graphical solutions for the single house and equivalent multiple houses which is the basis for the following discussion.

The diagrams in Figure 2-14 give the character of the long-term, time dependant temperature development in the ground. The two diagrams present two different ground heat exchangers distances: 5 m and 20 m. The black axes relate to the dimensionless, universal numbers, g-function and dimensionless time. The green axes relate to the particular example of the single system correspondingly to multiple equivalent reference systems.

The base line for temperature development is set by the very left data points. Here, the time interval is below one year. Accordingly, the very left point marks the temperature difference that appears within operation periods shorter than one year. This point, and not a temperature difference of zero, is selected as reference to determine the long-term temperature development in the ground.

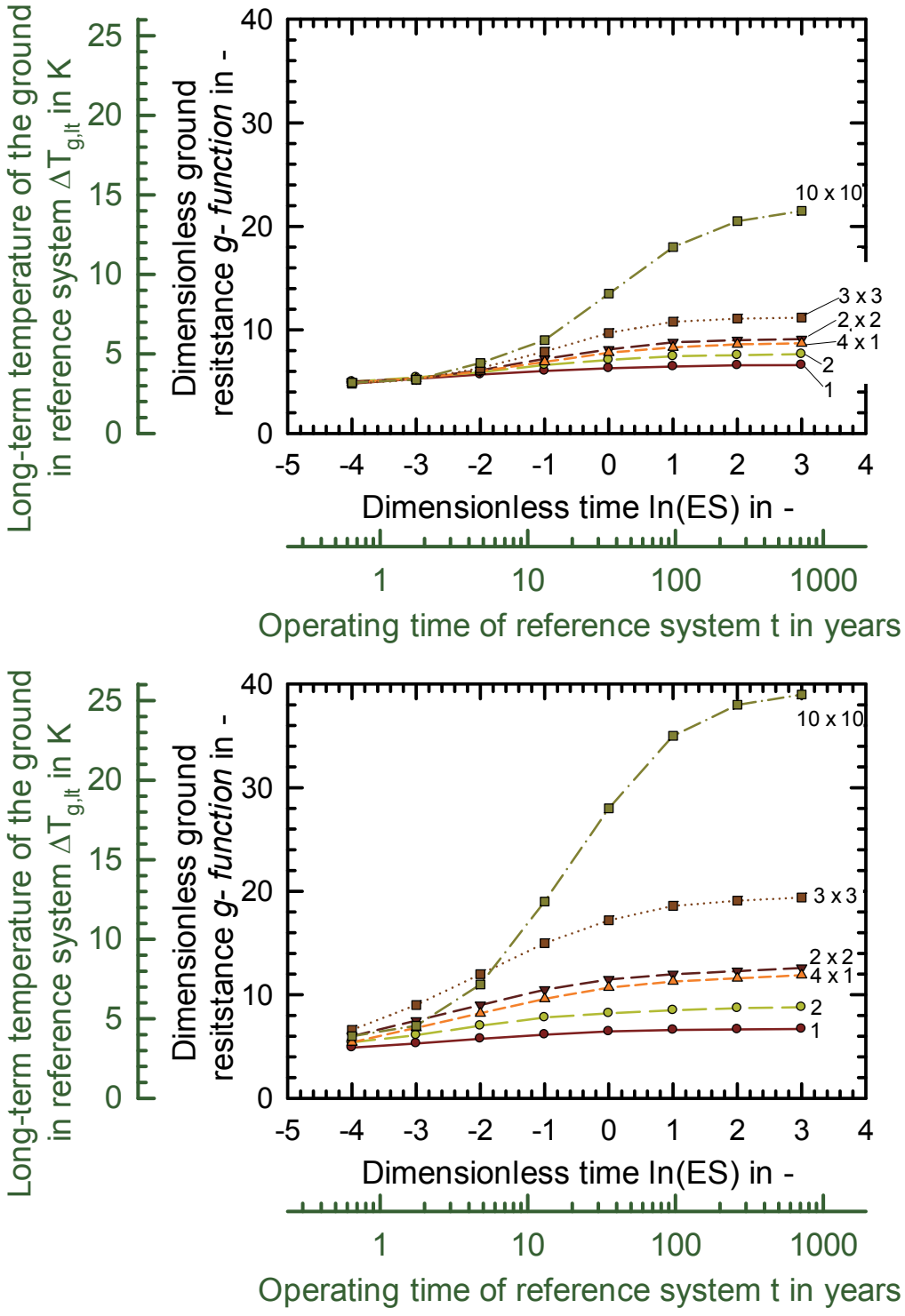

Figure 2-14: g-functions and temperature response vertical ground heat exchangers Top: GHX fields with a distance between the boreholes of 20 m. Bottom: g-functions for vertical ground heat exchanger fields with a distance between the boreholes of 5 m. The vertical ground heat exchanger field with 10x10 here has a distance of 10 m instead of 5 m. The outer, **green axes** are calculated for a number of ground heat exchangers 100 m deep which are all operated simultaneously with a heat load according to the simulation reference case, Figure 4-2. The given temperature difference $\Delta T_{g,lt}$ represents only the long-term temperature influence due to the ground's thermal capacity depletion. Constraints: $\frac{r_{GHX}}{H} = 0.0005$; λ=2 $Wm^{-1}K^{-1}$; ρ=2500 kg m^{-3};c_p=0.8 kJ kg^{-1} K^{-1}

In principle, Figure 2-14 reveals that the long term influence is small in the case of a single ground heat exchanger. In the example given the long-term temperature increase of the ground is around 1 K in the first 100 years of operation, mainly in the first three years (lowest line, outer green axis, year 1 to 100). Also, this single ground heat exchanger solution corresponds to fields with very large distances and not interfering ground heat exchangers.

In contrast to single ground heat exchangers, the temperature difference increases strongly for multiple ground heat exchangers. Between the 1st and 30th year of operation their long-term temperature development reaches significant values and furthermore has not reached steady state conditions. For periods longer than 10 years the temperature drop can be strong.

4 adjacent ground heat exchangers have an over-seasonal temperature drop of 4 K with a distance of 5 m and 2 K with a distance of 20 m under the given conditions and a 30 year time frame. 9 adjacent ground heat exchangers have an over-seasonal temperature drop of 8 K with a distance of 5 m and 3 K with a distance of 20 m. 100 adjacent ground heat exchangers have an over-seasonal temperature drop of 14 K with a distance of 10 m and 5.5 K with a distance of 20 m.

To sum up, the larger the number and the shorter the distance between the ground heat exchangers in the field the bigger is the influence on the temperature. The same applies to the required time until which steady state conditions are reached. Arranging many boreholes together will result in a slow depletion of the ground and a gradually decrease of the temperatures both at long time constants.

It is emphasized at this point that these theoretically very large over-seasonal temperature development is good to assess the benefits of regeneration but unlikely to happen in reality. Firstly, the ground heat exchanger field will in most cases be better designed and not be built in such a configuration. That means the ground heat exchanger field will be planned either with longer or more distanced ground heat exchangers. Secondly, after some years of operation such a poorly designed system would reach its permitted lower temperature limit and would accordingly stop to operate. Thirdly, the extracted heat flow rate would decrease because the colder source temperature for the heat pump would lead to a lower heat pump performance which means less heat extraction from the ground. This effect is not respected with the assumption of a constant annual heat extraction but would slightly reduce the calculated

temperature drop.

Of course, the over-seasonal effects differ for each particular case. The heat flow rates extracted, the depth of the heat exchangers and the ground properties vary for every system. Even so, the basic character of over-seasonal ground-cooling effect becomes obvious. Ground heat exchangers cannot be operated oblivious of other ground heat exchangers within the surrounding neighbourhood. Accordingly, the long-term effect applies particular to larger systems and multiple adjacent single systems as located in urban areas.

It is restated that 100.000 new ground source heat pumps are installed per year in Europe and it seems likely that in many cases 4 or more ground heat exchangers are built close enough to interfere with each other. Their long-time constants and interference will often be recognisable only decades later. In fact, ignoring the high long-term influence of ground heat exchanger fields damages the sustainable and continuous use of the ground as a renewable heat source.

What is the impact of solar or other thermal regeneration in this context? Periodically recharging the ground by solar energy or any other heat source will neutralise the long-term effect presented. In the case of complete solar regeneration the characteristic time of any g-function configuration will not reach more than one year, even if the ground heat exchangers do interact due to very close distances. Remarkable savings of the component length required are possible in the size of the over-seasonal temperature drop. Furthermore, the complex interaction of ground heat exchangers will vanish and the influences of ground properties, borehole depth, and geometric arrangement on the long term temperature behaviour will diminish. In short, regeneration means much less interference and complexity of the ground heat exchanger dimensioning. Any borehole field performs like multiple single ground heat exchangers that do not interfere.

To conclude, the long-term effects are very specific for each case as long as they are not fully regenerated. Partly recharging of the ground heat exchanger field dampens the over-seasonal effects described. Cutting half of the annual heat load means cutting half of the long-term temperature drop. Even so, the long term issue remains. Identical system will behave differently if they have no, 3, or 30 adjacent systems. The magnitude and character of long-term effects is relevant, which becomes very clear in the example given. This interference, however, vanishes with solar regeneration of the ground.

For this reason the annual regeneration of the vertical ground heat exchanger is an

attractive dimensioning goal. This allows easy designing, scaling and transferring correlations from a single to any configuration of vertical ground heat exchangers and more independence of the ground properties. To achieve this goal the use of uncovered solar thermal collectors as a heat source is attractive because they provide low temperature heat at very low costs. A method for the dimensioning of uncovered collectors to realize a complete regeneration is derived and documented in chapter 7.2 “Fully Regenerated Ground Heat Exchanger”.

It is restated that the long-term effects, Figure 2-12 No. 4, and the short-term effects (No. 1-3) are investigated separately. This separation of long and short term effects is a key point for the understanding of the results presented hereafter.

The simulations investigating the impact of solar energy are made for a single ground heat exchanger, which has a negligible long-term temperature drop. The remaining long-term influence of a single ground heat exchanger between the 2nd and the 20th year of operation is 0.4 K, Figure 5-15 . Accordingly, the dynamic system simulations are conducted for 2 years and assessed in the second year only. These simulations do not include the long-term effects described.

2.2.7 Short Term Validation of Simulation Model

The short term transient modelling of the ground heat exchanger is of high importance for the quality of system simulations. “Short” means all periods during which the g-functions will not apply due to transient effects within the ground heat exchanger. This is usually 2-3 hours. The inner thermal heat capacities and the large inner fluid volume result in a quite different heat transport process as for long-term operation. The short term description is important because, in contrast to conventional dimensioning tools, the system simulations are conducted in one minute time steps. Most simulation tools do not account for the intermittent operation of the heat pump, which is in many cases operated for 10 or 20 minutes only.

For this reason, model extension is made for the ground heat exchanger model used in throughout the system simulations. This model extension is the result of dynamic measurements with a ground heat exchanger conducted at ISFH. The measurements examine the short term quality of the ground heat exchanger model. The model extension and measurement results are made by Pärisch [46].

The experiment conducted is comparable to a step response and displayed in Figure 2-15. A constant inlet temperature is set at the ground heat exchanger inlet[1]. The mass flow rate is constant.

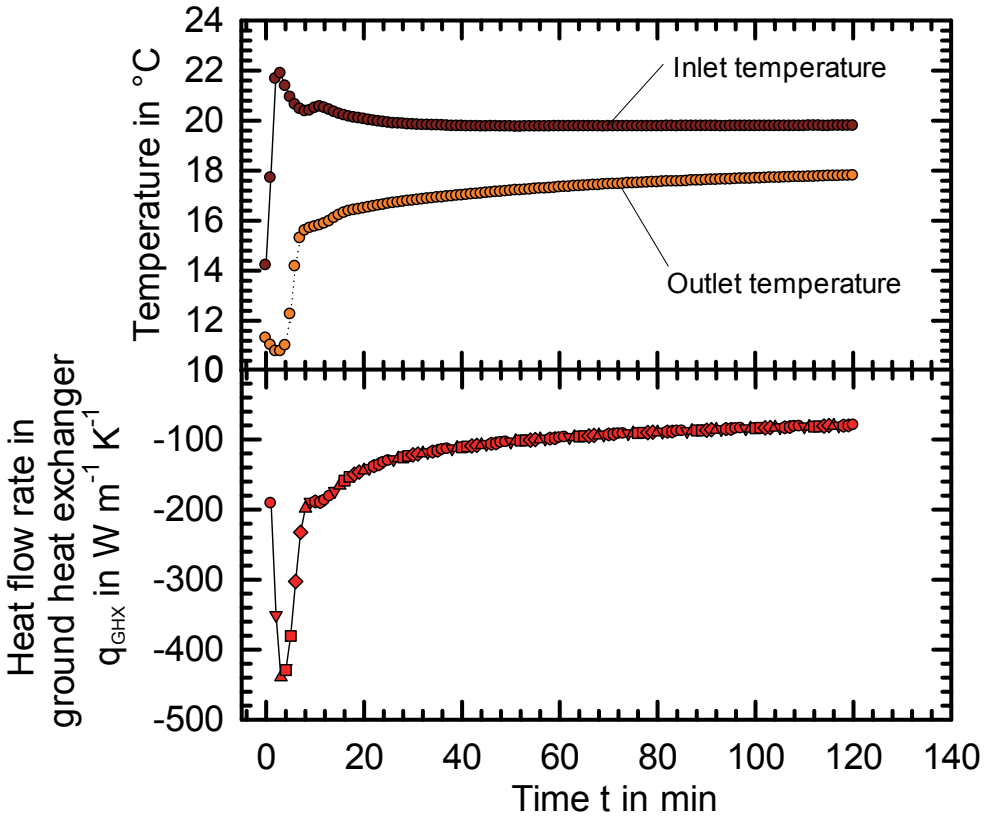

Figure 2-15: Top: Measured inlet and outlet temperature of the ground heat exchanger, Bottom heat flow rate inserted in the ground heat exchanger, mass flow rate 2250 kg h^{-1}, start of the experiment is at t=0

In the first minutes of operation enormous heat flow rates of up to 400 W m^{-1}K^{-1} occur at the ground heat exchanger, caused by the plug flow effect. The fluid in the ground heat exchanger, approx. 140 l, has ground temperature and is flushed out without being affected much by the inlet temperature conditions. The outlet temperatures converge only after one complete fluid circulation, then the heat flow rate diminishes.

In case of an intermittent heat pump operation a significant part of the heat transfer between the fluid and the ground is transferred during the standstill periods. For an extreme case the heat pump would only be operated long enough to flush the fluid out and then pause. The ground heat exchanger is then operated more as a ground heat

[1] Deviations of up to 2 K appear in the first two minutes due to capacity effects of the experimental setup. However, this deviation is much too small to cause the very high heat flow rates in the beginning of the experiment.

regenerator benefiting from capacity effects.

The ground heat exchanger simulation model [47] does not include short term heat capacity effects. Correspondingly, the ground heat exchanger model in the system simulation, see chapter 4, is configured with a pre-pipe to improve the short term quality of the simulations.

The pre-pipe is defined as a model of an adiabatic pipe. In the simulation this pipe model is positioned previous to the ground heat exchanger inlet. All fluid entering will pass once though this pipe model before it enters the ground heat exchanger model. During standstill the pre-pipe is operated in short circuit with the ground heat exchanger at low mass flow rates. This respects the heat exchange between filling and ground. Accordingly, the heat contained in the inner ground heat exchanger filling and fluid, here the pre-pipe, discharges to the surrounding ground.

The geometrical configuration of the pre-pipe is done according to Pärisch [46]. The pre-pipe is simulated with type 604 from [48]. Apart from the fluid it accounts for the mass in the pipe wall, which is simulated as a numerical mesh of nodes. The pipe has the length of the vertical ground heat exchangers depth.

The diameters are derived from the U-tube geometry. The outer pre-pipe diameter $D_{pre-pipe,out}$ is equal to the diameter of borehole D_{GHX} including the filling, Eq. 2-26. The inner pre-pipe diameter $D_{pre-pipe,in}$ is twice the U-tube pipe diameter $D_{GHX,U-tube}$, Eq. 2-27. The pre-pipe mantle properties between $D_{pre-pipe,out}$ and $D_{pre-pipe,in}$ are equal to the filling material.

$$D_{pre-pipe,out} = D_{GHX} = 2\, r_{GHX} \qquad \text{Eq. 2-26}$$

$$D_{pre-pipe,in} = 2 \cdot D_{GHX,U-tube} \qquad \text{Eq. 2-27}$$

The extension of the DST model with pre-pipe is now compared to the measurements and other simulation tools that respect heat capacity effects, see Figure 2-16.

One simulation model is the EWS model as TRNSYS type 451 [33], which is also used in the dynamic system simulation. The other model is a Comsol model [31], which is a detailed FEM model of the physical processes within the borehole, but not used in system simulations.

Overall, all simulation models show high agreement to the measurements and prove to have good quality in modelling short term effects that are dominating in the first 10 min of operation. Of course, 10 minutes is a rough approximation. These short term effects would have longer lasting dominance in deeper ground heat exchangers, at lower mass

flow rates or larger pipes. However, in the experiment presented deviations of around 1 K still remain after 10-30 minutes.

It is restated at this point that heat pumps in field measurements and simulations often run less than 30 min or even less than 10 min. The simulation quality for these short term effects and especially the plug-flow effect is therefore highly relevant for the system simulation, compare chapter 5.3.2.

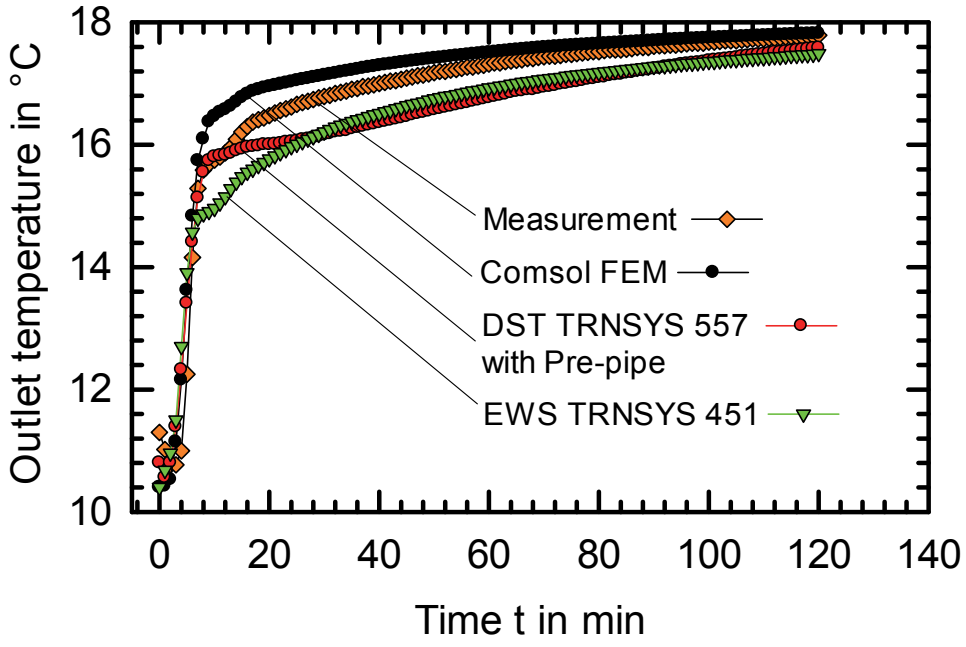

Figure 2-16: Measured and simulated outlet temperatures of different ground heat exchanger models corresponding to experiment in Figure 2-15

2.3 Uncovered Solar Thermal Collector

2.3.1 Working Principle and Description

Uncovered (or unglazed) solar thermal collectors absorb solar irradiance with a surface that permits a direct convective heat transfer of its irradiance absorbing surface to the ambient air. In contrast to conventional flat plate collectors, there is no transparent cover with an insulating air gap that reduces the thermal losses of the collector. Accordingly the uncovered collectors have a higher thermal loss coefficient and do not reach operating temperatures with a high difference to the ambient air. Typical stagnation temperatures are normally below 100°C even in summer. Two pictures of uncovered collectors are displayed in Figure 2-17.

Figure 2-17 Uncovered collectors: Left 8 different black polymer collectors during testing at ISFH, right: 650 m² of black metal roof collector for swimming pool heating in Nordstemmen, Germany

Uncovered collectors have several advantages. First of all they have a low price and a simple design as compared to covered collectors. Black polymer collectors reach prices of 40 € per m² in large fields and 100 € per m² for small fields [49, pp. 80–81]. Secondly, if the collector is supposed to provide heat at low operating temperatures close to or even below the ambient air temperature, the uncovered collector will compete with or even outperform the covered collector. At low temperature differences to the ambient the convective heat losses are low or there may be heat gains when there is an operation below the ambient air temperature.

Uncovered collectors are therefore applied in systems with low operating temperatures. The most widespread application is swimming pool heating, which demands an operating temperature close to the ambient air temperature. Uncovered collectors are also successfully used for water pre-heating in open district heating nets [49]. Another application often pursued is the combination of uncovered collectors on the heat source side of a heat pump. Here, the uncovered collector supplies heat to the heat pump evaporator at low temperatures.

There are a variety of different collector designs for uncovered collectors. The resulting collector efficiencies for different collector designs are displayed in Figure 2-18 according to the collector efficiency Eq. 2-32. A comprehensive description is given in Appendix A for the applied performance sets in this thesis.

The collector types have characteristic performances due to their design.

- Black polymer (swimming pool) collectors consist of extruded pipes or a polymer matrix that hold the fluid. In most cases the collector requires some mounting that fixes the collector onto the roof, Figure 2-17. (product examples: [50]–[52]

- Metal roof collectors are building integrated metal roof elements with piping at the rear side of the metal roof for heat transport. (product examples [53]–[55]
- Massive absorbers consist of concrete building elements used as heat sources for heat pumps, they are also a type of uncovered collectors. Since the first heat pump boom in the 1990ties they have been used as sources of heat pumps [56], [57].
- Uncovered photovoltaic thermal (PVT)-collectors transmit solar irradiation to heat and electricity. In many cases a rear piping is simply added to PV-modules or PV cells are glued to metal roof collectors [58], [59].
- Selective uncovered collectors have special optical properties with high absorption values for short wave radiation and low emissivity for long wave radiation (measured product [60]).

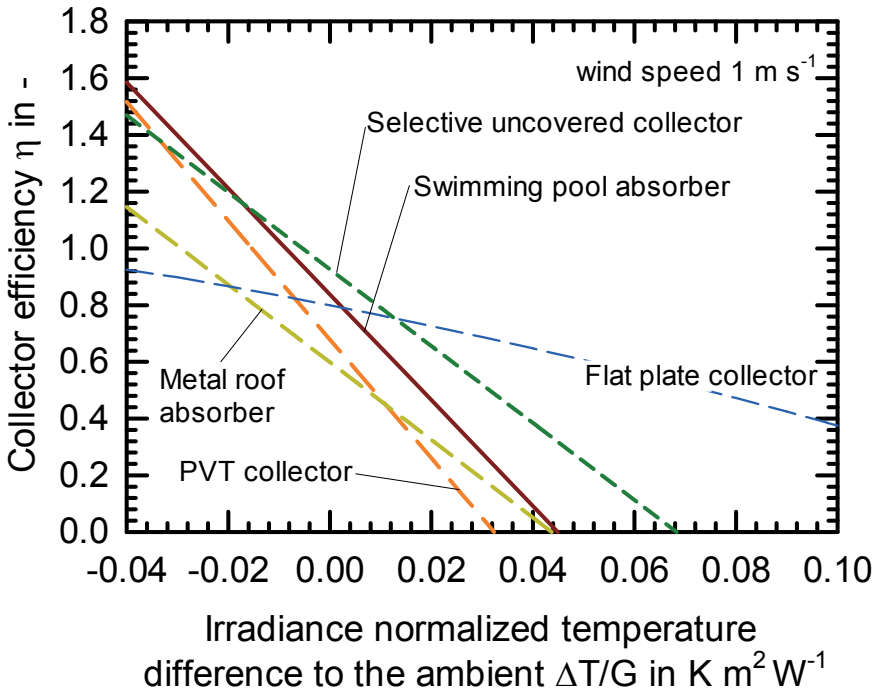

Figure 2-18 Efficiencies for a wind speed of 1 m/s representing different types of uncovered collectors. The applied performance parameters can be found in Appendix A. The efficiency of a standard flat plate collector is included, too. Note: In the efficiency calculation the irradiance G for covered and uncovered collectors is defined differently, see Eq. 2-33.

2.3.2 Heat Flow Rates for the Uncovered Solar Thermal Collector

[1]There are many possible energy fluxes at the system boundary of an uncovered collector. From the first law of thermodynamics [10, p. Gl. 2.26] the following energy balance results.

$$\frac{dE}{d\tau} = \dot{Q} + P + \sum \dot{m}(h + \frac{c^2}{2} + g_{grav} \cdot z) \qquad \text{Eq. 2-28}$$

For the sake of simplicity kinetic and potential energy of the working fluid are ignored. Furthermore, it is assumed that only two steady state mass flow rates, the air $\dot{m}_{air}$ and the fluid in the collector $\dot{m}_{fluid}$. The thermal energy flow rate for the collector fluid derives to $\dot{Q}_{coll} = \left(\dot{m} \cdot c_p \cdot \Delta T\right)_{fluid}$. The much more complex energy flow rate from air mass flow may contain rain or snow. In addition the air enthalpy change Δh_{air} possibly comprises sensible heat and latent heat. The latent heat can derive from melting, frost, condensation and evaporation (sublimation, desublimation) of humidity in the air. Figure 2-19 displays uncovered collectors with icing or condensation.

Figure 2-19 Uncovered collectors: Left metal roof collector in operation with condensation on the roof elements (darker grey). Right: Selective uncovered collectors with hoarfrost in the morning partly melted by sunlight [source Energie Solaire SA, Bernard Thiessen]

Moreover, three direct heat flow rates are assumed to appear at the collector: A convection heat flow rate to the ambient $\dot{Q}_{conv}$, conduction to the rear side of the collector $\dot{Q}_{side}$, and a heat flow rate from radiation exchange $\dot{Q}_{rad}$, which is seperated into the incoming short wave radiation $\dot{Q}_{SW}$ from the sun and the, under nearly all wheather conditions negative, long-wave radiation balance $\dot{Q}_{LW}$. In case of a PVT-

[1] Identifying all possible energy flow rates developed from discussion with Michel Haller during the collector modelling report of the IEA SHC Task 44 / HPP Annex 38 [61] p.3.

collector electricity P_{PV} might also be gained. The energy balance "simplifies" to:

$$\frac{dE}{d\tau} = \dot{Q}_{SW} + \dot{m}_{air}\Delta h_{air} - (\dot{Q}_{conv} + \dot{Q}_{side} + \dot{Q}_{coll} + P_{PV} + \dot{Q}_{LW}) \qquad \text{Eq. 2-29}$$

Incoming energy flow rates are defined positive.

2.3.3 Model of Uncovered Solar Thermal Collector

The physical parameters that solve the energy balance equation Eq. 2-29 are hard to obtain and impossible to adjust for every collector design and mounting situation in the field. In fact, every existing collector model does neglect some possible heat flow rates. In practical application the collector heat flow rate $\dot{Q}_{coll}$ is derived from linearised performance models. For a flat plate collector the Hottel-Whillier-Bliss equation applies, see for example [62, p. 292], Eq. 2-30.

$$\dot{q}_{coll} = F_R(\tau\alpha)_{avg}G' - F_R U_L \cdot \Delta T_{in-amb} \qquad \text{Eq. 2-30}$$

$\dot{q}_{coll}$	*Specific usable collector heat flow rate in* W m^{-1}
F_R	*Heat removal factor of collector in* -
G'	*Irradiance in collector plane in* W m^{-2}
U_L	*Loss coefficient of collector in* W m^{-2} K^{-1}
$(\tau\alpha)_{avg}$	*Effective transmittance-absorptance product of collector in* -
ΔT_{in-amb}	*Temperature difference between coll. inlet and ambient in* K

Soltau adjusts this equation to uncovered collectors [63, p. 263]. The net irradiance is defined G'' that includes long-wave radiation exchange. Second the thermal loss terms are extended with a linear wind dependency. From Eq. 2-31 the simplified Eq. 2-32 results:

$$\dot{q}_{coll} = F_R\alpha G'' - F_R U_L \cdot \Delta T_{in-amb} \qquad \text{Eq. 2-31}$$

$$\dot{q}_{coll} = (c_1 - c_2 \cdot u)G'' - (c_3 + c_4 \cdot u) \cdot \Delta T_{in-amb} \qquad \text{Eq. 2-32}$$

α	*Solar absorptance for (short wavelengths <3*µm*) in* -
G''	*Net irradiance according to* Eq. 2-34 *in* W m^{-2}
u	*Wind speed in* m s^{-1}
$c_{1,2,3,4}$	*Collector performance coefficients*

Note that G'', Eq. 2-33, is the net irradiance derived from a radiation balance for a surface with the same optical properties as the collector but at ambient temperature. The additional long wave radiation losses for higher collector temperatures are taken into account as the linearised part of the collector heat loss coefficients, see [63].

$$\alpha G'' = \alpha G' + \epsilon L_{sky} + \epsilon \sigma T_{amb}^4 \qquad \text{Eq. 2-33}$$

L_{sky}	*Incoming long wave radiation of sky in* W m^{-2}
σ	*Stefan-Boltzmann constant 5.67 10^{-8}* W m^{-2} K^{-4}
ϵ	*Hemispheric emissivity (long wave >3µm) radiation in* –

The same steady state equation as presented in Eq. 2-32 is used for the measurement of collector performance under steady state conditions (EN 12975 [64] or ISO 9806 [65, p. 85]), see Eq. 2-34. Note that this equation is related to the average collector fluid temperature difference and not the inlet temperature.

$$Q_{coll} = A_{coll} \cdot G'' \cdot \left(\eta_0 \cdot (1 - u \cdot b_u) - \frac{\Delta T_{avg-amb}}{G''} \cdot (b_1 - b_2 \cdot u) \right) \qquad \text{Eq. 2-34}$$

$$\text{With } G'' = G' + \frac{\epsilon}{\alpha}\left(G_{lw} - \sigma \cdot T_{amb}^4\right)$$

η_0	*Conversion factor of collector in* -
b_u	*Loss coefficient of conversion factor* s m^{-1}
b_1	*Collector loss coefficient* W K^{-1} m^{-1}
b_2	*Collector loss coefficient* J K^{-1} m^{-3}

For this equation many measured performance data sets can be found for numerous collectors, see also Appendix A. An example for the performance is given in Figure 2-20 for a selective uncovered collector.

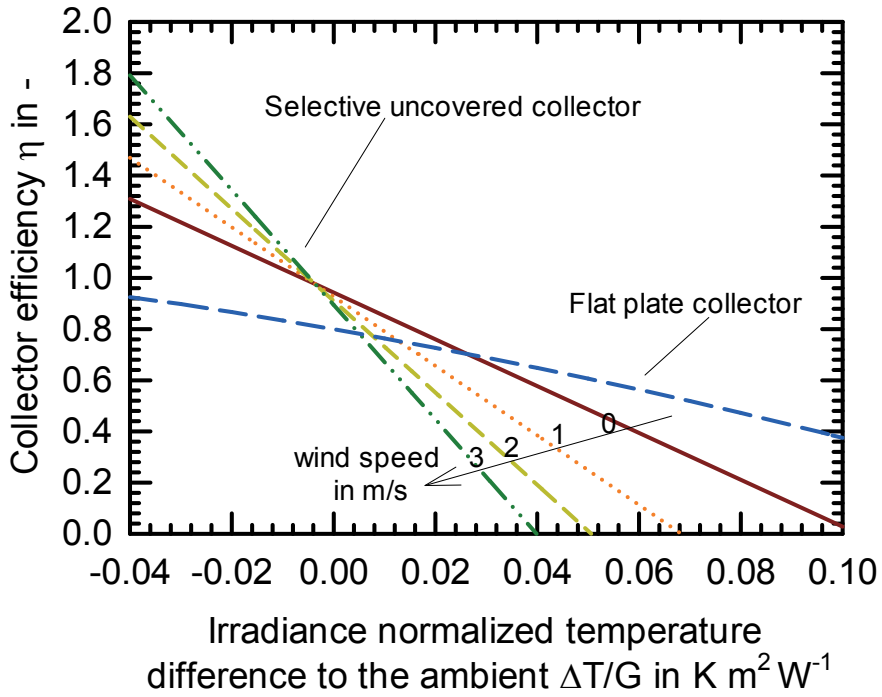

Figure 2-20 Comparison of collector efficiency curves for flat plate collector and selective uncovered collector. Note! The irradiance G for covered collectors is the total irradiance G´ and for the uncovered collectors the net irradiance G´´, see and Eq. 2-34.

In the dynamic simulations the uncovered collector is simulated with a more complex

model, type 203. It is also based on the steady state equation of Eq. 2-34, but further influences are included [66]: Incidence angle modifications, beam and diffuse irradiance, condensation yields, photovoltaic electricity production and capacity effects of the collector, Eq. 2-35.

$$\dot{Q}_{coll} + c_{eff}\frac{\delta T_{avg}}{\delta t} = \dot{Q}_{cond} + A_{coll} \cdot G''_{red} \cdot \left(\eta_0 \cdot (1 - u \cdot b_u) - \frac{\Delta T_{avg-amb}}{G''_{red}} \cdot (b_1 - b_2 \cdot u)\right)$$

Eq. 2-35

c_{eff} *Effective collector capacity in* kJ K^{-1}

$\frac{\delta T_{avg}}{\delta t}$ *Temperature – time derivative in K s^{-1}*

$\dot{Q}_{cond}$ *Usable collector heat flow rate from condensation in* W

G''_{red} *Reduced net irradiance in* W m^{-2} *see Appendix B*

The complete calculation description for the PV power, incidence angle modifier and condensation can be found in the Appendix B and in [66]. The most relevant information on the model is given in the following.

- Condensation of water from the air can appear at the collector surface if the collector operating conditions below the ambient air temperature. The water condensed provides an additional heat flow rate to the collector. This useful condensation heat gain is calculated with a model, from [67] and [68], that is successfully validated with an error of 10-20% of the overall performance or daily yields [69]–[71]. The simulation showed the condensation yield to be approx. 20 kWh/m² and 4% of the annual yield in combination with a ground heat exchanger, [72].
- Incident angle modifiers respect the lower collector performance at incident angle that are not perpendicular. Data measured on black polymeric collectors showed no significant incidence effect up to an angle of 50°[50, p. 39].
- The PV- power will reduce the available irradiance for thermal use and will be respected in case of a PVT- collector. The PV model applied is a performance model using data from standard test conditions, [73].
- Frost formation is not included in the model. Ice can increase the usable heat flow rate, but also diminishes the heat transfer from the absorbing surface of the collector to the fluid. Moreover, ice has a low absorptance of solar radiation. In any case, manufacturers and system owners are often sceptical about ice blocks developing on the roof as a potential source of injuries and accidents. As a result, the collector is not operated below outlet temperatures of 0°C in many real systems and also not in the simulations.

2.4 Figures for System Characterisation

Seasonal Performance Factor SPF

In most cases heat pump systems are assessed over the time frame of one year. Thus, Eq. 2-1 integrates the heat pump performance COP which defines the seasonal performance factor *SPF*, Eq. 2-36.

$$SPF = \int_{1\,year} COP\,dt = \int_{1\,year} \frac{Q}{P_{el}}\,dt \qquad \text{Eq. 2-36}$$

Depending on the context, seasonal performance factors are defined for different purposes, each with a different boundary. The seasonal performances used are defined in accordance with IEA SHC Task 44 / HPP Annex 38, see [74], [75]. The differences in the simulations of a conventional system without any solar assistance range from $SPF_{HPHS} = 4.12$ to $SPF_{SHP+} = 3.50$, Table 4-3.

$$SPF_{HPHS} = \int \frac{Q_{HP,H}}{P_{el,HP} + P_{el,SC,C} + P_{el,HS}}\,dt \qquad \text{Eq. 2-37}$$

$$SPF_{bSt} = \int \frac{Q_{HP,H} + Q_{SC,H}}{P_{el,HP} + P_{el,SC,C} + P_{el,HS} + P_{el,BU} + P_{el,CU}}\,dt \qquad \text{Eq. 2-38}$$

$$SPF_{SHP} = \int \frac{Q_{SH} + Q_{DHW}}{P_{el,total} - P_{el,DHW} - P_{el,SH}}\,dt \qquad \text{Eq. 2-39}$$

$$SPF_{SHP+} = \int \frac{Q_{SH} + Q_{DHW}}{P_{el,total}}\,dt \qquad \text{Eq. 2-40}$$

$Q_{HP,H}$	*Heat flow rate at heat pump condenser in* kW
$Q_{SC,H}$	*Heat flow rate from collector to hot storage in* kW
Q_{SH}	*Heat flow rate space heating demand in* kW
Q_{DHW}	*Heat flow rate for domestic hot water demand in* kW
$P_{el,HP}$	*Electric power consumption (p.c.) of heat pump in* kW
$P_{el,SC,C}$	*Electric p. c. of solar collector on HP source side only! in* kW
$P_{el,HS}$	*Electric p. c. of overall heat source in* kW
$P_{el,BU}$	*Electric p. c. of back-up / direct electric heat in* kW
$P_{el,CU}$	*Electric p. c. controller unit in* kW
$P_{el,total}$	*Electric p. c. of all electric units in the system*
$P_{el,DHW}$	*Electric p. c. for domestic hot water distribution in* kW
$P_{el,SH}$	*Electric p. c. for space heating distribution in* kW

In general, the seasonal performance factor is used that focuses on the sub-system in question. Most relevant for the end-user is SPF_{SHP+} because it takes into account the overall electricity consumption of the complete system. This is the electricity that must be paid for and this is used in most simulation analysis.

The seasonal performance factors SPF_{SHP} and SPF_{SHP+} include electrical penalties.

These penalties are defined to include simulation runs that do not quiet fulfil the given boundary settings, for example, the room temperature drops for some minutes below the given room temperature set-point. Such simulations are permitted for comparison but deviations are compensated for with the following penalties, Eq. 2-41 and Eq. 2-42.

$$P_{el,pen,SH} = UA_{bui}(\Delta T_{SH}(\Delta T_{SH} + 3)) \quad \text{Eq. 2-41}$$

$$P_{el,pen,DHW} = c_{p,H2O} \cdot \dot{m}\, \Delta T_{DHW} \cdot 1.5 \quad \text{Eq. 2-42}$$

$P_{el,pen,SH}$	*Electric penalty for space heating in* kW
UA_{bui}	*Heat loss value of building* kW K^{-1}, *(0.168* kW K^{-1} *simulation reference)*
ΔT_{SH}	*Temperature difference between room temperature and allowed lower room temperature in* K
$P_{el,pen,DHW}$	*Electric penalty for domestic hot water in* kW
$c_{p,H2O}$	*Heat capacity of water in* kJ kg^{-1} K^{-1}
$\dot{m}$	*Mass flow rate of tapped water in* kg h^{-1}
ΔT_{DHW}	*Temperature difference between tapped DHW temperature and the DHW set point temperature in* K

Energetic Weighted Quantities

For many investigations energetic weighted quantities supply very valuable information in a single number because they characterise a value not only over the time but with respect to a particular energetic quantity. For instance, the evaporator temperature of a heat pump has much more importance at high evaporator heat flow rates and furthermore should not be taken into account in periods of a heat pump standstill with no evaporator heat flow rate. This can be described by the weighting of the evaporator temperature with the evaporator heat flow rate. Eq. 2-43 gives an example for a temperature T(t) and an energetic quantity q(t). The weighted quantity T^* is given for continuous functions and discrete time steps.

$$T^* = \frac{\int q(t) \cdot T(t)\, \delta t}{\int q(t)\, \delta t} = \frac{\sum_i q(t_i) \cdot T(t_i)\, \Delta t}{\sum_i q(t_i)\, \Delta t} \quad \text{Eq. 2-43}$$

Specific ground heat exchanger length and collector area

The ground heat exchanger length is related to the heating demand for space heating Q_{SH} and domestic hot water Q_{DHW} to derive some specific and transferable results from the simulations. The specific ground heat exchanger length is defined as follows: $L' = \frac{L_{GHX}}{Q_{SH}+Q_{DHW}}$.

3 Combined Ground and Solar Heat Source

3.1 System Classification

Solar assisted heat pump systems can be classified in many ways. The three classical categories for systems are parallel, series and dual-source given by Duffie & Beckman [76, p. 127] or Freeman et. al. [62, p. 528]. This classic categorization of series, parallel and dual-source categorizes the system by the heat flow rate of the solar collector in relation to the heat pump's heat flow rate. The classification in this thesis uses the terms "hot side integration", and "cold side integration" instead.

The terms "hot side" and "cold side" integration relate to which side of the heat pump the solar heat is supplied. All system variations may include alternate heat sources, an alternate auxiliary heating, or thermal storage volume(s). Figure 3-1 displays a schematic overview of the categories. The terms "hot side integration" and "cold side integration" avoid confusion since many other components can be connected in series or in parallel in systems.

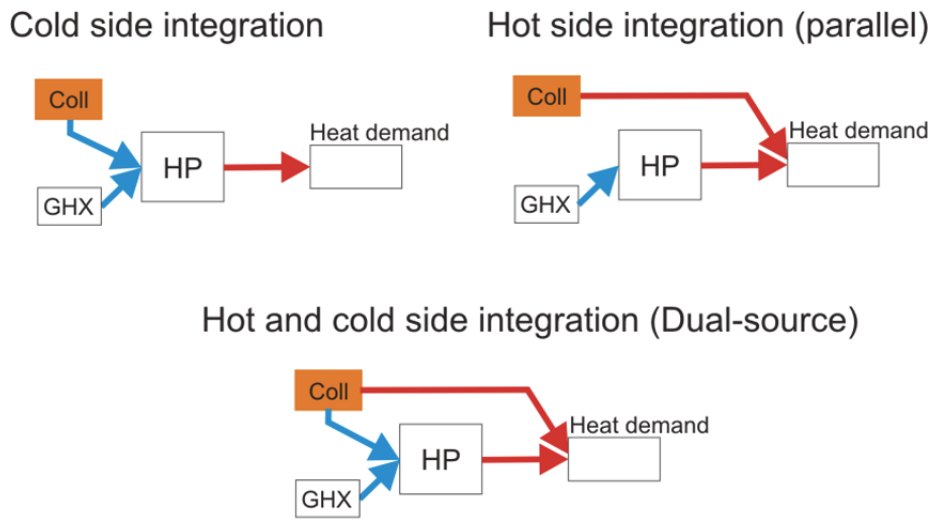

Figure 3-1 Categorization of solar heat pump systems: Cold side integration, hot side integration (parallel), hot and cold side integration (dual-source)

Note that the definition of hot side integration and dual- source are synonymic to the definition given by Duffie & Beckman [62, p. 528] and Freeman [77, p. 128]. The term cold side integration, however, is different compared to the classic definition of series systems. According to the definition of series systems the solar collector is the sole heat source for the heat pump and the solar collector can also provide heat directly to the heat demand. This results in a system similar to the hot and cold side integration (dual-source) but without alternate heat source for the heat pump. In this thesis, the

categorization cold side integration allows operating the solar collector and an alternative heat source, the vertical ground heat exchanger, on the heat pump's source side.

In addition, the systems are further categorized by their piping configuration on the hot side and cold side (Chapter 4.2 Hydronic System Description).

3.2 Literature Introduction

The following brief literature overview focuses on heat pump systems with vertical ground heat exchanger and uncovered solar collectors. There are broader reviews on solar assisted heat pump systems [43], [78]–[82]. The literature is divided into hot and cold side integration according to the system classification outlined in chapter 3.1.

Hot side integration of solar collectors, with over 50% market share [83, p. 82] in 2011/2012, is the most widespread combination of solar assisted heat pump systems. In essence, it is not different to conventional solar thermal systems with gas boilers or other auxiliary heaters, and the collector operates independently of the heat pump. The solar heat supplied replaces parts of the heat demand. A general calculation method for such heat pump systems is introduced by Anderson [84], see also [62, p. 691].

The most prominent simulation study is presented by Freeman, who simulated air source systems and identified hot side integration (parallel) as the best possible combination in 1979, [77]. Basically, this very general statement is still in line with recent simulation studies, [85]. Nonetheless, dual-source systems have the potential to outperform parallel systems, but this is usually linked to high effort and only small advantage, see e.g. [86], where ground source systems are compared to dual-source systems with ice storage.

While the majority of the presented investigations for solar hot side integration have been made for flat plate collectors, the calculation principles also apply to uncovered collectors.

Cold side integration systems are less elaborated in contrast to hot side integrated (parallel) ones. However, the combination of uncovered solar collectors and vertical ground heat exchangers is often investigated in this field of application.

Representative of early investigations is a Swedish study that reports a 2 K source temperature increase [87] cited in [43, p. 31], where a good overview is also given on further projects starting in the 70ties [43, pp. 29–40]. More recent simulations and

measurements report similar temperature improvements of 1.5 K in [43, p. 128] and 3 K in [88]. The observed performance improvement is moderate. Tepe, for example, finds a seasonal performance improvement of 0.3 [89]. Typically, higher improvements are reported only for undersized vertical ground heat exchangers [43, p. 99ff], [90, p. 806].

Another common but slightly converse finding is that solar regeneration leads to no electric savings or even additional consumption due to the pump electricity required [91][92, p. vi]. It is, therefore, often proposed to only use surplus solar energy for ground regeneration in dual-source systems. Many dual-source systems follow that principle. Typically, they perform nearly equal to hot side integration systems [93]–[95].

In summary, the collector cold side integration results in small improvements for the seasonal performance and source temperatures. This has been proven in several case studies. Field measurements also do not reveal any strong temperature increase.

In contrast to the seasonal performance, the borehole length is clearly influenced by the heat from the solar collector. The cold side integration allows shortening of the overall borehole length especially in the case of a larger borehole field correspondingly larger heat load. The systems are typically investigated by means of dynamic simulations in case studies. They appear in a variety of locations, system sizes, system concepts, reference system dimensioning and performance figures. As a result, a reasonable comparison is difficult, although it can be said that larger systems profit increasingly from solar regeneration. In other words, in larger systems the temperature drops down gradually and over-seasonally in systems without solar regeneration. Here, the vertical ground heat exchanger length can be reduced accordingly. The studies are discussed from smaller to higher heat demands in the following paragraphs.

Normally, the solar regeneration of vertical ground heat exchangers does not allow much ground heat exchanger length reduction. Swedish single family houses with 29 MWh/a heating demand do not show much potential of vertical ground heat exchanger reduction [43, p. 99]. Still, Lazzarin [94] proposes a vertical ground heat exchanger reduction from 200 m to 270 m due to solar regeneration. Here, the heating demand, which corresponds to Italian climate, is below 12 MWh a^{-1} and the calculations are made with EED.

The benefits of solar regeneration increase with raising heat load, which is shown for an example scaling from 12 MWh/a to 36 MWh/a [90]. In addition, solar regeneration allows the reduction of the possible distance between the boreholes from 6 m to 3 m.

Much larger systems of multi-family dwellings are simulated by Ménard. The system's annual heating demand ranges from 18 to 58 MWh a^{-1}. Uncovered collectors and vertical ground heat exchangers are found to be one of most cost effective solutions. Furthermore, the importance of regeneration is emphasised for compact vertical ground heat exchanger fields in urban areas [96, p. 26].

Even larger systems have been examined in combination with solar regeneration in North American climate. Chiasson simulates a school building with 16,000 m² building area, for which the vertical ground heat exchanger length could be reduced by 34% to 4050 m [97].

Another example of a large system [98] is highlighted. It clearly indicates the difference between larger and smaller fields, points out the possible reduction from 5920 m to 3783 m due to solar regeneration, and approaches the possible effects of solar energy by an analytical equation for the different effective thermal resistances from [44] (see also Eq. 2-18). In this study the time dependant resistances and heat flow rates in the ground are connected to particular possible heat flow rates of solar energy. The study, however, has the comparatively small focus of a 5 year time frame and does not extrapolate the findings to a principle understanding of solar energy and vertical ground heat exchangers.

Another example of an analytical calculation of the solar energy impact is given by Eskilson [20, p. 517]. For an example of summertime charging it is shown that the induced temperature change becomes negligible 3 to 6 six months later, in winter. Nonetheless, no discussion is made of the effects of solar energy that arise from the repetitive periodical solar recharging of the ground every summer.

To sum up, the hot side integration of a solar collector to a system is transferable from conventional solar assisted systems with boilers etc. The cold side integration of a collector shows a moderate or negligible improvement in the temperature for smaller systems. Larger systems in contrast reveal considerable potential for vertical ground heat exchanger shortening at equal performance. The separation of different influences of solar energy together with theoretical understanding is the key for a systematic assessment of solar ground regeneration.

3.3 Temperature Potential of Combined Heat Sources

3.3.1 Temperature Potential for a Heat Source

The heat pump efficiency depends on its heat source temperature T_{cold}, heat sink temperatures T_{hot} and its heat pump or exergetic efficiency ε_{HP} (Eq. 2-1). The heat sink temperature T_{hot} and the heat pump efficiency ε_{HP} are independent of the heat source. Consequently, the potential of a heat source can be assessed by a maximum possible heat source temperature T_{cold}.

The aim of defining such a maximum temperature T_{cold} is to provide a theoretical limit for single and combined heat sources that allows

1. The comparison of the potential of different heat sources
2. The assessment of current simulation and measurements results in the context of the possible limits
3. Application in simple spread sheet calculations (no dynamic simulations).

With this objective a theoretical temperature limit is defined using the following assumptions

1. Infinite size of components
2. No temperature losses due to the heat demand of the cold heat source and no change through thermal resistances within a component
3. No temperature dependant effects or limitations for the operation of the heat source such as freezing or air humidity

The theoretical maximum temperature on the cold side of the heat pump is calculated accordingly from steady state black box performance models of the components.

This approach is different to the typical assessment of solar collector heat sources. Normally, they are evaluated for a constant operating temperature by their yield [62, p. 672], [99] or so called energy potential [100] because they provide energy to the hot side of the heat pump. The energy yield is calculated using simulations or spread sheet calculation methods for a constant inlet temperature. This method is practical in the designing process, but does not allow the determination of a heat source's theoretical temperature limit. Moreover, the temperature shift is the essential aim of the solar assistance on the cold evaporator side.

The maximum source temperature description does not include any heat flow rates and accordingly no entropy or exergetic examination. Nonetheless, knowing this maximum

source temperature enables the calculation of the reversible heat pump efficiency. This would derive from Eq. 2-1 with an exergetic efficiency ε_{HP} of 1 and a known hot side temperature T_{Hot}. The following examination, however, is restricted to the maximum source temperature.

3.3.2 Maximum Temperature of Ground and Uncovered Solar Collector

In principle, a maximum heat source temperature can be defined for any natural heat source. The stagnation temperature is the maximum possible temperature at a time t for the uncovered collector $T_{x,UC}(t)$. The stagnation temperature $T_{coll,stag}$ results for $\eta = 0$ from the steady state for uncovered collectors Eq. 2-34

$$T_{x,UC}(\mathrm{t}) = T_{coll,stag} = \frac{\eta_0 \cdot (1 - b_u \cdot u)}{b_1 + b_2 \cdot u} G'' + T_{amb} \qquad \text{Eq. 3-1}$$

It is restated that the wind speed u relates to the wind speed above the collector. In all calculations presented here the wind speed from the weather data is therefore reduced by a factor of 0.5[1]. This wind factor is the same as used in the simulation framework [101, p. 6]. Therefore, the theoretical temperature potential calculated can be compared with the simulation results from the following chapters.

The maximum temperature of the vertical ground heat exchanger $T_{x,GHX}(t)$ at a time t is calculated using Eq. 2-9.

$$T_{x,GHX}(t) = T_{g,undis} - q \cdot \left(\frac{1}{2 \cdot \pi \cdot \lambda} \cdot g \left(\frac{t}{t_s}, \frac{r_{GHX}}{H} \right) \right) \qquad \text{Eq. 3-2}$$

For an infinite vertical ground heat exchanger the specific heat flow rate q is 0. This reveals a weakness of the concept since no seasonal storage effects can be included. Accordingly, Eq. 3-2 simplifies to Eq. 3-3

$$T_{x,GHX}(t) = T_{g,undis} \qquad \text{Eq. 3-3}$$

Generally speaking all other heat sources can be similarly calculated: covered collectors, horizontal ground collectors, air or water. The maximum temperature derives assuming an infinite size for the heat sources.

The maximum theoretical possible temperature $T_{x,t}$ is then defined in Eq. 3-4 as the

[1] Meteorological wind speed is measured at a height of 10 m above ground. The surface or collector near wind speed is therefore much slower.

maximum temperature of two heat sources, a hybrid system, at the time *t*. For the two heat sources, source 1 and source 2, this temperature is easily determined using the temperatures from steady state equations, here Eq. 3-1 and Eq. 3-3:

$$T_x(t) = \max\left(T_{x,source1}(t), T_{x,source2}(t)\right) = \max\left(T_{x,GHX}(t), T_{x,\mathrm{UC}}(t)\right) \qquad \text{Eq. 3-4}$$

An example of this temperature $T_{x,t}$ in the course of the day is displayed in Figure 3-4.

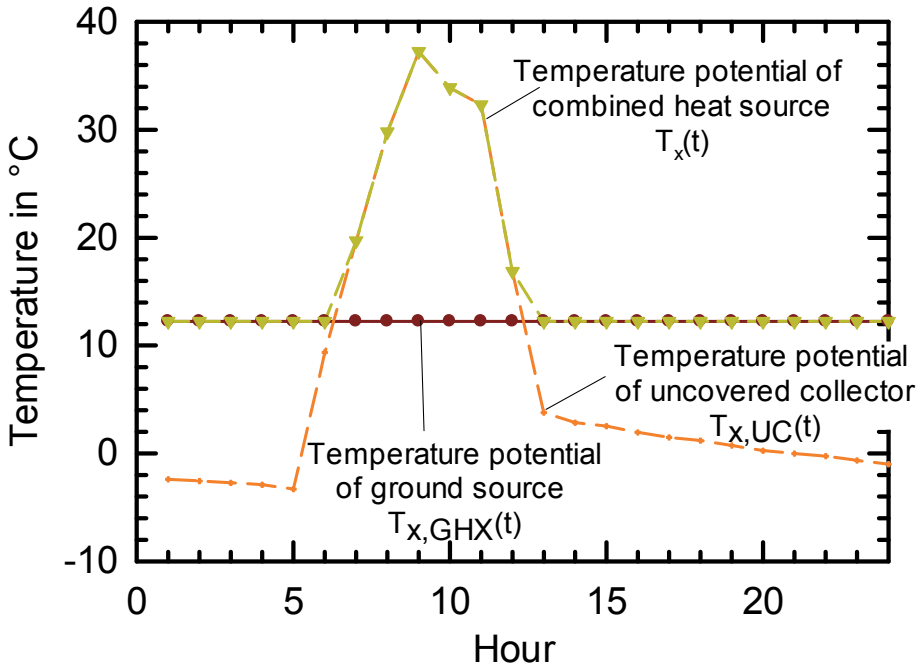

Figure 3-2 One day example of the temperature potential. The single heat sources: ground $T_{x,GHX}(t)$ and uncovered collector $T_{x,\mathrm{UC}}(t)$ and the combination of both sources $T_x(t)$

More relevant for the system assessment is not the instantaneous temperature $T_x(t)$, but a representative value T_x for a longer period– a year or a month. This temperature is defined using a heating demand function $\dot{q}(t)$ as a weighting quantity:

$$T_x = \frac{\int \max\left(T_{x,source1}(t), T_{x,source2}(t)\right) \cdot \dot{q}(t)\, dt}{\int \dot{q}(t)\, dt} \qquad \text{Eq. 3-5}$$

For an approximate constant heating demand, e.g. the domestic hot water, this equation simplifies to:

$$T_x = \overline{\max\left(T_{x,source1}(t), T_{x,source2}(t)\right)} \qquad \text{Eq. 3-6}$$
$$= \frac{\int \max\left(T_{x,source1}(t), T_{x,source2}(t)\right)\, dt}{t}$$

Any function or load pattern of the heating demand can be applied. For instance T_x can be calculated assuming a simplified space heat demand $\dot{q}(t)$ according to Eq. 3-7. In

this case the space heating demand is proportional to the temperature difference $\Delta T(t)$ between ambient air temperature $T_{amb(t)}$ and a constant room temperature T_{room}. Additionally, the space heating is taken into account only, if the average ambient temperatures of the last day T_{amb24} drops below $T_{SH,threshold}$, Eq. 3-8.

$$\dot{q}(t) = \dot{q}_{max} \cdot \frac{\Delta T(t)}{\Delta T_{max}} \quad \text{Eq. 3-7}$$

$$T_x = \frac{\int T_x(t) \cdot \Delta T(t) \cdot \Theta\left(T_{amb} - T_{SH,threshold}\right) dt}{\int \Delta T(t) \cdot \Theta\left(T_{amb} - T_{SH,threshold}\right) dt} \quad \text{Eq. 3-8}$$

With Θ as Heaviside- function, $\Theta \begin{cases} 0 : T_{amb24} - T_{SH,threshold} > 1 \\ 1 : T_{amb24} - T_{SH,threshold} \leq 0 \end{cases}$

In fact, solar radiation is in most cases not provided the whole day. Higher stagnation temperatures, therefore, occur during the day while at night the lowest ambient temperature and, with it, the highest heat demand occurs. It is accordingly advantageous to use a thermal storage capacity that makes beneficial conditions accessible over an extended time period.

Such a storage concept is also applied to the maximum source temperature. The concept of a temperature storage capacity is unusual, since in reality heat, not a temperature, is stored at a temperature level.

Nevertheless, a simple storage model for an ideal temperature storage is introduced. This temperature store is of finite size but has no thermal losses and is also applicable on a spread sheet basis. It allows the examination the storage size effects on the ideal temperature T_x.

This thermal storage capacity supplies its stored temperature over a period τ. Accordingly, at a time step t_s the store allows the use of temperatures from earlier time steps $t - \tau$ or with help of Eq. 3-4 the maximum temperature $T_{x,stor}(t)$ is calculated as

$$T_{x,stor}(t) = \max_{t_s \rightarrow (t_s - \tau)} \left(T_{x,source1}(t), T_{x,source2}(t)\right) \quad \text{Eq. 3-9}$$

The period τ depends on the storage size and the heat demand. This period τ represents the time, in which the amount of heat was taken from the storage by a fluctuating heat flow rate $\dot{q}(t)$ equivalent to the storage size $Q_{storage}$. In other words, integrating this heat flow rate over the period τ discloses exactly the thermal storage capacity. This correlation is expressed as

$$Q_{storage} = \int_{t_s - \tau}^{t_s} \dot{q}(t) dt \quad \text{Eq. 3-10}$$

Furthermore, $Q_{storage}$ is defined using a maximum heating rate $\dot{q}_{max}$ and the period τ_{size}, over which the storage can provide this maximum heating rate. Accordingly, the heat flow rate $\dot{q}(t)$ is smaller or equal than $\dot{q}_{max}$.

$$0 = \tau_{size} \cdot \dot{q}_{max} - \int_{t_s-\tau}^{t_s} \dot{q}(t)dt \qquad \text{Eq. 3-11}$$

The period τ is variable and must be calculated for every time step t_s in the course of the year. τ can be determined numerically at any time step t_s from a load pattern or function, according to Eq. 3-12. The principle of the iteration method is illustrated in Figure 3-3.

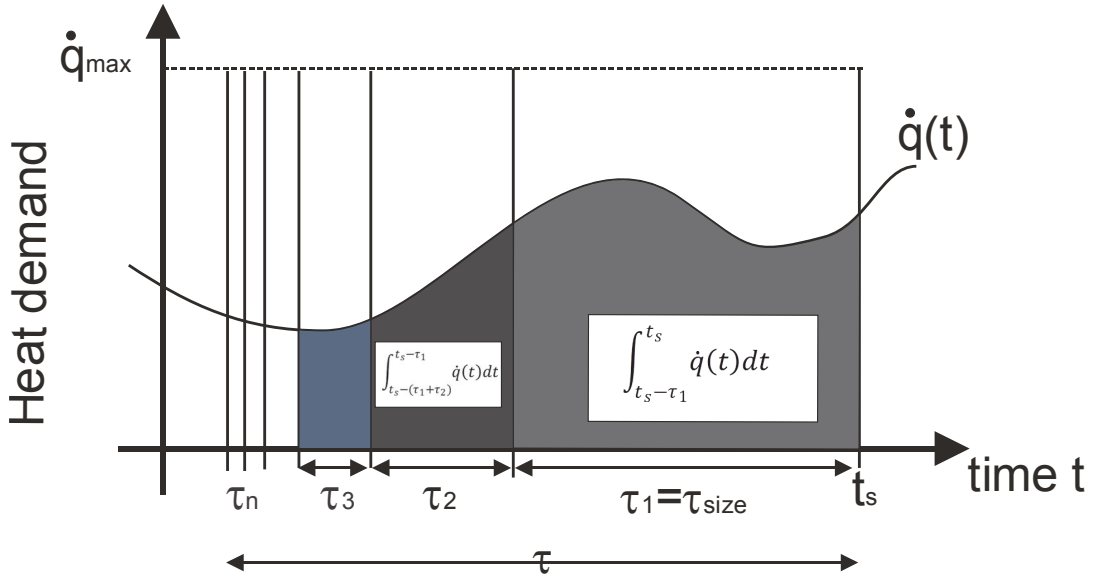

Figure 3-3 Illustration of iteration principle given in Eq. 3-12 for determination of τ

Basically, the period τ is calculated by stepwise integration of $\dot{q}(t)$ until there is no remaining heat capacity in the storage. The size of the next integration step is calculated from the maximum possible heat flow rate and the remaining heat capacity in the storage of the last integration step.

$$\tau = \tau_1 + \left(1 - \frac{\int_{t_s-\tau_1}^{t_s} \dot{q}(t)dt}{\tau_1 \cdot \dot{q}_{max}}\right) \cdot \tau_1 + \left(1 - \frac{\int_{t_s-(\tau_1+\tau_2)}^{t_s-\tau_1} \dot{q}(t)dt}{\tau_2 \cdot \dot{q}_{max}}\right) \cdot \tau_2 + \cdots \qquad \text{Eq. 3-12}$$

$$= \tau_1 + \tau_2 + \tau_3 + \cdots$$

$$with \quad t_1 = \tau_{size}$$

A lower limit for τ_n has to be set as a stop criterion for the iteration process, which should be in the range of the data time steps provided. For all results from spread sheet

calculations 5 iterations steps have been used *(t_1-t_5)* and the iteration is stopped for periods τ smaller than the time step of one hour.

Two heat demands are discussed: a constant heat demand and a space heating demand corresponding to the ambient air temperature Eq. 3-7.

Eq. 3-12 simplifies immensely for a constant heat demand heat demand $\dot{q}(t) = const.$ Correspondingly, Eq. 3-9 can be written as

$$T_{x,stor}(t) = \max_{t_s \rightarrow (t_s - \tau_{size})} (T_{x,source1}(t), T_{x,source2}(t)) \qquad \text{Eq. 3-13}$$

For space heating calculations Eq. 3-7 is used, which simplifies Eq. 3-12 to an expression with temperature differences instead of heat flow rates. The weighting can be done according to Eq. 3-8 and an example for the varying heating demand is given in Figure 3-4.

Finally, it is pointed out that temperature store may be located either on the hot or on the cold side of the heat pump as long as the heat flow rate $\dot{q}_{use}(t)$ and the storage size $Q_{storage}$ are located at the same side of the heat pump. In other words, the period, over which the heat pump benefits from the temperature conditions on its source side, may not necessarily lead to a system with cold storage. An alternative option is a shift of the heat load demand with a hot store. At beneficial temperature conditions on the cold side the heat pump can be operated and the heat stored on the hot side and subsequently consumed.

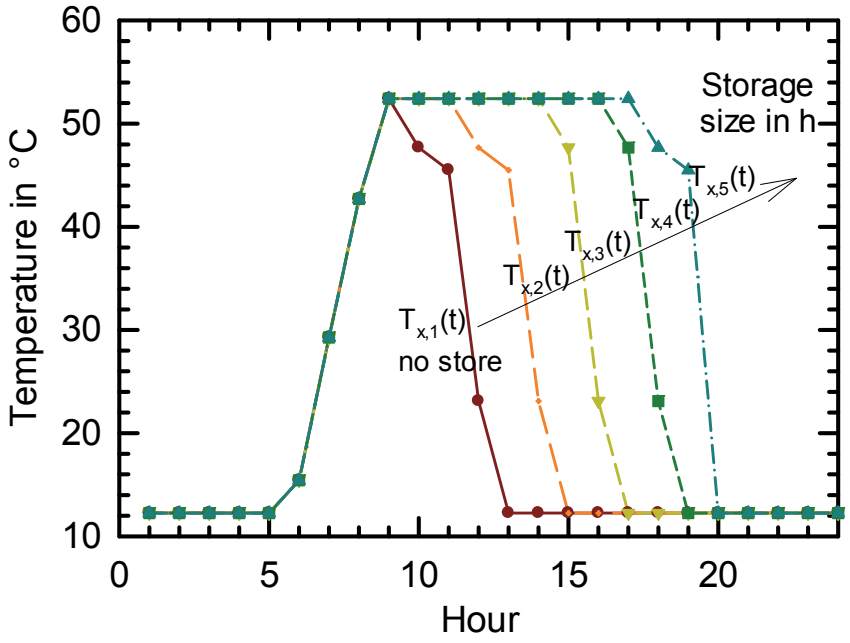

Figure 3-4 The temperature potential in the course of the day for different storage sizes from 1 to 5 hours. The heating demand q(t) is lower than the maximum heating demand. The storage capacity lasts longer than its defined size, the time τ_{size}.

3.3.3 Temperature Potential T_x for Strasbourg (tm2 Data)

The temperature potential introduced is calculated for the weather data of Strasbourg [102], [103] (central European climate) as an example. For this thesis Strasbourg is of special relevance because it is used for all simulations with the dynamic system model, see chapters 4. All results presented in the following section are calculated for a combination of an uncovered black polymer collector (performance data Table A-1) and a vertical ground heat exchanger of 100 m depth.

The temperature potential is presented in Figure 3-5 to illustrate the basic character for the mono heat sources $T_{(x,GHX)}$ and $T_{(x,UC)}$ as well as hybrid heat sources at a constant heat load according to Eq. 3-6. The values are average monthly values. Additionally, the hybrid heat source is presented for space heat demand weighted values $T_{(x,GHX+UC)-\boldsymbol{SH}}$ according to Eq. 3-8.

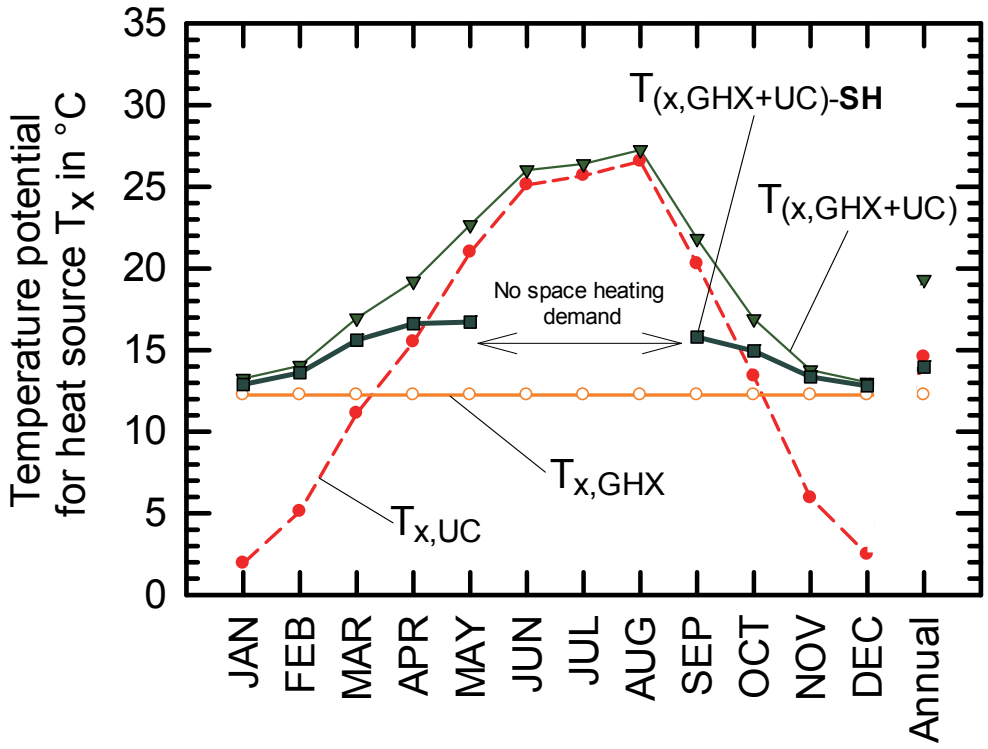

Figure 3-5 The temperature potential T_x for different heat sources and energy demands. Constant heat demand: $T_{x,GHX}$ for the vertical ground heat exchanger, $T_{x,UC}$ uncovered black polymer collector and $T_{(x,GHX+UC)}$ the combination of both. Varying heat demand $T_{(x,GHX+UC)-\boldsymbol{SH}}$ for the combined heat source

Annual values for the combined temperature potential increase significantly from 12.3°C to 19.3°C for a constant heat demand and in comparison to the ground source. In contrast, this improvement drops 7.0 K to 1.7 K, if related to the to the space heating demand.

The outcome for the temperature potential in the course of the year is disappointing

considering that T_x represents the potential for components of infinite size. In winter in particular the temperature increase is small for both demands investigated. In summer better improvements are achieved of up to 15 K by combination with the collector. Nevertheless, in spring and autumn the temperature is improved. From March to May a 4 K increase is achieved, while in autumn September and October the increase is 3 K. In the context of the application to buildings the space heating related $T_{(x,GHX+UC)-\boldsymbol{SH}}$ seems to be the appropriate figure, here 14°C. The potential $T_{(x,GHX)}$ is 12.3°C for vertical ground heat exchanger as sole source.

The potential can be increased with an additional thermal storage capacity, Figure 3-6. In winter the improvement is still negligible for small storages up to 4 h. The storage effect is, however, visible. Starting from 12.9°C without any store the annual temperature potential T_x raises to 14.0°C for a store that holds the capacity of 3 h of the maximum demand. A larger capacity of 12 h leads to a further increase up to 25°C and a considerable temperature increase of approx. 6 K even in winter.

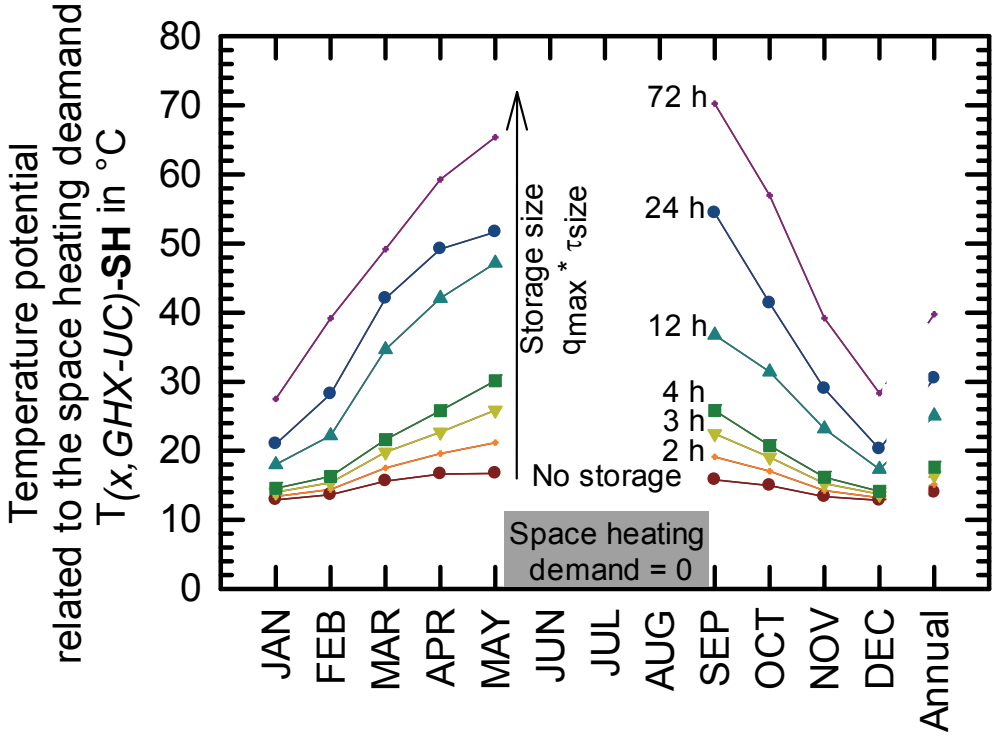

Figure 3-6 Temperature potential of the combined heat source $T_{(x,GHX,UC)-SH}$ for vertical ground heat exchanger and uncovered black polymer collector. The short-term storage capacity is varied. The values have been weighted to the space heating demand.

The results indicate that significant storage capacities will be necessary, if significant temperature increase is the goal. This correlation is certainly restricted to the combination of an uncovered collector and a vertical ground heat exchanger and other

combinations of heat sources, e.g. air or covered collectors, might come to different results.

Reducing the storage size to a time period τ is a useful but simplistic approach. The method lacks a clear transferability to real storage volumes. Each stored temperature maximum can be used only once and a gradual temperature decrease due to demand is not accounted for.

Nonetheless, the calculations give helpful orientation and reveal that larger storage sizes of 12 h are attractive. The size of 12 h is interpreted as large enough to store temperatures in winter during daytime and supply them until next morning while the store is continuously discharged. The heat pump measured (chapter 2.1.2) has an evaporator mass flow rate of 1900 kg h^{-1} for the 7.8 kW heat pump and a fluid density of 1048 kg m^{-3}. This results in a specific volume flow rate of roughly 250 l h^{-1} kW^{-1}. Accordingly, a storage size of 12 h would lead to 3 m^3 kW^{-1} or 15 m³ storage volume for a 5 kW heat pump. In the context of practical applications such large storages volumes seem unrealistic.

The overall heating demand in a building is usually a mix of a constant load for domestic hot water Q_{DHW} and a fluctuating space heating load Q_{SH}. The temperature potential $T_{(x,GHX+UC)}$ for a constant heat demand overestimates the possible temperature potential for domestic applications because it benefits from good conditions in summer, whereas the space heating related value $T_{(x,GHX+UC)-\boldsymbol{SH}}$ slightly underestimates the temperature potential of most applications since the space heating demand dominates in most systems. To conclude, in applications with seasonal and constant heat demand the temperature should be derived from both temperatures and heat demands. T_x can then be calculated as:

$$T_x = \frac{T_{(x,GHX+UC)} \cdot Q_{DHW} + T_{(x,GHX+UC)-\boldsymbol{SH}} \cdot Q_{SH}}{Q_{DHW} + Q_{SH}} \qquad \text{Eq. 3-14}$$

3.3.4 Six Locations in Europe

The weather conditions of a location determine the temperature potential T_x. Six different locations are investigated for a set of collector parameters. Moreover, the temperature lift T^*_{x-GHX} is defined according to Eq. 3-15 for easier comparison, because the ground temperature $T_{g,undis}$ also changes as a function of the location. This temperature lift is calculated for different storage sizes at six locations in Europe representing typical climates. For these calculations, the collector is orientated south

with a slope of 45° and the vertical ground heat exchanger is assumed to be 100 m. The results presented are determined for the space heating demand (compare Eq. 3-8).

$$\Delta T^*_{x-GHX} = T_x - T_{g,undis} \qquad \textit{with } T_x \textit{ according to Eq. 3-10} \qquad \text{Eq. 3-15}$$

At all six locations the temperature potential shift ΔT^*_{x-GHX} is moderate without thermal storage capacity, Figure 3-7.

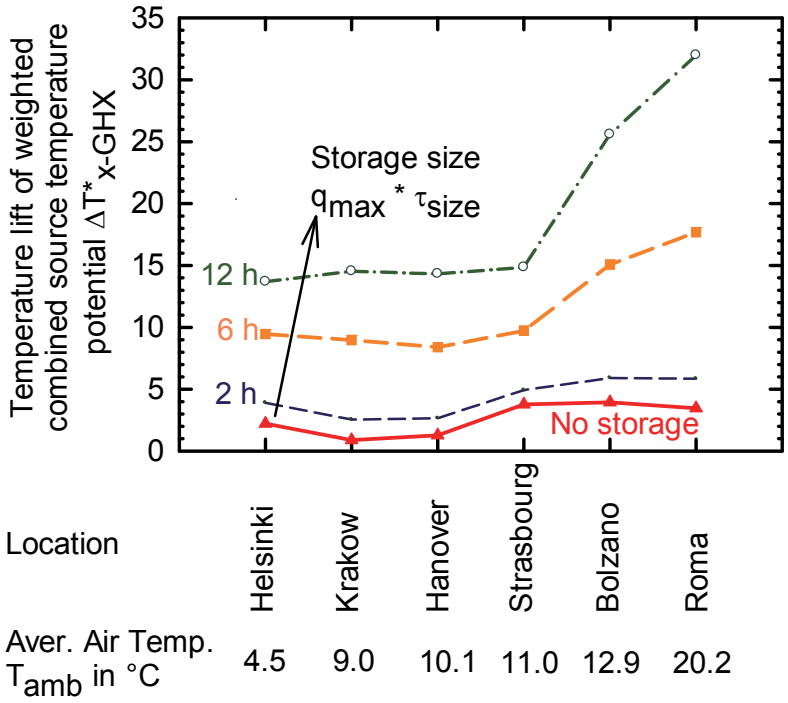

Figure 3-7 Temperature lift T^*_{x-GHX} of combined heat source compared to vertical ground heat exchanger temperature for six locations in Europe and related to space heating demand. The combined source is an uncovered black polymer collector 45° sloped and orientated south and a vertical ground heat exchanger of 100 m depth. The temperature is weighted with the space heating demand Q_{SH} ($\dot{Q}_{SH}$ = max @ T_{amb} = -10°C; $\dot{Q}_{SH}$ = 0 @ T_{amb} = +12°C).

For all locations the benefit is under 4 K. Furthermore, the impact has a clear dependency on the location, but no obvious trend is evident. The benefits of the combined source are dramatically increased for all locations, if a thermal storage capacity is included. A temperature storage of 12 h leads to a potential increase of at least 15 K, which is particular surprising in the case of Helsinki with hard winter conditions at a latitude of 60° north. Moreover, in particular Bolzano and Rome show huge potential with 26 K and 32 K temperature lift, although Rome has a small absolute space heating demand. A smaller storage size of 2 h has barely any effect on the temperature potential.

It should be kept in mind that the calculated temperature lift must be regarded in context of the parameter settings and heat load distribution applied. The values will differ

significantly, if weighted to space heating or a constant load, as pointed out in chapter 3.3.3. Higher temperature lifts would likewise be obtained for different load profiles with shares of constant loads or even summer heat loads.

Nonetheless, the results allow fast and useful orientation for the limits and benefits of a combined or hybrid heat source.

3.3.5 Different Collectors Types

The temperature potential also depends on the collector performance parameters applied since these parameters determine the stagnation temperature calculated.

The temperature potentials presented above are determined for a black polymer collector. Other collectors have different performances data sets, see Appendix A, which lead to other stagnation temperatures, Figure 2-18. The used irradiance in collector panes is reduced by 18% for the PVT- collectors, because the electricity leads to lower availability of solar radiation to be transformed into heat.

The results given in Figure 3-8 disclose significant differences between the collectors. In the following discussion keep two things in mind. Firstly, the baseline for the temperature potential is 12.3°C which represents the sole ground heat exchanger. Secondly, the collector performances given try to be representative but are not absolute. There will be PVT- collectors with higher stagnation temperatures as well as lower performing selective uncovered collectors. The results are discussed in three groups of collectors.

The first group, the PVT- collector, has the lowest stagnation temperature and also the lowest temperature potential. Without a storage capacity the increase of the temperature potential is below 1 K. With a storage capacity of 12 h it still stays below 20°C or 7 K increase.

The second group of metal roof and black polymer collectors shows a significantly higher potential. A yearly temperature potential of 14°C is reached without storage and 25°C with storage capacity of 12 h.

The third and best group, the selective metal absorber, reaches a temperature potential of 15°C without and 32°C with storage capacity. It is emphasised that the order and relations between the different collector types are constant for all investigated values, monthly, annual, with and without storage capacity.

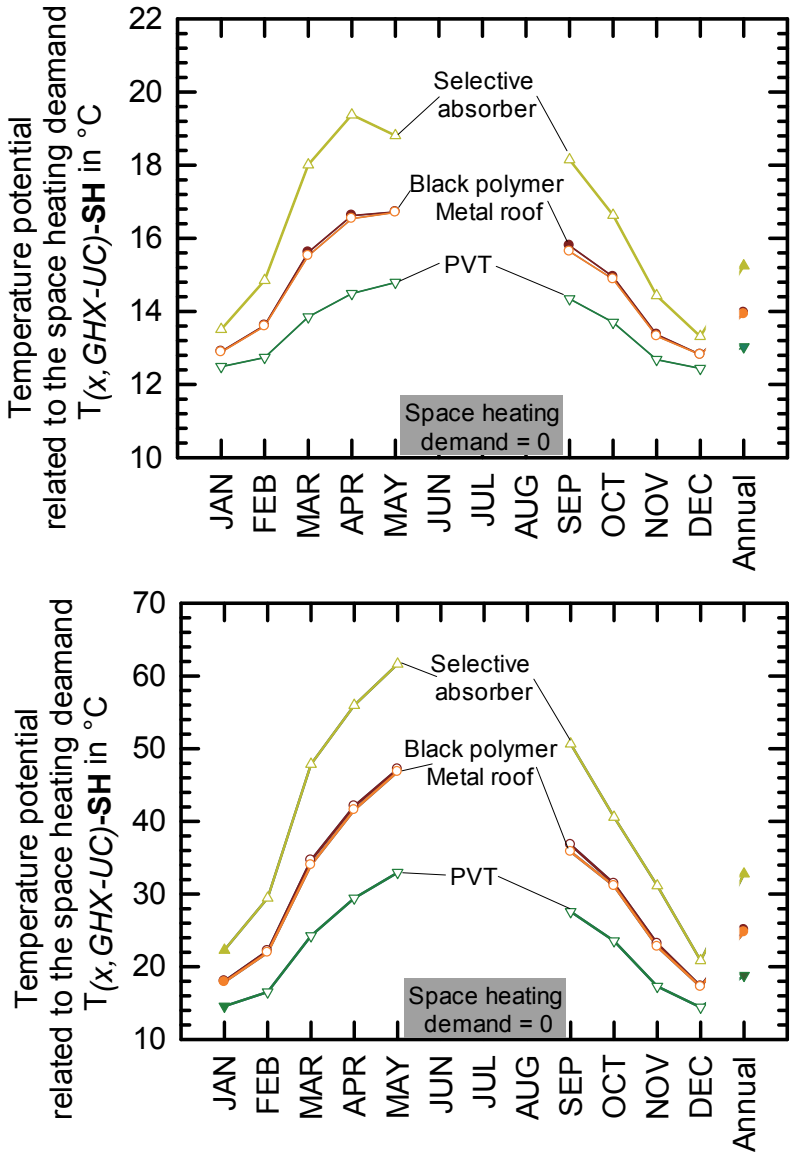

Figure 3-8 The monthly space heating weighted temperature potential in the course of the year for T_x^* in Strasbourg for different collector parameter sets. (Top) without storage, (bottom) with 12 h storage

To sum up, the collector parameters have a strong impact on the temperature potential especially when combined with storage capacities. For the examples presented the potential temperature lift could be nearly doubled with selective absorbers. On the other hand, inappropriate collectors, here the PVT-collector, show negligible potential even with an additional thermal storage capacity.

The agreement of the collector types for metal roof and black polymer collector is not intended. Of course, the given performance characteristics are examples and the collector performances of a particular collector can lead to different results. In other words changing the collector design, optical properties or thermal losses, affects the stagnation temperature and correspondingly its temperature potential.

This does, however, reveal the strong focus of the method on the collector stagnation temperature. Collector performances may differ significantly despite their nearly identical stagnation temperatures, see Figure 2-18. The method presented characterises the collector performance by only one parameter. Nonetheless, this parameter, the stagnation temperature, is determined by the parameters that define the whole range of the collector performance: the optical properties, the heat removal factor, and the collector heat losses.

3.3.6 Discussion

The presented temperature potential T_x provides a helpful method to assess the theoretical limits of combined heat source with moderate effort. For further discussion some simulation results are included. The energy weighted temperature potential (Eq. 3-14) is compared to simulation results, Figure 4-2 and Table 3-1.

As expected the simulation's finite components achieve lower temperatures as in the calculation of a theoretical potential presented. The calculated temperature lift ΔT^*_{x-GHX} is roughly in the same range for simulated and theoretical infinite components.

Table 3-1: Theoretical temperature potential and simulated source temperatures for different system concepts in Strasbourg and a vertical ground heat exchanger length of 110 m

Collector type	Setting		Simulation		Theoretical potential	
	Coll. Area	Cold storage volume	Source temperature[1]	Temperature lift	Temperature potential	Temperature lift
	in m²	in m³	in °C	in K	in °C	in K
No Coll.	0	0	6.0		12.4	
Swimming pool	10	0	8.0	2.0	14.7	2.3
Swimming pool	30	0	9.0	2.9	14.7	2.3
Swimming pool	15	1	8.8	3.8	16.8	4.4
Selective	10	0	8.2	2.2	16.7	4.4

The simulated temperatures are 6-8 K lower than the calculated temperature potential. This implies that the potential for improvements with the solar collectors is small, especially since the components have finite size and internal thermal resistances. Even without solar collector assistance high source temperatures are achieved, which is

[1] The corresponding simulation output is the energy weighted average evaporator temperature plus a constant temperature off-set of 2 K respecting the temperature spread at the evaporator.

perfectly in accordance with measured values in the field of 7,1°C [24, p. 94]. It is, in short, very difficult for the uncovered collector to improve the high heat source temperatures especially in winter when the heating demand is high.

The possible improvements with an additional cold storage capacity are not yet broadly evaluated, but show a clear potential here. The simulations conducted, however, include storage volumes only up to 1 m³. The corresponding theoretical value is calculated for 2 h. From today's perspective, large storages volumes of 10 m³ or 30 m³ do not seem justifiable with the efficiency obtained.

Nonetheless, the temperature potential formulated does not include over-seasonal temperature effects. In any case, other reasons than a high temperature potential, such as the shortening of the vertical ground heat exchanger for example, might make the combination with the uncovered collector an attractive goal. Additionally, the lower operating source temperatures of real components will also increase the impact of the solar collector support.

4 System Model

4.1 Simulation Setup and Reference Conditions

4.1.1 Reference Framework

The dynamic simulation of systems is a powerful scientific method to investigate system concepts and components in the course of one or several years. The system simulations are “numerical experiments” [62, p. 448] that are used for validating, developing or planning. The order of the model details depends on the purpose of the investigation. In the context of this thesis a high resolution model is developed to investigate and classify detailed component parameters by a sensitivity analysis. Additionally, transient effects are included that are relevant for 1 minute time steps. The system model, therefore, comprises the dynamic and transient modelling of the complete heat pump’s heat source and sink side, domestic hot water preparation, the space heating distribution system and the building.

The system model’s description and its implementation as well as the most important boundary conditions are presented in the following subsections. The general concept of the applied sub-models and boundary conditions is given in Figure 4-1.

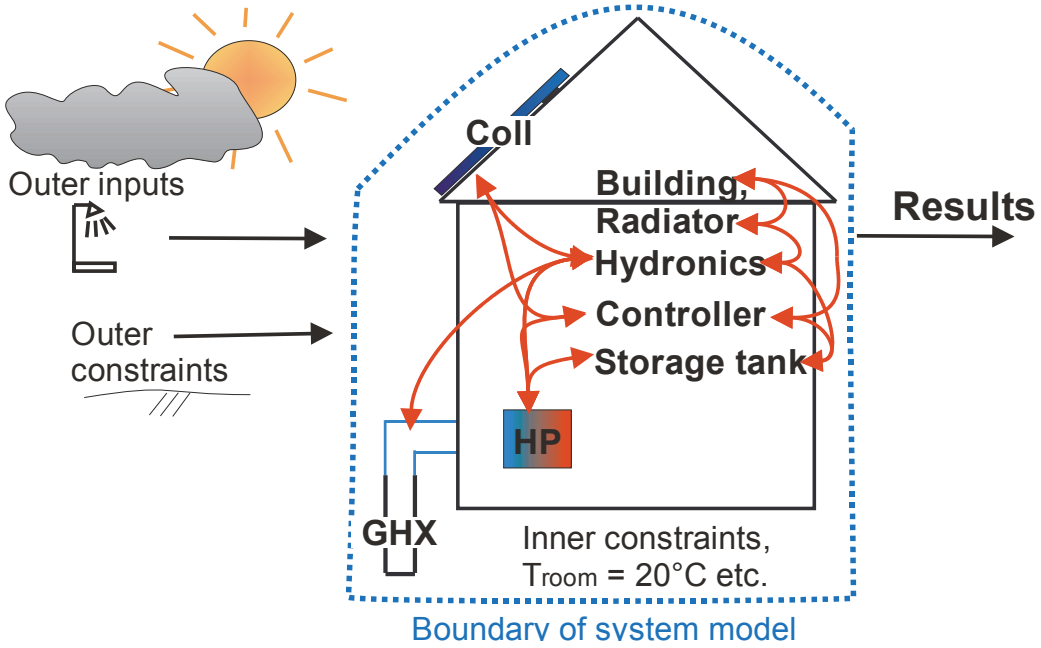

Figure 4-1: Overview of the system model with sub models, inner and outer boundary conditions

The system model is divided into sub-models. The sub-models for the solar collector, the vertical ground heat exchanger and the heat pump were introduced in chapter 2. Details are given in chapter 4.2 for the hydronic system, controllers and storage tank.

In principle, the setting up of a system model is extensive. In many cases the climate, heat distribution system or heating loads and the model choice itself influence the results. The results from one boundary set allow only rudimentary comparison to another set. These differences often appear even in the same development line of one single system model.

For this reason, a common simulation framework is used in this thesis to ensure the reproducibility and the comparability of the simulation results generated and presented. The applied boundary condition set is taken from IEA SHC Task44 / HPP Annex 38 [104] “Solar and heat pumps systems”.

The essential reference conditions are presented in Table 4-1. The complete description of the reference conditions is given in [101] and [103], e.g. the building model details such as walls, windows, ventilation, shading, internal loads etc.. The accordance of the developed system model of this thesis to the setting and applied modifications are documented as part of the work in IEA SHC Task44 / HPP Annex 38 [105, pp. 15–21]. The verification of the correct implementation and residual deviations are presented in chapter 4.1.2 Reference Data Check.

Table 4-1: Parameter settings overview for the main components in the system model. A similar version of this table was also used for system model description in [106].

Parameter	Reference value
Weather data	Average year in Strasbourg, France [102] tm2
Thermal load	
Heating demand building	Floor heating: 6.5 MWh / 140 m² = 46.6 kWh/m²a
Heating demand DHW	2075 kWh/a
Volume DHW storage	150 l (with solar DHW 300 l)
Heat pump	Extended parameters according to EN 14511-3
Heating capacity	7.9 kW (35°C heat source / 0°C heat sink)
COP	4.8 (35°C heat source / 0°C heat sink)
Vertical ground heat exchanger	
Ground properties	2 W m^{-1} K^{-1}; 2500 kg m^{-3}, 0.8 kJ kg^{-1} K^{-1}
Type of GHX	Double U pipe, outer pipe diameter 32 mm
Borehole resistance	0.08 K m W^{-1}
Solar thermal collector	Parameters according to EN 12975-2
Uncovered collector	Black polymer absorber according to table in Appendix A
Orientation	South, slope 45°

The system model represents a well-insulated single family building with a floor heating system. Two hydronic system concepts simulated are presented to illustrate the basic energy flow in the reference system. Figure 4-2 contains a Sankey-diagram for both.

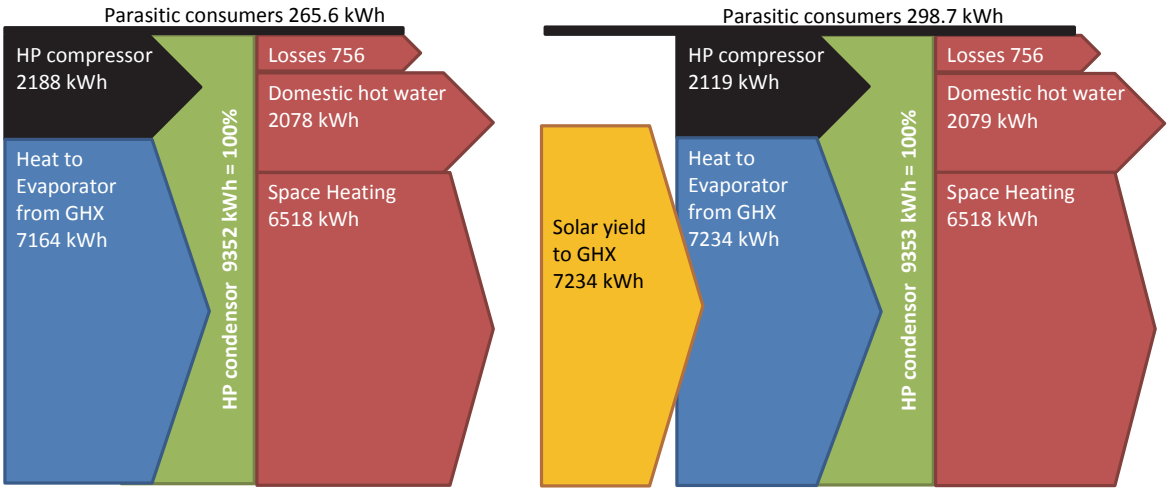

Figure 4-2: Sankey Diagram for annual energy flow rates for reference system according to IEA SHC Task44 / HPP Annex 38 conditions. The vertical ground heat exchanger has a length of 110 m. Left: The conventional system without solar assistance. Right: identical system to conventional system but with solar regeneration by 10 m² black polymer absorber

The first system (left) has a conventional dimensioned vertical ground heat exchanger. The second system (right) includes solar regeneration with an uncovered collector. There are only negligible changes in terms of performance between the systems, while the vertical ground heat exchanger is completely recharged. Around 10% of the overall electric consumption is caused not by the heat pump, but by auxiliary parasitic consumers such as pumps or controllers. The electrical consumption is presented in Table 4-2 and calculation details are given in Appendix C.

Table 4-2: Annual consumption of the different electricity consumers in the investigated systems

Consumer	Reference	With solar
Compressor	2187.6	2118.8
Pumps on the source side	53.0	87.3
Controller unit	100	100
DHW + Space heating distribution pump	82.5	82.5
Penalty Building	23.8	23.4
Penalty DHW	6.0	5.2
Direct electric heater	0	0
Overall consumption including penalty	2455.4	2417.4

The seasonal performance factors are very similar in both systems. With solar regeneration the heat pump compressor's performance SPF_{HPHS} is increased, though additional pump energy leads to nearly unchanged overall performance of the system $SPF_{SHP+,}$ Table 4-3. Furthermore, the boundary influence on the seasonal performance becomes obvious. The more the boundary encircles the heat pump the better the

efficiency becomes. The more additional thermal losses and auxiliary consumers are included, the lower the efficiency becomes. Hereafter, the overall system performance SPF_{SHP+} is used to avoid confusion. This is the most relevant figure from the perspective of the owner of a building.

Table 4-3: Seasonal performance systems for different boundaries of the reference system with and without solar regeneration for data of Figure 4-2 and Table 4-2; see chapter 2.4 for SPF- definitions

	SPF_{HPHS}	SPF_{bSt}	SPF_{SHP}	SPF_{SHP+}
Conventional system	4.12	3.94	3.60	3.50
With solar regeneration	4.19	4.01	3.66	3.56

4.1.2 Reference Data Check

The vast majority of systems are simulated in the central European climate. The chosen reference location is Strasbourg, where the simulated building has a space heating demand of 45 kWh $m^{-2}a^{-1}$. Apart from the heating demand the most decisive factor is the temperature level of the thermal load.

The domestic hot water demand is adapted from M/324 tapping cycle M (TC113N380 [107]) and (FprEN 16147 [108]) cited in [101, p. 16] and sums up to 2075 kWh/a. Hot water is tapped mostly at 45°C, but also includes a tapping at 55°C once a day and a bath tub once a week.

The building is heated by a floor radiator system, which is described as a large radiator with a heat capacity of 40.000 kJ. The radiator is dimensioned to supply the heating demand at the design conditions. At a nominal ambient temperature of -12°C the flow line temperature is 35°C with a return line temperature of 30°C. The system model is implemented in two configurations: with direct floor heating and with buffer storage tank. In either case, the correct implementation of the heating distribution system is checked by the yearly distribution of the temperatures and space heating energy.

The following part of the weather data input check and the verification of correct space heating implementation is cited from Bertram [105, pp. 15–21]. *The text includes some minor language and spelling changes.*

“

The reference climate data for Strasbourg, the simulation platform TRNSYS and the applied components are identical to the reference deck template of T44/A38. The

simulation results for the input data as weather, domestic hot water load etc. is identical. The correct implementation is verified with a task provided spreadsheet[1] for the output check. As an example Figure 4-3 shows values for monthly radiation in collector pane and Figure 4-4 for the temperature difference between clear sky and ambient air.

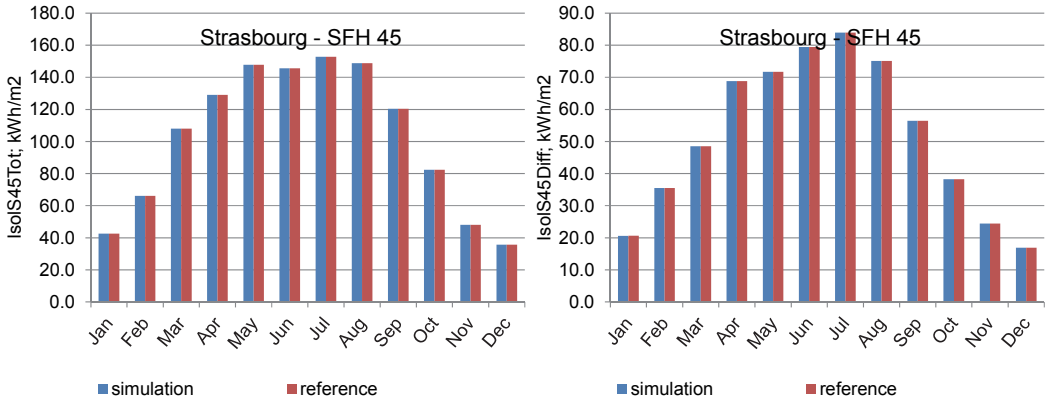

Figure 4-3: Total radiation in Collector pane (left) and diffuse radiation (right)

The simulated temperature difference between sky and ambient temperature is the only recognized difference to the reference input data. The reasons for this are unidentified. The differences which occur are small and, therefore, tolerated, see Figure 4-4.

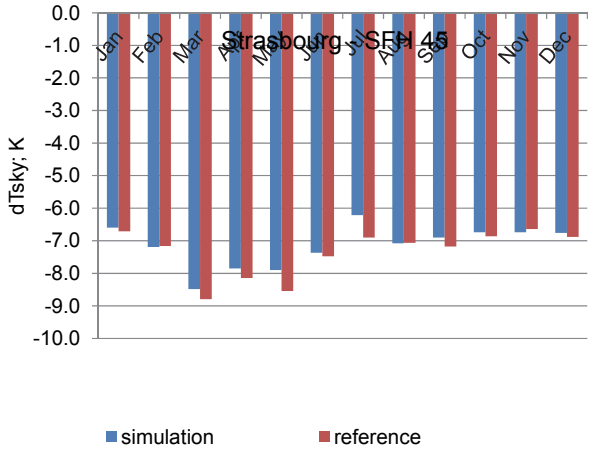

	Simulation	Reference	Difference in K
Jan	-6.6	-6.7	-0.1
Feb	-7.2	-7.2	0.0
Mar	-8.5	-8.8	-0.3
Apr	-7.9	-8.1	-0.3
May	-7.9	-8.5	-0.6
Jun	-7.4	-7.5	-0.1
Jul	-6.2	-6.9	-0.7
Aug	-7.1	-7.1	0.0
Sep	-6.9	-7.2	-0.3
Oct	-6.7	-6.9	-0.1
Nov	-6.7	-6.6	0.1
Dec	-6.8	-6.9	-0.1
SUM	-7.2	-7.4	-0.2

Figure 4-4: Monthly sums of the temperature difference between sky and ambient air temperature

The floor heating radiator is connected directly to the HP in the simulations and is displayed in Figure 4-5 (left). The following changes are implemented:

1. Direct hydronic connection of the heat pump to the floor heating system (radiator type 362)
2. The heat pump provides heat to the DHW and the space heating system. The

[1] T44A38_BUIComp_Cities_SFH.xls version 2.2

DHW preparation has priority over the space heating demand.

3. A hydronic bypass is inserted in parallel to the radiator, which ensures the constant nominal mass flow at the HP. This solution represents a hydronic pressure relief valve [or hydronic junction] in combination with a high-efficiency pump for the radiator. This enables an independent mass flow rate operation of the radiator and the heat pump. The thermostatic valve is operated with a PID control according to T44/A38 specifications.
4. The heat pump is controlled by its return line temperature. At the nominal max. heating point of -10°C ambient air temperature. The set point temperature for the return line is 32°C and 21°C at 15°C ambient air temperature. The hysteresis for the on/off control of the return line is 1 K. Furthermore, the heat pump controller has a minimum run-time of 3 minutes and a forced pause with a minimum reset time of 15 minutes.
5. The domestic hot water preparation for the heat pump has priority over the radiator.
6. The priority for the DHW leads to disruptions in the radiator heat supply. The room temperature temporarily decreases due to this lack of availability. This effect could be reduced by increasing the nominal heating capacity of the radiator by 7%, which lead to a significantly faster recovery of the room temperature.
7. The heat pump is parameterized according to own measurements. The heat pump applied was measured at constant mass flow rate of 900 kg/h at the condenser with a nominal power of 7.8 kW.
8. The mass flow rate for the radiator has no minimal off-set value.
9. A controller will turn off the radiator, if the room temperature exceeds 20.5°C.
10. The applied time step is 1 minute. The convergence and integration criteria are set to 0.001.

Further simulations are conducted with buffer or solar combi-storage tank in Figure 4-5 (right). These systems, however, do still contain the changes described (5. to 8.) applied to the directly connected HP. Correspondingly, small differences appear for the systems including the buffer compared to the SHC Task 44/HPP Annex 38 reference conditions and are also presented. The simulation results for the heating system with direct floor heating, described in Figure 4-5 (left), are presented in Figure 4-6 and Figure 4-7.

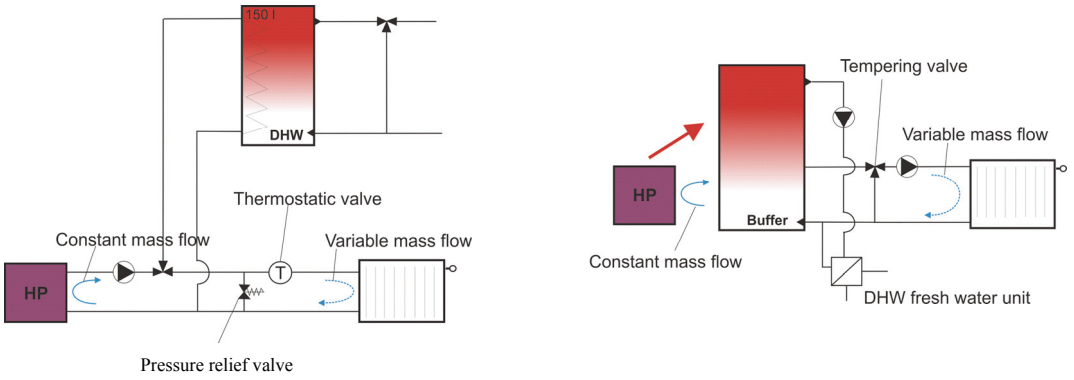

Figure 4-5 Hydronic concepts for the direct floor heating system (left) with pressure relief valve [or hydronic junction] and for the buffer system (right).

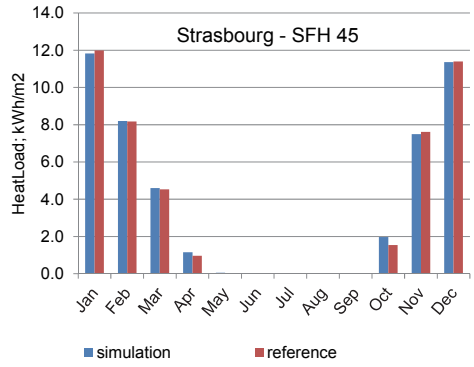

	Simulation	Reference	Diff. in kWh/mth	Rel. Deviation
Jan	11.7	12.0	0.2	2.1
Feb	8.1	8.2	0.0	0.6
Mar	4.5	4.5	0.0	-0.1
Apr	1.1	1.0	-0.1	-13.2
May	0.1	0.0	0.0	-123.3
Jun	0.0	0.0	0.0	
Jul	0.0	0.0	0.0	
Aug	0.0	0.0	0.0	
Sep	0.0	0.0	0.0	
Oct	1.9	1.5	-0.4	-24.5
Nov	7.4	7.6	0.2	2.3
Dec	11.3	11.4	0.1	0.9
SUM	46.3	46.3	0.0	0.0

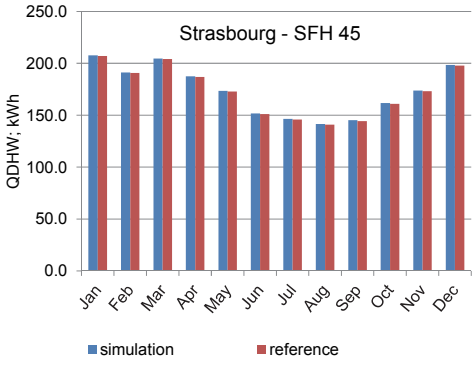

	Simulation	Reference	Diff. in kWh/mth	Rel. Deviation
Jan	207.1	207.0	0.0	0.0
Feb	190.7	190.7	0.0	0.0
Mar	204.1	204.1	0.0	0.0
Apr	187.0	187.0	0.0	0.0
May	172.9	172.8	-0.2	-0.1
Jun	151.5	151.1	-0.4	-0.3
Jul	146.3	145.9	-0.4	-0.3
Aug	141.3	140.9	-0.4	-0.3
Sep	144.9	144.3	-0.6	-0.4
Oct	161.3	160.9	-0.4	-0.3
Nov	173.3	173.1	-0.1	-0.1
Dec	197.9	197.9	0.0	0.0
SUM	2078.2	2075.6	-2.6	-0.1

Figure 4-6 Monthly space heating load (top) and domestic hot water load (bottom) in direct floor heating system

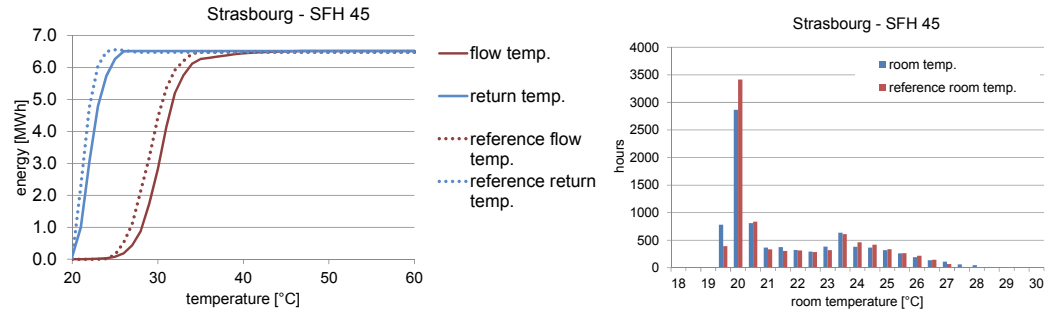

Figure 4-7 Temperature distribution of flow and return temperature and the monthly temperature room temperature in direct floor heating system

The simulation results for the heating system supplied by a buffer or combi storage, described in Figure 4-5 (right), are presented in Figure 4-8 and Figure 4-9.

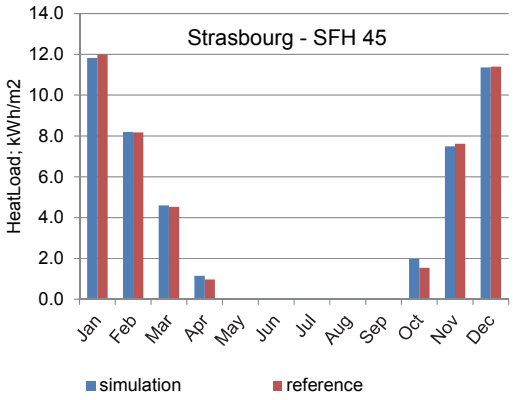

	Simulation	Reference	Diff. in kWh/mth	Rel. Deviation
Jan	11.8	12.0	0.2	1.4
Feb	8.2	8.2	0.0	-0.3
Mar	4.6	4.5	-0.1	-1.5
Apr	1.2	1.0	-0.2	-19.5
May	0.1	0.0	0.0	-110.2
Jun	0.0	0.0	0.0	
Jul	0.0	0.0	0.0	
Aug	0.0	0.0	0.0	
Sep	0.0	0.0	0.0	
Oct	2.0	1.5	-0.4	-27.1
Nov	7.5	7.6	0.1	1.6
Dec	11.4	11.4	0.0	0.3
SUM	46.7	46.3	-0.4	-0.9

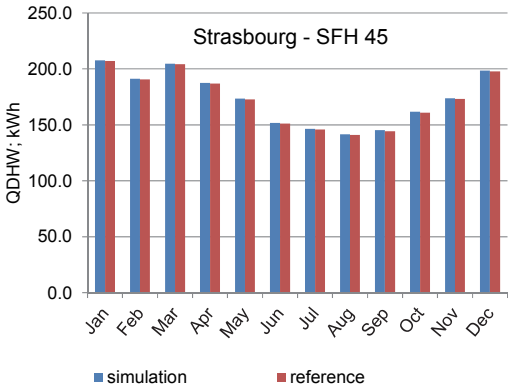

	Simulation	Reference	Diff. in kWh/mth	Rel. Deviation
Jan	207.6	207.0	-0.6	-0.3
Feb	191.2	190.7	-0.5	-0.3
Mar	204.7	204.1	-0.6	-0.3
Apr	187.6	187.0	-0.6	-0.3
May	173.5	172.8	-0.7	-0.4
Jun	151.7	151.1	-0.7	-0.4
Jul	146.5	145.9	-0.6	-0.4
Aug	141.5	140.9	-0.6	-0.4
Sep	145.2	144.3	-0.8	-0.6
Oct	161.7	160.9	-0.8	-0.5
Nov	173.8	173.1	-0.6	-0.4
Dec	198.4	197.9	-0.6	-0.3
SUM	2083.3	2075.6	-7.7	-0.4

Figure 4-8: Monthly space heating load (top) and domestic hot water load (down) in buffer system

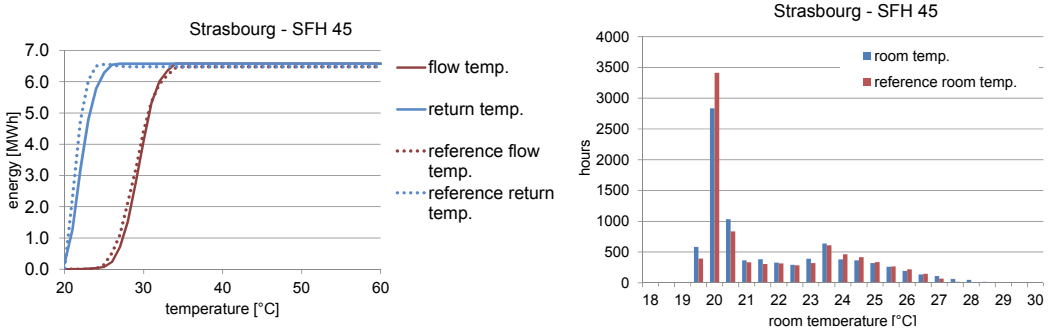

Figure 4-9: Temperature distribution of flow and return temperature and the monthly temperature room temperature in buffer system

On the whole, the implemented system shows good agreement with the task reference conditions with some slight but tolerable deviations compared to the IEA SHC Task44 / HPP Annex 38 conditions.

The differences in the annual heat demand for space heating and domestic hot water are at maximum 0.9% and are, therefore, negligible. In addition, all results of the simulation point in the same direction and slightly overestimate the heating demand compared to T44/38 reference conditions. Accordingly, relative efficiency figures and absolute consumption values are applicable for a fair comparison to other simulations.

The simulated temperature distribution slightly differs from the given reference conditions. Here, the simulations also slightly overestimate the operating temperatures. The temperature time and energetic weighted temperatures for flow and return line are given in Table 1. The differences are discussed with the yearly energy weighted temperatures.

The simulated buffer system has marginally higher temperatures. The differences are 0.1 K for the flow line and 0.4 K for the return line temperatures. These differences are tolerated and have a negligible influence on the system simulation results.

For the direct radiator higher differences occur. The differences are 1.5 K for the flow line and 0.5 K for the return line temperatures. These differences are minor, but nonetheless will have a distinguishable impact. The stationary measurements show for the heat pump a COP temperature sensitivity on the hot side of 0.07/K and 0.1/K depending on the temperature level of the condenser. In this context attention should be paid to the fact that (1) temperature sensitivity of the *SPF* is usually smaller than 0.1/K and (2) that the *SPF* is also determined by domestic hot water preparation and that (3) the characteristic temperature for the heat pump performance is not the flow or return temperature, but the average operating temperature. To conclude, a maximum difference of 0.1 in the *SPF* can be expected, due to the changed conditions in the direct floor heating.

An improved agreement for the temperature distribution will be achieved for the radiator with direct connection, if higher condenser mass flow rates are applied. The applied mass flow rate in the measurement of 900 kg/h is, however, already increased from the nominal manufacturer conditions of 700 kg/h. The necessary mass flow rate of approximately 1100 kg/h would, therefore, be unrealistically high.

Table 4: Flow and return line temperatures for the radiator in the reference and ISFH simulations

	Flow line in temperature °C			Return line temperature in °C		
Weighting quantity	Time	Energy 1 min. values	**Energy 1 hour values**	Time	Energy 1 min values	**Energy 1 hour values**
Reference System			**29.5**[1]			**21.8**[1]
Direct floor system	26.1	31.1	**31.0**	20.8	22.3	**22.3**
Buffer system	24.3	29.8	**29.4**	20.8	22.3	**22.2**

“

– End of citation.

[1] From rounded hourly values of document Buicomp_cities_SFHs_120404.xls version 2.2

The run-time characteristic is the most distinguishing feature and between the hydronic concepts with buffer and direct floor heating, Table 4-5.

Table 4-5:Overview on the heat pump settings and characteristic for the reference system with direct floor or buffer heating. The vertical ground heat exchanger has a length of 110 m and the DHW control has priority over the space heating.

Heat pump characteristic	Direct floor heating	Buffer
On-Off switches per year	10200	3560
Overall run-time per year	1144.4 h	1134.4 h
DHW controller		
Minimum run-time	5 min	2 point temperature control
Minum reset-time	25 min	
Space Heating controller		
Minimum run-time	3 min	10 min
Minum reset-time	15 min	15 min

The frequency and the overall run-time length for both hydronic concepts are displayed in Figure 4-10 for different run-time bins. Each bin represents a particular run-time period of the heat pump.

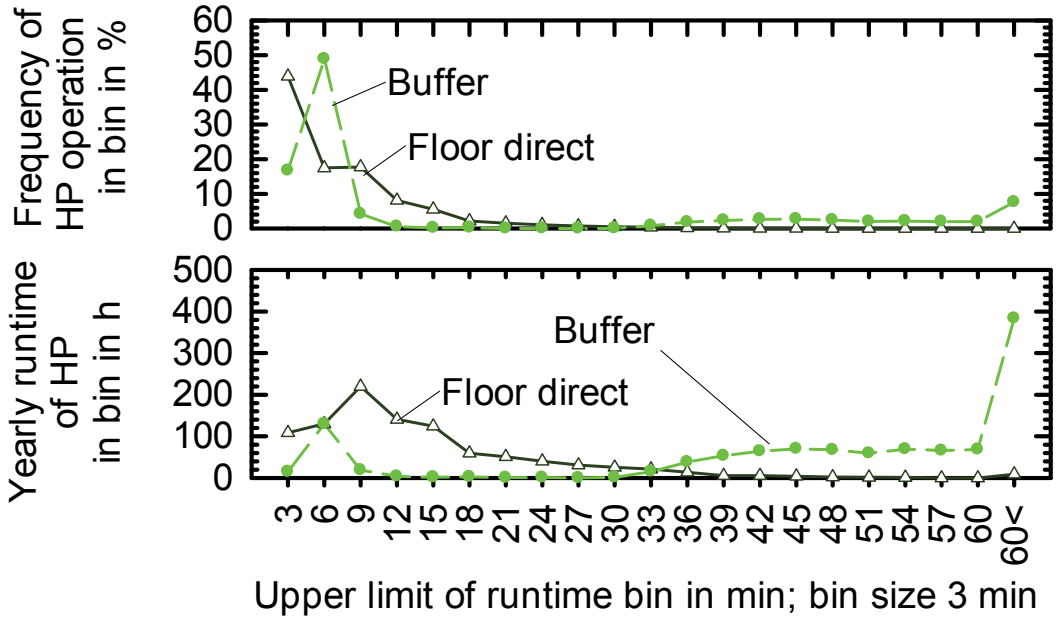

Figure 4-10: Comparison of systems with buffer and direct floor heating for different run-times the frequency (top) and the overall run-time (bottom) is shown

The direct floor heating system is determined by an intermittent heat pump operation. The varying power demand of the building and the space heating is covered by on and off switching of the heat pump at more or less constant nominal power conditions. Moreover, the controller settings for the heat pump are defined strictly in order to avoid overheating the building and corresponding additional building heat losses. As a result the direct floor heating has a characteristic run-time of below 10 min.

Frequent heat pump switching reduces the heat pump's lifetime. Field measurements, however, demonstrate that frequent on and off switching is typical for ground coupled heat pump systems. In the measured systems of Zottl [109] 4 out of 5 systems run for less than 30 min for more than 80% of their overall run-time. Another measurement in Switzerland reveals typical on-off-cycles from 6 to 10 min [110, p. 14 ff] for heat pump systems with direct floor heating in most weather conditions.

In contrast, much longer run-times are obtained in combination with a buffer storage tank. Here, the heat pump charges the buffer storage tank in longer intervals under nominal conditions. However, the buffer storage tank itself then supplies continuously heat to the system and delivers the varying demand of the load. Nevertheless, the domestic hot water tapping still induces some short time loading cycles with an average run-time of roughly 5 min, though the typical run-time intervals are over 30 min.

In principle, both concepts show similar and only small performance differences for different vertical ground heat exchanger lengths with and without solar regeneration; see Figure 4-11.

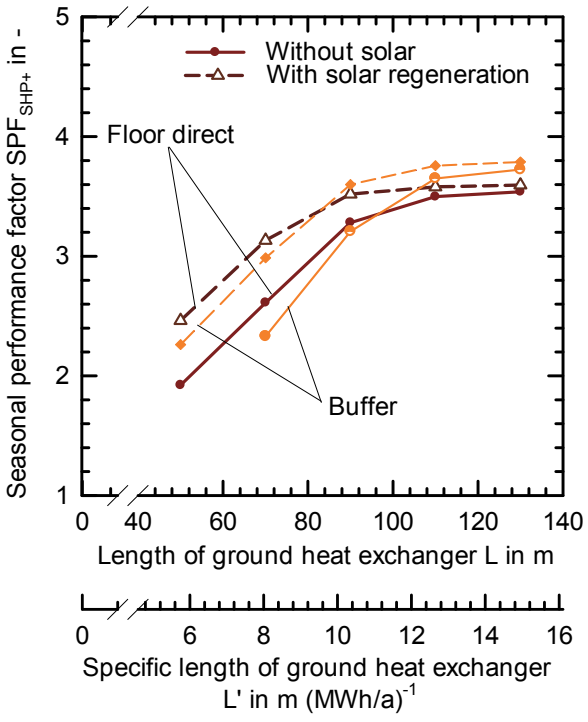

Figure 4-11: Seasonal performance factor for buffer and direct floor heating system with and without solar regeneration, black polymer collector of 15 m² collector area

At long heat exchangers the buffer concept has a 0.15 better seasonal performance. At 110 m vertical ground heat exchanger length the buffer system achieves a seasonal performance SPF_{SHP+} of 3.65 and the direct floor heating reaches a SPF_{SHP+} of 3.5.

On the other hand, the buffer concept declines more rapidly in its seasonal performance

for smaller vertical ground heat exchangers. This is explained by the lower temperatures at the vertical ground heat exchanger inlet, which occur for the buffer concept. If the allowed minimum temperature is met, a direct electric heater will substitute the heat pump and will instead deliver heat to the system. The set-point is -3°C at the vertical ground heat exchanger inlet (see chapter 2.2.2). The temperature difference remains around 0.8 to 1 K. In either case, both system concepts perform similar although they have a completely different runtime distribution.

The system's sensitivity on the minimum temperatures limit also becomes clear. More simulation results for this parameter are presented in section 5.3 Sensitivity Analysis.

4.1.3 Locations Outside the Reference Framework

In addition to the location of Strasbourg two other locations are simulated: Bolzano and Hanover. Strictly speaking every location demands for extensive location specific settings. The choice of location influences the controller settings, the size of the radiator, the ground temperatures and connected with this the cold water temperature and the domestic hot water demand.

In fact, the building related sizing depends mainly on the minimum ambient air temperature of the location. Fortunately, the minimum temperature for the three locations given is found to be similar: Strasbourg -9.70°C, Hanover -9.98°C, Bolzano -7.92°C. For the sake of simplicity the components and controller settings are not redesigned for the different locations. The impact of differences in the ground temperature between the locations is assumed to be minor and ignored. The monthly irradiation and the average temperatures for the locations is given in, Figure 4-12.

The main difference between the locations of Strasbourg, Hanover and Bolzano is the irradiance and its distribution in the course of the year. In one year Bolzano has 40% more radiation on the sloped collector. During winter the irradiance is 1.8 times higher than that of Strasbourg. It is restated at this point that the values are given for a particular orientation (South, 45° slope). Other orientations will certainly change these differences. Nevertheless, Bolzano offers much higher potential than Hanover or Strasbourg to use solar irradiation, while the monthly average temperatures especially in winter are similar at all three locations.

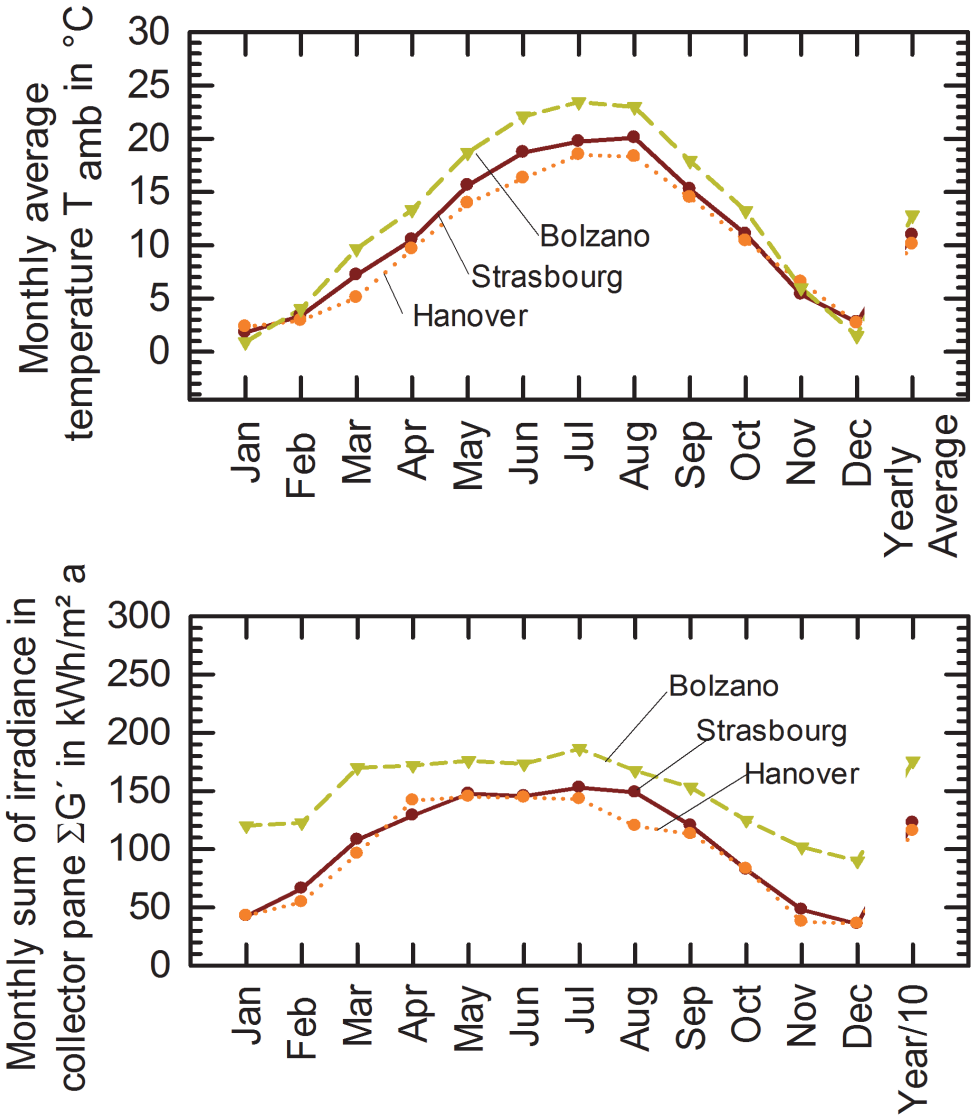

Figure 4-12 Monthly average ambient air temperature (top) and sum of irradiance in collector pane (bottom) for the locations Bolzano, Hanover, Strasbourg

A dynamic simulation was conducted for the three locations with the introduced reference building of the system model. The results are in accordance with expectations. Similar space heating demand is reached in Strasbourg (46 kWh $m^{-2}a^{-1}$) and Hanover (49 kWh $m^{-2}a^{-1}$). A lower space heat demand is required in Bolzano (29 kWh $m^{-2}a^{-1}$). The domestic hot water demand for all three locations is held constant 2075 kWh/a. The space heat demand in the course of the year is given in Figure 4-13.

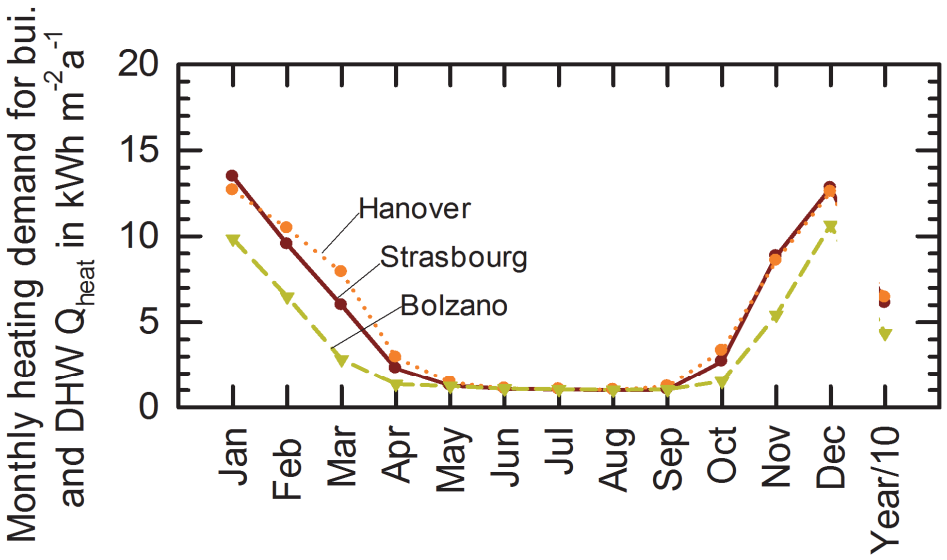

Figure 4-13 Monthly specific heat demand for building and domestic hot water. The building has a living area of 140 m².

4.1.4 Dimensioning of the Heat Pump

The heat pump is modelled according to a polynomial derived from measurements (chapter 2.1.2) with a nominal power of 7.8 kW[1] and around 6 kW for DHW preparation. The measurements extend to a prolonged temperature range and include the heating and cooling constants of the heat pump. The high quality of the data provided is the main reason to choose this particular heat pump size. Nevertheless, the sizing of the heat pump and the ratio of capacity installed to the capacity required are discussed in the following.

In addition to the domestic hot water demand, the heat pump must supply the space heating demand, which in Strasbourg is 4.1 kW under nominal conditions [103, p. 12]. Recknagel gives domestic hot water clear priority over the space heating in terms of heat pump dimensioning for the reference case. (Data applied: 5 kW/140 m² → 35 Wm^{-2} → DHW demand dominating for HP dimensioning [111, p. 984]).

The heating capacity required for domestic hot water is not only determined by the demand but also by the size of the domestic hot water storage. For the systems with direct floor heating a domestic hot water storage tank of 150 l was used, Figure 4-15.

The domestic hot water is prepared via a fresh water unit in the buffer tank system. The volume of the domestic hot water zone in the buffer tank is approximately 200 l, Figure 4-14.

[1] The nominal power is determined for a temperature of 0°C at the evaporator and 35°C at the condenser.

With this data set, a broad range of possible sizing recommendations can be found. The most generous dimensioning is proposed by the VdZ. Here, a single family house with 160 l storage volume requires a 15 kW heating capacity [112, p. 4]. Simple application of DIN 4708 [113] with peak load adapted to the real tapping profile reveals smaller capacities of 6.2 kW, which seems to be a more appropriate dimensioning. This result is confirmed by manufacturer dimensioning rules, which also determine significant smaller heat pump capacities of around 6.2 kW. The common calculation method includes in allowance for the living area and for each person (Low energy house: 40 W m^{-2}*140 m^{-2} +0.15 kW $person^{1}$ * 4 person = 6.2 kW [114, p. 42]).

In summary, the nominal heat pump power of 7.8 kW seems oversized, though much higher capacities can be found in the literature. Nonetheless, the heating capacity is realistic and representative for systems in the field, especially bearing in mind the ubiquitous practice of adding safety margins to the calculated heating capacity.

4.2 Hydronic System Description

4.2.1 Hot (Condenser) Side

Two heat distribution system concepts for the heat pump are investigated that represent typical and widespread system solutions, see for example [23, p. 179] or [115, p. 89]. The system concepts have already been introduced, Figure 4-5.

The first system is the floor heating system, in which the heat pump is directly connected to the floor heating radiator. The domestic hot water storage is prepared in a separated tank via an immersed heat exchanger. The second system is a system with buffer tank, to which the heat pump is connected. This buffer then supplies heat for the floor radiator and the domestic hot water system.

In this thesis, the buffer system concept is not simulated with a solar collector hot side integration. Uncovered collectors do not reach high solar fractions for space heating. Solar coverage for the more convenient solar domestic hot water is already limited, Chapter 5.1. Nevertheless, the detailed system integration is displayed in Figure 4-14.

The main features of the buffer storage tank are

- Two zone charging for different temperature levels of domestic hot water and space heating, see for example [116, p. 155]
- In a parallel concept the buffer integration allows the bypassing of the buffer tank. The heat pump can partly or completely be connected directly to the space

heating distribution, [23, p. 179].

- The space heating zone is discharged in the lower part of the tank. Its flow line passes a mixing valve. This valve mixes down the space heating flow to an ambient temperature dependant flow temperature for the space heating.
- The space heating return line flow is returned to the buffer via a stratifying manifold.
- The controller for domestic hot water charging has two temperature sensors (boiler control). The lower sensor determines the starting of the heat pump recharging. Accordingly, the upper sensor ends the charging.
- The domestic hot water zone is discharged by a fresh water unit.

The buffer system integration is complex and small changes in height and position of temperature sensors, inlet or outlet connection can significantly affect the heat pump performance and increase electrical consumption up to 50% [117]. The buffer solution presented is optimized by a procedure of trial and error. It achieves a similar performance as the direct floor heating system (Figure 4-11) and, therefore, allows good comparison to the direct floor heating systems.

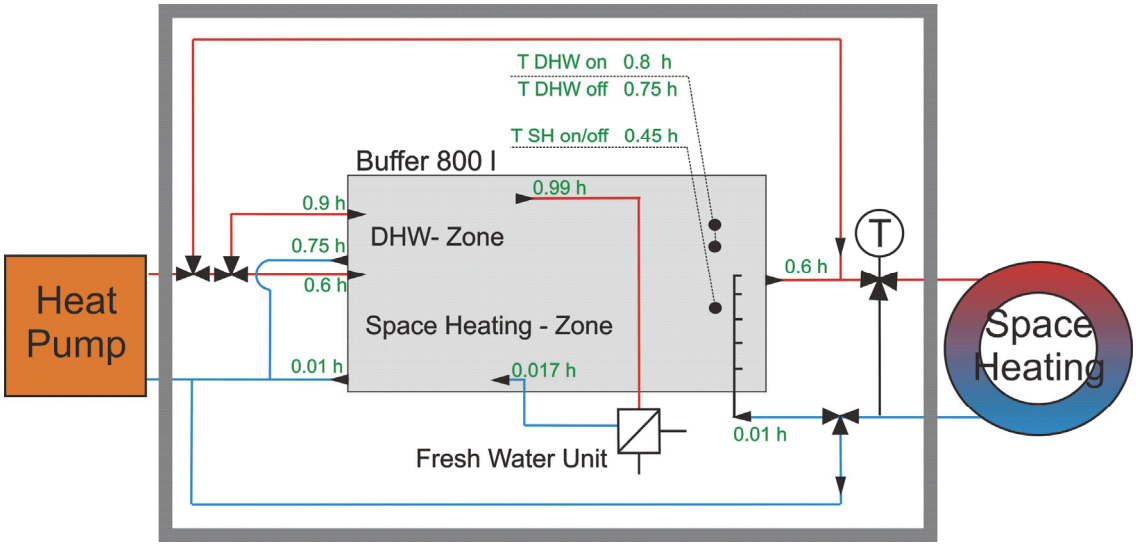

Figure 4-14: Detailed diagram for simulated buffer tank system with heat pump, space heating and domestic hot water The scheme includes temperature sensors for controllers, tempering valve for the space heating flow line, the relative heights of all inlet and outlet connections h are marked green. The grey box marks the boundary of the buffer storage concept. The effective overall heat loss coefficient of the 800 l storage tank to the ambient is 6.0 W K^{-1}

The heat pump is connected directly to the floor radiator in the floor heating system. Furthermore, it can be switched to heat a domestic hot water tank via an immersed heat exchanger. The domestic hot water storage tank has a volume of 150 l, if operated without solar hot side integration. With solar integration the domestic hot water storage

tank is extended to 300 l. The selected dimensioning is moderate but in good accordance with widespread rules of thump e.g. manufacturer guidelines [118, p. 107], which recommend 50 l/m² for flat plate collectors in central Europe. Hot side integration of flat plate collectors will also be simulated for comparison.

The details for the storage tank configuration temperature sensors etc. are presented with and without solar integration in Figure 4-15. The heat transfer coefficient for the immersed heat exchanger is a function of the collector area [119, p. 17], see Eq. 4-1

$$UA_{HX} = 88.561 \frac{\mathrm{W}}{\mathrm{m\,K}} \cdot A_{coll} + 328.19 \frac{\mathrm{W}}{\mathrm{K}} \qquad \text{Eq. 4-1}$$

A_{coll} - *Collector area in* m^{-2}
UA_{HX} - *Effective heat transfer coefficient of immersed HX in* $W\,K^{-1}$

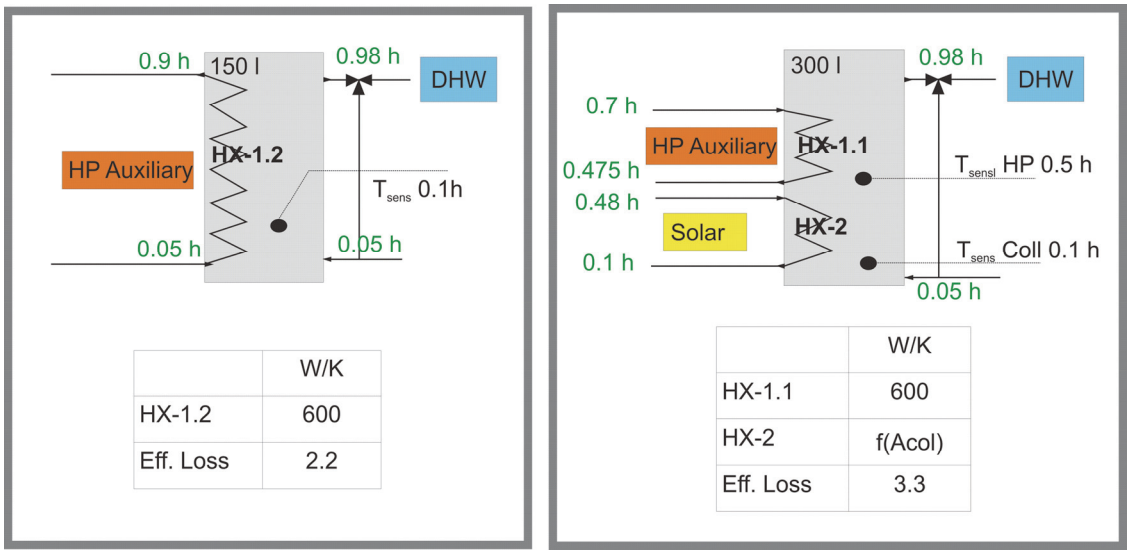

Figure 4-15: Diagram for domestic hot water (DHW) storage tank with and without solar hot side integration of uncovered collector. The scheme includes temperature sensors for controllers, the immersed heat exchangers HX including their effective heat transfer coefficients, the relative heights of all inlet and outlet connections h (green) and the effective overall heat loss coefficient of the storage tank to the ambient.

4.2.2 Cold (Evaporator) Side

System concepts with solar cold side integration are the focus of this thesis. There are two reasons for the cold side integration. One reason is the increase of the temperature at the heat pump's evaporator and the other reason is the thermal regeneration of the ground.

A helpful method for system visualisation is an energy flow chart or square view [79]. An example is given in Figure 4-16 (left) that shows all possible energy flows between the solar collector, vertical ground heat exchanger and a cold storage tank.

The energy flow charts can be misleading, however, because they suggest an explicit system concept, while numerous possible piping concepts are still possible even for a limited component number. This becomes clear for an example of a system without a thermal storage thermal tank. This case is given in Figure 4-16 (right) and has at least 3 significantly different piping concepts: parallel, series in-front and series behind, although at a first glance the energy flows suggest a rather clear connection. Another key point is that the order of the components in a thermal network influences their efficiency. Further details such as mass flow rates, positions of temperature sensors etc. also make a difference.

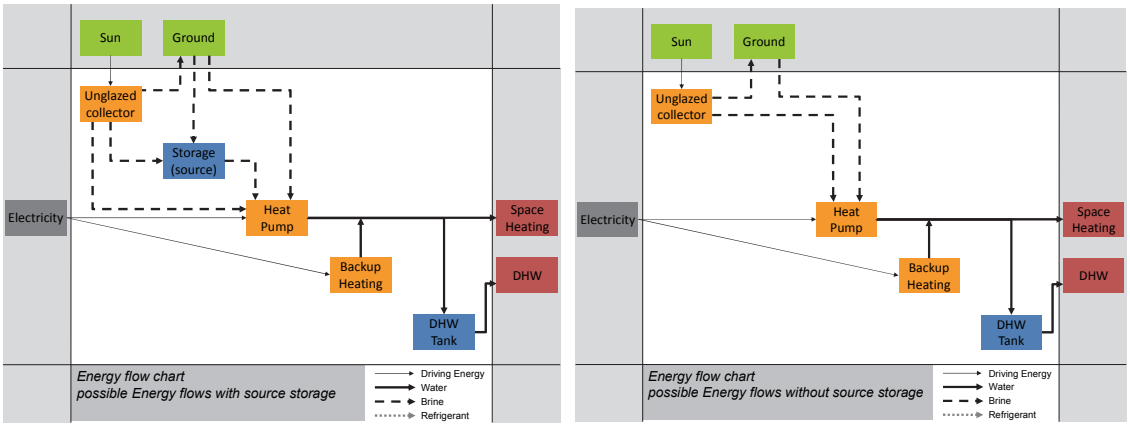

Figure 4-16: Energy flow chart / square view. All possible energy flows for solar collector, vertical ground heat exchanger Left: including a cold storage capacity. Right without cold storage capacity

Five source concepts and their basic ideas are presented and described in Figure 4-17 to Figure 4-22. The settings given below apply to all concepts.

The solar collector is controlled by a differential controller. The hysteresis is set to 6 K for starting the operation and to 3 K for ending it. The minimum run-time and the minimum reset time are 3 minutes. In the simulations the temperature sensor T_{upper} is positioned at the outlet of the collector or its last numerical segment. During standstill of the system the lower temperature T_{low} is saved from last time step with mass flow. Collector operation is permitted for temperatures of T_{upper} between 0° and 35°C.

The solar collector is operated at a specific mass flow rate of 30 kg m^{-2} h^{-1} to save energy for pumps. This is quite low, but will be varied and discussed in detail later (see Figure 5-9).

There is one exception for the collector mass flow in series systems No. 1 and No.2. If the heat pump is running, the evaporator pump will be switched on and operated at the nominal mass flow rate of the heat pump and oblivious to modes with lower mass flow rates. The heat pump operation is autonomous and depends on demand only.

0. **GHX only:** In this conventional system the vertical ground heat exchanger is the only heat source for the heat pump evaporator.

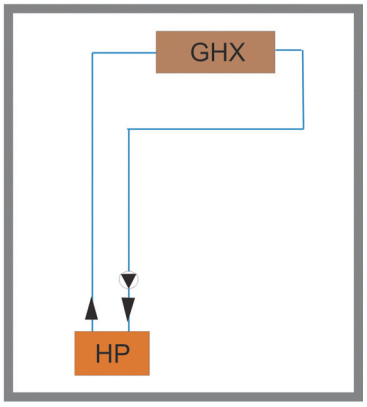

Figure 4-17: Conventional system with vertical ground heat exchanger (GHX) only

1. **Series in-front:** The collector can be switched on in series previous or in-front to the vertical ground heat exchanger. The collector will be switched on, if the collector is hotter than evaporator outlet. Accordingly, the coldest system temperatures from out of the evaporator, in case of recharging from the ground, lead to the highest possible collector efficiencies. The technical effort is low as only one additional switching valve and no additional pump is required. This system concept was also measured in the field (chapter 6.1).

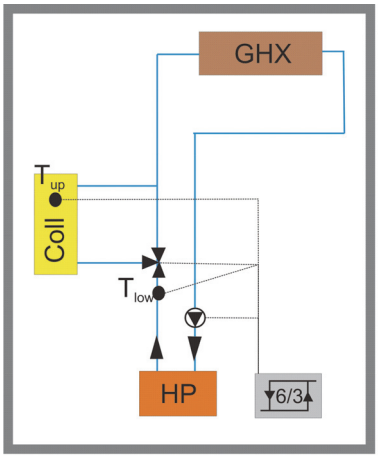

Figure 4-18: Cold side system concept: series in-front

2. **Series behind:** The collector can be switched on in series but behind the vertical ground heat exchanger. This concept is equal to series in-front, but with higher operating temperatures for the collector. This can have two effects: higher temperature levels at the HP inlet and extended collector operation even, if the outlet temperature of the heat pump is close to 0°C, because the collector is usually protected from operation below 0°C.

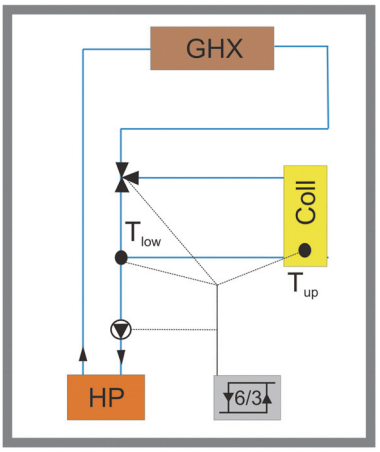

Figure 4-19: Cold side system concept: series behind

HP *heat pump evaporator,* GHX *vertical ground heat exchanger,* Cold Tank *cold storage tank,* Coll *solar collector,* 6/3 *2-point differential controller with its temperature sensor Tupper for the upper and Tlow for the lower temperature* *pipe with flow direction,* *pump,* *switching valve*

3. **Parallel:** Both heat sources, vertical ground heat exchanger and collector, are connected in parallel. This allows parallel operation of the collector and vertical ground heat exchanger and the collector can be operated as the sole heat source without passing the vertical ground heat exchanger. In this thesis the mass flow is divided in half, if the collector and the vertical ground heat exchanger are operated in parallel. This, configuration investigated, however, does not allow recharging the ground.

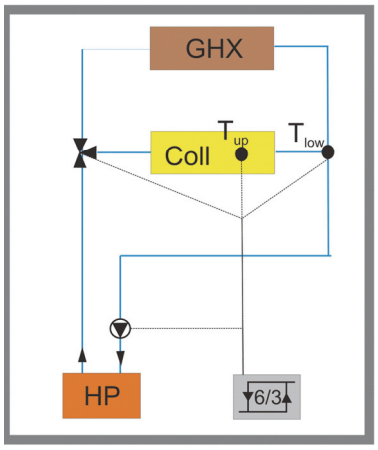

Figure 4-20: Cold side system concept: parallel

4. **Cold storage as hydronic junction for solar and ground**: Both heat sources supply heat directly to a cold storage tank. The mass flow rates of all components can be operated independently and the recharging of the ground is possible. This combination requires two additional pumps and a storage tank. All heat must pass the heat storage. The storage vessel is insulated (100 mm λ= 0.04 W m^{-1} K^{-1}).

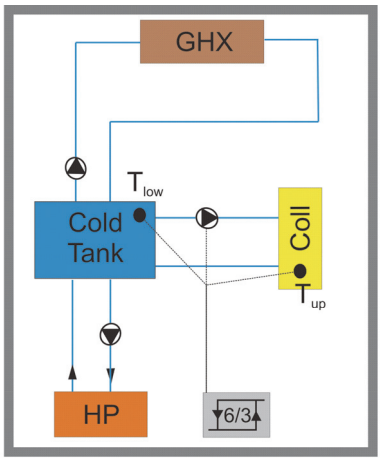

Figure 4-21: Cold side system concept: Cold storage as hydronic junction

5. **Cold storage capacity for solar only**. The cold storage tank charging is limited to the solar collector. The heat pump can either be switched to this cold storage or the vertical ground heat exchanger. The heat source is usually switched to the heat source with higher temperature. In contrast to the hydronic junction variation, it is, however, possible to discharge one heat source and save the heat in the other one. One additional pump, a switching valve and storage tank are required. The regeneration of the vertical ground heat exchanger is possible only with an additional pump. This solution is therefore not simulated, because the basic effects of a cold side storage capacity are covered in system 4.

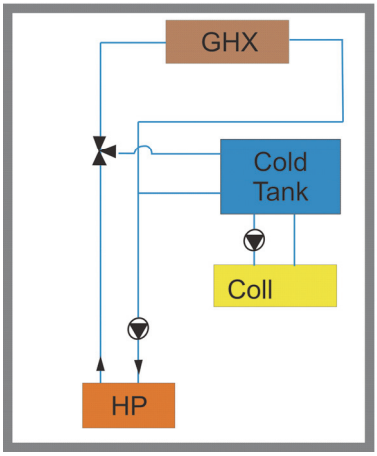

Figure 4-22: Cold side system concept: cold storage capacity for solar only

It is emphasized that a design optimization of system concepts on the cold side and especially the cold storage tank is as demanding as the design optimization on the hot side e.g. described by Haller [117]. Here too, small details can have an impact on the performance and the position of every temperature sensor, inlet and outlet can be optimized. Correspondingly, the cold storage tank is described in detail, Figure 4-23.

The cold storage tank can have two positive effects. Firstly, solar energy can be stored and, if available, and be subsequently provided. Secondly, the evaporator heating demand can be buffered. This heating demand of the evaporator can then be elongated using its storage capacity, which leads to longer but lower heat flow rates at the vertical ground heat exchanger.

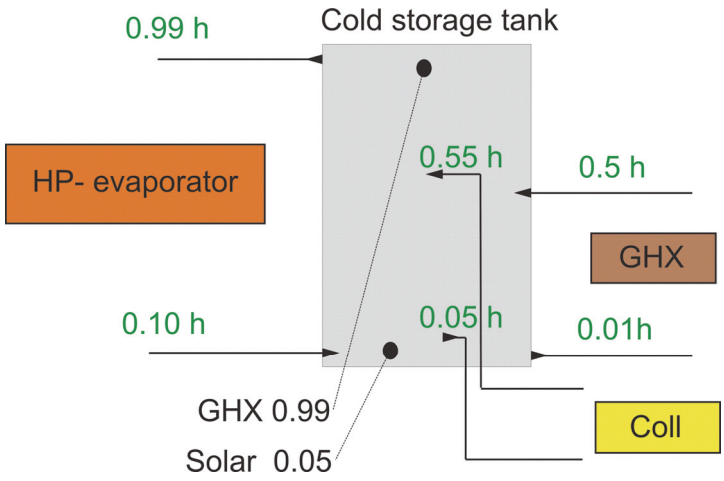

Figure 4-23: Cold storage tank integration to the evaporator side of the heat pump for the system concept given in Figure 4-21: Cold side system concept: Cold storage as hydronic junction

Some optimization proposals for the cold storage tank were already derived by Arnold within the context of a bachelor study [120]. This work investigates a dual-source system for flat plat collectors in combination with hot and cold side integration and contains a single parameter optimization for seasonal performance. The results are not included in this thesis. Nevertheless, they reveal the complexity of the systems and are valuable for further optimization. The improvements achieved are high for the collector yield but in the range of 0.1 in the seasonal performance.

Arnold [120, pp. 52–67] proposes three major changes. The first proposal is revolving connections for the vertical ground heat exchanger. The ground is then recharged with the highest storage tank temperature. Secondly, the storage tank's maximum temperature limit should be increased from 30°C to 60°C. Such high temperatures at the evaporator could be critical for the heat pump operation, but will be tolerable, if an additional tempering valve is added ahead of the evaporator. Thirdly, the controller that

manages the charging from the vertical ground heat exchanger can be optimized to minimize the pump run-time.

The concepts presented cover most of the possible hydronic solutions for a cold side integration of hybrid heat sources, but are implemented as one particular solution. Further optimization and slightly different concepts will lead to changes and presumably even improvements. Other components like e.g. ice or buried storages, cold storage tanks with immersed heat exchanger or several fluid loops with external heat exchanger will lead to shifts of the results to different temperature levels and heat gains.

It is assumed that differences made through further optimisation of concepts will be moderate and the system solutions presented allow the understanding of the general concept. In any case, the variations without cold storage, in particular, are extremely well elaborated in the field and have seen the results of a broad optimisation process.

The corresponding simulation studies are presented in chapter 5.2.

4.2.3 Combination of Hot and Cold Side Variations

In principle, every combination of the hot side can be combined with every system concept of the cold side integration. On the hot side three concepts are presented: 1) direct floor heating, 2) direct floor heating with solar 3) buffer system. On the cold side of the heat pump 6 system concepts are presented, of which 5 (No. 0 – No. 4) are implemented.

The focus of the simulations is the collector cold side integration. It will be shown subsequently that the application range of uncovered collectors for hot side integration is limited, chapter 5.1. As a result, the combination of hot and cold side is even less appealing. The systems investigated apply solar heat in the majority of cases on the cold side, in the minority on the hot side and on an exemplary basis on both sides.

In chapter 5.4.1, the solar collector supports the hot and cold side of the heat pump. Such systems promise to increase the overall performance by intelligent channelling the solar heat to the point in the system, where it has its maximum effect on the overall performance. The right controller and assessment of such a point of maximum effect, however, is difficult, because the combination of hot and cold side even bears the danger of reducing the system's performance. In several cases the combined hot and cold side systems perform less well than a system with solar hot side integration only [77], [121].

A theoretical calculation for the switching point is proposed by Haller & Frank [122], while Pärisch et. al. [11] demonstrate some control strategies in combination with stagnation cooling and also stress the danger of performance losses in the system due to combination of hot and cold side.

4.3 Component and System Models

4.3.1 Applied Models, TRNSYS Versions and Simulation Methodology

Numerous models are assembled to form the developed system model. An overview of the applied models and their origin is given in Table 4-6. These component models and their level of detail or simplification also have a strong influence on the validity of the overall system model. For instance icing is not included in most components despite their operation of temperatures below 0°C. Even the choice of the model can influence the results (chapter 5.3.2).

Table 4-6: Implemented component models in the TRNSYS system model. A similar version of this table was also used for system model description in [106]

Description	Type No.	Reference / comment
Hot and cold storages tanks		
	340	[123], the cold storage tank is recompiled to allow operation below 0°C
Vertical ground heat exchanger		
modified with pre-pipe	557a, 604	[48] TESS + modification according to [124] [48] TESS
Hydronic components		
pipes, valve, multi-valve, pump	709, 11, 469, 803	[48] TESS, [125] standard, [48] TESS, [125] standard
Controller		
On-off, DHW storage, W-interpreter, forcing function, value recall (1), value recall (2)	911, 890pro, (-), 14, 93, 899	[48] TESS, Source [101], [126], [127], [125] standard, [125] standard, ISFH
Output		
Pin-sorter, printer, integrator (1), integrator (2)	1576, 24, 339, 55	[48] TESS, [125] standard, [125] standard, [125] standard
Building		
Internal loads and applied types are used according to task44 template	56 -	[125] standard [101], [126] non-standard
Collectors		
Uncovered collector (PVT-) collectors, covered collector	203, 832v500	[66] non-standard, [128] non-standard
Heat distribution:		
Radiator with PID controller	362	[129] non-standard
Weather data reader, dew-point calculation, sky temperature	109, 33, 69p	[125] standard

The complete rebuilding of the system model would presumably not lead to exactly the same results even though much effort was invested to obtain a transparent and reproducible system model. Simply the full documentation of every parameter for all types (one storage tank has 130 input parameters, one vertical ground heat exchanger at

least 40 parameters), their connections and the applied scaling formulas for pipes and storage tanks etc. in every detail exceeds the possible documentation length.

Moreover, the process of modelling itself involves ongoing model configurations and debugging of the sub- and system model and implementation. This fundamental modelling process is called the “simulation pipeline” [130, p. 3]. This means for modelling different system concepts with the aim to compare them that every single model change, improvement and pug anywhere in the model needs to be transferred and checked for all existing system models to ensure their comparability. These modifications must be implemented throughout the whole modelling process and to all system model configurations. Otherwise different results from “System A” and “System B” cannot be clearly traced back to the intended changes between A and B. The intended differences between A and B interfere with differences that are caused by system model deviations.

To ensure the comparability of system results a single system model was developed that includes all hydronic system configurations investigated. This multi system model allows switching between the hydronic configurations by simply activating or shutting down hydronic valves. Strictly speaking the system model is therefore a system**S** model of multiple systems. As a result, all changes in the system models identically apply to all system configurations at once. For instance a change in the weather data file or a modified time constant of a heat exchanger in a storage tank automatically is connected to all system configurations.

In summary, the developed system model ensures high simulations quality and allows even small differences between the systems configurations to be quantified exactly.

4.3.2 Plausibility and Balances

The system model is implemented to the TRNSYS simulation environment. Here, different components, (types) are compounded to one system (deck). From the perspective of TRNSYS the components themselves are independently calculating black box models, which are connected within TRNSYS by their in- and outputs. During the simulation internal algorithm of TRNSYS then numerically solves the equations that connect the components [125, p. Documention Part 1]. Even differential equations can be solved [131].

A point often overlooked is that the quality of the solution found depends on the numerical settings for the error tolerances set by the user. The quality of the results

obtained is the trade-off for the simulation run-time. High limits for the convergence lead to fast solutions and low computing costs, but at the price of a higher error or, in other words, more inaccurate results. In all results presented the simulations are conducted with a tolerance for the integration error and a convergence error of 0.001. The TRNSYS version utilized is 17.01.25.

Furthermore, heat balances for the complete system and some components are made to ensure the quality of the simulation results. Table 4-7 gives the annual heat flow rates and the error in the second year of operation. All other results presented are also taken from the second year of operation.

The thermal energy differences of the components between the start and the end of the simulation from thermal capacity differences are neglected because they are assumed to be small compared to the overall heat flow rates. All simulations have been checked in their balances and the given example in Table 4-7 is representative for all simulations presented. In systems without solar assistance all deviations are smaller than with solar assistance.

Table 4-7: Heat balances for systems of Figure 4-2 with solar (right) in the second year of operation. The relative balance error is related to the maximum heat flow rate within the balance.

Heat balance system	Balance error in kWh	Rel. balance error in %
Overall System	20.3	0.21
including all components and connecting pipes		
Subsystems		
Heat pump	0	0
DHW storage tank	0.28	0.000
Collector loop	1	0.013
Evaporator side:		
GHX, collector, pipes, evaporator	11.4	0.152

5 Transient System Simulation Results

5.1 Solar Hot (Condenser) Side Integration

In general, solar hot side integration can be used for space heating assistance or solar domestic hot water preparation. The solar domestic hot water preparation is less demanding for the solar collector performance. In summer the heating demand occurs at low operating temperatures and high solar irradiances. Normally conventionally designed solar domestic hot water systems can supply the entire heat demand during the summer season. In most cases solar domestic hot water systems are well elaborated standardized systems with flat plate collectors. Uncovered collectors have lower collector yields, but also a lower price.

Four different collector types are simulated with the system layout given in Figure 4-15. All systems achieve clear improvements in the seasonal performance, Figure 5-1. The improvement, however, is moderate even for extremely large collector areas.

The collector type has a decisive influence, while the size of the collector above 15 m² has no influence on the system performance. As to be expected, the system with selective collector performs best. It achieves *SPF* improvements up to 0.6. This means the SPF_{SHP+} increases from 3.5 to 4.1. All other collector types achieve performance improvements of roughly 0.4 or below. Moreover, the improvement due to solar assistance on the hot side decreases rapidly for smaller vertical ground heat exchangers independently of the collector size. The effect of solar heat on the hot side has the opposite impact as its use on the cold side. This will be demonstrated subsequently in Chapter 5.2.

The decrease of the heat demand due to solar assistance on the hot side does not influence the temperatures on the cold evaporator side of the heat pump. All simulations presented in Figure 5-1 show no change in the minimum inlet temperature of the vertical ground heat exchanger (ΔT_{min} <0.01K).

In a second step the selective collector, the best performing collector type, is compared to a typical flat plate collector (η_0=0.8; a_1=3.5 W $m^{-2}K^{-1}$; a_2=0.015 W $m^{-2} K^{-2}$) [119, p. 16]. The collector areas are varied while the domestic hot water storage volume of the 300 l is held constant.

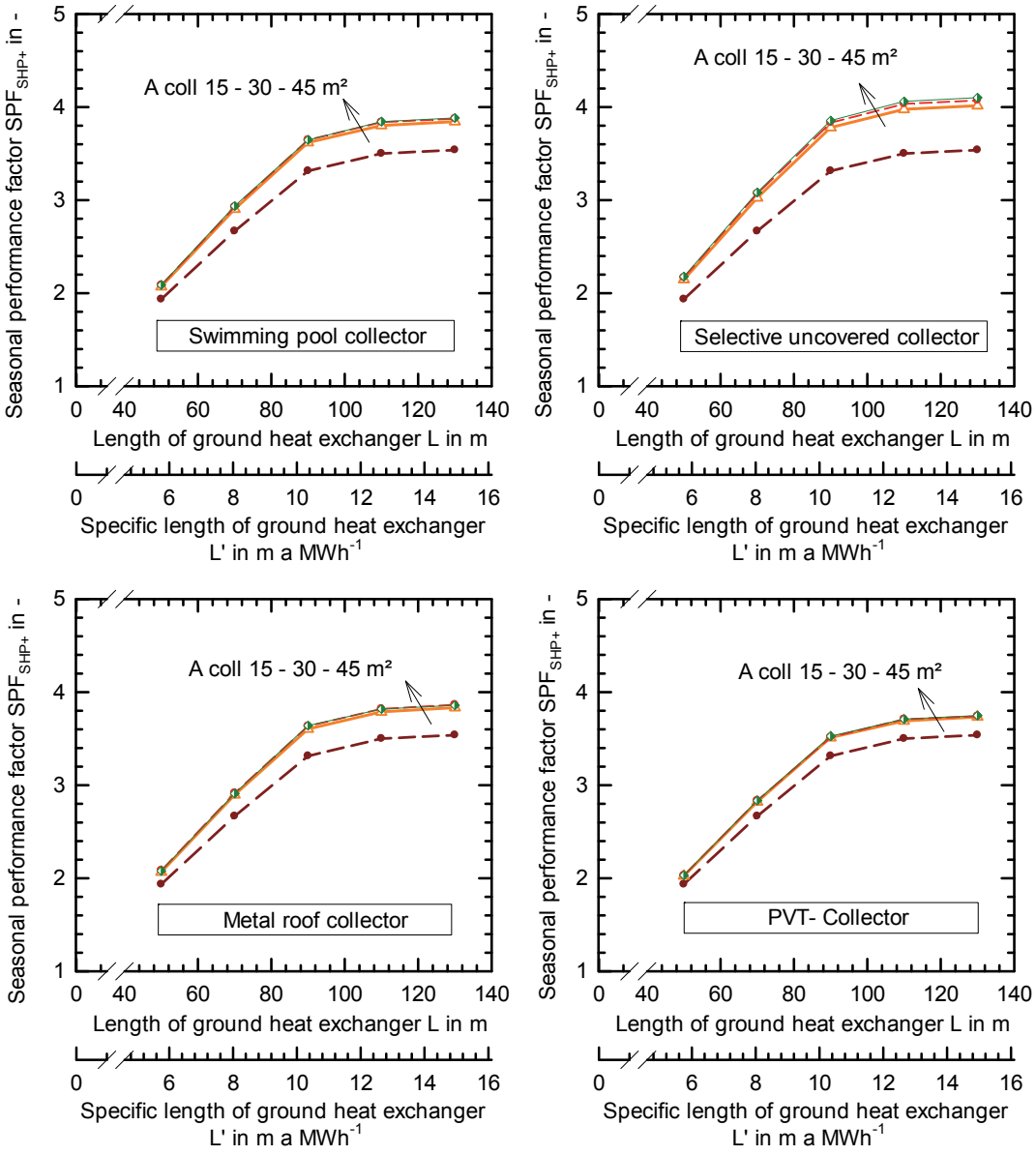

Figure 5-1: Seasonal performance factor SPF_{SHP+} of systems with vertical ground heat exchanger and solar domestic hot water assistance for different collector types and collector areas of 15/30/45 m². (top left): Black polymer collector, (top right) selective uncovered collector, (bottom left) metal roof collector (bottom right) PVT- collector. The performance data from Appendix A is applied.

The solar fraction for the domestic hot water $s_{d,DHW,2}$ is defined[1], Eq. 5-1, to evaluate the impact of the solar assistance. Here, Q_{use} is the consumed domestic hot water energy and $Q_{AUX,DHW-store}$ is the heat delivered to the storage tank from an auxiliary heater- here the heat pump. It is emphasized that this definition of the solar fraction is related to the domestic hot water demand only.

[1] The widespread definition for the solar fraction $s_d = \frac{Q_{sol}}{Q_{sol}+Q_{AUX,DHW-store}}$ is not used because it regards solar overheating of the storage volume in summer as useful energy; see [75] Abb. 6.

$$s_{d,DHW} = 1 - \frac{Q_{AUX,DHW-store}}{Q_{use}} \qquad \text{Eq. 5-1}$$

The flat plate collector achieves considerably higher seasonal performances and solar fractions than the uncovered collector, Figure 5-2. The flat plate collector performs better not only for collectors of the same size but also in absolute numbers. A flat plate collector of 10 m² reaches solar fractions of over 60% and seasonal performance of nearly 5. The uncovered collector, on the other hand, performs significantly below these figures. Its maximum solar fraction is 33% with a seasonal performance of 4.3.

In addition, the performance stagnates even for larger collector areas. This especially applies to the uncovered collector, for which the solar fraction nearly stagnates between 20 m² and 30 m² collector area.

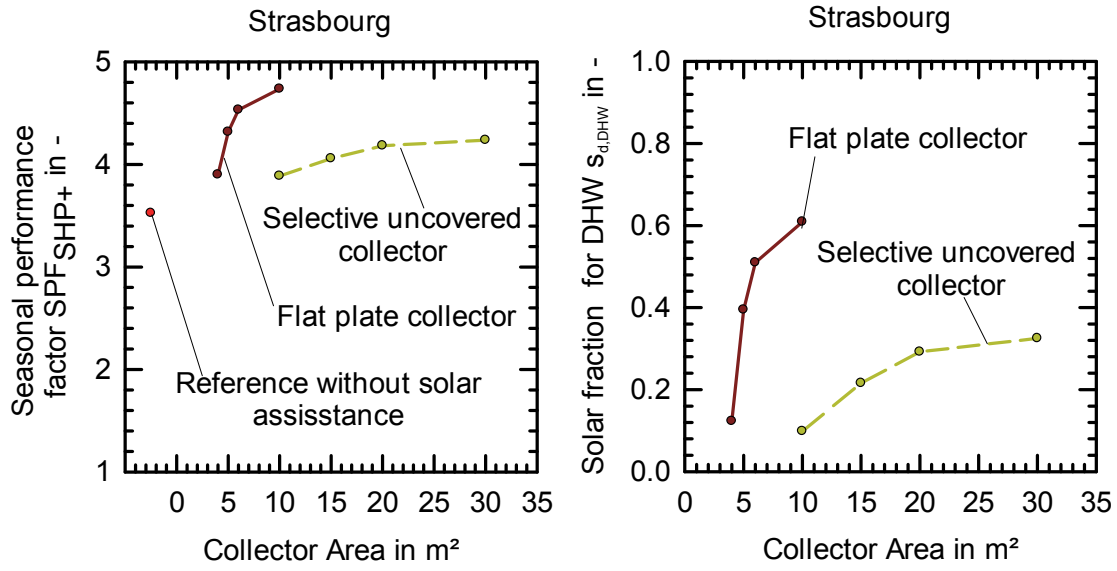

Figure 5-2 Flat plate collector and uncovered selective collector for domestic hot water application in dependency of the collector size. The vertical ground heat exchanger length is 110 m and the domestic hot water storage volume is 300 l for all variations. Left: the seasonal performance SPF_{SHP+}, Right: the solar fraction $s_{d,DHW}$

As pointed out earlier, the collector impact on the system depends on location. This applies in particular to uncovered collectors because of their high dependency to the ambient conditions. Therefore, the identical system with flat plate collector and selective uncovered collector are also simulated in Bolzano (Italy) and Hanover (Germany) and discussed on the basis of the solar fraction. Weather data information can be found in chapter 0.

The systems show a high dependency on location, Figure 5-3. In Hanover, which has weather similar to Strasbourg, very similar simulation results are obtained. Here, the flat plate collector clearly outperforms the uncovered collector. In Bolzano both collector

types gain high solar fractions for domestic hot water. The flat plate collector is still better than the uncovered collector, but the difference between the collector types is somewhat diminished. Consequently, other aspects such as cost or architectural integration will be of increasing importance.

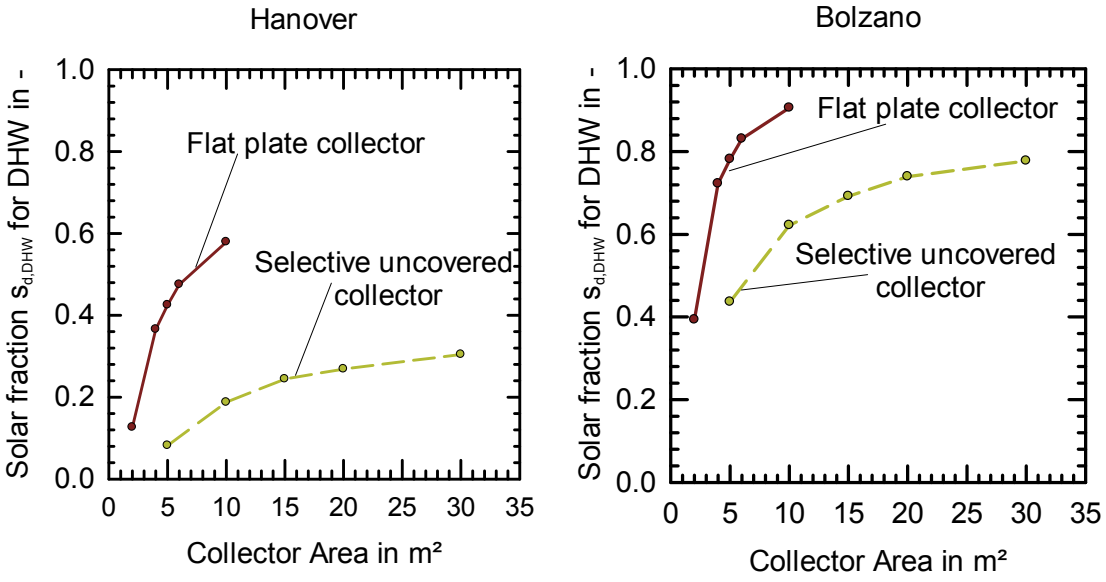

Figure 5-3 Solar fraction for domestic hot water in dependency of the collector. The covered collector area is varied between 2 and 10 m² and the uncovered collector is varied between 5 and 30 m². Left: Hanover, Right Bolzano

To conclude, the results show higher performance increases on the hot side than on the cold side. Nonetheless, these improvements are small compared to the integration of a small conventional flat plate collector. The application of any kind of uncovered collectors for solar domestic hot water assistance seems therefore unlikely in central or northern European countries. In contrast, uncovered collectors may be an interesting alternative in more southern climates. Further analysis beyond this thesis should include economic aspects and climates with even higher irradiance and ambient temperature conditions.

5.2 Solar Cold (Evaporator) side Integration

5.2.1 Seasonal Performance and Minimum Temperatures

The most elaborated system configuration for solar ground regeneration with uncovered collector is the system configuration series in-front (see chapter 4.2.2). This combination is simulated with an uncovered black polymer collector for different collector sizes from 5 to 30 m² collector area and different vertical ground heat exchanger lengths. The simulation outcomes are presented in Figure 5-4 for the seasonal

performance factor SPF_{SHP+} and additionally for the dimensioning criteria the minimum inlet temperature T_{min} in Figure 5-5. The results displayed are central for the understanding of the results presented hereafter.

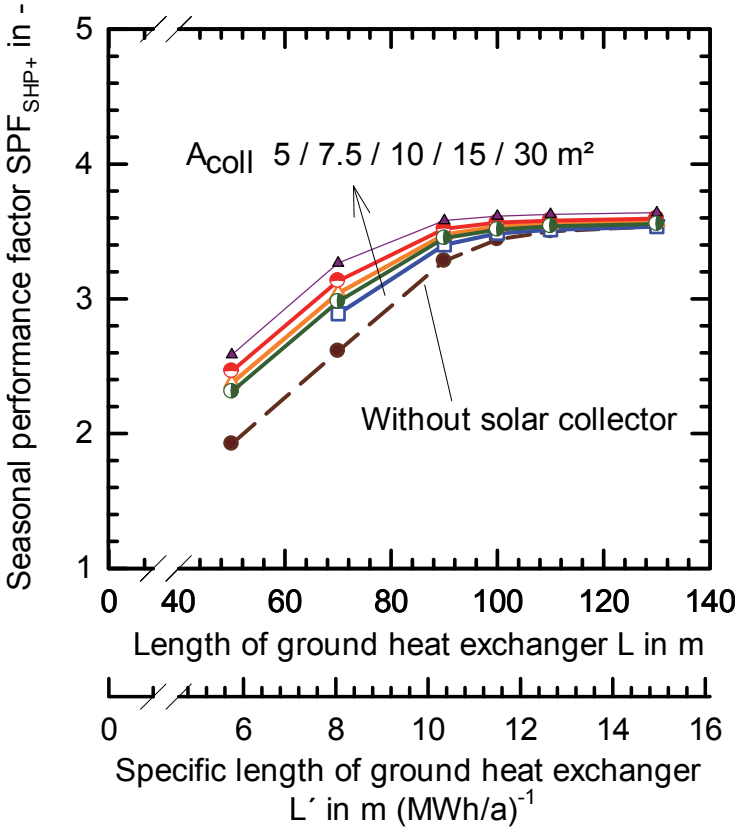

Figure 5-4: Simulated seasonal performances for the reference system conditions of Task 44 / Annex 38. The vertical ground heat exchanger length and the collector area are varied. The system concept is series in-front with a black polymer collector.

The collector induced efficiency improvement is small compared to the reference case without solar collector. For long vertical ground heat exchangers the improvement in the SPF_{SHP+} is below 0.2 for collector areas up to 30 m². The impact of the collector rises significantly, however, for smaller vertical ground heat exchanger lengths. Here, improvements up to 0.6 are reached due to the collector compared to the case without collector. An even annual balance in the ground is already achieved for 10 m² collector area.

The minimum temperature T_{min} is a key figure because it determines the dimensioning of the vertical ground heat exchanger length. The simulations reveal that this temperature can be shifted by 1-2 K compared to the reference case without solar collector. This corresponds to 10-20% shortening of the vertical ground heat exchanger.

Moreover, the temperature shifts are constant off-sets compared to the reference system without solar support. Of course, the shift is only constant until the allowed minimum

temperature (bivalence-point) is reached. If the minimum temperature condition is met, here -3°C, the direct electric heater temporarily replaces the heat pump.

The constant value of 1-2 K indicates that the solar induced shift arises more from long-term influences within periods of months or longer and not from a solar ground charging close to the minimum temperature appearing. A short term or direct influence would be highly sensitive to the collector area. In addition, a short term effect causing the temperature shift should also be dependent on the collector temperature level. The effect would be increased with shorter ground lengths, if this were the case.

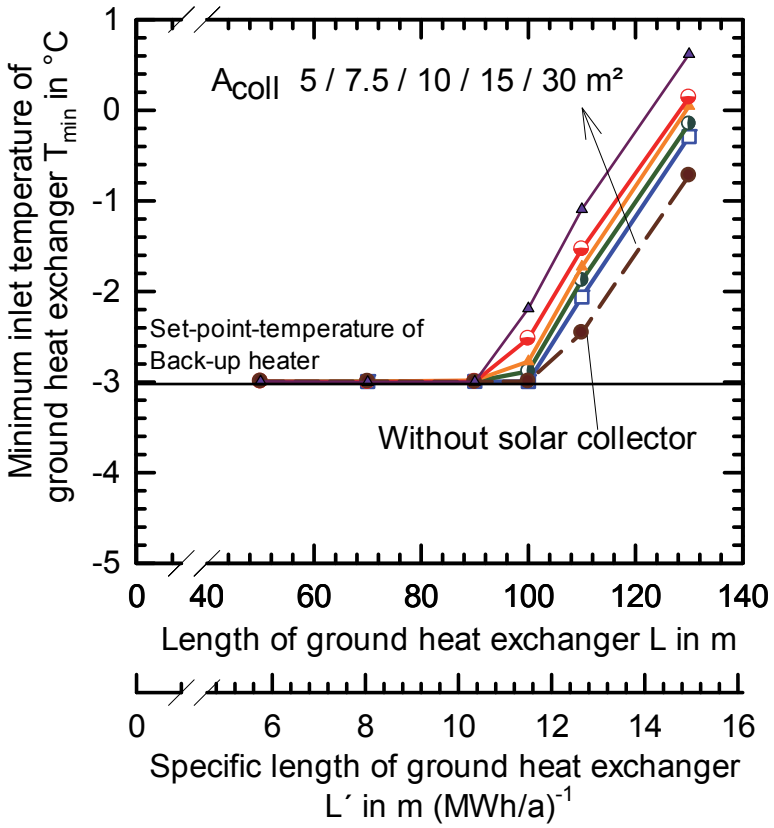

Figure 5-5: Simulated minimum inlet temperatures for the reference system conditions of Task 44 / Annex 38. The vertical ground heat exchanger length and the collector area are varied. The system concept is series in-front with a black polymer collector.

The effect of increasing solar impact with smaller vertical ground heat exchangers is more visible looking at all the source temperatures and not only at the minimum values. For instance, the system with 15 m² collector area increases the energy averaged temperature of the heat pump evaporator by 2.1 K for 130 m and by 3.4 K for 50 m ground heat exchanger length.

The simulations prove to be a powerful tool because they reveal a detailed insight into a number of variations that cannot be derived from measurements. The seasonal performance factor SPF_{SHP+} and the minimum inlet temperature $T_{min,}$ are both

important. Together they allow the parallel discussion of the system's efficiency and dimensioning. Furthermore, it becomes clear that both aspects could not be discussed independently and that constraints like the minimum inlet temperature for the vertical ground heat exchanger can have a decisive impact on the results.

5.2.2 System Concepts

The system concept on the cold side (chapter 4.2.2) determines the solar impact on the seasonal performance SPF_{SHP+} and the minimum inlet temperature T_{min}, Figure 5-6.

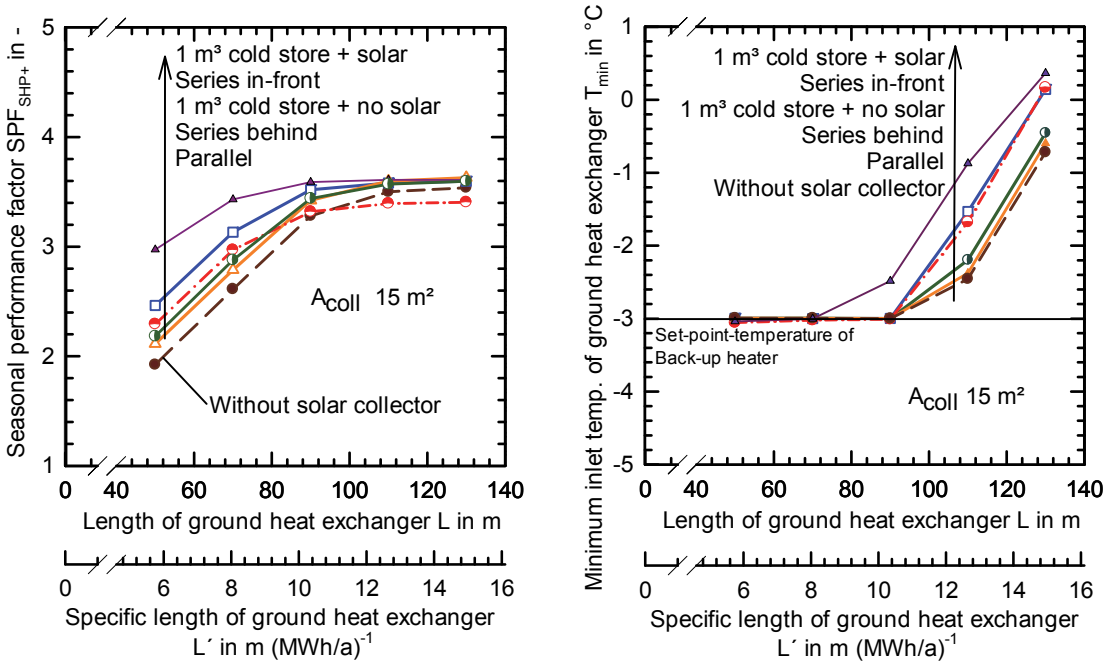

Figure 5-6: Variation of cold side system concepts with 15 m² uncovered black polymer collector

The seasonal performance factor is identical for all system concepts in the case of long vertical ground heat exchangers. The system without solar assistance, but with a 1 m³ glycol storage tank performs even less well than the reference system. Instead the concept has more pump consumption and lesser temperatures due to the necessary controller hysteresis. The additional storage capacity does not lead to higher source temperatures without solar assistance.

The system with glycol storage tank and solar collector performs best. This applies for the minimum inlet temperatures and the seasonal performance factor. This system improves the *SPF* by 0.8 for 70 m vertical ground heat exchanger. The minimum inlet temperatures are shifted by approx. 1.6 K. In addition, it is restated that further optimization of this concept appears possible.

The second system in terms of efficiency and minimum temperatures is the series in-

front system. All other systems perform significantly less for both criteria, T_{min} and SPF_{SHP+}.

A storage size of 1 m³ seems rather large for the resulting improvement. In comparison the storage volume of the domestic hot water tank is 150 l. In further simulations the storage volume was therefore reduced to 100 l to determine the viability of downsizing this cold storage volume.

Unfortunately, a smaller cold storage volume also leads to a performance drop down at smaller ground heat exchanger lengths, Figure 5-7.

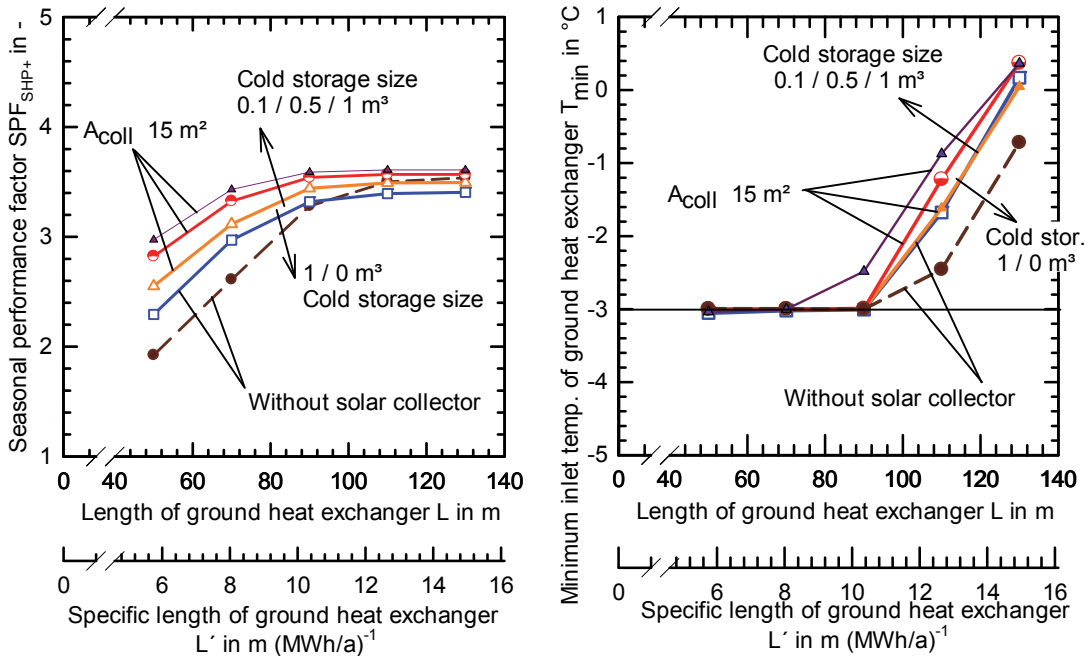

Figure 5-7: Seasonal performance factor (left) and minimum inlet temperatures (right) for variation of the cold storage volume 0.1/0.5/1 m³ and 15 m² uncovered black polymer collector in comparison to other system configurations without collector

The reduction to 0.1 m³ brings no improvement compared to 15 m² without any storage volume. In terms of efficiency a storage volume of 0.5 m³ achieves nearly the same improvement as the 1 m³ storage volume, while the improvement for the minimum inlet temperature is visibly 0.35 K lower than with a 1 m³ storage volume. Therefore, a volume appears necessary of at least 1-0.5 m³ or approximately 100-50 l per MWh usable heating demand.

All things considered, the system configuration with cold storage volume has the best performance and highest potential for downsizing the vertical ground heat exchanger. Large cold storage capacities are nonetheless required to achieve significant effects. The series in-front hydronic system achieves the highest improvements from all concepts without a cold storage volume.

5.2.3 Uncovered Collector and Even Ground Balance

The even heat balance of a ground heat exchanger is an interesting dimensioning goal, see chapter 2.2.2 and chapter 7.2. The focus of the current chapter is a parameter study on the collector yield varying some of the most sensitive parameters: the collector area, the mass flow rates, and the collector type. The study has an instructive character as the later development dimensioning rules respect these influences as part of the collector performance data required.

It is emphasized that the collector yield presented can change significantly in different systems (Figure 4-2), while the otherwise often presented seasonal performance remains more or less identical.

Figure 5-8 displays the energy balance of the ground and the collector yield. The results correspond to the simulations of Figure 5-4. A perfect 100% evenly balanced vertical ground heat exchanger is not achieved for any collector size. Depending on the collector area the ground is partly regenerated with smaller collectors and overcharged for larger collector areas. Most simulated configurations have an uneven balance Figure 5-8 (left). Only for the 10 m² collector area is the ground approximately fully regenerated without overloading.

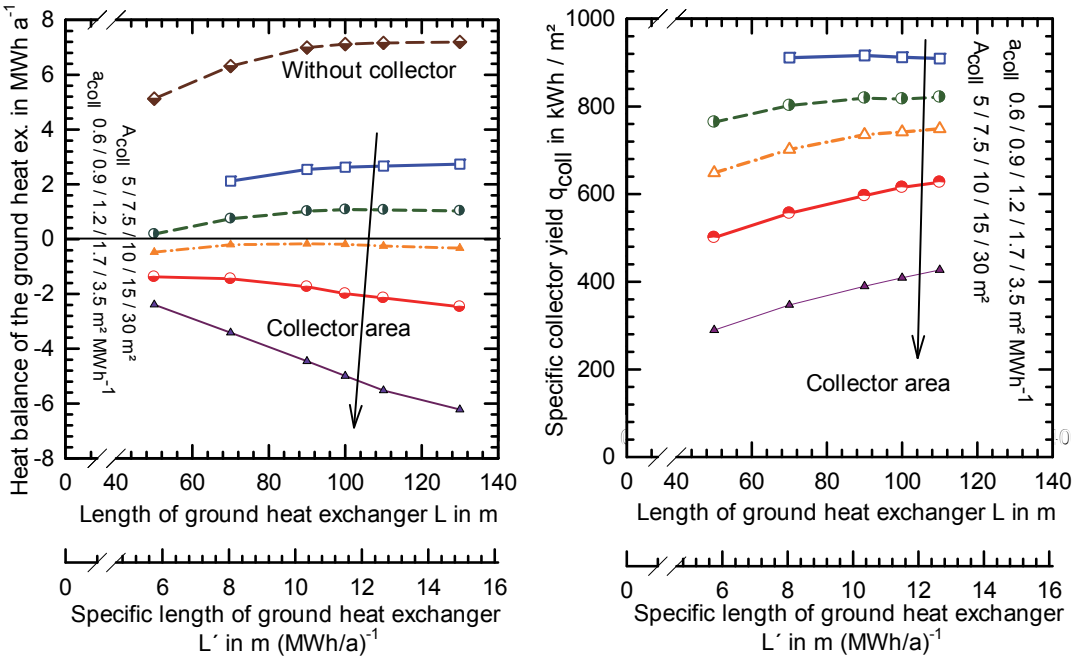

Figure 5-8: Energy balance of vertical ground heat exchanger (left) and specific collector yield (right) for varying collector areas of a black polymer collector in system concept series in-front

The achieved collector yields are impressive. Values of over 600 kWh m^{-2} are reached for the case of full regeneration. Smaller collector areas reach collector yields of over 900 kWh m^{-2} and recharge two thirds of the extracted heat with 5 m² for a complete

single family house. The total solar radiation in collector pane is 1227 kWh m^{-2}. Moreover, the specific yield is extremely sensitive to the collector area. The specific collector yield decreases to 400 kWh m^{-2} or even lower for higher collector areas.

Apart from the collector area two essential parameters, the specific collector mass flow rate and the collector type, are investigated in the following section.

For swimming pool applications, typical for uncovered collectors, high mass flow rates of 80-110 kg h^{-1} m^{-2} are common [50, p. 64]. These recommendations cannot simply be transferred to systems with ground regeneration for the following two reasons. Firstly, solar heat is less valuable on the cold side. Although it increases the heat pump efficiency, it does not directly replacing primary energy. Secondly, many uncovered collectors types, especially building integrated ones, do have a significant pressure drop in contrast to simple black polymer collectors, and high mass flow rates bear the risk of causing high electrical pump consumptions. The mass flow is therefore kept low at rates of 30 kg m^{-2} h^{-1} for the regeneration of the ground. If operated in series with the heat pump, however, the mass flow rates will be set equal to the evaporator mass flow rate of 1900 kg h^{-1}.

The collector mass flow rate for regeneration is investigated in a parameter study with values between 10 and 100 kg h^{-1}, Figure 5-9.

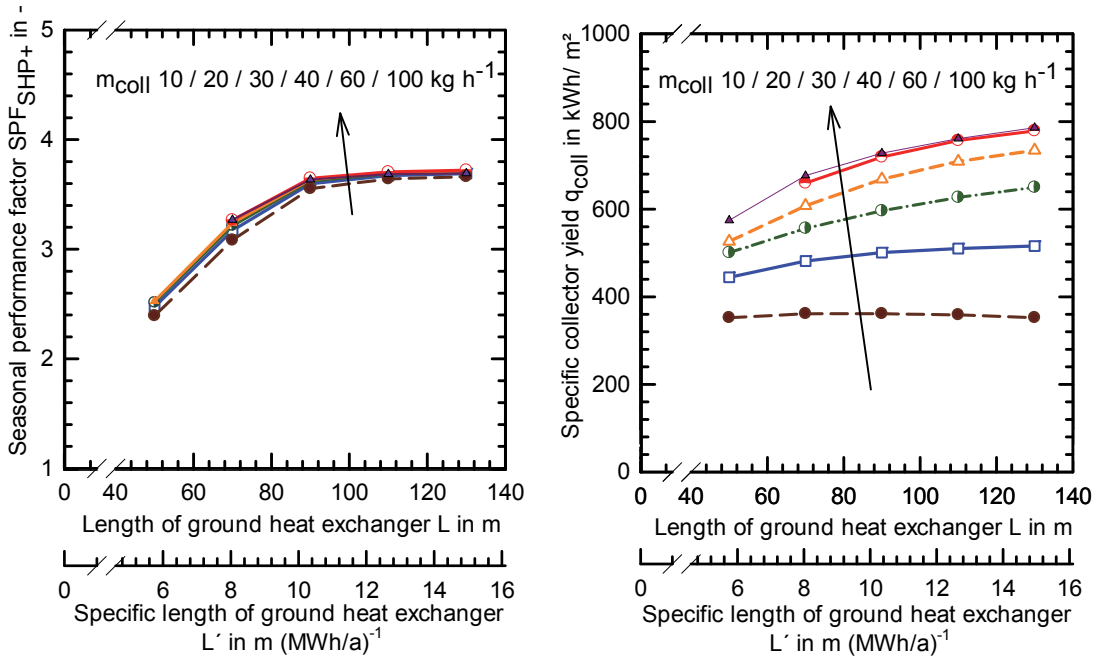

Figure 5-9: Variation of collector mass flow rate from 10 to 100 kg h^{-1} m^{-2} for different vertical ground heat exchanger lengths and 15 m² black polymer collector in system concept series in-front. Left: Seasonal performance factor $SPF_{SHP+,}$ Right: specific collector yield.

The results show a significant influence on the collector yield up to 40 kg m^{-2} h^{-1} while

the influence on the seasonal performance with collector is negligible. In the simulations the mass flow rate is 30 kg m^{-2} h^{-1}, which is a very conservative design. On the other hand, mass flow rates over 40 kg m^{-2} h^{-1} do not significantly increase the yield.

The collector type has an impact on the collector yield, too. Four different collector types are simulated with performance data from Appendix A at a flow rate of 30 kg h^{-1} m^{-2}, Figure 5-10.

The influence of the collector type on the collector yield spans approximately 20% from the worst to the best performing collector. The influence on the seasonal performance factor is negligible. In other words, for ground regeneration the collector type will have a moderate influence on the sizing and the choice of collector and presumably other aspects such as building integration or price will make the decision for or against a certain collector type.

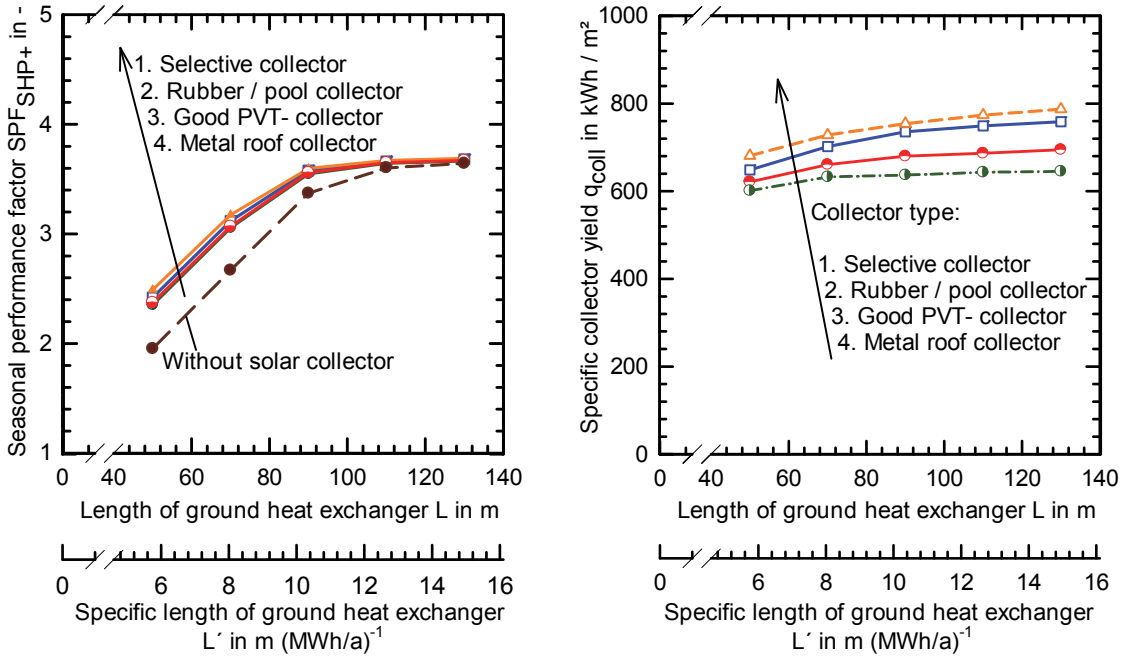

Figure 5-10: Seasonal performance factor SPF_{SHP+} (left) and collector yield for different vertical ground heat exchanger lengths in dependency of collector types and a constant collector area of 15 m²

5.2.4 Distribution of Temperatures

The simulated temperature distribution provides an insight when viewed with the integral yearly values. The distributions for the two most interesting fluid inlets are discussed: The inlet of the vertical ground heat exchanger and the heat pump evaporator. The results are given in Figure 5-11 for a vertical ground heat exchanger length of 110 m and collector areas from 0 to 30 m².

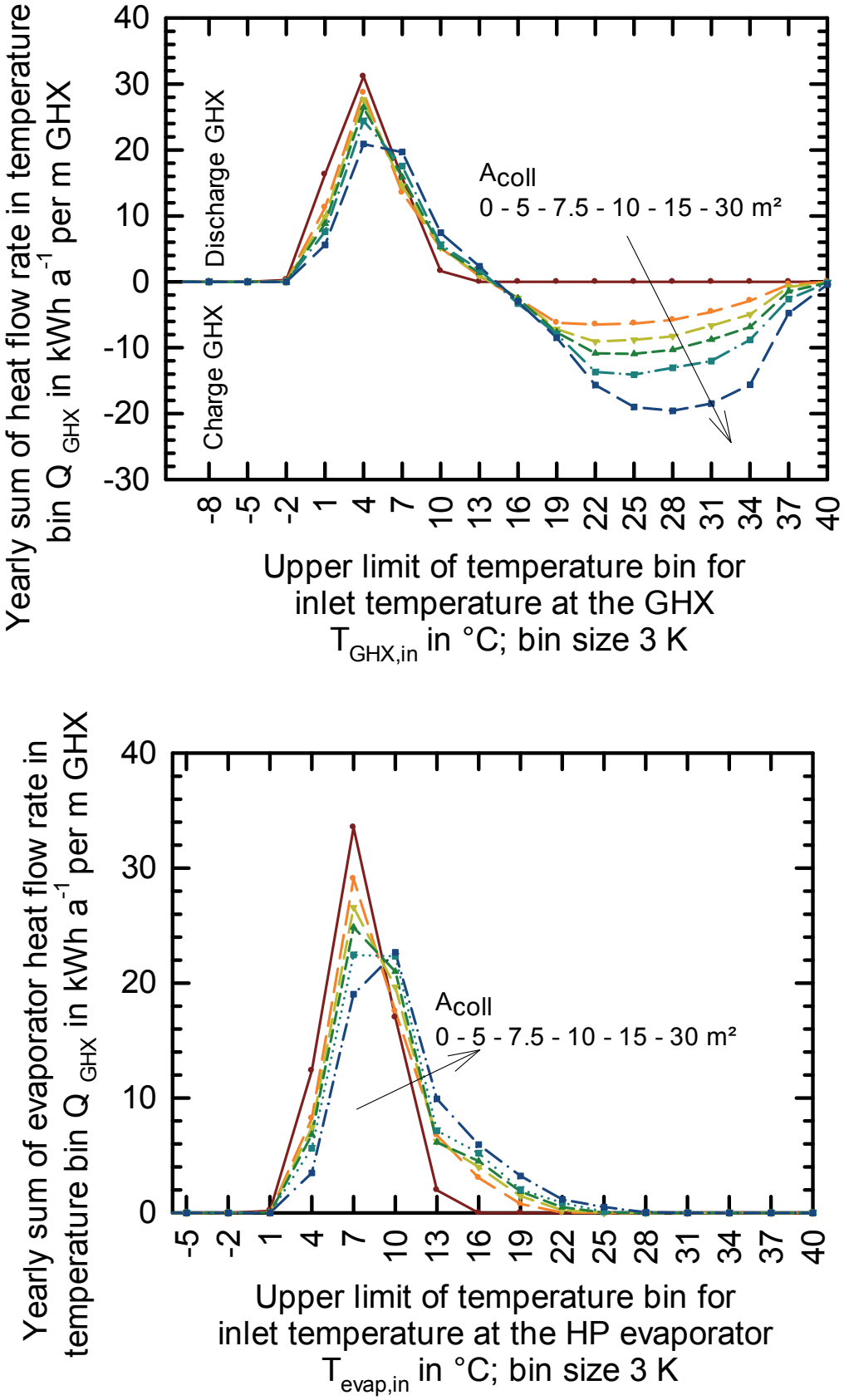

Figure 5-11: Temperatures at inlet (top) of the ground heat exchanger and of the evaporator inlet (bottom), 110 m GHX, black polymer collector

The temperature distribution is displayed in energy vs. temperature bins. In a particular temperature range, the temperature bin, the heat flow rates that appear within this bin are integrated. Thus, each data point represents the integrated energy heat flow rate of the evaporator or ground heat exchanger (y-value) that appeared in a particular temperature range or bin of its inlet temperature (x-value).

The inlet temperature of the vertical ground heat exchanger (top) is a very characteristic point in the system because it is either the evaporator or the collector outlet temperature. Correspondingly, it is colder than the evaporator inlet temperatures, which are shown in the bottom figure.

The collector yield to the vertical ground heat exchanger is mainly charged above 11°C while the heat discharge occurs below 10°C. The collector heat causes this temperature distribution shift to higher values not only for the vertical ground heat exchanger but also the temperatures of the heat pump evaporator. Here, the temperatures can be partly lifted to 15°C or even above. The shift of the source temperatures with higher collector areas can be clearly identified, though the shift is small and moves towards higher temperatures only reluctantly even with large collector areas.

Nonetheless, the whole temperature distribution does shift. This means all temperatures are lifted including the minimum, sizing relevant temperatures. Yearly average temperatures of 6°C for 10 m² and of 7.4°C for 30 m² are reached starting from an average and energy weighted evaporator temperature of 4.1°C.

The temperature shift is compared between systems with solar integration on the hot and the cold side, Figure 5-12. The systems with hot side integration use flat plat collectors because they achieve higher and more typical solar fractions than is achieved with solar hot side integration with uncovered collectors. The simulated systems with flat plate collectors are also presented and described in [106].

Two basically different system concepts with flat plate collectors are simulated. In the first system a 5 m² flat plate collector assist the domestic hot water preparation. In the second system the collector with 15 m² and 30 m² also supports the space heating in combination with solar combi-store of 800 l volume. These systems represent typical solar direct systems and achieve high solar fractions up to 34% and seasonal performances SPF_{SHP+} up to 6 and correspond to systems presented in [106].

The source temperatures are influenced little in such systems with hot side integration despite their solar fraction of up to 34%. The cold side integration with 15 m² uncovered

collector area has much graeter influence on the source temperatures. This applies correspondingly for the optional shortening of the vertical ground heat exchanger.

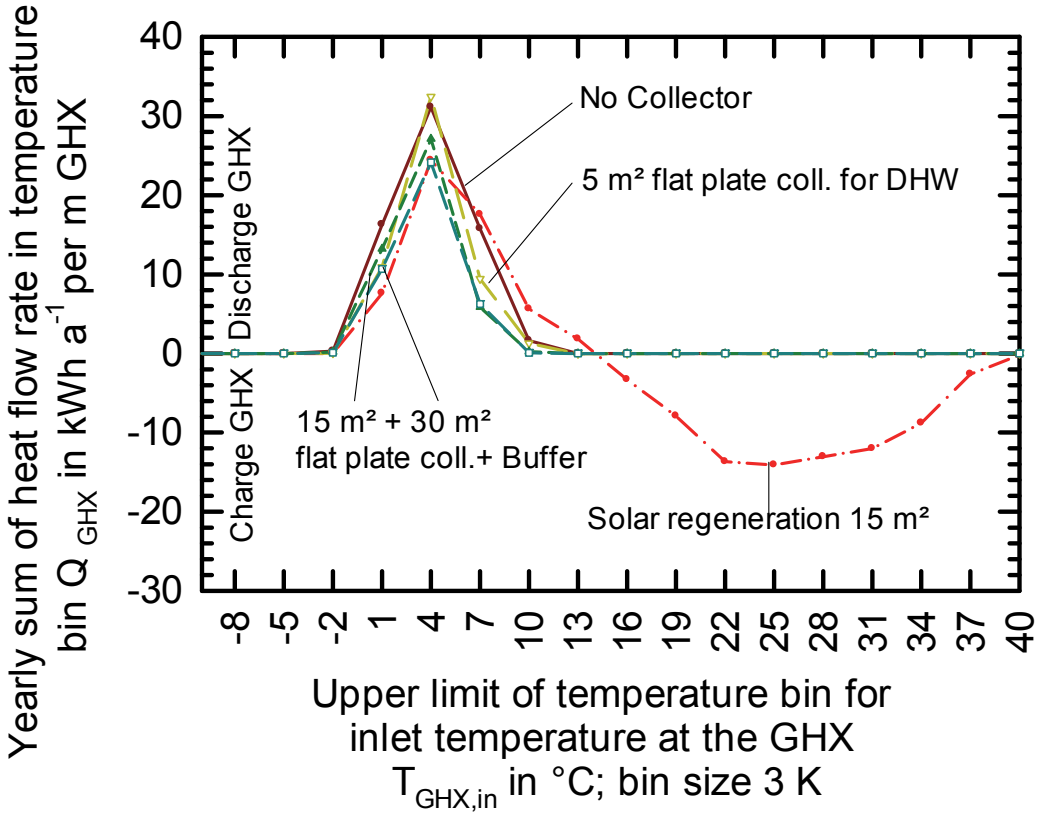

Figure 5-12: Temperatures at the vertical ground heat exchanger inlet for different systems at 110 m GHX length, solar regeneration system with 15 m² uncovered black polymer collector, domestic hot water and buffer concepts for space heating assistance with flat plate collector

5.2.5 Shortening the Ground Heat Exchanger

The simulations presented in this chapter have also been published in Annex G to Report C3 of IEA SHC Task 44 / HPP Annex 38 [105, pp. 11–22].

The solar regeneration is of minor relevance for the seasonal performance in conventionally dimensioned systems. However, the temperature level of the vertical ground heat exchanger is lifted and its length can be reduced. The character of such downsized systems is examined also on monthly data basis for 4 different systems with nearly identical seasonal performance SPF_{SHP+}. The vertical ground heat exchangers are gradually reduced while the heat source side is assisted by an uncovered collector and a glycol storage tank (Figure 5-13).

1. The reference system without any solar collectors is the starting point for this investigation. The vertical ground heat exchanger length is 110 m, which is just above the minimum temperature limit of -3°C (compare Figure 5-5) (**#1**

Reference).

The seasonal performance SPF_{SHP+} is 3.50.[1]

2. The same system with identical vertical ground heat exchanger length is simulated with 15 m² uncovered black polymer collector (**#2 Reference+coll**). The system configuration for the collector integration on the cold side is series before (compare Figure 5-5).

   The seasonal performance SPF_{SHP+} is 3.55.

3. The system is identical to system #2 but with a smaller vertical ground heat exchanger of 90 m. (**#3 Downsize+coll**). (compare Figure 5-5)

   The seasonal performance SPF_{SHP+} is 3.48 .

4. The most downsized system has a vertical ground heat exchanger of 70 m, a black polymer collector with an area of 15 m² and an additional glycol storage tank with a volume of 1 m³ (**#4 Downsize+coll+tank**). (compare Figure 5-6).

   The seasonal performance SPF_{SHP+} is 3.44.

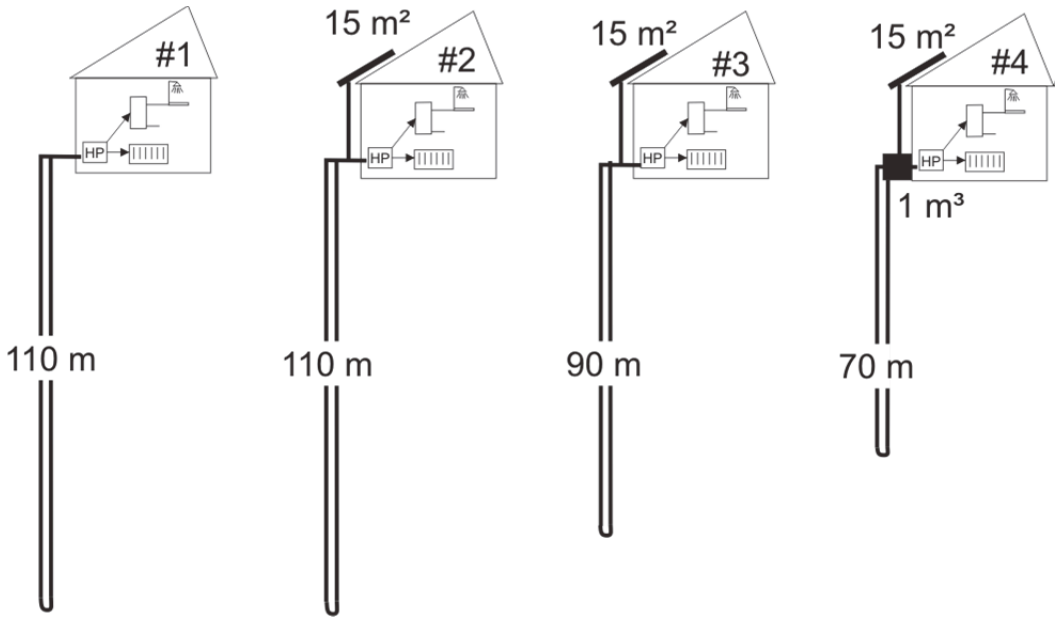

Figure 5-13: Systems #1 to #4 for downsized vertical ground heat exchanger length from 110 m to 70 m by solar assistance on the cold side and a glycol storage tank of 1 m³. The uncovered black polymer collector has a collector area of 15 m². All 4 systems have a nearly identical seasonal performance SPF_{SHP+} between 3.55 and 3.44.

All four systems have very similar seasonal performances and overall electrical consumption although their vertical ground heat exchanger length is reduced. The solar

[1] The reference systems without a solar collector and with smaller ground heat exchangers have a decreased performance of 3.3 for 90 GHX length and 2.7 for 70 m GHX length.

collector allows shortening by approx. 20 m or 18%. Even further downsizing is possible by another 20 m, which is 36% of the reference length, if the system is combined with a 1 m³ cold storage tank.

The shortening of the vertical ground heat exchanger is not only an economical question of optimization. (The solar collector or cold storage tanks will increase the investment costs.) It extends in general the application range of vertical ground heat exchangers in areas with drilling depth restrictions and allows, as indicated previously, sustainable operation in general.

Moreover, the monthly energy distribution, Figure 5-14, already gives rise to the subject of the electrical load in the course of the year. The shortening of the vertical ground heat exchanger leads to lower compressor consumption but at the price of higher parasitic auxiliary consumer loads and the direct electric heater.

In the example given the electric load distribution differences are minor and all three systems with solar collector reveal very similar energy flows. The solar heat is injected to the ground mainly in summer. Here, the compressor energy can be reduced, while the consumption of the parasitic auxiliary consumers is increased. The performance of the systems with reduced boreholes decreases slightly because the temperature limit for the vertical ground heat exchanger is met. The direct electric heater causes additional consumptions in January and December. In the systems presented the additional winter load is small and negligible compared to the benefit from the shortening of the vertical ground heat exchanger. Nevertheless, this discloses clearly the necessity to assess not only the overall electrical consumption but also take into account the seasonal distribution of the electrical load.

Generally speaking, it is always tempting to balance solar benefits, typically appearing in summer, with smaller components that lead to more consumption in winter. On an annual basis the systems perform well although their electric load in winter is high.

Much more imbalanced systems with high winter loads but similar seasonal performances are presented in chapter 5.4.2 for an air heat source and in chapter 5.2.5 for solar assisted systems without any ground source.

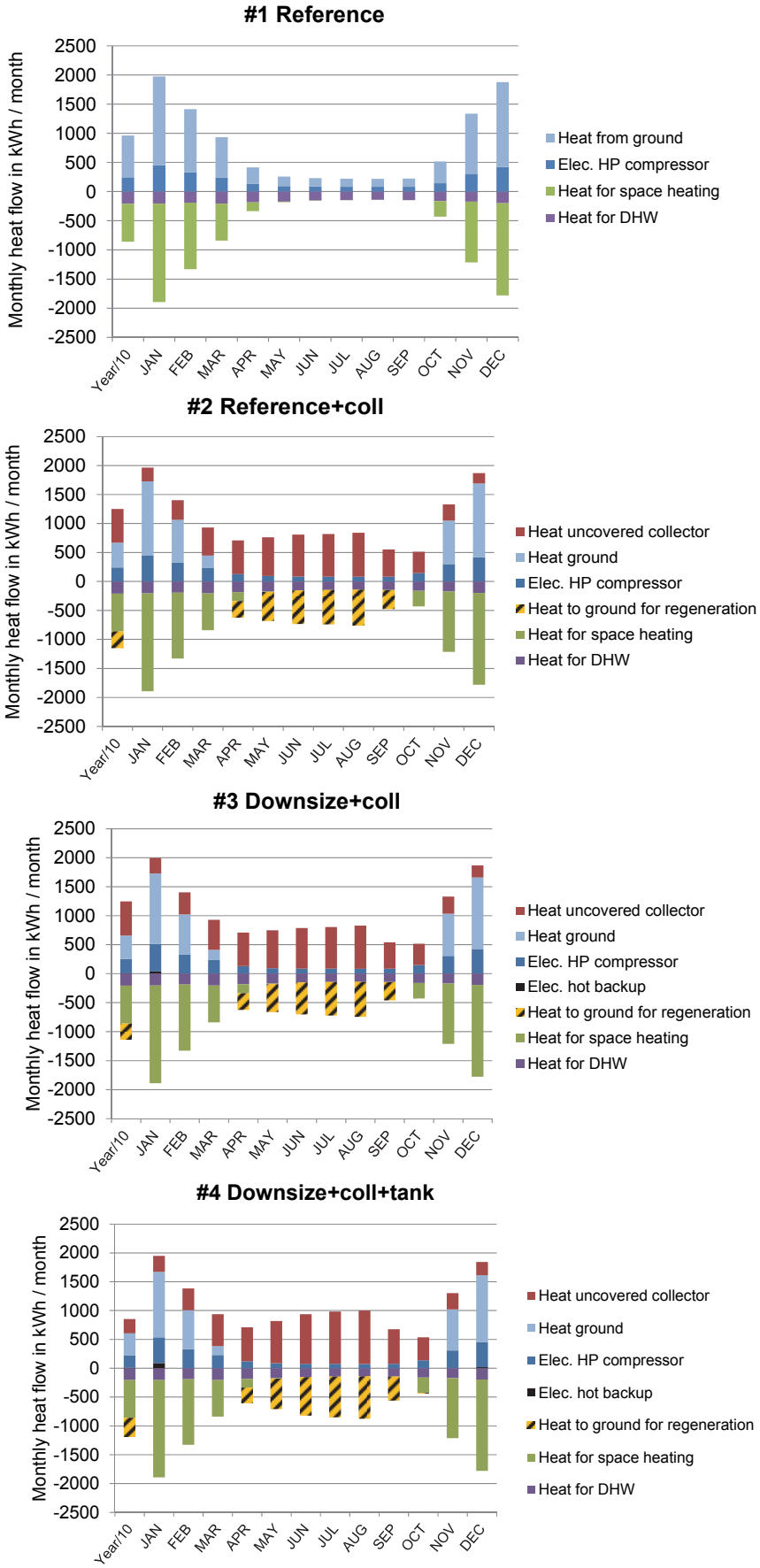

Figure 5-14: Monthly energy net flow rates of components for the simulated systems from top to bottom: #1 reference with 110 m GHX without solar; 15 m² black polymer in systems #2 reference+coll with 110 m GHX; #3 Downsize+coll with 90 m GHX; #4 Downsize+coll with 70 m GHX and 15 m².

5.3 Sensitivity Analysis

5.3.1 Introduction

The detailed dynamic simulation of complex systems is time consuming and economically not feasible in the planning process of smaller systems. The high effort arises from the immense amount of comprehensive model specifications, connections and detailed parameterization that is required. Moreover, the implemented models usually have high calculation costs of more than 1 hour per simulation, which makes numerical optimization difficult. As a result, dynamic simulations are often restricted to the context of research and development.

As pointed out before, every set of boundary conditions or any system model modification leads to different results. The results are transferable, if changes appear. Most systems, however, behave comparably to applied changes. A simple sensitivity analysis is conducted for the system to derive a transferable and general understanding of the main influences.

The major part of the sensitivity analysis from section 5.3.4 to 5.3.7 is made for one particular design point. At this reference point the parameter investigated is varied in the system model while all other parameters are held constant. The reference point is defined for two system concepts: without solar collector and one system with solar cold side integration series in-front with 15 m² uncovered black polymer collector. Both systems have a vertical ground heat exchanger length of 110 m.

The influences are grouped by location parameters, properties of the ground, design parameters of the vertical ground heat exchanger, and heat pump parameters.

5.3.2 GHX Model

Numerical parameters and the choice of the vertical ground heat exchanger model have an important influence on the simulated outcomes. The simulation run-time necessary, some numerical parameters and the model choice are discussed.

For conventional ground source heat pump systems the simulation run-time considered can be essential. Several years of operation might pass before a quasi-steady state is reached in the ground temperature regime. As pointed out before, a single vertical ground heat exchanger has the smallest long-term influence of all possible vertical ground heat exchanger configurations. Nevertheless, the influence of the simulation run-time on the results is investigated. Figure 5-15 shows the result of a simulation for 20

years with a single vertical ground heat exchanger.

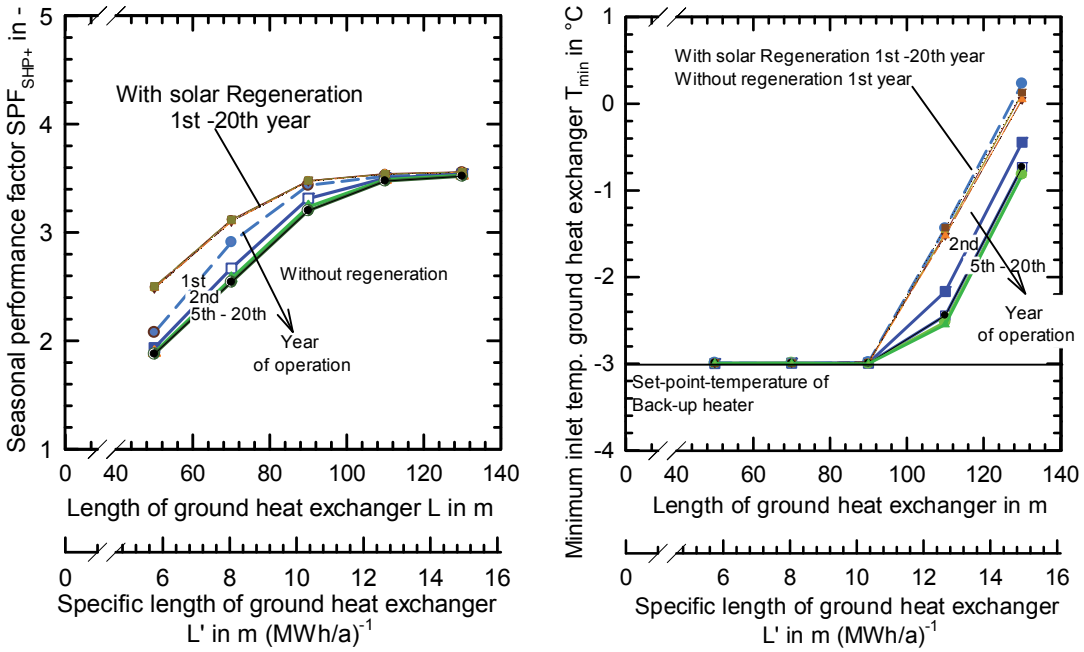

Figure 5-15: Variation of the simulation run-time for the seasonal performance SPF_{SHP+} and T_{min} with and without solar regeneration in a series in-front system with 15 m² black polymer collector

The systems with solar regeneration reveal absolutely no long-term shifting of the seasonal performance SPF_{SHP+} and the minimum inlet temperatures T_{min} from the first year of operation.

The quasi-steady state equilibrium is reached after 5 years without solar regeneration. Already in the second year of operation the seasonal performance factor is only around 0.1 higher than the value in the 20th year and even smaller off-sets appear for most operation points. For the minimum inlet temperature the drift between the 2nd and the 20th year of operation is 0.4 K.

The simulation run-time can be reduced immensely accepting this error of 0.4 K for systems without regeneration. All simulations values are therefore taken from the second year of operation because in systems with regeneration no long-term influence appears and in systems without regeneration the only noticeable influence is 0.4 K between the 2nd, 5th or 20th year of operation. This 0.4 K off-set is neglected in all simulation results presented.

Furthermore, the influence of some numerical parameters has been tested for the applied DST model with pre-pipe. The parameters checked are: ground layer thickness, number of radial nodes and number of axial nodes of the model. In the example given these have a negligible or no influence, Table 5-1.

Table 5-1: Influence of numerical parameters in the reference system without solar regeneration. The vertical ground heat exchanger is simulated with the DST- model with pre-pipe and has a length of 110 m².

Varied parameter	Value Reference/min/max	SPF_{SHP+} Min / Max	T_{min} Ref +/-
Thickness of ground layer in m	160/160/3000	0.0024	0.066
No. of radial segments	1/1/30	Influence < 0.002	
No. of axial segments	10/1/30		

Finally, the simulation results can be very dependent on the choice of the model. For illustration two different vertical ground heat exchanger models are compared.

All simulations in this thesis are conducted with the duct ground storage (DST-) model with pre-pipe [34]. The model is validated by Pärisch [124] in the same project that comprises this thesis. The model proves to have a high accuracy for small time steps and transient operation. In the figures presented the model has the number #A.

The alternate model (#B) presented is the same (DST-) model [34], but without pre-pipe extension. This model has no fluid and filling capacity and accordingly shows strong deviations in measurement during the starting sequences of the borehole operation. The following model comparison has also been presented in [106].

The two models are simulated in systems with and without solar regeneration, Figure 5-16, and with and without a buffer storage tank, Figure 5-17.

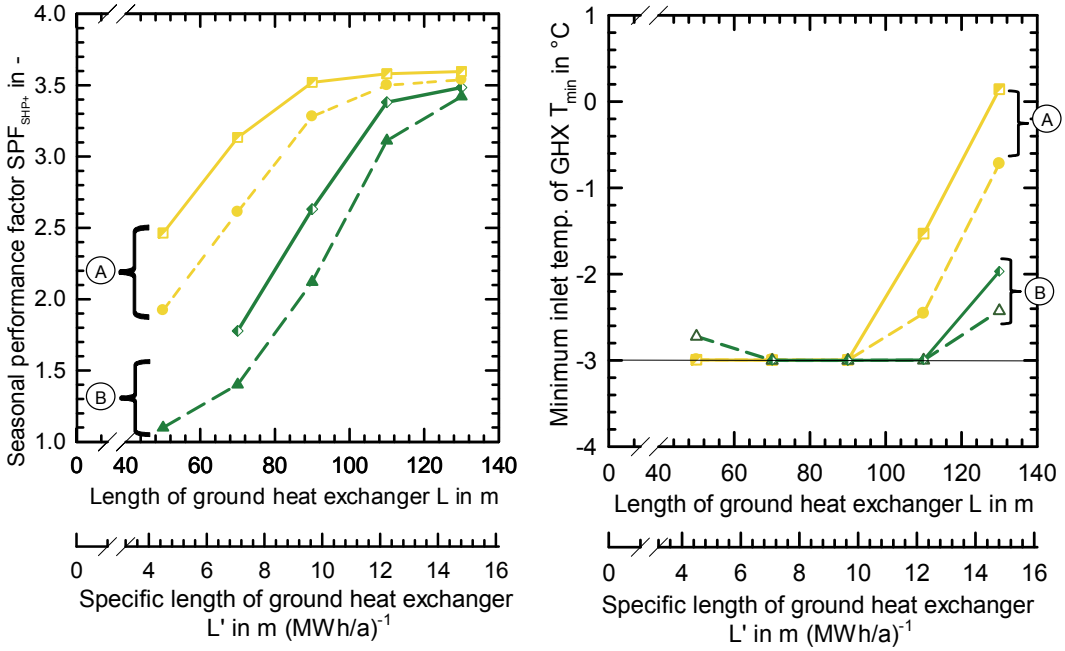

Figure 5-16: Comparison of simulation models for vertical ground heat exchangers with and without solar regeneration in seasonal performance factor and $T_{min,}$ The models compared are: #A – DST model with pre-pipe; #B – DST model without pre-pipe

The simulations with buffer storage tank reflect the influence due to different kinds of operation characteristics. The detailed parameter settings for the model configurations

are given in Appendix E. The results disclose clear deviations between the models especially for the minimum inlet temperatures at smaller vertical ground heat exchangers.

The lowest performance and lowest minimum inlet temperatures are simulated with the DST model (#B). This outcome is convincing because the model has no pre-pipe and therefore a much lower heat capacity in comparison to the DST model with pre-pipe (#A). The pre-pipe and its additional heat capacity lead to a lower, but longer lasting heat extraction from the borehole, which has a positive effect on the source temperatures. These are around 2 K with pre-pipe. In simulation with short time steps it is essential to include transient effects in the borehole model.

The DST-model with pre-pipe (#A) has higher seasonal performance values in correspondence to the temperatures. Seasonal performance falls significantly for shorter vertical ground heat exchangers. Both, minimum temperature and seasonal performance are more sensitive to the model choice than to the influence of solar assistance.

The model differences in the systems with buffer are very similar, Figure 5-17. Here, the DST model without pre-pipe (#B) has also the lowest temperatures and seasonal performances. The differences between with buffer and direct floor heating are also minor. This is highlighted because the buffer tank charging leads to a different heat pump run-time distribution with less on-off-cycles, compare Figure 4-10.

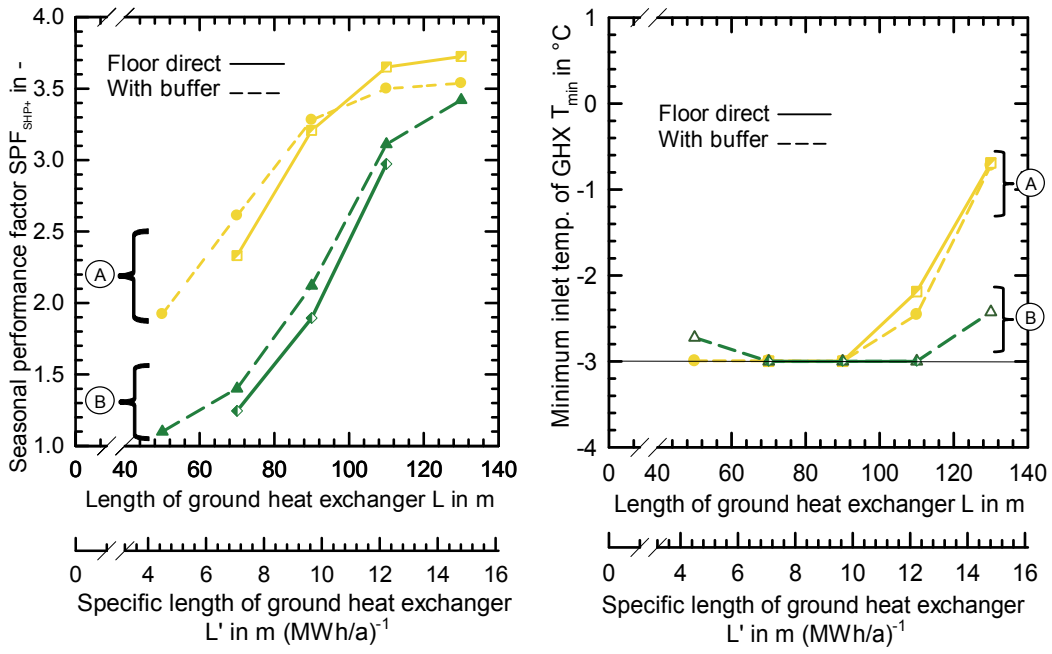

Figure 5-17: Comparison of ground heat exchangers models in systems with direct floor heating and with buffer system. Systems have no solar assistance. Left: simulated seasonal performance factor SPF_{SHP+}. Right: minimum inlet temperature $T_{min.}$ The compared models are: #A – DST model with pre-pipe; #B – DST model without pre-pipe

The differences between models mainly concern the minimum temperatures and therefore the shortening of the ground heat exchanger. The differences in the performance are minor for longer heat exchangers.

In summary, the choice of model can have an impact on the simulation results. The DST-model with pre-pipe (#A), which is utilized in all system simulations, gives higher temperatures and seasonal performances compared with the DST model (#B) without pre-pipe. The widespread DST model without pre-pipe (#B) , which leads to the smallest temperatures and correspondingly the longest vertical ground heat exchangers, does not include capacity effects.

5.3.3 Ground Temperature Limit

The vertical ground heat exchanger is protected from excessly cold temperatures by a direct electric heater (chapter 2.2.2). The temperature $T_{protect}$ limit for the electric heater activation is varied between -5°C and +2°C in systems with a single vertical ground heat exchanger with lengths from 50 m to 230 m, Figure 5-18. These temperature limits cover the range of limits given by the VDI 4640 [17] for safe operation with water, for which 2 K safety distance from 0°C should be kept to certainly avoid freezing in the heat exchangers. Freezing of the evaporator heat exchanger usually means the complete destruction of the heat pump.

The results reveal no influence for long vertical ground heat exchangers and a large influence for shorter vertical ground heat exchangers. Even further shortening is possible through solar assistance, Figure 5-18 right. The performances shift around 1 K due to solar support.

Even with very long vertical ground heat exchanger lengths the performance is connected to the ground temperature regime and rises only marginally. An operation with water seems unrealistic despite the solar assistance on the source side.

The results are also presented for shorter ground heat exchanger lengths up to 130 m in [106].

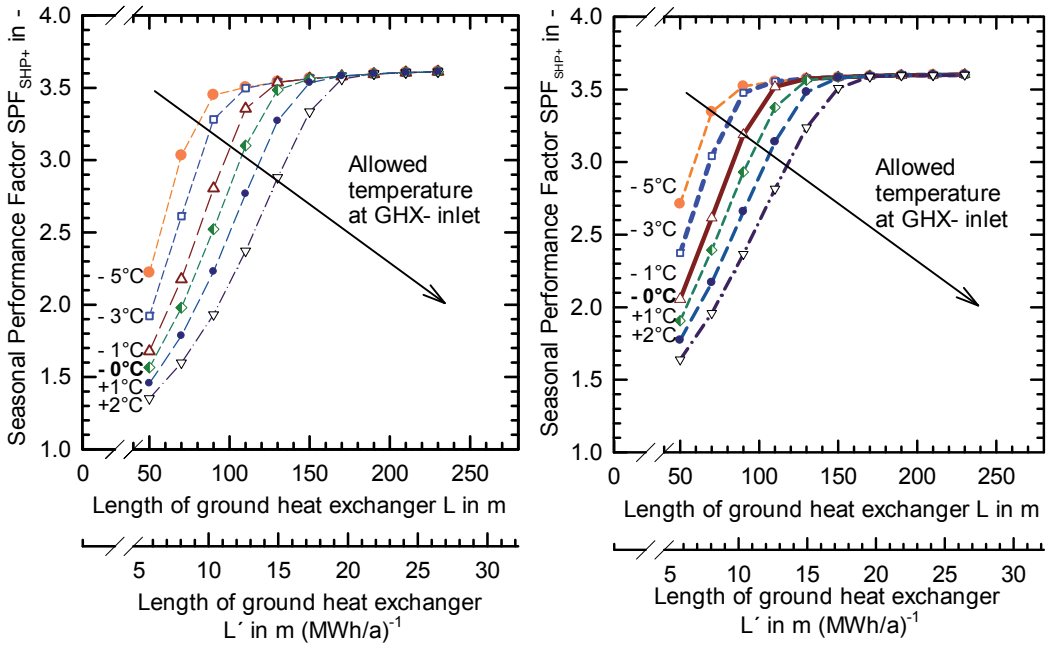

Figure 5-18: Seasonal performance factor for different vertical ground heat exchanger lengths between 50 and 230 m for varying setting temperatures for the direct electric heater temperatures (bivalence temperature) left without solar regeneration, right with 15 m² black polymer collector connected series in-front

5.3.4 Location Parameters

The varied location parameters concern the vertical ground heat exchanger, for which the following variations are implemented

- The undisturbed ground temperature for the vertical ground heat exchanger was changed in the simulations. In the model the initial surface temperature, the maximum, minimum and average preheating temperatures of the internal storage volume temperatures (Parameters. 30, 33, 34, 36, Appendix E) and the surface temperature (input 3) have been changed by a constant off-set.
- The heat conductivity and the volumetric heat capacity of the ground are varied by changing the parameters (Par 40, 41) of the vertical ground heat exchanger model. The values are derived from VDI-4640 part 2 [132, p. 7] and cover the majority of existing ground properties.
- The previously discussed temperature limit (see chapter 0) is a location parameter because it is a fixed legal restriction connected to the particular location. The limit was varied according to the description in chapter 0.

All values applied are presented in Table 5-2 and the results in Figure 5-19.

The following findings can be derived from the parameter variation:

- The most sensitive parameter for the seasonal performance is the temperature limit $T_{protect}$.
- The most sensitive parameter for the minimum temperature limit T_{min} itself is the ground temperature. The influence would certainly be linear over the complete investigated temperature range, but the minimum temperature cannot decrease below the set temperature limit $T_{protect}$. Accordingly, the maximum decrease of the parameter is confined to a lower limit. The same applies for low values of the heat conductivity of the ground and many values in the following.
- If the lower limit T_{min} is reached due to variation of a parameter, the seasonal performance will be strongly influenced.
- The maximum decrease of T_{min} has an off-set of around 0.7 K with and without solar collector because the reference temperature of the systems with and without solar assistance is different, too. In general, the systems with solar collector reveal a slightly lower sensitivity.
- The heat capacity of the ground has a small influence only on the SPF_{SHP+} and T_{min}. The heat capacity alone has a clear linear influence.

Table 5-2: Overview on the location parameter range for the sensitivity analysis displayed in Figure 5-19

Varied parameters	Unit	Refe-rence	Max	Min
Heat conductivity ground λ	W m^{-1} K^{-1}	2	1	4
		100%	50%	200%
Heat capacity of the ground c_p	MJ $m^{-3}K^{-1}$	2	1.3	2.5
		100%	65%	130%
Undisturbed ground temperature $T_{g,undis}$	°C	12.5	+17.5°C	+7.5°C
Temperature limit of the location $T_{protect}$	°C	-3	+2°C	-7°C

Reference Values		Without solar	With solar
SPF_{SHP}	-	3.60	3.66
T_{min}	°C	-2.14	-1.52

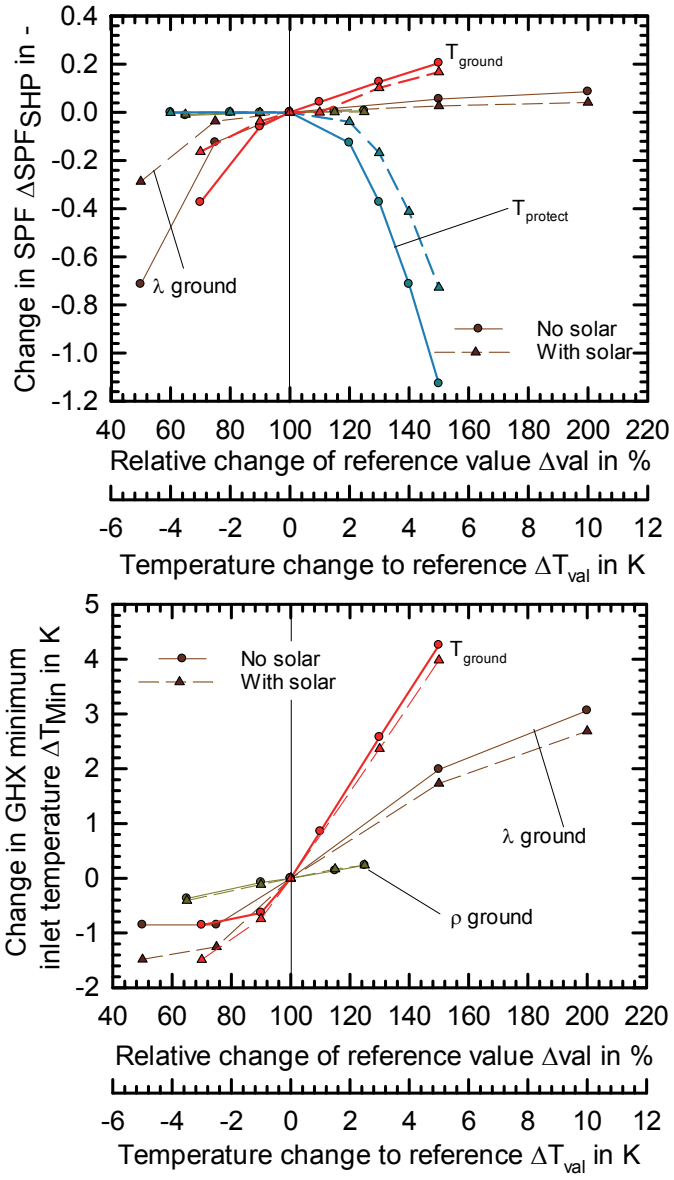

Figure 5-19: Sensitivity of the seasonal performance factor SPF_{SHP} and for the minimum inlet temperature T_{min}. The varied parameters are the undisturbed ground temperature, the heat conductivity, the heat capacity of the ground and the temperature limit for the vertical ground heat exchanger minimum inlet temperature

5.3.5 GHX core

The parameters of the inner properties of the vertical ground heat exchanger have been varied to determine their sensitivity in the system. All of the parameters studied can be influenced by choice of material or design parameters. Changes are made for the analysis within the vertical ground heat exchanger model, which is the DST-model [57] with pre-pipe [133]. The configurations are made as follows:

- The **borehole resistance** R_b has been changed from 0.03 to 0.2 m K W^{-1}, which represents the complete range of from extremely good to very bad resistances. Loose [41, p. 53] gives examples of 0.05 m K W^{-1} for good to 0.15 m K W^{-1} for bad resistances. Koenigsdorff uses [23, p. 225] uses values from 0.3 to 0.24 m K W^{-1} for an analytic sensitivity analysis.

  In contrast to all other investigations, in this thesis the simulations are performed with another DST-model implementation: the type 557**c_thermal_resistance_known.** (In all other simulations type 557**d_design_model** was used.). The reference value of the borehole resistance is determined at 0.08 m K W^{-1} by a geothermal response test performed in the simulation with the design model in the reference case. The required internal coupling resistance R_a is calculated to 0.235 m K W^{-1} by EED [35] from the design parameters. Detailed information about the calculation of the thermal resistances within the borehole for EED and the DST model can be found in [42] Eq. 7/10/28.
- The **U-tube diameter** is varied for different U-tube diameters radii r1. The tubes are positioned at a distance of 30 mm to the diameter of the drilled borehole R_2. This 30 mm distance is reasonable to encapsulate the tubes in case of leakage and is the legally demanded minimum safety distance [134, p. 36] in Lower Saxony, Germany. The geometrical parameters of the pipes can differ slightly depending on the manufacturer specifications. Some pipe diameters for polyethylene tubes can be found in [135, p. 64], [136, p. 165] and [137, p. 4]. The positioning distance piece for the U-pipes is measured at a sample from [137, p. 11] for the default U-tube and then transferred to the other tube sizes. The geometrical data applied is given in Figure 5-4 and Table 5-3.

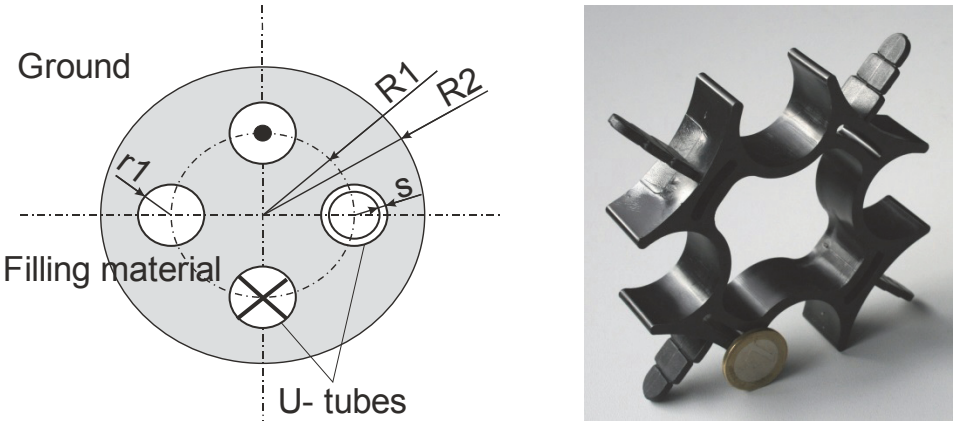

Figure 5-20: Left: Applied geometric parameters of the vertical ground heat exchangers for different pipes. The radii can be calculated as R1 = R2 – $30_{distance}$- r1, Right: Spacer for U-Tube pipes in a vertical ground heat exchanger

Table 5-3 Applied geometric parameters of the vertical ground heat exchangers for different U-tube diameters.

Outer diameter		1 x 32	2 x 25	2 x 32 (Default)	2 x 40	2 x 50
Nominal diameter		1 x DN 25	2 x DN 20	2 x DN 25	2 x DN 32	2 x DN 40
Percentage diameter		50%	78%	100%	125%	156%
R1	mm	29	33	40	58	60
R2	mm	75	75	86	108	114
r1	mm	16	12.5	16	20	25
S	mm	3	2.3	3	3.7	4.6

- The **thermal properties of the filling material,** the heat conductivity of the filling material λ_{fill} and its heat capacity ρ_{fill}, are varied in a range that extend the properties of current filling materials.

  The heat conductivity λ_{fill} is varied from 0.6 to 3 W $m^{-1}K^{-1}$ and the heat capacity of the filling material ρ_{fill}, is included only in the extended model within the pre-pipe wall capacity. This influence is varied from 1.3 kJ kg^{-1} K^{-1} to very high values of 5.3 kJ kg^{-1} K^{-1}, which are significantly higher than typical values presented in [135, p. 130]. The reference value is 2.65 kJ kg^{-1} K^{-1} and also used in the experimental model validation for the prepipe conducted by Pärisch [124].

The results are displayed in Figure 5-21 and Table 5-2.

The following findings are derived:

- The low impact of the parameters on the seasonal performance is a surprise, though minimum temperature sensitivities are well in accordance with expectations. Furthermore, the minimum inlet temperature is decreased for

higher borehole resistances R_b while higher heat conductivities or capacities for the filling and the U-tube lead to higher minimum inlet temperatures. In other words, a good filling material, bigger U-tubes or a low borehole resistance reduces borehole length necessary. The performance, however, is hardly improved.

- The **pipe diameter** of the U-tube improves the minimum inlet temperature. The pipes contain more fluid and also achieve a better heat transfer rate through a larger heat transfer area. Both effects will presumably have a positive influence on the minimum temperature.
- The **borehole resistance** R_b beyond 130% leads to an only slight decrease in the minimum temperature because it is hitting the temperature limit of the direct electric heater. Even so, the performance is only slightly decreased in this range.
- Low heat conducting **filling material** or a small **pipe diameter** reduces the minimum temperatures more in systems with solar collector than in systems without solar collector. In both cases the temperatures drop to their lower possible limit. With a solar collector the solar yield is slightly decreased because of the higher operating temperature. The positive impact of the solar collector is also reduced and the annual collector yield is 5% smaller.

Table 5-4: Overview on the location parameter range for the sensitivity analysis displayed in Figure 5-19.

Varied parameters	Unit	Min	Refe-rence	Max
Thermal borehole resistance	Km W^{-1}	0.03	0.08	0.2
		38%	100%	250%
Heat conductivity of filling material	W m^{-1} K^{-1}	1	1.7	3
		59%	100%	176%
Heat capacity of filling material	kJ kg^{-1} K^{-1}	1.3	2.65	5.3
		50%	100%	200%
Diameter U-tube	mm		See Table 5-3	
		50%	100%	156%

Reference Values			Without solar	With solar
	SPF_{SHP}	-	3.60	3.66
	T_{min}	°C	-2.14	-1.52

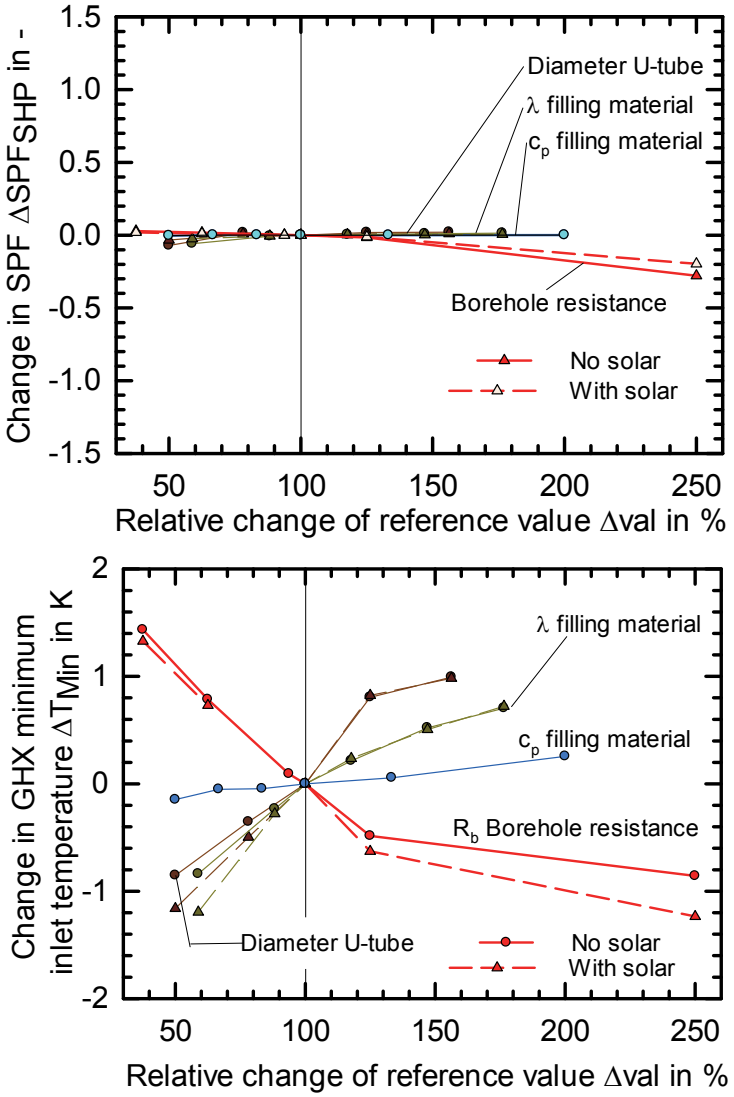

Figure 5-21: Sensitivity of the seasonal performance factor SPF_{SHP} and for the minimum inlet temperature T_{min}. The reference point is a system with 110 m according to Figure 5-4. Solar system concept is series in-front with 15 m² black polymer collector.

5.3.6 Ground heat exchanger

Constraints set in context of the estate induce the design of vertical ground heat exchangers in many real applications. Some of these parameters are varied to determine their sensitivity. The following configurations are made:

- The **vertical ground heat exchanger length** has been varied.
- The **vertical ground heat exchanger distance** is varied for 6 GHXs with 18.3 m length each. This corresponds to an overall length of 110 m, which is the reference case with one single vertical ground heat exchanger. The results presented are taken from the second year of operation.
- **Ground buried connecting pipe,** Figure 5-22, models have been added to the system model between the heat pump and the vertical ground heat exchanger and the length of the pipes is varied. (In the reference case no connecting pipe is simulated. The heat pump is directly above the vertical ground heat exchanger.) The buried pipes are defined as a non-insulated PE-pipe with an inner diameter of 69 mm and buried in a depth of 1.4 m [137, p. 27] simulated with the type 952 [138]. The model calculates the heat conduction in the ground around a pipe with a numerical strictly cylindrical mesh of capacity nodes. Outside this cylindrical mesh the undisturbed ground temperature is set as boundary condition as a function of depth and surface temperature. Heat conduction is considered only.

  

  Figure 5-22: Buried horizontal connecting pipe at ISFH test facility

  Two cases are simulated. One case is for the typical point of 110 m vertical ground heat exchanger and the other case is for short vertical ground heat exchangers of 50 m length. The presented minimum temperature difference ΔT_{min} is given for the temperature between buried pipe and the GHX inlet.

The results are displayed in Figure 5-23 and Table 5-7.

The following findings are derived:

- The **length of the vertical ground heat exchanger** has a strong influence on seasonal performance and on ground temperatures. The temperature limit for the vertical ground heat exchanger can clearly be identified for shorter vertical ground heat exchangers.

- The **distance between 6 adjacent boreholes** is investigated. Slight differences appear compared to the reference system with a single vertical ground heat exchanger. The set temperature limit $T_{protect}$ is hit in most of the variations displayed because of interference between the vertical ground heat exchangers. A single vertical ground heat exchanger of the same length does not reach this limit.

  The results still reveal two interesting points. Firstly, the reference temperature is lower than for a single heat source and does not increase significantly with higher distances. Secondly, systems with solar collector show nearly constant values for the $SPF_{SHP+,}$ even though the temperature limit is met. In contrast, the SPF_{SHP+} decreases strongly of the systems without solar collector.

  To conclude, reducing the borehole distance might increase the interference effects between the systems and especially in systems without solar regeneration. On the other hand, the enlargement of a vertical ground heat exchanger field does not lead to greatly improved conditions.

- The **length of the buried connecting pipes** influences the minimum inlet temperature significantly. This leads to a large increase of the seasonal performance of 1.6 in case of short vertical ground heat exchangers (here 50 m). The improvement of the seasonal performance for long vertical ground heat exchangers is small, below 0.1 and therefore it is not presented. Looking at the graphs, the buried horizontal ground heat exchanger can be understood as a sort of extension to the vertical ground heat exchanger.

  The minimum temperature, which is measured directly at the ground heat exchanger inlet, is influenced by the buried pipe. This temperature rises strongly in systems that do not meet the lower temperature limit. In systems above the limit the impact of the buried pipe length is lower. This can be seen for the short ground heat exchangers. In principle, these systems still hit the temperature limit $T_{protect}$, however, the temperature directly at the inlet of the vertical ground heat exchanger is slightly increased with longer connecting pipes.

  On the whole, the influence of a buried pipe is very comparable to the influence of lengthening the vertical ground heat exchanger. However, the results should not be overestimated because the model and its assumption enclose no validating reference. Many potentially important influences are neglected such as rain, icing, interference between pipes, long term influences outside the mesh etc.

Table 5-5: Overview on the location parameter range for the sensitivity analysis displayed in Figure 5-23

Varied parameters4	Unit	Min	Refe-rence	Max
Distance of boreholes[1]	m	3	6	9
		50%	100%	150%
Length of boreholes	m	50	110	130
		45%	100%	118%
Length of connecting pipes long GHX 110 m	m		0	30
			100%	127%
Length of connecting pipes short GHX 50 m	m		0	30
			100%	160%

Reference Values		Without solar	With solar
SPF_{SHP}	-	3.60	3.66
T_{min}	°C	-2.14	-1.52

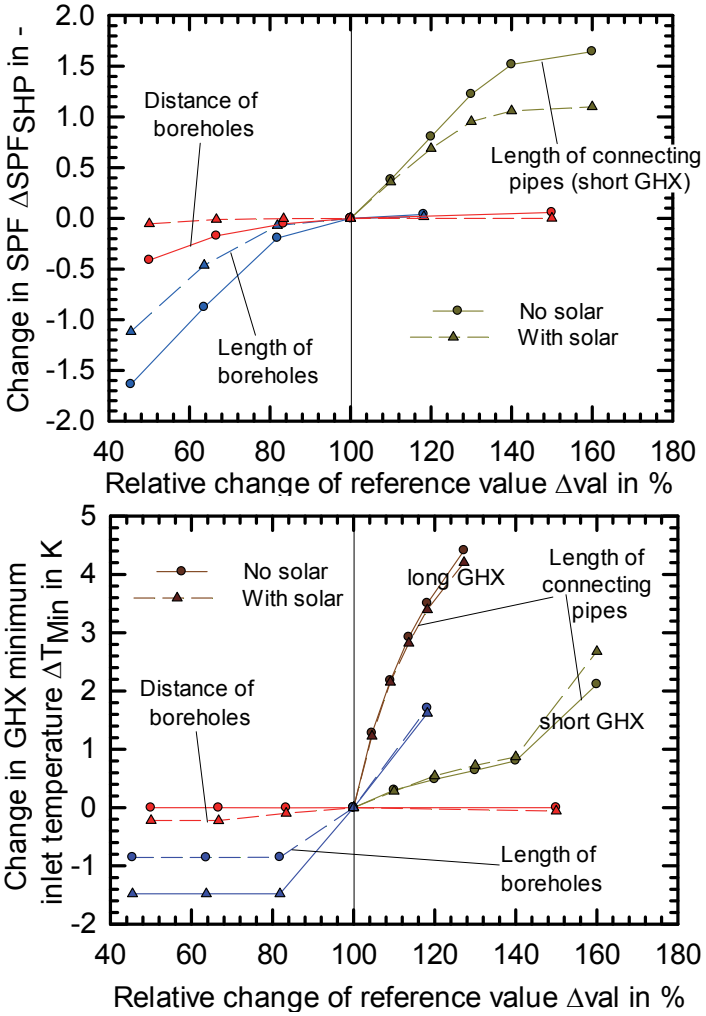

Figure 5-23: Sensitivity of the seasonal performance factor SPF_{SHP} and for the minimum inlet temperature T_{min}. The design parameters are varied for the vertical ground heat exchanger. The system concept with solar is of the type series in-front with 15 m² black polymer collector.

[1] The reference values are not the same as for a single GHX.

Without solar: SPF_{SHP+} = 3.48, T_{min} = -3°C; With solar: SPF_{SHP+} = 3.65, T_{min} = -2.77°C.

5.3.7 Heat Pump

The impact of the heat pump size and heating-up constant are unknown in terms of the system simulation. The following variations are made to determine their sensitivity:

- The heat pump's transient thermal characteristic is described by a **heating and cooling time constant** of the heat pump. The heating constant has been varied. The cooling constant is not investigated, but has a lower impact on the system performance [16, p. 95]. The reference value of 30 s in the simulation is determined experimentally. The value is much smaller than the default value of the simulation model 180 s.
- The **size of the heat pump capacity** is varied. The heat pump characteristic at 100% capacity is derived from measurements, see chapter 2.1.2. These measured performance data points for electric power, heat and mass flow rates are multiplied by a scaling factor, from which new polynomials are extracted according to Eq. 2-2 and Eq. 2-3. The new, scaled polynomials are calculated with the same least-square fit procedure as for nominal conditions.

  The system simulations are subsequently repeated with the heat pump model scaled polynomials. The mass flow rates are reduced accordingly. No other parameters in the system model are modified. This includes the dynamic time constants of the heat pump.

  This scaling approach of the heat pump capacity is well suited for investigation of scaling effects of the heat pump size. Nonetheless, the scaling certainly does not represent realistic heat pumps on the market, if extrapolated to a broader scaling range.

  It's assumed that the heat pump capacity and the dynamics of the system are dependent on each other. The variations are, therefore, repeated with the buffer storage tank system. The buffer system has a different system dynamic and fewer heat pump on-off cycles.

The results of the parameter variation given in Table 5-7 are presented in Figure 5-24.

Table 5-6: Overview on the location parameter range for the sensitivity analysis displayed in Figure 5-23

Varied parameters	Unit	Min	Refe-rence	Max
Heating time constant of heat pump	s	10 33%	30 100%	180 600%
Scaling for the HP capacity	kW	4.56 60%	7.8 100%	8.36 110%

Reference Values		Without solar	With solar
SPF_{SHP}	-	3.60	3.66
T_{min}	°C	-2.14	-1.52

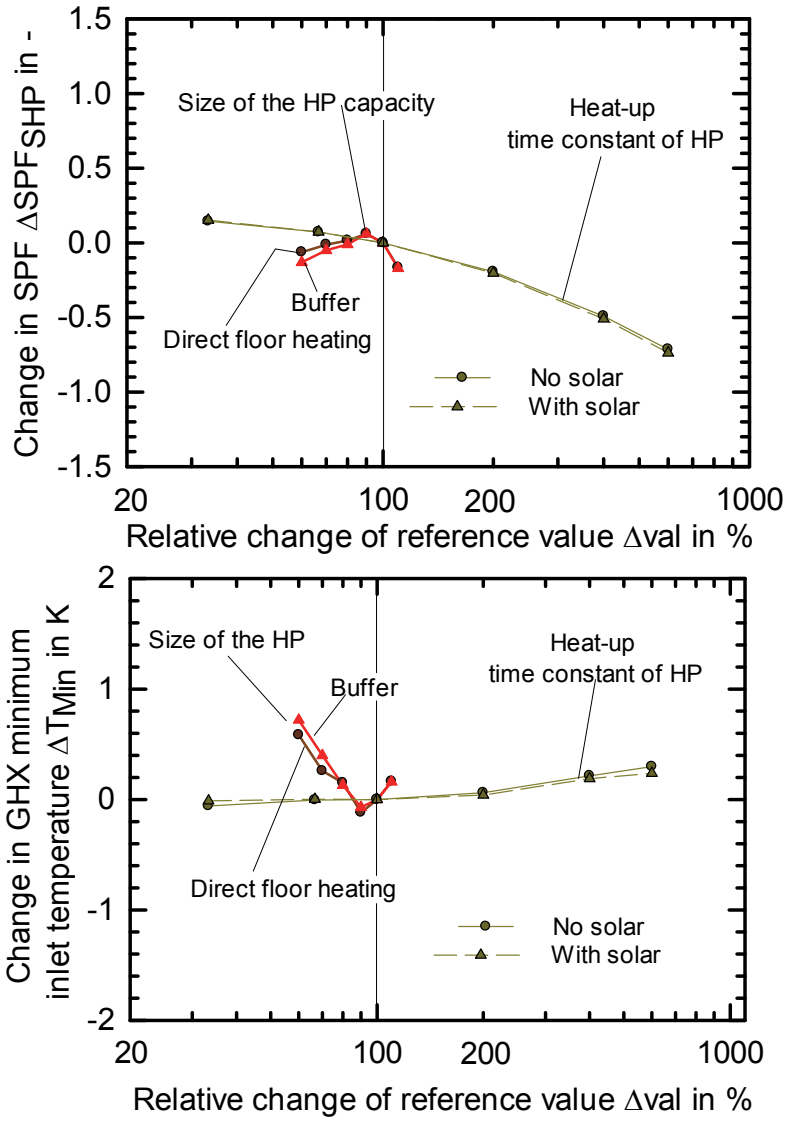

Figure 5-24: Sensitivity of the seasonal performance factor SPF_{SHP} and for the minimum inlet temperature T_{min}. The varied parameters are design parameters for the vertical ground heat exchanger. The system concept with solar is of the type series in-front with 15 m² black polymer collector. The varied parameters are the heat pump capacity (100%=7.8 kW) and the heat-up constant of the heat pump (100%=30 s)

The following findings are derived:

- The **heating time constant** has a significant influence on the seasonal performance and hardly any influence on the minimum inlet temperature of the vertical ground heat exchanger. Between the reference value of 30 s and the default value of 180 s for the component there is a performance difference of approx. 0.2. Improvements can be achieved in the system with smaller heating constants.
- The **heat pump capacity** is the only parameter investigated that reveals a non-monotonic function in this sensitivity analysis. The seasonal performance has a maximum at 90% of the reference heat pump capacity. At the same capacity the minimum inlet temperature shows a minimum. The minimum temperature increases by 0.8 K for the smallest heat pump. The impact of the heat distributing concepts, with floor heating or buffer, is small. Both concepts decrease up to around 0.15 in their seasonal performance for smaller heat pumps and up to 0.2 for larger heat pumps.

  The most obvious difference between the concepts is that the heat pumps with higher capacities have higher mass flow rates, a more intermittent operation, smaller maximum runtimes, Figure 5-25 (top), and longer overall run-times, Figure 5-25 (bottom).

  The inlet temperature minimum is explained by two opposing trends.

  One trend is the lower heat flow rate at the evaporator for decreasing capacities. These lower heat flow rates lead to an increasing minimum temperature for smaller heat pumps (see Eq. 2-18).

  The other, more complex trend is dominated by transient effects, compare chapter 2.2.2, of the vertical ground heat exchanger. The complete recirculation of the fluid in the ground heat exchanger pipes takes approximately 7 minutes, while the transient influence on the temperature level is longer. The fluid in the ground heat exchanger, here 220 l, in addition to the ground heat exchanger of the filling and the pipe material reduce the temperature response during each starting interval.

  Accordingly, very large heat pumps, which have a high heat flow rate but small runtimes, can benefit from transient effects. In other words, the minimum temperature T_{min} decreases because the maximum runtime period of large heat

pumps decreases significantly. The transient effect during the starting period in consequence compensates for the higher heat flow rate of the evaporator and the minimum temperature decreases.

These two trends interfere with each other and lead to higher minimum temperatures T_{min} for very small or very large heat pumps, whereas for moderate dimensioning a minimum of T_{min} is reached, see in Figure 5-24.

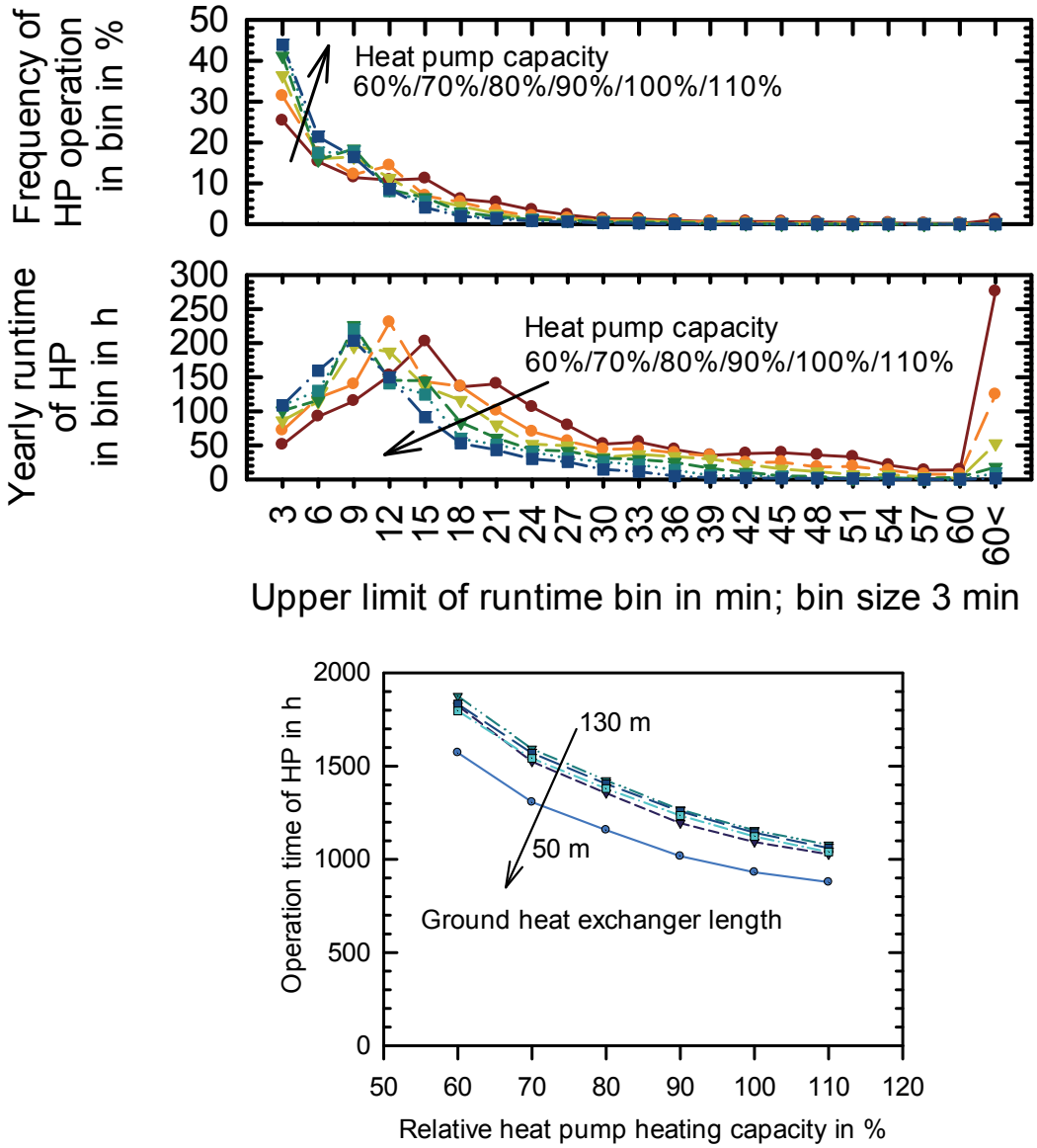

Figure 5-25: Top: Run-time distribution of the heat pump in the system with floor heating for different heat pump capacities for 110 m vertical ground heat exchanger length. Bottom: the overall run-times for different vertical ground heat exchangers from 50 to 130 m. The off-set between 50 m and 70 m is induced by direct electric heating

The seasonal performance maximum can only be explained partly by the aforementioned effects. One clear trend, however, is the increase of cycling losses for heat pumps with higher capacity. The higher capacity leads to more on

and off cycles and thus to more cycling losses that reduce the seasonal performance. In the reference case simulated the larger heat pumps run mostly for 10 min or even less. The short cycling losses lead to a higher fraction of starting losses in each runtime interval. Having a time constant of 30 s the heat pump reaches 98.2% of its nominal power after 2.5 min., compare data from chapter 2.1.3. The cycling losses as a result occur in the first 3 minutes of a cycle. Correspondingly, the cycling losses have an increasing impact in shorter sequences of some minutes and a reduced influence for longer operating sequences.

The performance drop of roughly 0.1 for smaller heat pumps with longer runtimes appears to have no plausible reason. Detailed analysis identified the heat pump as the main reason for this decrease. The temperature development simulated on the evaporator and condenser side does not explain the occurring differences.

Two explanations are found: Firstly, computational errors might have an influence. The energy balance for the heat pump with 110% reveals differences of $\pm$ 0.4‰, which corresponds to 4.5 kWh a^{-1}. This might be an indication for unrecognized numerical faults, because no balance error occurs in the reference case simulation. Secondly, systematic errors might appear for the applied scaling method of the heat pump coefficients. The fitted polynomials might systematically reduce the heat pump performance for smaller heat pump capacities.

Moreover, the SPF_{SHP+} maximum found appears for the ground heat exchangers with a length of 110 m and 130 m but not for smaller depths. In other words, the discussed maximum depends on the particular heat pump capacity but its characteristic also depends on the vertical ground heat exchanger length, see Figure 5-26. This characteristic seems reproducible also in a complete different system simulation setup because very comparable simulation results are presented by Kjellsson [43, p. 93]. Likewise, the impact of the heat pump capacity on the seasonal performance changes as a function of the ground heat exchanger length.

In general, the results disclose the system's complexity and demonstrate the difficulty to interpret the simulation results. The heat pump capacity and its changed runtime distribution affect many dependencies that cannot be separated and interfere

simultaneously: The heat pump's dynamic time constant, the evaporator heat flow rate, the plug-flow effect, and also the operation of the direct electric heater. The simulation results do not permit to clearly identify one parameter to the occurring system behaviour. In most cases the influence of the heat pump capacities is, however, moderate and in the range of 0.1 to 0.2 in the SPF_{SHP+}.

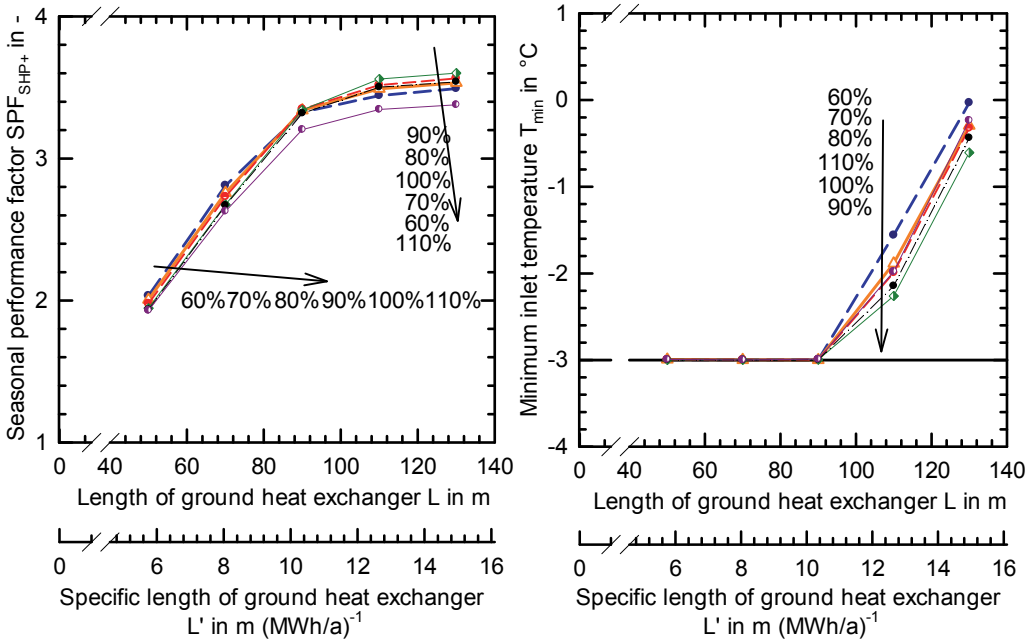

Figure 5-26: Seasonal performance factor SPF_{SHP+} and minimum inlet temperatures T_{min} for different heat pump capacities between 60% and 110% and vertical ground heat exchanger lengths.

5.3.8 Discussion of Sensitivity Analysis

The sensitivity analysis develops a detailed understanding of the heat pump system and the influence of solar thermal regeneration. It is restated that the sensitivity presented is a single parameter analysis. A multi-parameter interference of influences was not examined. In addition, the relative change of a parameter can be very different. For instance, a 10% change is large value in the case of the vertical ground heat exchanger length, while it is a comparatively small value for the ground thermal conductivity.

In the case of the **seasonal performance factor SPF_{SHP+}** the most sensitive parameters are the length of the vertical ground heat exchanger L (or the connecting pipe in case of a short vertical ground heat exchanger), the temperature limit $T_{protect}$ and the heat conductivity of the ground λ_{ground}. All other parameters influence the performance moderately with less than 0.5. Of course, this applies only to the parameter range investigated. Only the inner vertical ground heat exchanger parameters are emphasized. They have hardly any influence on the seasonal performance in the system

configuration investigated.

Moreover, nearly all parameters influences are non-linear. In fact, the possible improvement of performance seems limited, as a positive parameter change does not significantly improve the performance. Even a 5 K higher undisturbed ground temperature leads to an improvement of only 0.2 in the seasonal performance.

The **minimum inlet temperature T_{min}** is sensitive to more parameters than the performance. The most decisive ones are the location parameters T_{undis} and λ_{ground} and the design parameters: vertical ground heat exchanger length L and the connecting pipe length for short lengths of L. Decreases of T_{min} occur as well as significant increases. Furthermore, the limiting temperature $T_{protect}$ for the direct electric heater is one obvious reason for non-linear behaviour of the minimum temperatures. It is highlighted, that transient effects have an impact on the minimum temperatures, although the influence is moderate.

Some of the results are compared to literature values. These include one simulation study on systems with vertical ground heat exchangers and solar assistance [43] and the analytic sensitivity analysis for the minimum inlet temperature by Koenigsdorff [23, p. 225]. It is restated that the studies are only qualitatively comparable because their particular simulation setup differs.

In principle, the simulation study by Kjellsson produces comparable results. Systems with long vertical ground heat exchangers show nearly constant seasonal performance of approx. 3.5 [43, p. 99]. Moreover, all influences investigated lead to performance decreases but no increase. The vertical ground heat exchanger length is identified as one of the most important system parameter and shows a clear non-linear characteristic.

Significant differences between the studies, however, do appear for parameters connected to vertical ground heat exchanger in context with the solar collector.

A change of 40% in the borehole resistance causes a shift in the minimum temperature T_{min} by 1.5 K [43, p. 124]. The same change of 40% leads to a change of 2 K in the analytical study [23, p. 225]. In contrast, this thesis' simulations show a shift of only 0.6 K, Figure 5-21. The reduced sensitivity of the thermal resistances in the vertical ground heat exchanger is explained by the improved modelling of the transient, dynamic effects within the vertical ground heat exchanger in the system.

Large improvements due to solar collectors are also found with shorter vertical ground heat exchangers by Kjellsson, [43, p. 99]. Here, the performance improvements achieve

values of 1, which is twice as high as found in this thesis, compare Figure 5-4. The Kjellsson simulations show an abrupt performance reduction compared to the shallower performance drop in this thesis. The difference is also assumed to be caused by the utilization of the DST-pipe without pre-pipe, Figure 5-16.

In summary, while the system model established is comparable to other studies, the improved vertical ground heat exchanger model reveals a less sensitive characteristic due to the now included inner thermal capacities. This more stable behaviour applies in particular to the seasonal performance in context with the borehole resistance and all parameters in the ground heat exchanger core.

A validation of the dynamic system model's sensitivity analysis against field measurements is of course desirable but it would require excessive effort to obtain applicable measurement data from systems in the field. Furthermore, such a measurement needs to be very accurate and the same applies to the components' properties, e.g. the heat pump performance. To give an example, the validation of the heat pump capacity sensitivity presented, see Figure 5-26, would involve 30 exactly identical systems that would operate with identical components with identical user load patterns, ground properties and weather conditions for 2 years. In the example given, the difference in the SPF_{SHP+} simulated is 0.2. This means other influences of the same magnitude on the system need to be excluded otherwise the sensitivity cannot be measured and the simulation validated. This example also highlights the general difficulty to validate a complex system model against system measurements in the field.

5.4 Further Systems

5.4.1 Solar Hot and Cold side Integration

The use of solar heat on the hot and on the cold side of the heat pump is temping. This combination increases simultaneously the seasonal performance (Figure 5-16) and achieves the solar regeneration of the ground (Figure 5-4). As already indicated previously in chapter 4.2.3, combined systems are, however, in many cases complex and not just the sum of a hot and a cold side integrated system.

Nevertheless, such a combined system with hot and cold side integration is simulated. Here, solar domestic hot water preparation is combined with cold side integration series in-front. The controller that switches between the hot and cold side has a simple priority control. In this strategy the switching of the collector to the hot side has priority over the

switching to the systems' cold side.

High collector yields are reached on the hot and on the cold side, Figure 5-27. In both cases, however, the solar heat gain Q_{sol} is smaller than in case of mere operation on either hot or cold side.

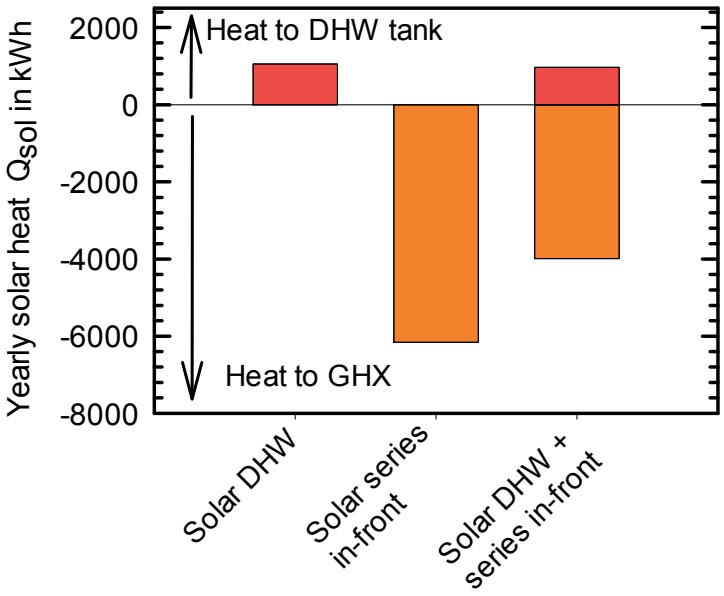

Figure 5-27: Solar yield comparison of three different system concepts. All systems have the same 15 m² selective uncovered collector and a vertical ground heat exchanger length of 110 m.

The performance of each system concept compared to the other concepts depends very much on the vertical ground heat exchanger length; Figure 5-28. For long vertical ground heat exchangers the system will perform best, if solar heat is only used on the hot side. For shorter lengths the combined system performs best. It benefits from the effects of ground regeneration and still achieves performance improvements due to solar domestic hot water preparation. As a result, the combined system solution has the highest performance for shorter heat exchangers.

In general, correlations for the combined systems are hard to deduce since the combined systems certainly are strongly dependent on sizing and controller strategies. This is made clear by a control strategy that has already been proposed by Kjellsson. Here, the controller settings depend on the season. The controller priorities are switched between summer and winter. This controller achieves a high seasonal improvement, but at the same time the strategy reduces the collector heat to the cold side to 8% of the overall collector yield [43, p. 146]. Accordingly, only 6% of evaporator demand is supplied by solar energy. In this case the collector is not really supporting the vertical ground heat exchanger in terms of regenerating the ground. Therefore, it will not have the just presented beneficial effect for smaller vertical ground heat exchangers, [43, pp. 99 &

104].

In summary, the simultaneous use of the solar heat on the cold and hot side can be beneficial and an interesting solution, but requires very intelligent controlling. The deduction of general recommendations is difficult if derived from a particular set of dimensions and location. Changing these conditions will presumably lead to a change of the optimum strategy.

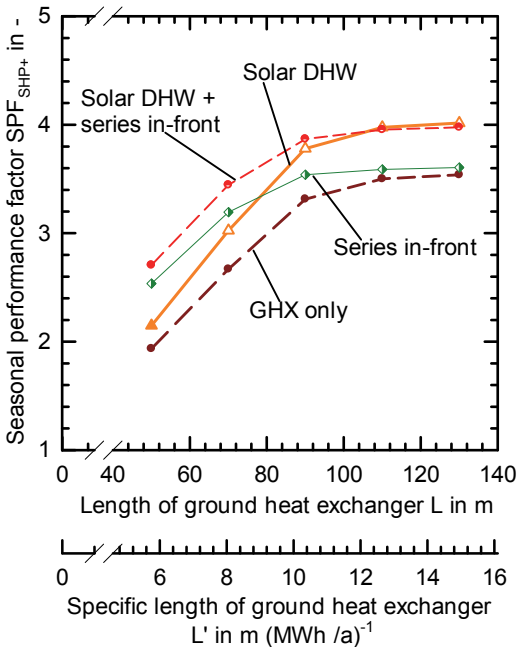

Figure 5-28: Seasonal performance factor SPF_{SHP+} for different system integrations on the hot and/or the cold side of the heat pump. All solar assisted systems have an identical solar collector area of 15 m² selective uncovered collector and a vertical ground heat exchanger length of 110 m. The order of system performance changes depending on the vertical ground heat exchanger length.

5.4.2 Comparison of Air and Ground Heat Exchanger Systems

Heat pump systems with an air heat source are the technology competitor to heat pumps with a ground heat source. The main advantage of air heat source systems is their lower installation costs, which can be down to half of the price for ground source systems [5, p. 20]. They also require less effort for installation. On the other hand, air source heat pumps are clearly less efficient, especially when low ambient temperatures and high heat demands occur. Air heat source pumps are therefore widespread and clearly dominating in southern Europe [13, p. 12].

Simulations are conducted with the reference system introduced in chapter 4, but with an air heat source instead of the vertical ground heat exchanger.

The applied air heat exchanger model and implementation is a design model, which is validated against a measurement with an error of 10% in the heat transfer rate, it is

documented in [139, p. 27]. The model is implemented in TRNSYS as type 880 [140][1]. The applied model coefficients for the fan's electric consumption and air flow have been derived from measurement. Condensation heat gains are respected in terms of a constant value and also gained from measurement data. Frost effects are not accounted for.

In Strasbourg, the simulated SPF_{SHP+} is 2.78 for the air system without solar assisstance. This is in good agreement to field test measurements. Typical measured values in central Europe are SPF_{SHP+} 2.8 [141, p. 3]. The often cited ISE study give values of the SPF_{bSt} between 2.3 and 3.4 for Germany [142, p. 55].

In particular the correct description of parasitic auxiliary consumers is important. In the simulations the electrical consumptions are 5% for the fan and 10% for the direct electric heater. These values are well in the range of the measurements [142, p. 84], although the system model slightly underestimates the fan consumption by 2 % while the direct electric heater is overestimated by around 5% compared to measured average values.

The underlying question for the comparison is to find out the differences between ground and air heat sources- especially in the course of the year. Three system concepts are simulated: an air heat source, a vertical ground heat exchanger without and one with solar cold side integration series in-front. The vertical ground heat exchanger length is 110 m. The uncovered solar collector for regeneration is selective and has an area of 15 m². The three systems are simulated at three different locations: Bolzano, Strasbourg and Hanover, (chapter 0).

In general, systems for Bolzano show a lower performance, while the systems in Strasbourg and Hanover perform approx. 0.3 better and have very similar results, see Table 5-7. This is due to the higher relative fraction of domestic hot water in Bolzano. With warmer climates the fraction of space heating demand decreases, while the domestic hot water demand stays constant. Hanover and Strasbourg have a similar performance since their similar climates lead to a similar ratio of space heating and domestic hot water. This effect is independent of the heat source.

[1] The implemented TRNSYS type 880 is provided by the solar thermal systems working group at the European Research Academy (EURAC), Italy. Many thanks goes to the whole working group and especially to Matteo D`Antoni and Roberto Fedrizzi.

Table 5-7: Annual seasonal performance factor SPF_{SHP+} for air and ground source heat pumps with and without solar regeneration at three different locations for the same reference systems

Heat source	Strasbourg	Hanover	Bolzano
Air-only	2.92	2.93	2.59
GHX-only	3.50	3.57	3.21
GHX + regeneration	3.60	3.64	3.33

The impact of the domestic hot water fraction on the seasonal performance becomes even more clear in the course of the year when lower seasonal performances are reached in summer. An example is given for Bolzano and Strasbourg in Figure 5-29. Bolzano has obviously the shorter heating period, which leads to a lower annual performance.

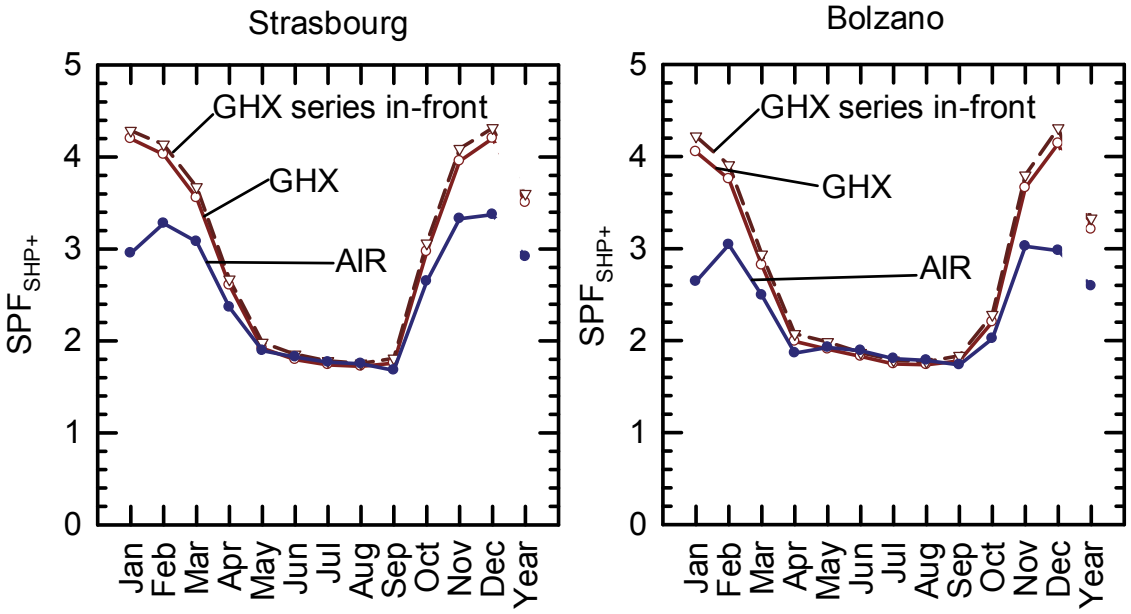

Figure 5-29: Seasonal performance for Bolzano and Strasbourg for the heat sources air, vertical ground heat exchanger with and without solar regeneration in the course of the year.

The monthly heat demand is correlated with the monthly electric consumption for a significant comparison of the heat sources. Further, both values are related to the living area of the building Q_{use}, which is the heating demand per living area. E_{el} is the monthly electric consumption per m² living area. These figures correlate surprisingly well for all three locations Figure 5-30.

The main difference for the heat sources appears in winter for higher heat loads. Here, the ground heat source has an electrical demand of 3.0 kWh $m^{-2}month^{-1}$. The air heat source has a 50% higher electrical demand of 4.5 kWh $m^{-2}month^{-1}$. The difference between the systems with and without solar regeneration is visible- but small.

In a first approximation the development of the electrical demand is linear. Correspondingly, a linear regression analysis is conducted to derive a transferable

correlation from the simulation results, Table 5-8. However, these derived correlations are limited to the simulated systems and boundary conditions. Especially the air heat source indicates these limitations. It shows a much more scattered distribution than the ground heat source, and at higher heat demands a tendency is seen for consumptions above the linear trend. Further influences as controller settings and the systems' setup will also influence the consumption.

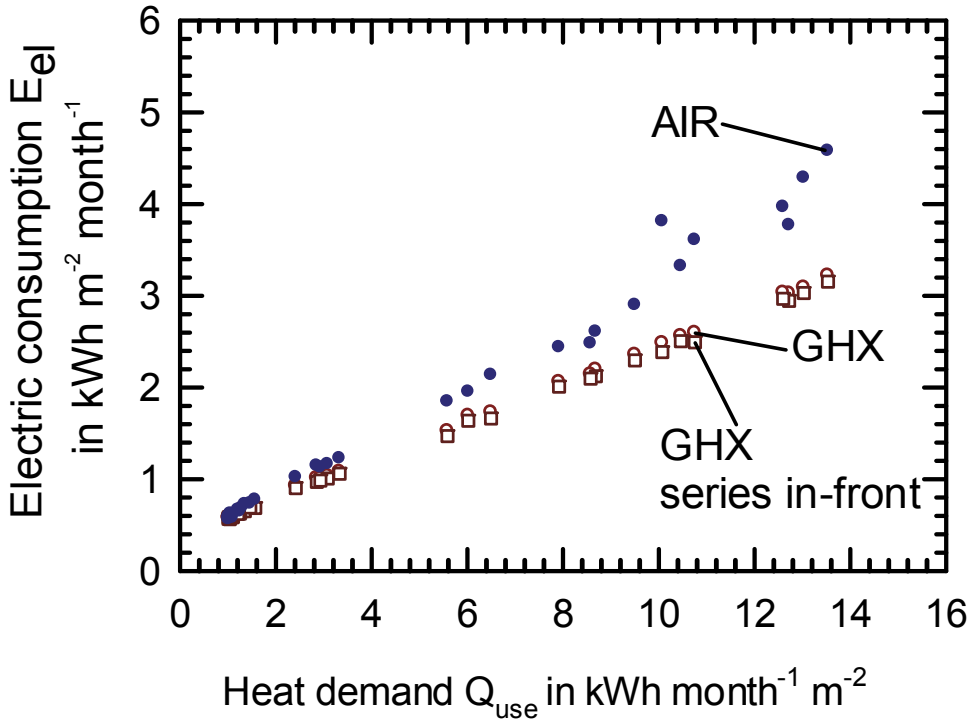

Figure 5-30: Monthly electrical consumption vs. heat demand per m² living area for the reference building and domestic hot water demand for the locations of Strasbourg, Bolzano, Hanover

It should be noted that the heating demand depends on the ambient air temperature and the solar irradiance. The electric consumption does not correlate this well over the ambient air temperature because the heating demand is also strongly influenced by the irradiance available.

To conclude, the deeper analysis of the heat sources reveal a much higher difference between the ground and the air heat source as it would be expected by the annual seasonal performance. In winter the electric consumption of the air heat source systems is 50% higher than in systems a with ground heat source. The seasonal performances of 2.9 for the air source and 3.5 for the ground source meanwhile suggest lower differences. This difference is large and it is especially relevant in the context of an increasingly regenerative and volatile electricity supply.

Table 5-8: Regression of the average electric load for air and ground heat source systems of three different types and at three different locations.

$E_{el} = d_0 + d_1 \cdot Q_{use}$				
	d_0	d_1	R	SD
all units are monthly values	kWh m^{-2}	-	-	kWh m^{-2}
Air	0.270	0.296	0.993	0.152
GHX	0.386	0.208	0.999	0.019
GHX series in-front	0.376	0.203	0.999	0.224

5.4.3 Systems without Ground Heat Exchangers

The results presented in this chapter have also been published in Annex G to Report C3 of IEA SHC Task 44 / HPP Annex [105, pp. 11–22]

The solar assisted heat pump systems without any vertical ground heat exchanger are attractive. Such systems can be planned, prefabricated and build without considering the ground conditions. Such a system is simulated. It consists of a glycol filled cold storage tank as described in Figure 4-21 “Cold storage as hydronic junction”, but without any vertical ground heat exchanger.

Additionally, the following settings have been changed:

- The minimum temperature on the cold side of the heat pump is extended to -10°C. The restrictions for the minimum ground temperature are no longer relevant. There has also been defined an upper temperature limit of 35°C for the cold storage side.
- The storage tank is simulated as an insulated cylindrical storage tank filled with glycol. The tank is placed in an environment with an constant ambient temperature of 15°C. The tank itself has an insulation of 150 mm thickness and a heat conductivity of 0.04 W m^{-1} K^{-1}. A heat transfer to the ground or the building is not considered.
- A selective uncovered solar collector is used as the only heat source for the system.

It is emphasized that these simulations have the character of a feasibility study and do not reach the high quality of the before presented simulations with vertical ground heat exchanger. Many of the applied models have not been validated in this temperature range (e.g. the heat pump or the storage tank) and fewer variations are made. The controller and the components can be optimized further.

The glycol storage volume and the collector area are varied. The seasonal performance simulated reach a respectable SPF_{SHP+} of 2.8 for uncovered collector areas of 30 m² and a cold storage volume of 5 m³, Figure 5-31. This is the same performance as in a system with air heat source. Still such systems have surplus solar heat in summer, which could also be used on the hot side of the heat pump.

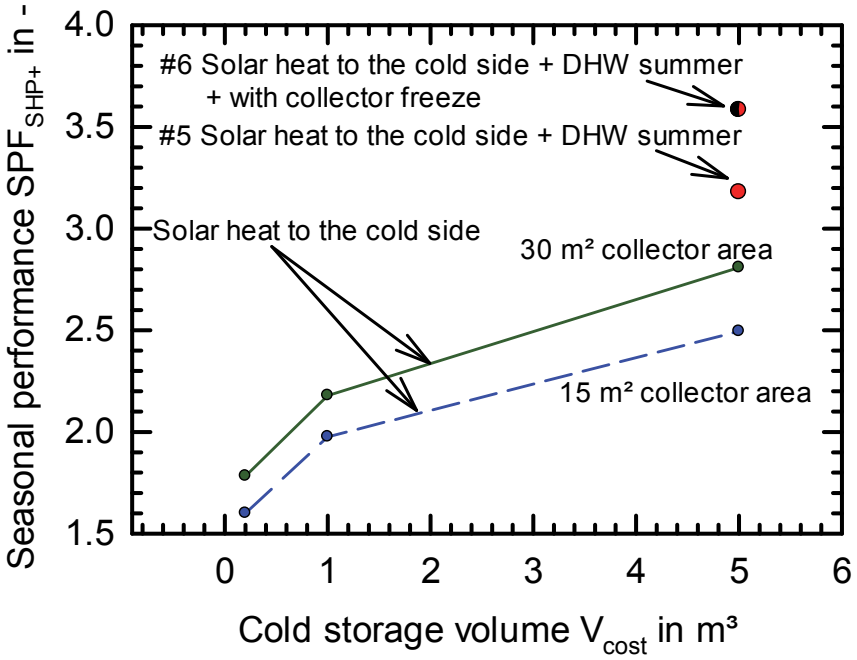

Figure 5-31 Seasonal performance factor for systems without vertical ground heat exchanger different cold storage volumes and collector areas. The applied collector is an uncovered selective collector. The systems #5 and #6 are using solar heat also for domestic hot water preparation during summer.

Following the four systems already investigated #1 to #4 in chapter 5.2.5 (shortening the vertical ground heat exchanger), two further systems have been defined.

5. The system #5 “solar heat to the cold side + DHW in Summer” consists of a 30 m² selective uncovered solar collector, which is operated on the cold side only. In summer the direct use of solar energy for domestic hot water preparation is also possible. During this period the solar collector can be switched between hot and cold side. A simple priority controller is used with the priority to the hot side. (The domestic hot water priority in summer is also successfully used by Kjellsson [43, p. 146] in combination with vertical ground heat exchangers, but with dramatic decrease for the solar ground regeneration.) Summer is defined as the period in which the 24 h average of the ambient temperature is above 15°C.

   The seasonal performance SPF_{SHP+} is 3.18.

6. The system #6 is the same system as #5 but with one important change for the

collector controller settings. In winter a restricting limit for the collector operation is the frost protection described in chapter 0. The collector frost protection is unlocked and the collector can be operated even below 0°C. Heat gains from frost formation or the change of the optical properties on the collector are not included in the collector model.

The seasonal performance SPF_{SHP+} is 3.58.

The simulations reveal comparatively high seasonal performances, Figure 5-31. The system #6 outperforms the conventional vertical ground heat exchanger system with an SPF_{SHP+} of 3.5. Nevertheless, for a reasonable comparison other aspects have to be taken into account, too. This is especially the peak load consumption of the system, which rises significantly in the system without vertical ground heat exchanger, Figure 5-7.

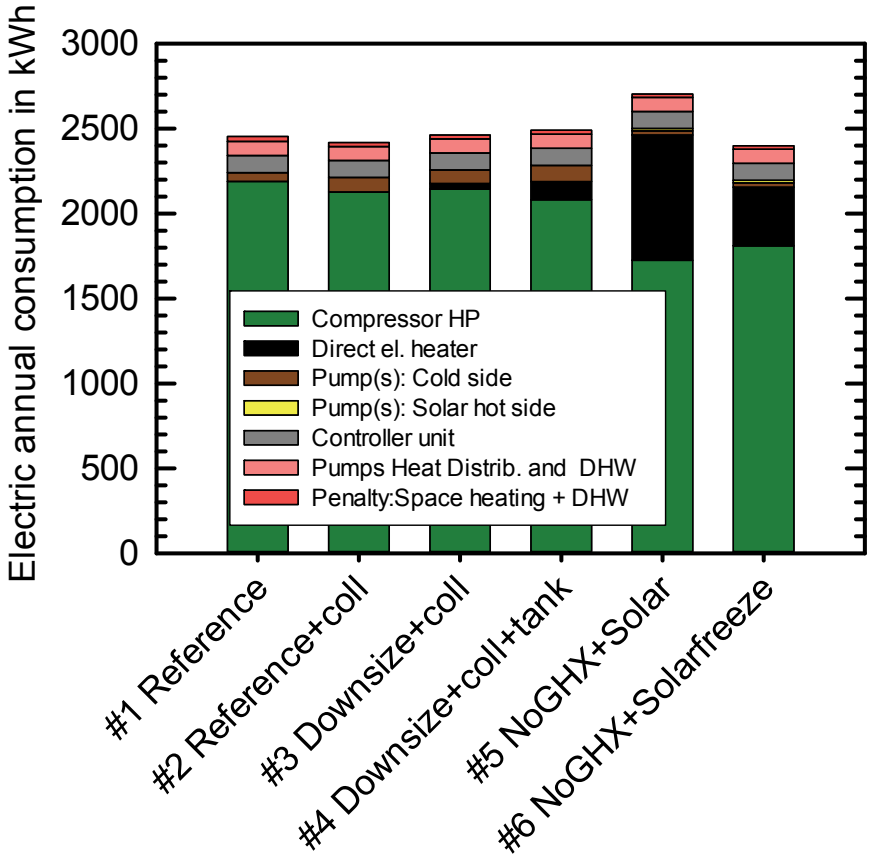

Figure 5-32 Annual overall consumption of systems #1 to #4 for downsized vertical ground heat exchanger length from 110 m to 70 m by solar assistance and a glycol storage tank of 1 m². The systems #5 and 6# have no vertical ground heat exchanger at all but 30 m² selective uncovered collector and a 5 m³ cold storage tank. The fraction for the direct electric heater is dominant in systems without vertical ground heat exchanger, because the lower temperature limit for the heat pump source side is met.

As to be expected the systems with #5 and #6 have their peak load in the winter; Figure 5-33. Accordingly, the distinguishing feature of the systems compared to vertical ground heat exchangers is not the overall performance but the distribution of their electric consumption. In the developing framework of an increasing renewable energy supply these seasonal distribution aspects will be decisive.

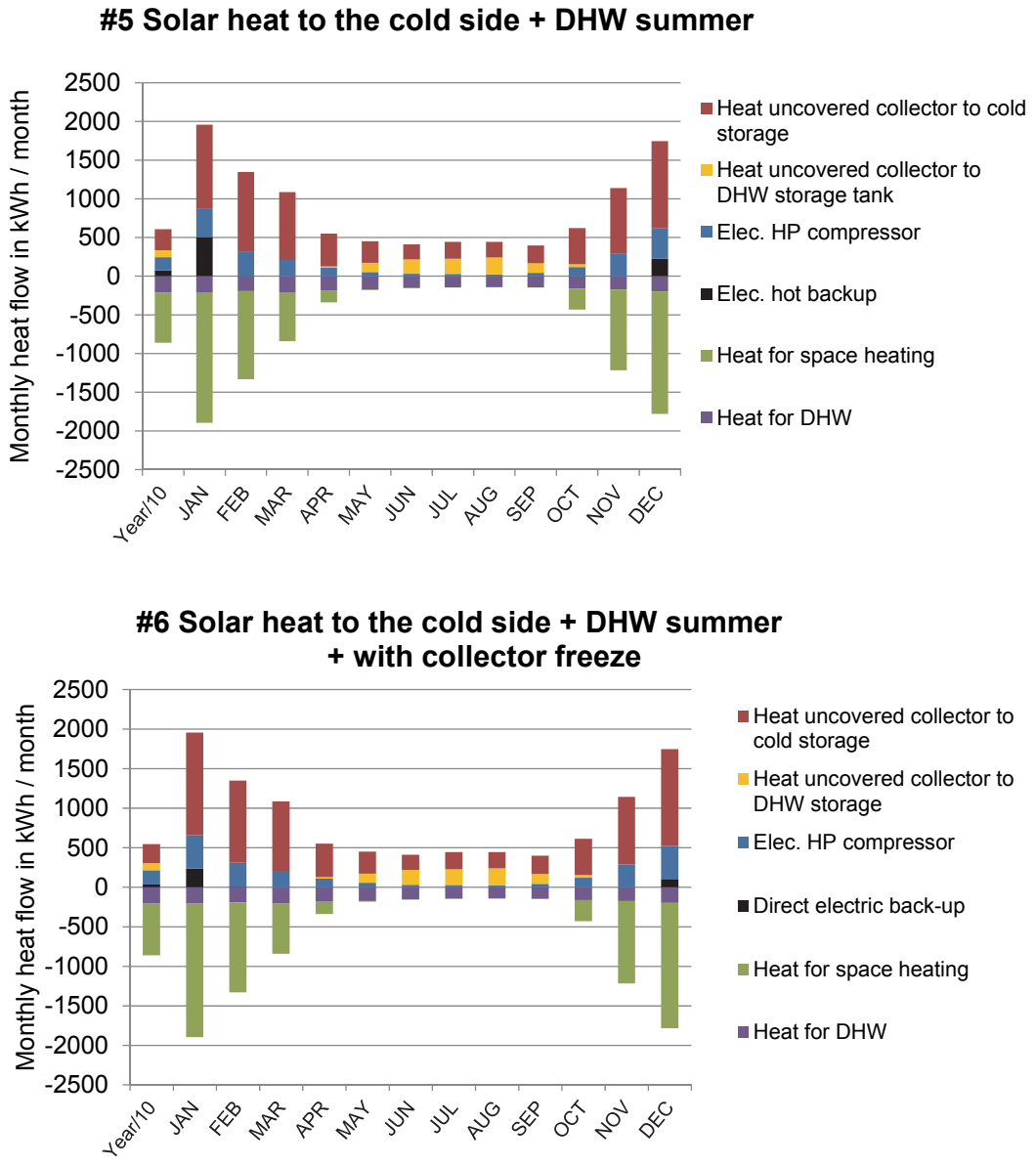

Figure 5-33 Monthly heat flow rates for the systems #5 and #6 without vertical ground heat exchanger. Both systems have 30 m² uncovered selective collector, a 5 m^3 glycol storage tank and solar DHW preparation in summer. System 6# allows collector operation at temperatures below 0°C

6 System Measurements

6.1 Systems Measured

6.1.1 Description

Background

This section describes the system measurements that are the basis for the dimensioning rules validation presented in chapter 6.2. The system measurements were conducted as part of two research projects before the beginning of this thesis, see chapter 1.3. All three heat pump systems consist of an uncovered solar thermal or a solar PVT collector and a vertical ground heat exchanger. The system configuration for all three systems is series in-front, Figure 4-18.

The measurement set-up for the collector is basically identical in all three systems. In the measurement sensors were used that were calibrated at the accredited collector test centre at ISFH. The temperature sensors are mounted inline. The measurement extended standard uncertainty for the sensors measuring the heat flow rate measurement is 2.5% at nominal conditions. Heat balances of all measured components on the cold heat pump side, however, revealed an error of 6.6% related to the annual heat demand. The solar irradiance is measured with a pyranometer in the collector pane. It is calibrated and has an extended standard deviation of 2.8% at 940 W m^{-2}. The ambient air temperature is also measured in the collector pane with a ventilated sensor. Multiple further data is measured. The scan interval applied is 60 s and 30 s for data recording.

Limburg

The Limburg system is situated in Limburg an der Lahn, Germany and was commissioned in September 2006. It was monitored over the period from October 2006 to June 2008, Figure 6-1 (left).

The ground heat exchanger consists of 14 vertical pipe-in-pipe heat exchangers with 17 m depth with a spacing of 4 m between them. They are arranged in a 2 x 7 grid formation. The zinc metal roof collector has an area of 43.7 m², is orientated south east and has a 10° slope. The heat pump has a nominal power of 15.8 kW and a COP 4.4 for 0°C source and 35°C sink temperature.

The 300 m² building has an annual measured heating demand of 36 MWh a^{-1} and a low temperature heat distribution system with floor and wall heating radiators.

Klein Köris

The Klein Köris system south of Berlin, Germany, is commissioned in 2006, which is much earlier than the beginning of the monitoring in November 2007, Figure 6-1 (right). The monitoring ended in June 2008, so only 8 months are measured. Even so, the heating demand of 29.2 MWh a^{-1} is comparable to the system in Limburg.

The vertical ground heat exchanger consists of 2 double u-tubes with a depth of 75 m installed with a 6.1 m spacing. The uncovered collector is orientated south with a slope of 45° and has an area of 19.8 m².

The heat pump has a nominal power of 10.9 kW with a COP 4.6 at a condenser temperature of 35°C and a source temperature of 0°C. In addition this heat pump has a direct electric back-up heater of 9 kW.

The hydronic installation of the system is identical to the other systems with one exception. A by-pass valve is installed parallel to the solar thermal collector.

Figure 6-1 Two Systems with roof integrated uncovered zinc collector marked in **red**. Left: System in Limburg with 44 m² collector area; Right: Klein Köris System with 20 m² collector area

Dreieich

The system in Dreieich near Frankfurt a. M., Germany , Figure 6-2, was measured from March 2009 to June 2011.

The system consists of a 39.4 m² unglazed PVT collector with a slope of 16° and an azimuth angle of -24°. Three ground heat exchangers are installed with a depth of 75 m. The pipe-in-pipe heat exchangers were installed with a 5 m spacing arranged in a straight line. The 12 kW heat pump was replaced after 1 year of operation. The COP in the first year of operation was 4.65 and in the second year 4.8. The heat pump has a de-super heater integrated in a 150 l DHW storage tank.

The heating demand of the building was much higher than planned. In the first year of

operation was 35.0 MWh a^{-1} and 40.8 MWh a^{-1} in the second year. The heating demand was planned to be 27.8 MWh a^{-1}.

Figure 6-2 System in Dreieich with PVT- collectors; front: Meteorological weather unit with pyrgeometer and pyranometer

6.1.2 Measurement Results

All the measured systems use the heat from the uncovered collector only on the cold side. Consequently, the heat flow rates measured on the cold side are analysed. The systems are characterized by the heat flow rates on the cold source side, Figure 6-3.

The character of the heat flow rates is identical for all three systems. In winter the ground is the main heat source and the heat demand is high. In summer the solar collector recharges the ground and the heat demand is low. The collector supplies up to 100 kWh per m^{-2} of collector per month. The monthly net charging of the ground is approximately 15 kWh $month^{-1}$ per meter of ground heat exchanger. This is 10 kWh $month^{-1}$ per meter less than for winter discharge. During transition periods the collector supplies a significant part of the heat load for the evaporator.

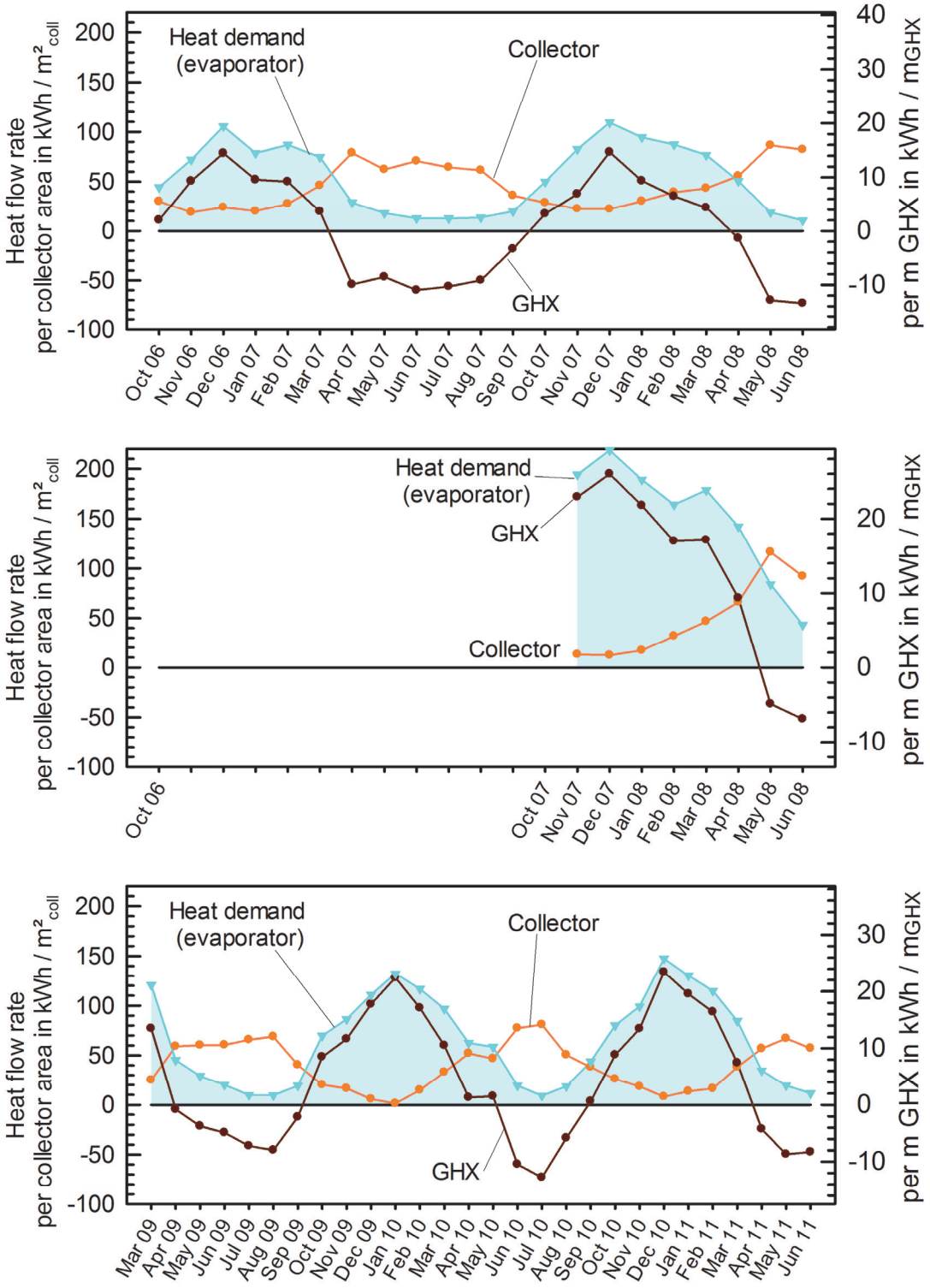

Figure 6-3 Heat flow rates at the heat pump evaporator (blue area), the ground heat exchanger and the collector for the three measured systems. The left y-axis gives the collector specific heat flow. The scaling is identical for all three graphs. The right y-axis gives the specific heat flow rates related to the ground heat exchanger length.
Top: Limburg system, Middle Klein Köris system, Bottom Dreieich system

It is emphasized that the collector heat fraction is lower in autumn periods than in spring. This is explained by the temperature level of the ground heat exchanger. Fully recharged in autumn, it provides higher temperatures than in spring when it is fully discharged after the heating season. Consequently, the collector recharges and is used less in autumn conditions than in spring, even if the ambient conditions and heat demand are the same as in spring.

Attention should be paid to the heating seasons in Limburg, which were extraordinary mild especially in 2006/2007. Here, the collector operated on average 10 K below ambient temperature and even then supplied only 25% of the heat demand on a monthly basis. In other words, even in climates with such warm winters the collector field would need to have a size of 175 m² instead of 43.7 m² to completely supply the required heat. Moreover, this is calculated on a monthly basis and neglects heat storage.

The heat balance of the systems is very different. In the Dreieich system there is a net heat demand from the ground despite the solar regeneration of 50-70 kWh per m. The Limburg system has a balanced ground heat exchanger. 5 kWh are injected per meter ground heat exchanger and year. The Klein Köris system has not been measured for a complete year, but it seems likely that the heat flow rates will not be balanced due to the very high specific heat demand from the vertical ground heat exchanger.

In general, the uncovered collector's operating temperature is strongly connected to the ambient air conditions, Figure 6-4. The average collector operating temperature is similar to the ambient temperature within a limit of maximum of 10 K offset. In most months the difference is significantly less than this.

The collector temperatures are also of interest for the ground source. Temperatures that are too high may damage the pipe's polymeric material or at least require the use of more expensive and temperature stable material. Furthermore, the temperatures in the ground are often limited by legal constraints, e.g. in ground water reservoirs containing drinking water.

A maximum temperature of 38°C was measured. This is in agreement with the other systems which had 35°C. Accordingly, no material problems are expected for most polymeric materials. This also allows retrofitting of systems that have yet no solar collector for regeneration. Nevertheless, the temperatures will become relevant if the system temperatures rise. This should be considered for hotter climates, for high performing selective collectors or in the case of very large collector fields.

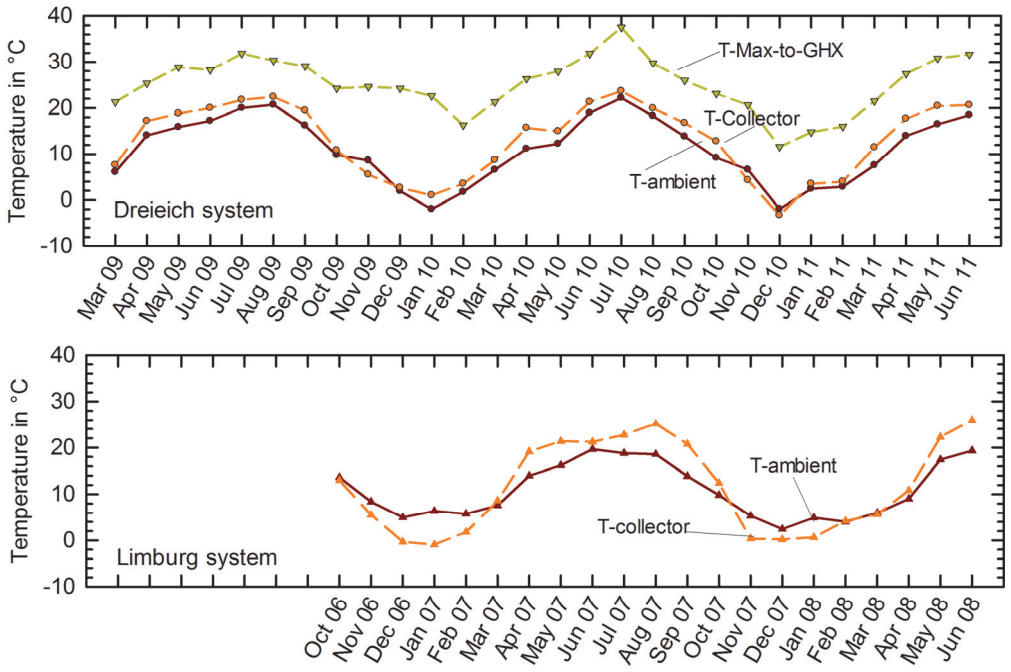

Figure 6-4 Monthly averaged ambient temperatures and energy weighted collector temperatures, Top: Dreieich system with maximum measured inlet temperature to the ground heat exchanger[1]. Bottom: Limburg system

The seasonal performance is measured in both systems, but for different system boundaries. In the Limburg system the seasonal performance SPF_{bst} is 3.5 for both years. In the Dreieich system the seasonal performance factor SHF_{SHP} is 4.0 in the first year and 4.2 in the second year. Direct comparison of the two systems is tempting. The systems, however, have different source and sink temperatures, climates, heat pump efficiencies, and component dimensioning and, therefore, do not allow general rules to be deduced by simple comparison. Nevertheless, the data is provided to IEA SHC Task 44 / HPP Annex 38 (Subtask A), in which the results of field test measurements are analysed in the context of many measured systems.

The field test measurements preclude assessing the impact of the solar heat on the source side because this requires a reference system without solar assistance for comparison. Correspondingly, the impact of the solar energy can only be quantified in the context of simulation that allows an exact system reproduction.

Such a comparative simulation is done for the Dreieich system data and is presented and discussed in the BiSolar-WP project [121], [7]. The energy weighted temperature

[1] The temperature to the ground heat exchanger is measured in the building, so “high” temperatures of 20°C can also arise from the room temperatures.

difference with and without collector is determined at 3 K in the first year of operation and 4.3 K in the 20th year of operation. The temperature difference is calculated for the heat source at the heat pump evaporator inlet. These simulation results belong to a case study, which mixes long-term and short term influences, and, therefore, do not allow extrapolation to other systems.

To conclude, the data, temperatures and component specific mass flow rates measured provide valuable reference values for other measured systems and simulations. They cannot be used to make general conclusions about the impact of solar energy on the source side because there is no reference system without solar regeneration.

6.2 Collector Yield Prediction with Utilizability Method

6.2.1 Introduction of the Utilizability Method

The utilizability method calculates the monthly collector yield with a minimum of data required. It offers a simple way of dimensioning series systems (see Chapter 4.2.2) in combination with existing programmes for vertical ground heat exchanger dimensioning. In such programmes as EED [35] or EWS [37] the monthly collector yield calculated can be applied as a cooling load. The method is also an essential part of the proposed sizing method for fully regenerated ground heat exchangers, see chapter 7.2.

The input data for the calculation model has been reduced to the minimum necessary. The input data required includes: Collector performance coefficients, the hourly global irradiation in the collector pane and monthly values for the average ambient temperature, wind speed and vertical ground heat exchanger temperature.

The method is derived from the calculation method for the collector yield introduced by Duffie and Beckman [62, p. 700]. It is presented as the daily utilizability method, which calculates the "monthly average daily useful energy gain" $\overline{Q_u}$. Basically, the calculation determines the dependency on solar irradiance and thermal losses due to a collector temperature difference to the ambient. It is defined according to Eq. 6-1 using the daily average utilizability $\overline{\Phi}$, which represents the usable part of the daily irradiation.

$$\overline{Q_u} = A_{coll} \cdot F_R(\overline{\tau\alpha}) \cdot \overline{H_T} \cdot \bar{\Phi} \qquad \text{Eq. 6-1}$$

with
$\overline{Q_u}$ *Monthly average daily useful energy yield in* kWh d^{-1}
F_R *Collector heat removal factor in* -
$(\overline{\tau\alpha})$ *Monthly average transmittance-absorptance in* -
$\overline{H_T}$ *Monthly average daily radiation in collector pane in* kWh d^{-1} m^{-2}
$\bar{\Phi}$ *Daily utilizability in* -
A_{coll} *Collector area in* m^{-2}

The method uses monthly values and is applicable only for systems with constant or slowly changing collector operating temperatures over the course of the month. Accordingly, it is very well applicable for ground coupled systems in combination with solar thermal collectors.

The determination of the daily utilizability $\bar{\Phi}$ is crucial for the determination of the collector yield. Daily utilizability is defined as "the sum for a month, over all hours and all days of the radiation on a tilted surface [$I_T = G'_T$] that is above a critical level [$I_{TC} = G'_{TC}$] divided by the [sum of the] monthly radiation" [62, p. 700]. This daily average utilizability $\bar{\Phi}$ is defined according to Eq. 6-2. Here, G'_T is used instead of I_T and G'_{TC} instead of I_{TC}.

$$\bar{\Phi} = \sum_{days} \sum_{hours} \frac{\left(G'_{T,i} - G'_{TC}\right)^+}{\bar{H}_T\, N} = \frac{1}{H_T} \sum_{i=t_1}^{t_2} \left(G'_{T,i} - G'_{TC}\right)^+ \qquad \text{Eq. 6-2}$$

with
$\bar{\Phi}$ *(Daily)*[1] *utilizability in* -
$\overline{H_T} \cdot N = H_T$ *Monthly sum of radiation in collector pane in* kWh d^{-1} m^{-2}
t_1, t_2 *Time at begin and end of the month usually in* h
$G'_{T,i}$ *Average radiation collector pane in time step i (usually hours) in* Wm^{-2}
G'_{TC} *Monthly critical radiation level in* W m^{-2}

The + indicates that only positive differences are included.

The critical radiation level I_{TC} is a constant monthly value. It is a function of the collector parameters and the representative temperature conditions for the collector, the collector inlet temperature T_i and the ambient temperature T_{amb}. It is defined according to Duffie Beckman according to Eq. 6-3 as:

[1] From the perspective of the author "daily" is a misleading prefix for the utilizability because it is always calculated as a value from monthly sums. It is, therefore, clearly a monthly-related value and used to determine monthly averaged daily values. To avoid further confusion "utilizability" is hereafter used for $\bar{\Phi}$ without any additional "monthly" or "daily", but always related to a period of one month.

$$G_{TC} = \frac{F_R U_L (\bar{T}_i - \bar{T}_{amb})^+}{F_R (\tau\alpha)_n \cdot \frac{(\overline{\tau\alpha})}{(\tau\alpha)_n}} \qquad \text{Eq. 6-3}$$

with

G_{TC}	*Monthly critical radiation level in* W m^{-2}
F_R	*Collector heat removal factor* F_R in -
U_L	*Collector overall heat loss coefficient* U_L *in* W m^{-2} K^{-1}
$\bar{T}_i$	*Representative monthly collector inlet temperature in* °C
$\bar{T}_{amb}$	*Representative monthly ambient temperature in* °C
$(\tau\alpha)_n$	*Perpendicular effective transmittance absorptance product in* -
$(\overline{\tau\alpha})$	*Average effective transmittance absorptance product incidence angle dependent in* -

6.2.2 Motivation for Modification of Utilizability Method

The utilizability method introduced requires a modification when used with uncovered (PVT-) collectors and systems with low temperature heat demand. Two additional effects have to be considered: Convective gains and radiation use for PV- electricity production. Figure 6-5 displays the collector yields measured correlated to the irradiation measured in the collector pane for daily or monthly periods.

The convective gains without irradiation have most obviously to be respected. During periods with low irradiance the collector yield measured clearly exceeds the solar irradiance offered. Accordingly, irradiance is no longer the dominating heat source of the collector, but there are also **convective heat gains** from the ambient air. In periods with low irradiance particularly, these convective gains can provide a significant part of the daily or monthly usable heat.

The Dreieich system with **PVT-collectors** additionally converts solar radiation to PV electricity. It shows the lowest thermal yields. Although irradiance related performance differences do not clearly prove any reduction by irradiation from the PV production, it still is an indicator for a generally reduced thermal output. In any case, the fraction of irradiance that is converted to PV electricity has to be respected.

In fact, the difference between Klein Köris and Limburg highlights the dependency of the collector yield to the operating temperature level. Under identical radiation conditions the collector yields differ up to 50%, although the two systems have similar thermal collector performance characteristics and system layouts. Consequently, for a reliable yield prediction the temperature level has to be accounted for- in terms of a critical radiation level or otherwise. The method for utilizability is thirdly modified for usability reasons. The collector heat removal factor F_R and the collector overall heat loss coefficient U_L parameters are related to the collector inlet temperature. In contrast,

the widespread **performance data from EN- 12975** is related to the average fluid temperature of the collector. Most data, therefore, for uncovered collectors is not applicable to the original form of the utilizability equation. The loss terms in the equation for utilizability must, for this reason, be modified.

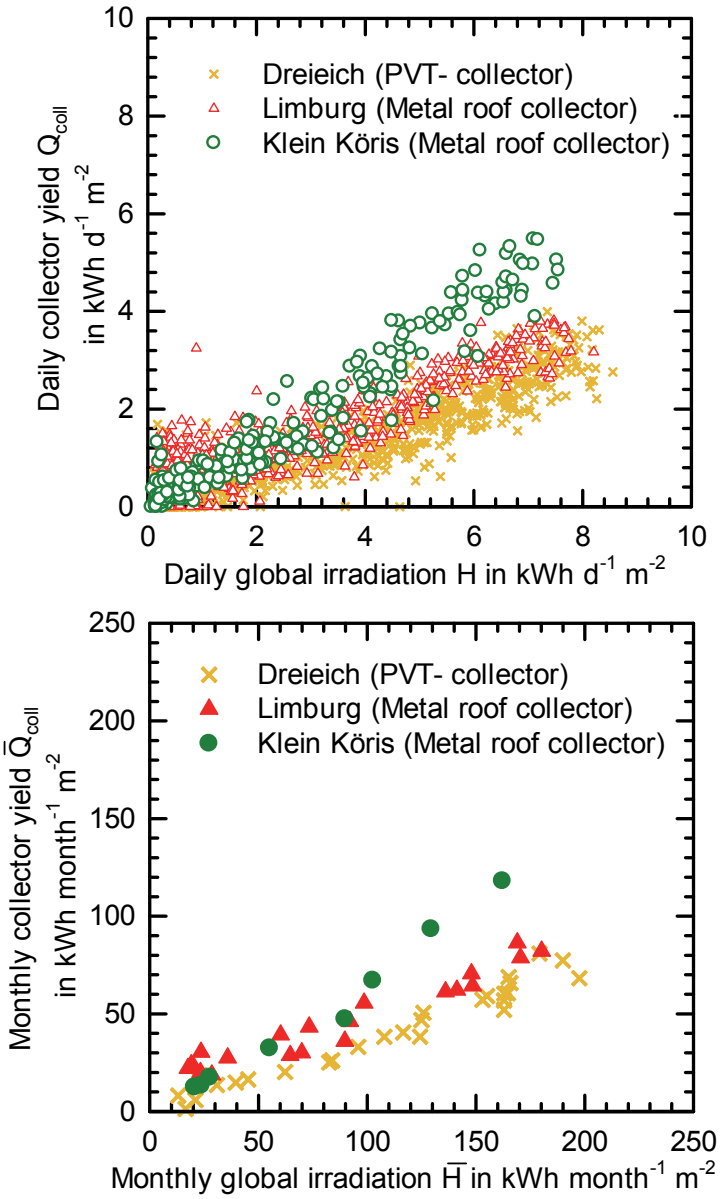

Figure 6-5: Daily (top) and monthly (bottom) measured collector yield and global irradiation in collector pane for the three systems measured: Dreieich, Limburg, Klein Köris

6.2.3 Modified Utilizability Method

Modifications to EN- 12975 Performance Data

The equation Eq. 6-3 is modified in context with uncovered collector and for use of performance parameters from standard test procedures. Basically, the mean temperature

related collector performance coefficients are adopted to allow the connection with performance data from EN- 12975. For this adoption the equations Eq. 6-4 and Eq. 6-5 [143, p. 16] are used with the constraint that the loss coefficient for unglazed collectors is temperature independent:

$$\eta_0{}' = (\tau\alpha)_n \cdot F_R \qquad \text{Eq. 6-4}$$

$$b = U_L \cdot F_R \qquad \text{Eq. 6-5}$$

with
- $\eta_0{}'$ *Collector conversion factor including wind losses in* -
- $(\tau\alpha)_n$ *Perpendicular effective transmittance absorptance in* -
- F_R *Collector heat removal factor F_R in* -
- U_L *Collector overall heat loss coefficient related to absorber temperature in* W m^{-2} K^{-1}
- b *Collector overall heat loss coefficient related to average fluid temperature in* W m^{-2} K^{-1}

The absorptance α for unglazed collectors replaces the effective absorptance transmittance product needed for covered collectors. Moreover, the loss terms b and η_0 are integral and correspond to loss coefficients including the wind dependent losses. In correspondence to the representative temperatures both, b and η_0, are calculated for a characteristic average wind speed $\bar{u}$. As a result, equation Eq. 6-3 for the critical monthly radiation level G_{TC} derives to Eq. 6-6. The critical radiation level represents the radiation limit at which the collector reaches a stagnation temperature equal to load or collector temperature $\bar{T}_{avg}$. There is, consequently, no critical radiation for load temperatures below or equal to the ambient air temperature.

$$G_{TC} = \frac{b \cdot \left(\bar{T}_{avg} - \bar{T}_{amb}\right)^+}{\eta_0{}' \cdot \frac{\bar{\alpha}}{\alpha_n}} = \frac{(b_1 + b_2 \cdot \bar{u}) \cdot \left(\bar{T}_{avg} - \bar{T}_{amb}\right)^+}{\eta_0 \cdot (1 - b_u \cdot \bar{u}) \cdot \frac{\bar{\alpha}}{\alpha_n}} \qquad \text{Eq. 6-6}$$

with
- $\bar{u}$ *Representative wind speed in* m s^{-1} -
- $\bar{T}_{avg}$ *Representative monthly average collector/load fluid temperature in* °C
- $\bar{T}_{amb}$ *Representative monthly average ambient temperature in* °C
- $\frac{\bar{\alpha}}{\alpha_n}$ *Ratio of effective incident solar absorptance to perpendicular solar absorptance in* -
- b_1, b_2, b_u, η_0 *according to EN-12975-2 see chapter 0*

For $\bar{\alpha}/\alpha_n$ a value of 0.95 is adapted from [62, p. 198]. This equals an angle of incidence of approximately 50° for a black body and should represent a conservative estimate for all flat surfaces. It is emphasized that the average collector temperature is the only variable connected to the behaviour of the system. All other parameters, such as the collector performance, radiation or wind speed stay either constant or are independent from the sizing of the vertical ground heat exchanger and the actual heat demand.

Method Extension to Convective Gains

Convective gains can become usable heat gains, but only for collector operating temperatures below the ambient air temperature. Correspondingly, the utilizability, defined in Eq. 6-2, is extended by a convective term ϕ_{conv} respecting possible additional convective heat gains from the ambient air. The proposed equation for ϕ_{conv} is presented in Eq. 6-7 and the extended equation for the utilizability is given in Eq. 6-8. This correlation determines the convective gains from the collector loss coefficients and the monthly average temperature difference to the ambient surroundings.

$$\phi_{conv} = (b_1 + b_2 \cdot \bar{u})\left(\bar{T}_{amb} - \bar{T}_{avg}\right)^{+} \cdot \zeta \qquad \text{Eq. 6-7}$$

$$\bar{\Phi} = \frac{1}{H_T}\left(\phi_{\text{conv}} + \sum_{i=t_1}^{t_2}\left(G'_{T,i} - G'_{TC}\right)^{+}\right) \qquad \text{Eq. 6-8}$$

with ϕ_{conv} *Additional monthly heat gains by convection in* kWh month^{-1}
ζ *Run-time coefficient, 0.33 of solar collector*

The + indicates that only positive differences are included.

The run-time ζ is clearly an empirical parameter, which reduces the heat gain obtained by monthly values. It is assumed that the convective heat gains occur only intermittently and are not obtained continuously for the whole month, although the average temperatures suggest so. In the following calculations $\zeta = \frac{1}{3}$ is used which corresponds to 8 hours of operation with convective gains per day.

Modification for PVT- Collectors

The utilized PV- electricity production has to be considered in addition to the convective gains. The electricity production reduces the irradiance for heat conversion available and affects the critical radiation level. Correspondingly, the available global irradiance G'_T in the collector pane is reduced by the PV electricity produced. For the calculation the electric PV efficiency at standard test conditions $\eta_{PV,STC}$ is used in Eq. 6-9:

$$\bar{\Phi} = \frac{1}{H_T}\left(\zeta \cdot (b_1 + b_2 \cdot \bar{u})\left(\bar{T}_{amb} - \bar{T}_{avg}\right)^{+} + \sum_{i=t_1}^{t_2}\left(1 - \eta_{PV,STC}\right)\left(G'_{T,i} - G'_{TC}\right)^{+}\right) \qquad \text{Eq. 6-9}$$

with $\bar{\Phi}$ *Utilizability in* -
ζ *Run-time coefficient, 0.33*
$\bar{u}$ *Representative wind speed in* m s^{-1} -
$\bar{T}_{avg}$ *Representative monthly avg. coll/load. fluid temperature in* °C
$\bar{T}_{amb}$ *Representative monthly ambient temperature in* °C
t_1, t_2 *Time at begin and end of the month usually in* h
$\eta_{PV,STC}$ *Electric efficiency under STC, if collector is a PVT coll. in* -
$G'_{T,i}$ *Avg. radiation coll. pane in time step i (usually hours) in* W m^{-2}

G_{TC} Monthly critical radiation level in W m^{-2}
b_1, b_2, b_u, η_0 according to EN-12975-2

For better comprehension the utilizability is discussed for the systems measured. The data is given in Appendix D. For low heat demands, in summer, values of 0.6 to 0.7 are typical. Accordingly, only 60% of a summer month's irradiance could be harvested by the collector. With rising heat demand, in winter and transition periods, a large variety of utilizability values between 0.6 and 1.8 occur. Values greater than one emphasize the importance to include convective heat gains- especially in periods of a high heat demand. Here, the collector yield exceeds the monthly available irradiance.

Having determined the modified utilizability $\bar{\Phi}$, the monthly collector yield Q_u can be calculated with Eq. 6-10.

$$Q_u = A_{coll} \cdot \eta_0 \cdot (1 - b_u \cdot \bar{u}) \cdot H_T \cdot \bar{\Phi} \qquad \text{Eq. 6-10}$$

The expression is identical to Eq. 6-1, except that it uses the average collector loss terms and the monthly radiation sum H_T according to Eq. 6-4 and Eq. 6-5.

Herewith, a calculation is derived that allows the monthly collector yield to be calculated with only two equations, Eq. 6-9 and Eq. 6-10. Furthermore, the calculation now accounts for convective gains, possible PV electricity production and uses standard EN-12 975 performance parameters.

Of course, at a first glance the calculation still seems cumbersome for practical application, but this is not the case. On the contrary, the collector area and the load/collector temperature are the only free variables in the context of dimensioning a particular system. All other input parameters are constant for a particular location and collector orientation.

6.2.4 Obtaining the Required Data

The method described requires input data, which is specified in the following.

The collector performance data of 12975-2 b_1, b_2, b_u, η_0 has to be used and should be provided by the collector manufacturer. Some parameter sets are given in Appendix A. The value used for the collector area A_{coll} should be the same that is used as for the collector performance determination, usually the aperture collector area.

The meteorological data must be adapted to the collector pane. Several sources of data are available, see for example [144], [102]. The characteristic wind speed $\bar{u}$ and the ambient air temperature $\bar{T}_{avg}$ are monthly average values. Note that the wind speed in

the data is adopted for use with the collector performance measured directly above the collector. Until no better correlation is available, Haller in IEA SHC Task 44/ Annex 38 [101, p. 1] proposes a reduction of 50% for $\bar{u}$ of the meteorological wind speed.

The characteristic average load or collector temperature $\bar{T}_{avg}$ represents the characteristic monthly temperature level for the collector. In contrast to the other input parameters, it has to be calculated. It is proposed that the average ground heat exchanger temperature be used as load or collector temperature $\bar{T}_{avg}$. This temperature is derived then from the planning of the ground source. A method is proposed in chapter 7.2 for an equilibrated ground heat exchanger.

In part regeneration ground heat exchanger the average fluid temperature should be used for the solar yield calculation. This assumption is checked with the measurement data, Table 6-1 and Figure 6-6. The differences between measured ground heat exchanger and collector temperature are below 1 K for the annual average values. Higher deviations, up to approx. 2.5 K for monthly values, seem possible, although atypical, and the standard deviations are 1.3 K or less. The deviation is small especially in summer at high collector yields.

As a result, the data measured demonstrates that the average ground source temperature used for the calculation of the collector yield and the resulting difference are tolerable within planning uncertainty.

Table 6-1: Temperature difference between average energy weighted collector and vertical ground heat exchanger temperature

Difference of T_{coll} - T_{GHX}		Limburg	Klein Köris	Dreieich
Average	K	0.4	2.3	-0.9
Maximum deviation	K	-2.7	4.0	-2.3
Standard deviation	K	1.3	1.3	0.54

The Klein Köris system is emphasized. Here, a pressure relief valve is installed in parallel to the collector, which leads to the higher deviations, due to simultaneously different mass flow rates in the collector and the vertical ground heat exchanger.

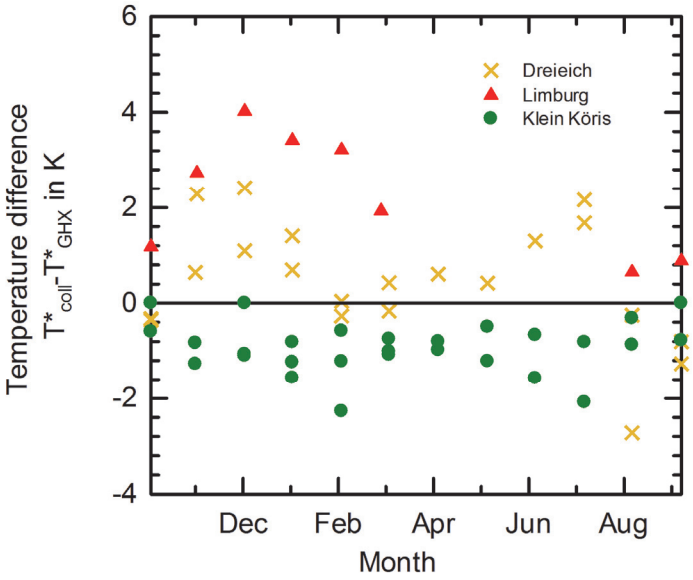

Figure 6-6: Monthly temperature difference in three systems measured between the average fluid temperature T^* in the vertical ground heat exchanger T^*_{GHX} and the solar collector T^*_{coll}

6.2.5 Validation of Utilizability Method

The utilizability method described has not been used before for vertical ground heat exchanger systems. Simplifications are made to allow a simple and lucid calculation. For instance, the method does not account for long-wave radiation losses, heat capacity effects, pipe losses, condensation, controller thresholds etc. Furthermore, most meteorological input data and the load/collector temperature are applied as monthly averaged values. In short, the method requires validation.

The method is validated against the data measured from the three systems presented in chapter 6.1.

The utilizability calculated for the three systems is displayed in Figure 6-7 and correlated against the monthly collector heat measured. Furthermore, a regression analysis is conducted with the monthly values. The statistical correlation coefficient R is 0.9846 and tests the quality of the regression and, correspondingly, the calculation method for the utilization. The standard error of estimate is 4.5 kWh m^{-2} $month^{-1}$.

In fact, the data in Figure 6-7 reveals that the utilization calculated slightly underestimates the collector yield. This underestimation tends to appear especially in months with higher yields above 60 kWh m^{-2} $month^{-1}$ and appears in all three systems.

In addition the method is validated against the dynamic system simulations, chapter 4. The system is simulated in the Strasbourg climate with an 8 m² black polymer collector and 110 m vertical ground heat exchanger. The collector is integrated series in-front on the cold side. The weather data applied for simulation and utilizability method are

identical. The simulated energy weighted monthly collector or load temperatures are also an input for the utilizability method.

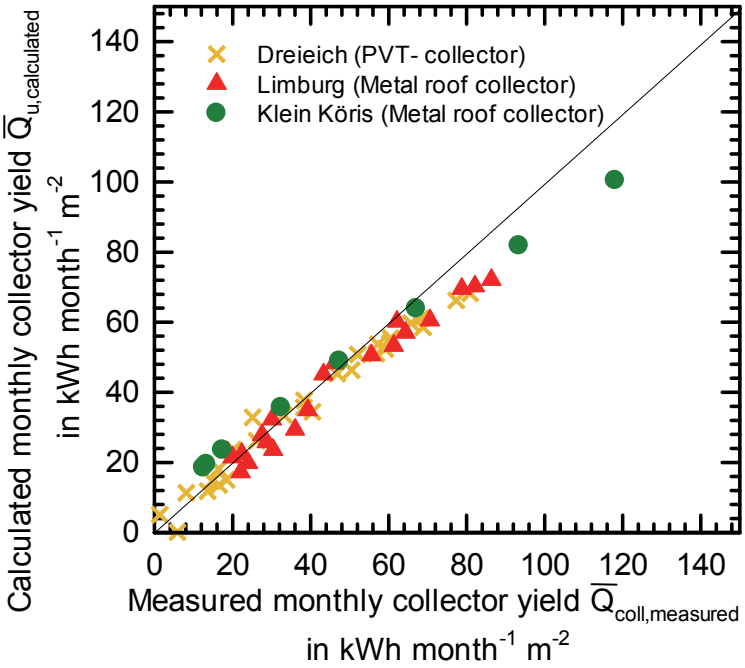

Figure 6-7: Monthly utilizability calculated $Q_{u,calculated}$ correlated against the monthly collector yield measured $Q_{coll,measured}$

The calculation methods, utilizability and dynamic simulation, deliver results with a high agreement and a statistical correlation coefficient R of 0.999. The standard error of estimate is 2.0 kWh m^{-2} month^{-1}. The result of the regression analysis performed is conducted for the same constraints as for the measurements. The data is presented in Figure 6-8.

All things considered the modified utilizability method is applicable with high accuracy for uncovered collectors in combination with vertical ground heat exchangers. Compared to the measurement the method delivers values approximately 10% lower than the measured energy yield. Compared to the simulations the method retrieves collector yields 1.2% lower than the collector yield in the dynamic simulation.

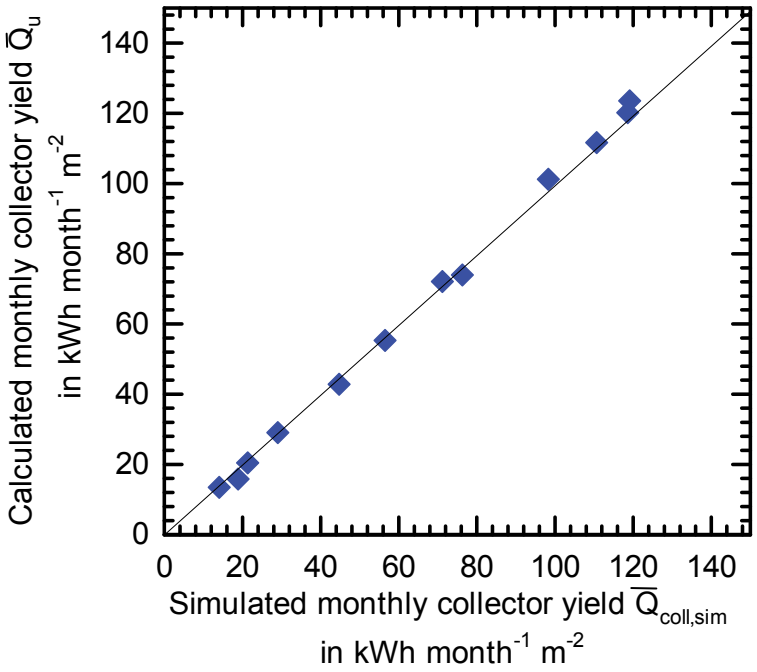

Figure 6-8: Monthly calculated $Q_{utilization}$ correlated against the simulated monthly collector yield

7 Planning

7.1 Adjacent Systems in Residential Areas

Multiple single vertical ground heat exchangers in residential areas act as a field of ground heat exchangers. The minimum distance of 5 m or 6 m between boreholes [17], section 5.1.1 or a placement to the estate boundaries as often demanded by local authorities does not prevent the interference between adjacent but autonomous systems, [145].

This kind of influence is complex and has clear long-term character effects as outlined in chapter 2.2.5. It depends on the ground properties, the geometry of the ground heat exchangers, and, of course, on the amount of heat extracted. The more ground heat exchangers are arranged adjacent to each other the higher the interference and the longer the time to reach a steady temperature regime.

As an exemplary case a set of four neighbouring houses is calculated. Each of the houses has the same heat load which is the well-known simulation reference case. Two cases are assumed. The first case is the reference case without solar regeneration. The second case is the reference system with full solar regeneration. The specific heat extraction is very conservative and at 65 kWh per m borehole without solar regeneration. The current VDI 4640-2 guideline allows for much higher extraction rates 100-150 kWh per m [17, p. 16].

The heat loads are the results of dynamic system simulations, which are then used as input data for Earth Energy Designer (EED). EED calculates the minimum temperature in the course of the year as a function of the heat load. The basis for the calculation is the Eskilson equation, Eq. 2-18. Recent validation for borehole fields with heat injection and extraction can be found in [146, pp. 83–84] for building heating and cooling loads.

A constant load file leads to incorrect results because the heat extraction is influenced by the long-term temperature drop. On the other hand, systems with solar regeneration have no long-term temperature drop and the heat extraction change is small in systems without regeneration.

The results of the calculation reveal two major characteristics. Firstly, there is, as to be expected, no temperature drop for systems with solar regeneration, but a clear ongoing temperature drop without regeneration. Secondly, the temperature drop rises for shorter distances between boreholes. For 15 m distance the long term effect is a drop of 3 K.

With solar regeneration the long-term effect is negligible even for very small distances between ground heat exchangers.

Clear interferences of more than 1-2 K will appear in comparatively small fields of 4 single ground heat exchangers operated with well insulated small houses, if operated without regeneration. Many systems that are currently installed [13] are likely to cause these effects, which will only become visible after decades.

Note that the EED results presented only aim to represent the long term effects. The absolute values of the minimum temperatures calculated do not match the dynamic simulation results. This is due to the fact that the peak load runtimes from the dynamic simulations are applied. These maximum heat pump runtimes are around 2 h and seem to be much too short to characterize the effective peak loads in EED. Assuming higher peak loading times will simply shift all minimum temperatures to lower values.

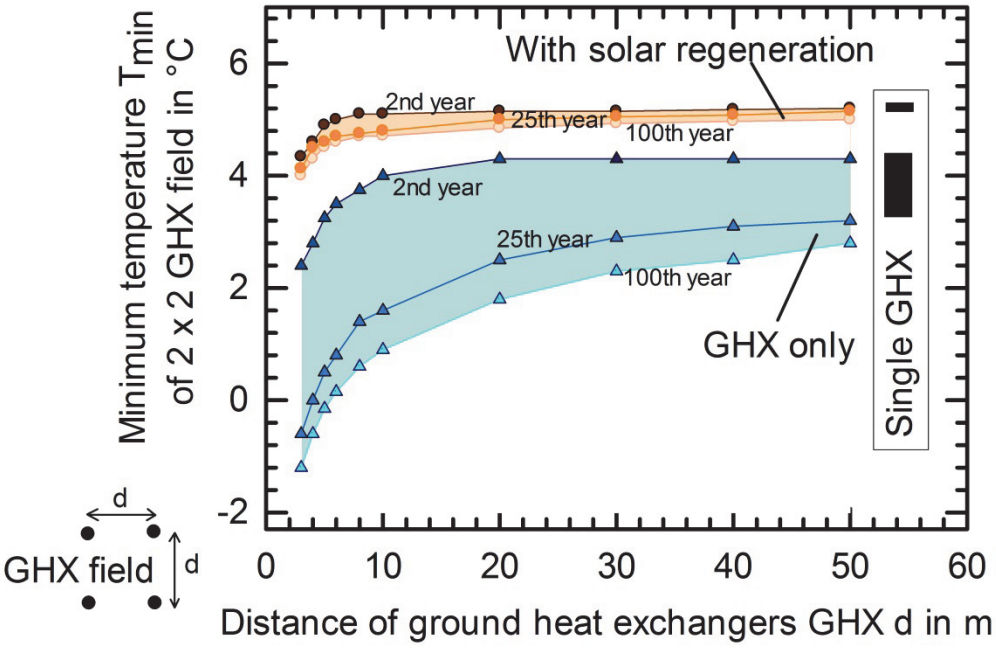

Figure 7-1: 2x2 Ground heat exchanger field with the heat load of four reference simulation systems and varying distances d between the ground heat exchangers. The blue temperatures represent a system without solar regeneration and the red lines represent systems with solar regeneration. The temperature drop for a single heat ground heat exchanger is also given (black boxes)

7.2 Fully Regenerated Ground Heat Exchangers

7.2.1 Analytical Solution for Balanced Ground Heat Exchangers

In accordance to Eskilson any load pattern can be formulated as a train of heat pulses of the temperature in a vertical ground heat exchanger to be calculated [20]. In most cases

monthly heat pulses are considered and then superimposed. The temperature change due to a single heat pulse ΔT_{pulse} between the borehole wall and the undisturbed ground temperature $T_{g,undis}$ can then be expressed for a single vertical ground heat exchanger according to Eskilson [20, p. 516] Equation 22 or introduced in the basics as Eq. 2-12:

$$\Delta T_{pulse} = \frac{\dot{q}_{pulse}}{4\,\pi\lambda} \cdot \left(\ln\left(4\frac{\alpha_g t_{pulse}}{r_{GHX}^2}\right) - \gamma\right) = \frac{\dot{q}_{pulse}}{4\,\pi\lambda} \cdot \Delta T'_{pulse} \qquad \text{Eq. 7-1}$$

With $5 r_b^2 \alpha^{-1} \cong t_b < t_{pulse} < 0.1 \cdot t_s = 0.1 \cdot \frac{H^2}{9\,\alpha}$

$\dot{q}_{pulse}$	*Specific heat flow rate during pulse* in W m^{-1}
λ	*Ground heat conductivity in* W m^{-1}K^{-1}
α_g	*Temperature diffusivity in* m² s^{-1}
r_{GHX}	*Borehole radius in* m
t_{pulse}	*Duration of the pulse in* s
γ	*Euler constant* ~0.5772
$\Delta T'_{pulse}$	*Dimensionless temperature drop due to pulse in* -

Following Eskilson the remaining temperature drop ΔT_{cov} after the recovery time t_{cov} is [20, p. 516] Equation 23

$$\Delta T_{cov} = \frac{\dot{q}_{pulse}}{4\,\pi\lambda} \cdot \ln\left(\frac{t_{cov} + t_{pulse}}{t_{cov}}\right) = \frac{\dot{q}_{pulse}}{4\,\pi\lambda} \cdot \Delta T'_{cov} \qquad \text{Eq. 7-2}$$

With $t_b < t < 0.1 \cdot t_s - t_1$

It is restated that these fields can be treated as a group of single vertical ground heat exchangers as long as the net heat extraction is zero and they are arranged at a certain distance to each other. This certain distance, outside of which no penetration of the temperature field occurs, is according to Eskilson 6 m (radius = 3 m) [20, p. 514].

For closer distances interaction may occur in dependency of the heat load and the ground properties. Assuming such a small distance this will lead to periodical temperature interference, but will have no long-term effect. The simulations with strongly reduced distances in shallow fields down to 3 m, section 5.3.6, reveal only little difference compared to single vertical ground heat exchangers. Even smaller distances than 3 m seem therefore feasible without significant change compared to a single vertical ground heat exchanger.

Eskilson points out that “any pulse train may be expressed by superposition of single pulses”. Accordingly, the two equations for pulses and subsequent recovery allow calculating the temperature drop ΔT_k for any train of heat pulses $\dot{q}_{pulse,n}$. At the time k the temperature drop ΔT_k is the sum of the current pulse $\Delta T_{pulse,k}$ according to Eq. 7-1 and the recovery of previous pulses $\Delta T_{cov,k}$ according to Eq. 7-2:

$$\Delta T_k = \Delta T_{pulse,k} + \Delta T_{cov,k} \quad \text{Eq. 7-3}$$

$\Delta T_{cov,k}$ accounts not only for the temperature drop due to recovery of a single pulse, but the recovery of all other pulses before the current pulse $\dot{q}_{pulse,k}$. This can be calculated using Eq. 7-2 and with i being the first and n being the last pulse before the current pulse:

$$\Delta T_{cov,k} = \sum_{i=1}^{n} \Delta T_{cov,t_i \rightarrow k} = \quad \text{Eq. 7-4}$$

$$\sum_{i=1}^{n} \frac{\dot{q}_{pulse,i=1}}{4\,\pi\lambda} \cdot \ln\left(\frac{t_{i=1\rightarrow k} + t_{pulse,i}}{t_{i=1\rightarrow k}}\right) + \cdots + \frac{\dot{q}_{pulse,n}}{4\,\pi\lambda} \cdot \ln\left(\frac{t_{n\rightarrow k} + t_{pulse,n}}{t_{n\rightarrow k}}\right)$$

This rather generic equation for $\Delta T_{cov,k}$ simplifies tremendously, when applied to annually regenerated vertical ground heat exchangers and heat pulses of uniform monthly duration. The constraint of annual regeneration allows neglecting all induced temperature drops before the beginning of the previous year.

As an example the temperature recovery is given for the month of March $\Delta T_{cov,mar}$. Eleven recovery temperature drops $\Delta T'_{cov,1\ldots11}$ from the eleven previous months need to be accounted for. Correspondingly, the impact from April one year before is included. The impact from March one year before is not. It is postulated that in an annually and fully regenerated vertical ground heat exchanger all heat induced influences from previous periods level out after one year and can, therefore, be ignored.

$$\Delta T_{cov,k=mar} \quad \text{Eq. 7-5}$$

$$= \frac{1}{4\pi\lambda} \sum_{i=jan}^{dec} \dot{q}_{jan} \cdot \Delta T'_{cov,jan\rightarrow mar} + \dot{q}_{feb} \cdot \Delta T'_{cov,feb\rightarrow mar} + \dot{q}_{apr}$$

$$\cdot \Delta T'_{cov,apr\rightarrow mar} + \cdots + \dot{q}_{dec} \cdot \Delta T'_{cov,dec\rightarrow mar}$$

$$with\ \Delta T'_{cov,month\rightarrow k=mar} = \ln\left(\frac{1\ month + t_{month\rightarrow k=mar}}{t_{month\rightarrow k=mar}}\right)$$

$$= \frac{1}{4\pi\lambda} \sum_{i=jan}^{dec} \dot{q}_{jan} \cdot \Delta T'_{cov,2} + \dot{q}_{feb} \cdot \Delta T'_{cov,1} + \dot{q}_{apr} \cdot \Delta T'_{cov,11} + \cdots + \dot{q}_{dec}$$

$$\cdot \Delta T'_{cov,3}$$

$$with\ \Delta T'_{cov,x} = \ln\left(\frac{x\ months + 1\ month}{x\ months}\right)\ all\ time\ intervals\ in\ s$$

The temperature drop at the outer borehole radius at the end of a month at a certain month k is then expressed as:

$$\Delta T_k = \Delta T_{pulse,k} + \Delta T_{cov,k} = \frac{1}{4\pi\lambda}\left(\dot{q}_{pulse,mar} \cdot \Delta T'_{pulse}\right) + \sum_{i=jan}^{dec} \dot{q}_i \cdot \Delta T'_{cov,k-i} \quad \text{Eq. 7-6}$$

As an example for the recovery in one year the response is calculated for one single monthly pulse induced in January of 10, 25, 50 and 75 W/m, Figure 7-2.

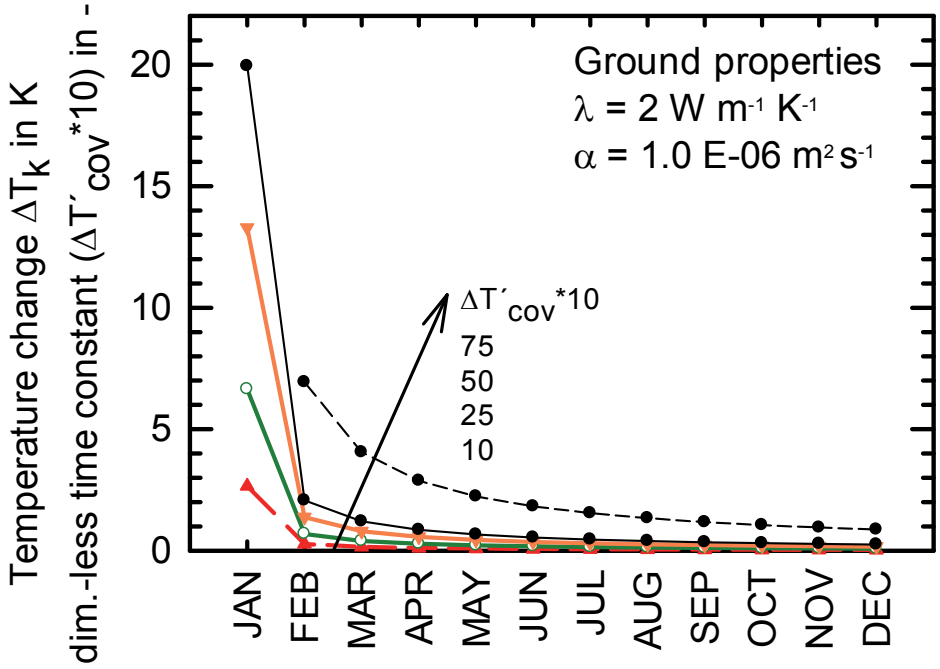

Figure 7-2: Dimensionless ground response $\Delta T'_{cov,} \cdot 10$ and the absolute ground temperature response ΔT_k at the borehole radius for a single monthly pulse in January of 10/25/50/75 W m^{-1} K^{-1}. The temperatures correspond to the temperature at the end of the month.

Figuratively speaking each monthly time constant $\Delta T'_{cov,x}$ is the characteristic response to a single month pulse x months later. Of course, each time constant has to be multiplied with the corresponding heat load eleven, ten, nine etc. months ago. Then the heat loads of the past eleven months and the pulse in the current month determine the temperature response.

To give an example: in March the temperatures are affected by April of the previous year. The heat load of April has a time constant for 11 months earlier, this would be April ($\Delta T'_{cov,11} = \Delta T'_{cov,apr\rightarrow mar}$), and has to be multiplied with the heat load from eleven months earlier here April $\dot{q}_{apr}$.

The dimensionless time constants $\Delta T'$ depend only on the length of the pulses and the duration it has passed. Once calculated for one year the eleven time constants can be reused for all other months in the year as long as monthly values are investigated. The same applies to the time constant for the pulse although in this case ground properties

and borehole radius are compulsory parameters and have to be adapted depending on the specific location.

As a result, the dimensionless time constants in connection with regenerated vertical ground heat exchangers make possible a refined expression for the borehole temperatures in the course of the year. The twelve monthly temperature drops in the course of the year at the end of each month $\overrightarrow{\Delta T}$ can then be calculated best by the use of a matrix:

$$\overrightarrow{\Delta T} = \frac{1}{4\pi\lambda} \cdot \boldsymbol{\Delta T'} \cdot \overrightarrow{\dot{q}_{pulse}}$$

with

$$\boldsymbol{\Delta T'} = \begin{pmatrix} \Delta T'_{pulse} & \Delta T'_{cov,feb\rightarrow jan} & \Delta T'_{cov,mar\rightarrow jan} & \cdots & \Delta T'_{cov,dec\rightarrow jan} \\ \Delta T'_{cov,jan\rightarrow feb} & \Delta T'_{pulse} & \Delta T'_{cov,mar\rightarrow feb} & \cdots & \Delta T'_{cov,dec\rightarrow feb} \\ \Delta T'_{cov,jan\rightarrow mar} & \Delta T'_{cov,feb\rightarrow mar} & \Delta T'_{pulse} & \cdots & \Delta T'_{cov,dec\rightarrow mar} \\ \cdots & \cdots & \cdots & \cdots & \cdots \\ \Delta T'_{cov,jan\rightarrow dec} & \Delta T'_{cov,feb\rightarrow dec} & \Delta T'_{cov,mar\rightarrow dec} & \cdots & \Delta T'_{pulse} \end{pmatrix} \qquad \text{Eq. 7-7}$$

$$\boldsymbol{\Delta T'} = \begin{pmatrix} \Delta T'_{pulse} & \Delta T'_{cov,11} & \Delta T'_{cov,10} & \cdots & \Delta T'_{cov,1} \\ \Delta T'_{cov,1} & \Delta T'_{pulse} & \Delta T'_{cov,11} & \cdots & \Delta T'_{cov,2} \\ \Delta T'_{cov,2} & \Delta T'_{cov,1} & \Delta T'_{pulse} & \cdots & \Delta T'_{cov,3} \\ \cdots & \cdots & \cdots & \cdots & \cdots \\ \Delta T'_{cov,11} & \Delta T'_{cov,10} & \Delta T'_{cov,9} & \cdots & \Delta T'_{pulse} \end{pmatrix}$$

$\overrightarrow{\Delta T}$	*Vector for monthly temperatures at outer ghx radius*
λ	*Heat conductivity of the ground in* W m^{-1}K^{-1}
$\overrightarrow{\dot{q}_{pulse}}$	*Vector for monthly heat loads in* W m^{-1}
$\boldsymbol{\Delta T'}$	*Matrix for dimensionless time constants for the ground heat exchanger*

Because all eleven $\Delta T'_{cov,x}$ are independent of ground properties and heat loads, once calculated the eleven temperature drops $\Delta T'_{cov}$ apply to all monthly calculations in any ground or borehole configuration. For each system only $\Delta T'_{pulse}$ must be calculated depending on the ground properties and the borehole radius. Likewise, within the matrix $\boldsymbol{\Delta T'}$ the time constant $\Delta T'_{pulse}$ is the only variable dependant on the ground properties and borehole radius. The matrix $\boldsymbol{\Delta T'}$ is given in the Appendix F.

To conclude, the calculation of the temperature in the regenerated vertical ground heat exchanger simplifies immensely as only one year of previous heat pulses and no geometry of the borehole field need to be considered. With the equation presented the yearly temperature profile $\overrightarrow{\Delta T}$ at the end of the month can be calculated for any given train of monthly heat pulses $\overrightarrow{\dot{q}_{pulse}}$ with a minimum of effort.

It is emphasized that the result calculated, the temperature profile $\overrightarrow{\Delta T}$, is the temperature at the borehole radius r_{GHX}. The calculation of the minimum fluid temperature

additionally requires the consideration of the borehole resistance and the temperature response of a peak heat pulse according to equation Eq. 2-18. This concerns not only the dimensioning of the vertical ground heat exchanger correspondingly the calculation of the minimum inlet temperature, but also the calculation of the characteristic monthly solar collector temperature $\overline{T_{avg}}$, which is discussed in the following paragraphs.

In principle, the dimensioning approach for solar collectors and vertical ground heat exchangers are different. Normally, the fluid temperature is the input parameter and the collector energy yield is the calculated result. In contrast, for the vertical ground heat exchanger the fluid temperature is the calculated result and the heat extraction is the required input data. The dimensioning of the collector area in hybrid systems demands combination of both calculation methods. This enables dimensioning the collector area depending on the climate, heat exchanger length, ground properties, collector parameters and a given heat demand.

The collector yield is determined with the developed utilizability method, see Eq. 6-10, as a function of the characteristic monthly load temperatures $\overline{T_{avg}}$. This characteristic load temperature is calculated as a function of the monthly heat load according to Eskilson, see Eq. 2-18. Both equations will be combined and solved to retrieve the necessary collector area, for which an equilibrated balance of the ground is achieved. The collector area is determined iteratively.

The equation for regenerated vertical ground heat exchanger temperatures requires some modification in order to combine it with the utilizability method. In fact, the equation calculates the temperature at the borehole radius, Eq. 7-7, for any train of heat pulse. The representative monthly fluid temperature is calculated using the analytic Eskilson solution for the vertical ground heat exchanger, Eq. 2-18. This equation is modified for application with the collector with the aim of calculating the representative load or collector fluid temperature in a month $\overline{T_{avg}}$:

$$\overline{T_{avg}} = T_{g,undis} - \frac{\dot{Q}_{g,lt}}{L} R^{\#}_{g,lt} - \frac{\dot{Q}_{net,p}}{L}\, R^{\#}_{g,p} - \frac{\overline{\dot{Q}_{coll,peak}}}{L} \cdot R^{\#}_{peak} - \frac{\overline{\dot{Q}_{coll}}}{L} R^{\#}_{b} \qquad \text{Eq. 7-8}$$

The following simplifications can be made for fully regenerated vertical ground heat exchangers

- No long term heat extraction $\dot{Q}_{g,lt} = 0$
- The periodic temperature drop $\frac{\dot{Q}_{net,p}}{L}\, R^{\#}_{g,p}$ is calculated not with a sine curve, Eq.

2-22, but with a monthly heat load distribution and the matrix according to Eq. 7-7

Attention should be paid to the fact that the heat flow rate of the collector is charging the vertical ground heat exchanger and therefore counts negatively. The fluid temperature is increased. Together with Eq. 7-8 and using the assumptions presented the monthly average collector temperatures can be calculated with Eq. 7-9:

$$\overrightarrow{\overline{T_{avg,coll}}} = \overrightarrow{\overline{T_{g,undis}}} - \frac{1}{4\pi\lambda} \cdot \boldsymbol{\Delta T}' \cdot \overrightarrow{\dot{q}_{ghx,pulse}} - \overrightarrow{\overline{\dot{q}_{coll,peak}} \cdot R^{\#}_{peak}} - \overrightarrow{\overline{\dot{q}_{coll,eff}}} \cdot R^{\#}_{b} \qquad \text{Eq. 7-9}$$

$\overrightarrow{\overline{T_{avg}}}$	*Vector for monthly average collector temp. in* °C
$\overrightarrow{\overline{T_{g,undis}}}$	*Vector for undisturbed ground temperature in* °C
$\overrightarrow{\dot{q}_{ghx,pulse}}$	*Vector for monthly net heat loads in* W m^{-1}
$\boldsymbol{\Delta T}'$	*Matrix for dimensionless time constants for the GHX*
$\overline{\dot{q}_{coll,peak}}_i$	*Average peak heat load in month i in* W m^{-1}
$R^{\#}_{peak_i}$	*Average peak load resistance in month i in* m K W^{-1}
$\overrightarrow{\overline{\dot{q}_{coll,eff}}}$	*Vector for effective collector heat flow rate in in* W m^{-1}
$R^{\#}_{b}$	*Borehole resistance in m* K W^{-1}
λ	*Heat conductivity of the ground in* W m^{-1}K^{-1}

Heat flow rates discharging the ground count positive. Heat flow rates charging the ground count negative.

The equation given requires additional input data for the solar collector. All values, however, can be estimated from data that is compulsory for the utilization method and that is already used for the collector yield calculation. The inputs required are the effective collector heat flow rate $\overrightarrow{\overline{\dot{q}_{coll,eff}}}$, the average collector heat peak load $\overline{\dot{q}_{coll,peak}}_i$, and the characteristic average operation peak runtime t_{peak}. This peak runtime is needed for the calculation of the characteristic peak time resistance $R^{\#}_{peak_i}$.

The values required are calculated from the utilizability data by simplification. The monthly effective collector heat flow rates $\overrightarrow{\overline{\dot{q}_{coll,eff}}}$ are calculated by the monthly utilizability Q_u and the overall run-time of the collector in the month $t_{runtime}$. The utilizability is already known and the monthly overall run-time is determined as the time, during which the solar irradiation level is above the critical radiation level G_{TC}. All values needed are determined previously as part of the collector yield calculation. In spreadsheet calculations $t_{runtime}$ is derived by counting cells. The run-time allows the calculation of the monthly characteristic collector heat flow rate $\overline{\dot{q}_{coll,eff}}\sim$ from the utilizability according to Eq. 7-10.

$$\overline{\dot{q}_{coll,eff}\sim} = \frac{Q_u}{t_{runtime} \cdot L} \qquad \text{Eq. 7-10}$$

$\overline{\dot{q}_{coll,eff}\sim}$ is a good first order approximation of the average collector heat flow rate, although the time-averaged value underestimates the characteristic heat flow rate of the collector if compared to results from simulations and measurements. Differences appear particularly in summer periods with low critical radiation levels G_{TC} when high heat flow rates together with high irradiance are responsible for high collector yields and operating temperatures. In these summer months, however, long daily average run-times of over 12 h can appear. As a result, the calculated $\overline{\dot{q}_{coll,eff}\sim}$ is too moderate and underestimates the effective collector temperatures. The calculated collector heat flow rates derived by $\overline{\dot{q}_{coll,eff}\sim}$ are often lower in summer than in winter. The time averaging leads to underestimated heat flow rates and therefore lowers the calculated effective collector temperatures. This is not in accordance with the measurement results, Figure 6-3.

To compensate for this effect, an empiric correction term is applied to increase the effective collector heat flow rate $\overline{\dot{q}_{coll,eff}}$ in summer. For this reason the effective collector heat flow rate $\overline{\dot{q}_{coll,eff}}$ is calculated according to Eq. 7-11 which increases $\overline{\dot{q}_{coll,eff}\sim}$ mainly during the summer months.

$$\overline{\dot{q}_{coll,eff}} = \frac{Q_u}{t_{runtime} \cdot L} \cdot \max\left(1, \frac{Q_u}{\sum_{jan}^{Dec} \overline{Q_u}}\right) \qquad \text{Eq. 7-11}$$

The impact of this empiric correction term on the effective heat flow rate is presented in Figure 7-3 which uses the reference system of an example discussed in the next chapter.

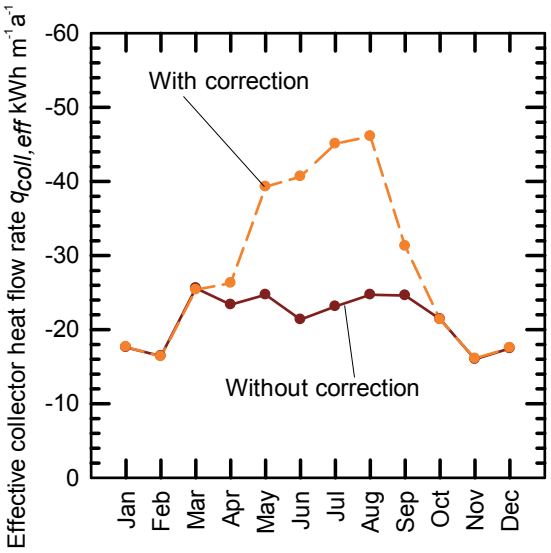

Figure 7-3: Effective collector heat flow rate with and without correction for the parameters and heat flow rates of the simulation reference system

Having calculated $\overline{\dot{q}_{coll}}$ allows the determination of the peak load temperature response of the vertical ground heat exchanger. This is done using Eq. 2-21, which derives to Eq. 7-12.

$$\overline{\dot{q}_{coll,peak}} \cdot R^{\#}_{peak} = \frac{\overline{\dot{q}_{coll,eff}} - \overline{\dot{q}_{ghx,pulse}}}{2 \cdot \lambda \cdot \pi} \cdot \left(\ln\left(\frac{\sqrt{4 \cdot \alpha_g \cdot t_{peak}}}{r_{GHX}} \right) - \frac{\gamma}{2} \right) \qquad \text{Eq. 7-12}$$

$$t_{peak} = \frac{t_{runtime} \cdot 0.5}{days/month}$$

It is emphasized that $\overline{\dot{q}_{coll,peak}}$ is the increased heat flow rate compared to the average monthly net heat load $\dot{q}_{ghx,pulse}$. It is not the actual heat flow rate of the solar collector $\overline{\dot{q}_{coll,eff}}$.

In summary, the utilizability method for the collector yield can now be combined with the vertical ground heat exchanger dimensioning. The equations required are Eq. 7-9 to Eq. 7-12. The method can be realized with a spread sheet calculation and the required input data is reduced to a minimum. The collector area is then iterated until an equilibrated balance in the ground is achieved, Figure 7-4.

This, in fact, allows the solar collector area to be calculated for any vertical ground heat exchanger length in any number, geometrical and load configuration as long as there is an equilibrated heat balance for the ground.

The following parameters are needed to apply the dimensioning method presented:

- Monthly thermal load profile (without solar regeneration) for charging and discharging the ground.
- Hourly values for solar irradiance in the collector pane, wind and ambient air temperature
- Collector performance parameters according to EN- 12975-2 for the uncovered collector and collector area
- Ground properties, undisturbed ground temperature, vertical ground heat exchanger length and borehole resistance

With slight modifications the method presented can also be reused for the dimensioning of the vertical ground heat exchanger length. For this case the maximum heat pump power and its run-time are required. Eq. 2-9 delivers the requested minimum inlet temperatures as a result with a minimum additional effort since no over-seasonal heat flow rate occurs and the periodical term from Eq. 7-12 can be reused. All other data has already been acquired.

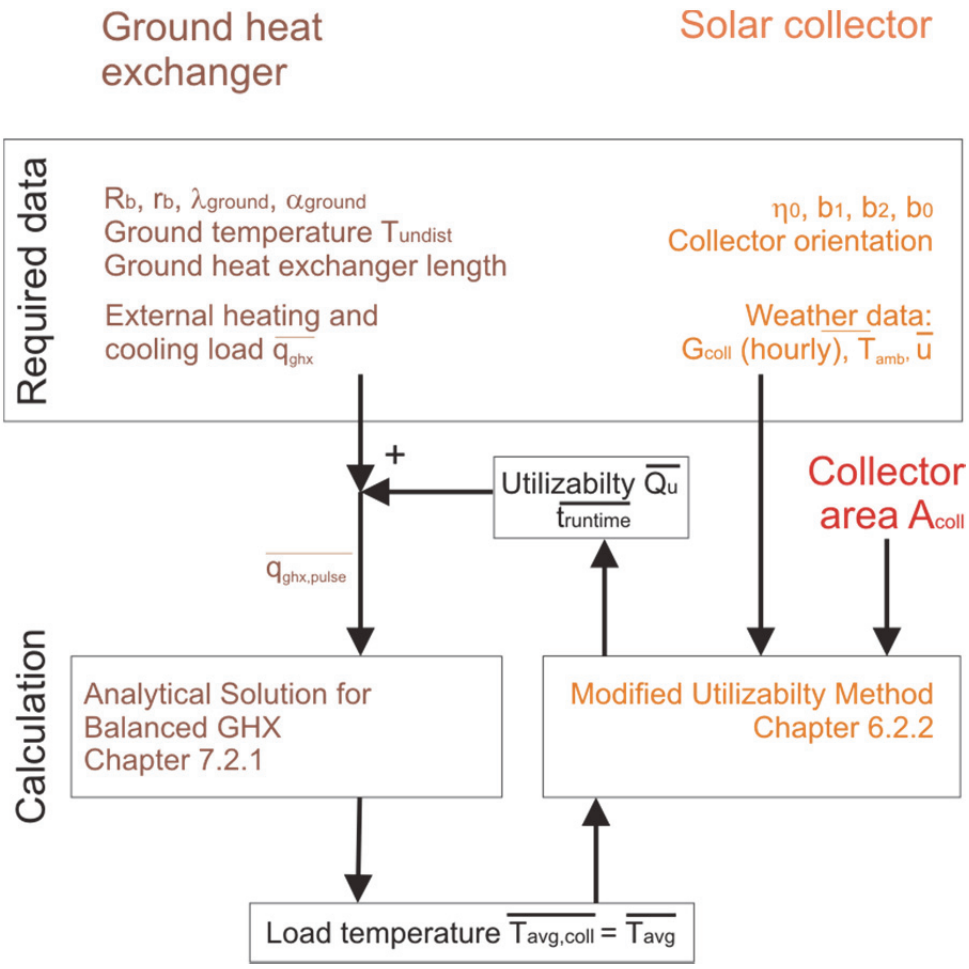

Figure 7-4: Calculation overview for iterative determination of collector area for complete regeneration of the vertical ground heat exchanger by combining the model for the utilizability method and the modified vertical ground heat exchanger model of Eskilson, The collector area A_{coll} is varied until an equilibrated balance in the ground heat exchangers is reached within the time frame of one year ($\Sigma q_{ghx,pulse} = 0$)

7.2.2 Example and Comparison to Dynamic Simulation

The monthly calculation method presented for the balanced vertical ground heat exchanger and the collector area is validated with the dynamic system model developed and already broadly discussed. The analytical solution also gives a good example of such systems over the course of the year.

The reference conditions are used from section 4.1.1 for the validation of the dimensioning method. The applied parameter set is given in table Table 7-1.

For the input required, the monthly evaporator heat flow rate, values from system simulation without solar regeneration are the starting data set to ensure realistic planning conditions. The evaporator heat flow rate changes due to the solar impact on evaporator temperatures. The difference in the given case, however, is only 1% and therefore negligible.

Table 7-1 Conditions and parameter set for the calculation example and validation of dimensioning method for collector area

Component	Description	Detailed information
Heat load	8.6 MWh a^{-1} 140 m² single family house 45 kWh m^{-2}	Chapter 4.1.1
Climate	Strasbourg	Chapter 4.1.1
Vertical ground heat exchanger	110 m Double U-tube 2 x 32 (default) R_p = 0.08 K m W^{-1}	Table 5-3
Ground properties	λ= 2 W m^{-1} K^{-1}, ρ = 2000 kg m^{-3}	Appendix E
Uncovered Collector	Black polymer collector azimuth 0°, tilt 45°	Appendix A
Hydronic variation	Cold side integration “series behind”	Chapter 4.2.2

The calculation method and the dynamic simulations are validated according to the following procedure.

Firstly, the collector area for an equilibrated balance is determined according to the input data in Table 7-1 using the iterative spreadsheet calculation procedure described in Figure 7-4. Secondly, a detailed transient system simulation is conducted with one minute time steps. The peviously determined collector area is now an input parameter for the simulation and all other input parameters are identical to the values used for the monthly calculation method. The results of both methods are then compared and discussed on the basis of monthly results and a regression analysis for the collector yield, the effective collector temperature and the net heat exchange of the ground.

The net monthly heat flow rate of the vertical ground heat exchanger $\dot{q}_{net}$ in a year is defined as the monthly sum of evaporator and collector heat flow rate. For a well balanced vertical ground heat exchanger the sum of all monthly $\dot{q}_{net}$ is zero. For the given conditions the calculated collector area for an equilibrated balance is 9.58 m².

The regression analysis conducted assesses the quality of the model.

The effective collector temperature is compared to the simulated energy weighted average collector temperature. The statistical correlation coefficient R is 0.977 and the standard error of estimate is 1 K for $T_{avg,coll}$. The statistical correlation coefficient R is 0.991 and the standard error of estimate is 5.1 kWh m^{-2} $month^{-1}$ for the monthly collector yield Q_u. The yearly differences are 33 kWh $m^{-2}a^{-1}$ for the collector yield, 0.2 K in the collector temperature and 2.2 W $month^{-1}$ m^{-1} for the net monthly heat demand $\dot{q}_{net}$. The net heat flow in the dynamic simulations is 2.2 kWh/m for the ground heat exchanger balance.

In summary, the simulation and the monthly calculation method agree astonishingly

well.

In addition, the analytic solution gives an inside view on the temperature consistence of the effective collector temperature over the course of the year. The shares of each temperature compound according to Eq. 7-1 are displayed in Figure 7-8 for the example calculated.

The influence of solar heat on the ground temperature becomes very clear. The ground temperature is above the undisturbed ground temperature in summer due to high collector yields. In winter the ground temperature is lower than the undisturbed ground temperature because the heat demand dominates. Furthermore, a slight elongation of higher temperatures can be seen in autumn. The temperature spreads increase moreover in summer up to 8 K while they are at 3 K in winter since higher heat flow rates appear.

On the whole this leads in summer to characteristic collector fluid temperatures of around 20°C which are mainly achieved by the borehole and peak shares and not by the ground temperature. In winter the characteristic collector temperature still reaches 10°C although the heat pump will probably be operated at lower inlet temperatures during this period.

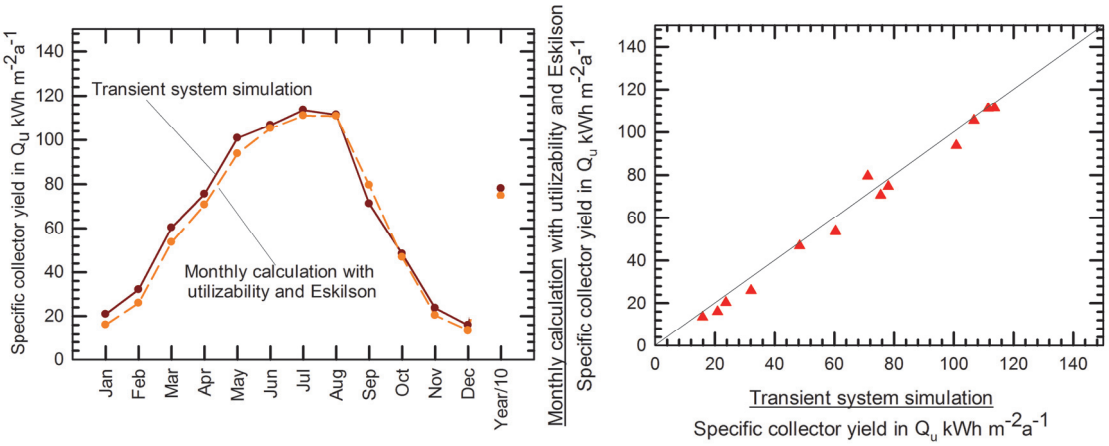

Figure 7-5: Monthly calculated and simulated specific collector yield $Q_{utilization}$ in the course of the year (left) and in regression analysis (right).

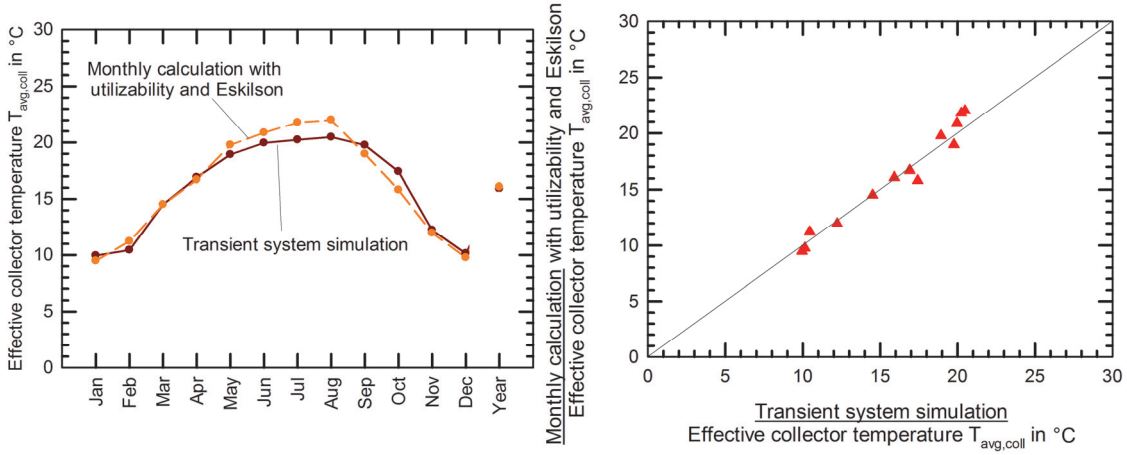

Figure 7-6: Monthly calculated effective collector temperature and simulated energy weighted collector temperature in the course of the year (left) and in regression analysis (right).

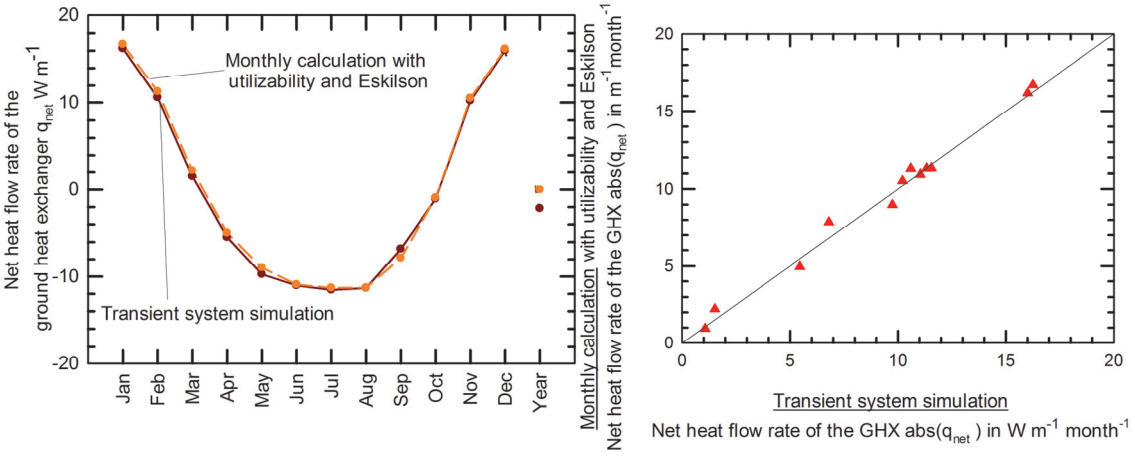

Figure 7-7: Monthly calculated and simulated net heat flow rate in the course of the year (left) and in regression analysis (right).

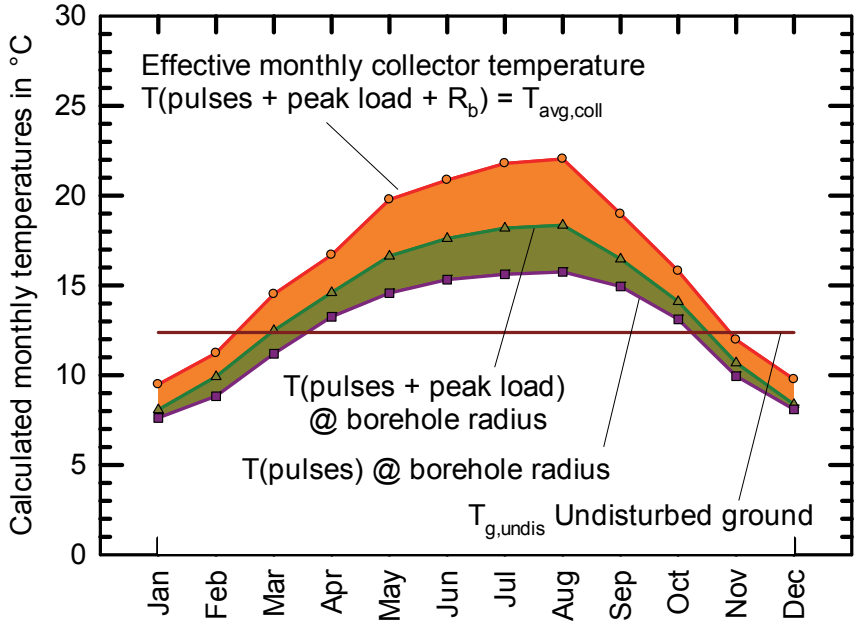

Figure 7-8: Monthly calculated temperature of the effective collector temperatures and the temperature shares for the different specific resistances

7.3 Practical Advice for Planning

Rules of thumb are important for feasibility checks in the early planning stage and for fast assessment of systems.

Both the dynamic simulations and the systems measured allow such specific parameters to be derived. The aim and purpose of these rules is then the sizing of the solar thermal collector for an even heat balance in the ground on an annual basis. It is restated that the equilibrated ground heat exchanger negates interference of ground heat exchangers. As a result, the specific values are valid for any ground heat exchanger field configuration.

In the reference system simulated an equilibrated balance is obtained with an black polymer collector of approx. 10 m², a ground heat exchanger of 110 m and an usable heat demand of 8.6 MWh a^{-1}. This amounts to **1.1 m² collector area per MWh** of usable heat for full regeneration.

These values correspond to a well-insulated building with 45 KWh/m² heating demand, 140 m² living area and a comparatively large dimensioned heat pump with 7.8 kW, which is in this case 1 m² uncovered collector per 10 m ground heat exchanger. Higher heating demands per installed heat pump capacity or smaller dimensioned ground heat exchangers will change these specific values. In the case of heat loads in less well insulated buildings higher specific collector areas are required to achieve an equilibrated balance. The same applies for lower performing collectors, the simultaneous generation of PV- electricity, a less beneficial orientation of the collector or a large borehole resistance. In other words, higher specific collector areas can be required, of up to 2 m² per MWh or 4 m² per m borehole under unfavourable conditions and high heat loads per m borehole.

To give some additional orientation, specific values are presented in Table 7-2 for the simulation reference system and the measured systems in Limburg and Dreieich.

The transfer of specific values is limited. The values measured differ compared to the simulation. For instance, the heating period in the measured systems is much longer than in the simulations [Simulation (Oct.-Apr.), Limburg (Sep-Apr) and Dreieich (Sep-May) Figure 5-14 and Figure 6-3]. The collector types used are a moderately performing PVT-collector in Dreieich and a metal collector in Limburg.

Table 7-2 Specific values for collector and vertical ground heat exchanger for example in dynamic simulation chapter 7.2.2 and the measured systems Limburg and Dreieich, chapter 6.1

		GHX	Solar collector	Heat pump
Simulation	Size	110 m	9.6 m²	7.8 kW
	Hot heat demand specific size	12.8 m/MWh	1.1 m²/MWh	0.9 kW/MWh
	Annual net heat flow cold side	2.2 kWh/m	770 kWh/m²	0.9 MWh/kW
	The hot side heat demand is 8.6 MWh and the cold side is 7.4 MWh.			
Measurement Limburg	Size	238 m	43.7 m²	15.8 kW
	Hot heat demand specific size	6.6 m/MWh	1.2 m²/MWh	0.44 kW/MWh
	Annual net heat flow cold side	-5 kWh/m	550 kWh/m²	1.6 MWh/kW
	The measured demand is 36 MWh at the condenser and 24.8 MWh at the evaporator.			
Measurement Dreieich	Size	225 m	39.4 m²	12 kW
	Hot heat demand specific size	6.4 m/MWh	1.1 m²/MWh	0.34 kW/MWh
	Annual net heat flow cold side	60 kWh/m	440 kWh/m²	2.5 MWh/kW
	The hot side heat demand is the useful heat 35 MWh in the first year of operation and 30.1 MWh at the evaporator.			

Apart from the specific differences both measured systems have a very similar specific size. The specific sizes related to the hot side heat demand are 1.2 m² MWh^{-1} for the collector and 6.6 m MWh^{-1} for the ground heat exchanger. The system specifications as a lower seasonal performance and the different use of the collector leads, however, in the case of Limburg to an equilibrated ground balance and in the case of Dreieich to a clearly imbalanced system with 60 kWh m^{-1} a^{-1} net heat extraction from the ground.

To conclude, the specific values give reliable orientation and presumably allow the planning of very similar systems with the same or similar components. The specific values do not, however, permit blind transfer to any system configuration. Detailed planning with the proposed planning method, chapter 7.2.1, must follow first order approximate estimations from these specific values.

More detailed calculation is recommended, if other hydraulic or controller concepts are involved.

8 Summary and Conclusion

Heat pump systems are studied with the hybrid heat source combination of vertical ground heat exchangers and uncovered solar thermal collectors. The benefits for this combination are quantified and dimensioning methods are developed.

The dominating heat source in these systems is the vertical ground heat exchanger. In contrast to the uncovered solar collector the ground delivers a reliable high temperature level for the heat pump, which is independent of the climate conditions. At the same time, however, the temperature level will decrease severely over the years if too much heat is extracted from too many adjacent and interfering boreholes. In extreme cases this over-seasonal temperature drop reaches more than 10 K between initial years of operation and quasi-steady state conditions. This long term effect in particular makes the dimensioning of conventional vertical ground heat exchangers complex and planning difficult.

It is demonstrated through systematic analysis that these long-term effects are eliminated by solar thermal regeneration which leads to shorter ground heat exchangers, simpler system dimensioning and easy scaling of systems. The benefit possible from solar regeneration equals the long term effect. Correspondingly, regeneration is especially attractive in large systems and in the case of adjacent systems in urban or residential areas. An example calculation shows an over-seasonal temperature drop of 3-4 K of four adjacent boreholes with very low heat extraction rate of 65 kWh per m and 10 m distance. This long-term influence vanishes with solar regeneration. It is emphasised that 100,000 ground coupled systems are currently built per year in Europe. Neglecting the interference between adjacent single systems will result in over-seasonal ground temperature decline.

Within the seasonal timeframe solar energy can be utilised directly or stored over shorter periods. Thus, two other methods are employed to assess the benefit over the period of a year. Firstly, a theoretical maximum source temperature is defined for infinite components, the temperature potential. Secondly, the systems are studied in “numerical experiments” through dynamic system simulations.

This temperature potential addresses the possible improvement due to solar regeneration, but it neglects all long term storage effects. The results are disappointing and disclose a clear maximum for this combination. The temperature potential improvement due to solar energy input is 5 K for heating loads for infinite components.

Better potential, however, is identified for more southern European climates and large short term storage capacities. This method has proved, nonetheless, to be a simple but effective way to assess hybrid heat sources.

Numerical experiments are conducted with dynamic system simulations to determine the benefits of finite components and including up to 1 year storing effects. The system model developed adopts component models that are validated and parameterised in measurements for application with solar collectors. These validated sub models are the starting point for the system simulations. In addition, the framework for system simulation is applied according to conditions from the SHC Task44/ HPP Annex 38 "Solar and Heat Pumps". This allows high reproducibility and comparability to subsequent studies.

The simulation results are consistent to the temperature potential and show a small improvement in efficiency for this hybrid heat source of 0.1 in the seasonal performance factor. Nonetheless, the impact of solar assistance increases with undersized vertical ground heat exchangers and allows shortening the boreholes by about 10%.

Many further simulations are conducted to identify possible optimisations and developments as well as to validate the developed designing methods.

For instance, an additional large cold storage of approx. 0.5 to 1 m³ allows a 20% shortening of the ground heat exchanger. The monthly electric loads have also been investigated, but these did not turn out to be greatly influenced by solar regeneration. Revealing is the comparison to an air heat pump. It discloses an immense difference of ground coupled systems with 50% lower electric monthly winter load. The uncovered collector application on the hot side seems not attractive, although the simulations indicate some potential for selective collectors in southern climates for domestic hot water preparation. Moreover, some studies with the solar collector as the only heat source reveal attractive options, but also give rise to other aspects such as electrical peak loads, safe collector operation and collector modelling under freezing conditions.

Finally, a comprehensive sensitivity analysis is conducted. In dynamic system simulations most parameters are less sensitive as to be expected from steady state calculations. This stable behaviour changes abruptly if the system is operated at the given limits of its components. As a result the systems are non-linear if the component dimensioning limits are met and the electrical back-up must temporarily take over or freezing of the collector appears and the collector is switched off. In principle, component operating limits make the systems and its analysis extremely complex.

Some specific system parameters have been derived from simulations and three measured systems. An equilibrated ground balance is achieved for 1.1 m² collector per MWh of annual heating demand. This specific value is helpful for quick assessment, but does not replace good planning and system realisation. Deviations will appear due to collector type and orientation and the seasonal performance and thermal losses in the system.

A more accurate design method is derived from the utilizability method for collector yield prediction on a monthly basis. The simplifying method requires only a minimum of data: hourly irradiance, ambient air temperature, collector performance and expected ground source temperature level. Validation showed good agreement with the data measured from the systems and the dynamic system simulations.

Moreover, the method can be combined with the analytic solution for the ground heat exchanger dimensioning. It calculates the necessary collector area for the cases of an even heat balance in the ground. In this case any borehole field configuration can be simplified as many single ground heat exchangers. This method agrees well with the dynamic system simulation.

This dimensioning for an equilibrated balance case appears to become more relevant. High and reliable system efficiencies, guaranteed by constant ground temperatures, are crucial in the context of a renewable dominated energy system especially in colder climates. Ground heat exchanger heat pumps have increasing market dissemination, though air source heat pumps are gaining market share. In the long term, the thermal regeneration will presumably become more relevant. In this context uncovered solar collectors are a simple and cost efficient way to ensure the sustainable use of the ground heat reservoir and allow the broad dissemination of ground coupled heat pumps as a cornerstone of renewable energy supply.

APPENDIX

Appendix A Performance Data of Uncovered Collectors

Table A-1: Collector performance parameter sets representing different types of unglazed collectors

Collector type		Black polymer	Metal roof	Selective absorber	Efficient Unglazed PVT
η_0	-	0.858	0.634	0.943	0.73
p_u	s m^{-1}	0.023	0.056	0.017	0.07
p_1	W $m^{-2}K^{-1}$	13.91	11.32	9.15	15.8
p_2	J $m^{-3}K^{-1}$	3.52	1.49	4.42	3.78
ε	-	0.81	0.7795	0.22	0.81
α	-	0.95	0.931	0.97	0.95
ε/α	-	0.85	0.84	0.23	0.85
cp	kJ $m^{-2}K^{-1}$	23.94	9.9	17.72	22.83
U_{int}	W $m^{-2}K^{-1}$	100	40	100	80

The performance data represents collectors of a certain collector type. The data has been derived from averaging the measured coefficients from similar collectors, some of them tested at ISFH, to ensure manufacturer independent but characteristic performance values.

Appendix B Collector Performance Calculation

The complete calculation of the uncovered (PVT-) collector performance with TRNSYS type 203 is documented either in the type documentation or in

M. Stegmann, E. Bertram, G. Rockendorf, and S. Janßen, "Model of an unglazed photovoltaic thermal collector based on standard test procedures," in Proceedings of ISES Solar World Congress, Kassel, Germany (2011).

$$\dot{Q}_{coll} + c_{eff}\frac{\delta T_{avg}}{\delta t} = \dot{Q}_{cond} + \mathrm{A_{coll}} \cdot \mathrm{G''_{red}} \cdot \left(\eta_0 \cdot (1 - \mathrm{u} \cdot \mathrm{p_u}) - \frac{\Delta \mathrm{T_{avg-amp}}}{\mathrm{G''_{red}}} \cdot (\mathrm{p_1} - \mathrm{p_2} \cdot \mathrm{u})\right)$$

The applied radiation is reduced and must be calculated accordingly

$$G''_{\mathrm{red}} = \left(\left(G' \cdot \mathrm{k_{PV}}\left(\Theta, \frac{\mathrm{G_{dif}}}{G_{dir}}\right)\right) - \frac{\mathrm{P_{el,PV}}}{A_{PV}}\right) \cdot \mathrm{k_{Th}}\left(\Theta, \frac{\mathrm{G_{dif}}}{G_{dir}}\right) + \frac{\epsilon}{\alpha}\left(G_{lw} - \sigma \cdot T_{amb}^4\right);$$

$$k\left(\Theta, \frac{\mathrm{G_{dif}}}{G_{dir}}\right) = k_{\Theta,\mathrm{dir}}(\Theta) \cdot \left(1 - \frac{G_{dif}}{G'}\right) + k_{\Theta,\mathrm{dif}}(\Theta_{\mathrm{dif}})\frac{\mathrm{G_{dif}}}{G_{dir}}$$

The photovoltaic energy production diminishes the available radiation for thermal use and is calculated with the effective performance model from Wagner using only standard performance data of the PV-module

$$P_{el,PV} = \eta_{STC} \cdot \eta_{rel}\, G' \cdot \mathrm{k_{PV}}\left(\Theta, \frac{\mathrm{G_{dif}}}{G_{dir}}\right) \cdot A_{PV}$$

$$\eta_{rel} = (1 + c_T \cdot (T_{cell} - T_{STC}) \cdot \left(1 + \frac{U_{T,STC}}{U_{MPP,STC}} \cdot \ln\left(\frac{G'}{G'_{STC}}\mathrm{k_{PV}}(\ \ )\right) - \frac{R_{PV,STC} \cdot I_{MPP,STC}}{U_{MPP,STC}} \cdot \left(\frac{G'}{G'_{STC}}\mathrm{k_{PV}}(\ \ ) - 1\right)\right)$$

The condensation heat flow rate $\dot{Q}_{cond}$

$$\dot{Q}_{cond} = A_{coll} \cdot \frac{R_L}{R_D}\frac{\Delta h_v}{p_0 c_L} Le^{m-1}\, u_{conv}[p_s(T_{abs}) - p_s(T_D)]$$

Nomenclature of collector performance calculation

c_{eff}	*Effective heat capacity of collector* kJ K^{-1}
$\frac{\delta T_{avg}}{\delta t}$	*Temperature time derivative* K s^{-1}
$\dot{Q}_{cond}$	*Collector heat flow rate at collector due to condensation in* W
G''_{red}	*Reduced irradiance for thermal collector model in* W m^{-2}
Θ	*Incidence Angle of radiation in* °
k_{PV}, k_{Th}	*Incident angle modifier (IAM) for PV or thermal performance in* -
$k_{\Theta,\mathrm{dif}}(\Theta_{\mathrm{dif}})$	*Incident angle modifier for diffuse radiation (in most case $k(\theta = 56°)$)*
G_{dif} / G_{dir}	Ration between diffuse and direct irradiance in collector pane
$\dot{Q}_{cond}$	*Condensation heat gain in* W
R_L	*Gas constant of air (R_L = 0.2871* kJ kg^{-1} K^{-1}*)* kJ kg^{-1} K^{-1}
R_D	*Gas constant of water (R_D = 0.4614* kJ kg^{-1} K^{-1}*)* kJ kg^{-1} K^{-1}
Δh_v	*Evaporation enthalpy of water in* kJ kg^{-1}
p_0	*Air pressure in* mbar
c_L	*Specific heat capacity of ambient air in* kJ kg^{-1} K^{-1}
Le^{m-1}	*Lewis number (Le = 0.87 for water vapour in air) in* -
u_{conv}	*Convection loss coefficient in* W $m^{-2}K^{-1}$
$p_s(T)$	*Water vapour saturation pressure at absorber temperature T in mbar*
T_{cell}	*Temperature of PV cell in* K
T_{STC}	*Temperature of PV cell at standard test conditions in* K
c_T	*Temperature coefficient for electrical power of PV-module in* K^{-1}
$U_{T,STC}$	*Temperature voltage UT at standard test conditions in* V
$U_{MPP,STC}$	*Voltage at maximum power point at standard test conditions in* V
$R_{PV,STC}$	*Parameter of effective performance model in* Ω
$I_{MPP,STC}$	*Current at maximum power point under standard test conditions in* A
$U_{MPP,STC}$	*Voltage at maximum power point under standard test conditions in* A
G'_{STC}	*Irradiance at standard test conditions in* W m^{-2}

Appendix C Calculation of Auxiliary Consumers

The calculation of the pump consumption is also described in

Bertram, E., Dott, R., Mojic, I., Lerch, W., Heinz, A., Haller, M.Y., Carbonell, D., Bunea, M., Winteler, C. and Ochs, F. 2013. Annex G Summary reports for simulations with T44A38 boundary conditions (Final Draft - Dec. 2013). Technical Report #Annex G to Report C3. IEA SHC / HP Programme. (to be published 2014).

“

For the calculation of parasitic electric consumption for controllers and pumps three different calculation methods are applied. The three methods are detailed, run-time calculation and constant values.

As the most simple calculation method constant values are used. The method is used for consumers that are not affected by the simulation. Values are displayed in table 3.

The second, more detailed method is used for pumps with constant mass flow rate. The operation time of pumps is recorded in the simulations. Herewith, the consumption is calculated together with the pressure drops shown in table 2.

As third method a detailed calculation is used for pumps with variable mass flow rate in the course of the simulation. This only applies to the cold side of the heat pump. Here, the pressure drop is calculated mass flow rate dependent within the simulation for every time step (1 minute).

The detailed calculation of the pump consumption is conducted for pumps with variable mass flow rate. The hydronic power P_{hyd} represents the power to overcome the hydronic resistance for operation of the components: solar thermal collector, vertical ground heat exchanger or heat exchanger of the heat pump evaporator.

This calculation is performed within the simulation for every time step. The pressure drop is determined with help of Eq. 1 and Eq. 2 [136, p. 21 ff] applying the actual mass flow rate for the operated components in the particular time step.

$$P_{hyd} = \dot{V} \cdot \Delta p = \frac{\dot{m}}{\rho} \cdot \Delta p \qquad \text{Eq. 1}$$

$$\Delta p = R \cdot l + \sum \Delta p_{installations} = \left(l \cdot \frac{\lambda}{d} + \sum \zeta\right) \cdot \frac{v^2 \cdot \rho}{2} \qquad \text{Eq. 2, } \textit{with}$$

$\dot{V}$	*Volume flow rate in* m³/s
R	*Pressure drop per m in* Pa/m,
l	*Pipe length in* m,
d	*Pipe diameter in* m,
λ	*The pipe friction (no unit),*
ζ	*Resistance coefficient for installations (no unit),*
v	*Fluid velocity in* m/s,
ρ	*Density in* kg/m³

The required ζ values for the vertical ground heat exchanger loop installations like valves, T-pieces etc. are taken from [136] and sum up to 17 for all installations. The pressure drops in the pipes of the borehole heat exchanger are calculated temperature and borehole length dependent with type 586 [147], a model for piping network calculation, for an ethylene-glycol water mixture of 30%. The ζ values for the collector loop and evaporator heat exchangers loop are derived from assumptions for the typical pressure drop and fluid velocities under nominal conditions. Installations are also included. From a typical collector pressure drop of 70 mbar [118, p. 26] a ζ value of 87.5 is derived for the complete loop. For the evaporator heat exchanger a typical pressure drop of 100 mbar derives to a ζ value of 222.

The hydronic energy E_{hyd} for the pump calculation is determined for the duration of the simulation from the hydronic power in each time step i with the duration t. Together with the pump efficiency derives the overall energy consumption E_{el}:

$$E_{el} = \frac{E_{hyd}}{\eta_{pump}} = \frac{\sum_i P_{hyd,i} \cdot t_i}{\eta_{pump}} \qquad \text{Eq. 3}$$

The pump efficiency η_{pump} is assumed to be 0.3 see for example [148, p. 80]. However, this leads to uncharacteristic low hydronic powers especially for low flow rates. Accordingly, these values are not realistic, because the pump efficiency also decreases rapidly for low flow rates. In addition, standby consumption has to be respected. To ensure more realistic calculations a minimum value of 10 W for the hydronic power is used for the calculation, even if lower hydronic powers have been calculated.

The **run-time calculation of the pump consumption** is applied for pumps with constant mass flow rates. Consequently, the overall energy consumption E_{el} is also calculated with help of Eq. 2 and Eq. 3, but with a constant pressure drop. Table 2 displays the calculated or otherwise assumed pressure drops. For the control unit a central controller unit is assumed that has system independent consumption. The constant consumption values are presented in Table 3.

Table 2 Pressure drops of pumps for run-time calculation

Pump	Pressure drop in mbar	Reference/ Remarks
Collector loop (Collector, piping system, HX)	300	[149]
Cold Storage loop	130	Heat pump evaporator [150, p. 187] + hydronic junction [151]

Table 3 Constant consumption data used for SPF calculation

Consumer Pump or Controller	Consumption in kWh/a	Reference/ Remarks
Heat distribution for space heating	70	[152]
Loading DHW storage	12.8	Calculation from run-time 320 h, exemplary pump power 40 W
Central controller unit	100	Estimated from measured data of [24, p. 104]

“

End of citation

Appendix D Utilizability Data

D.1 System Limburg

Table D.1: Monthly energetic values and temperatures calculated and measured for the system Limburg

Month	$\Sigma G'_T = H_T$ kWh mon.$^{-1}$ m^{-2}	Q_{Coll} kWh mon.$^{-1}$ m^{-2}	G_{TC} W m^{-2}	Q_u kWh mon.$^{-1}$ m^{-2}	$\overline{\Phi}$ -	$\overline{T}_{amb}$ °C	$\overline{T}^*_{BHX,avg}$ °C	$\overline{T}^*_{Coll,avg}$ °C
Oct-06	70	30	62	32	0.8	13.6	13.9	16.0
Nov-06	29	19	-0	23	1.3	8.4	6.1	5.8
Dec-06	19	24	-0	20	1.7	5.0	2.3	1.0
Jan-07	23	20	-0	22	1.5	6.4	1.9	1.5
Fep-07	36	28	-0	28	1.3	5.8	1.9	2.5
Mar-07	92	46	39	48	0.9	7.6	6.7	9.1
Apr-07	170	79	166	70	0.7	14.0	19.0	20.4
May-07	141	62	114	60	0.7	16.2	20.6	20.7
Jun-07	148	71	128	61	0.7	19.7	24.2	24.7
Jul-07	148	64	151	57	0.6	18.8	24.1	24.7
Aug-07	136	61	156	53	0.6	18.6	24.3	24.7
Sep-07	90	36	161	29	0.5	13.9	18.8	20.1
Oct-07	65	29	88	26	0.7	9.8	11.6	13.3
Nov-07	20	22	-0	22	1.8	5.3	2.9	0.2
Dec-07	18	22	-0	17	1.6	2.4	0.1	-0.7
Jan-08	24	30	-0	24	1.7	4.9	0.8	0.4
Fep-08	60	39	10	35	1.0	4.1	2.1	4.4
Mar-08	73	43	-0	45	1.0	6.0	4.6	5.7
Apr-08	99	56	41	51	0.9	9.1	10.0	10.6
May-08	169	86	132	72	0.7	17.4	22.8	22.6
Jun-08	180	82	180	70	0.6	19.3	26.5	26.4
Oct-06	70	30	62	32	0.8	13.6	13.9	16.0

D.2 System Klein Köris

Table D.2: Monthly energetic values and temperatures calculated and measured for the system Klein Köris

Month	$\Sigma G'_T = H_T$ kWh mon.$^{-1}$ m^{-2}	Q_{Coll} kWh mon.$^{-1}$ m^{-2}	G_{TC} W m^{-2}	Q_u kWh mon.$^{-1}$ m^{-2}	$\overline{\Phi}$ -	$\overline{T}_{amb}$ °C	$\overline{T}^*_{BHX,avg}$ °C	$\overline{T}^*_{Coll,avg}$ °C
Nov-07	24	13	-0	19	1.4	3.3	0.2	0.9
Dec-07	21	12	-0	18	1.5	2.4	-0.5	0.4
Jan-08	28	17	-0	24	1.4	3.8	-0.1	1.0
Fep-08	55	32	-0	36	1.1	4.8	1.2	3.9
Mar-08	90	47	28	49	0.9	5.0	2.0	6.1
Apr-08	103	67	-0	64	1.0	9.1	4.9	8.3
May-08	162	118	-0	100	1.0	16.5	12.2	15.4
Jun-08	129	93	-0	82	1.0	16.0	15.7	17.7

D.3 System Dreieich

Table D.3: Monthly energetic values and temperatures calculated and measured for the system Limburg

Month	$\Sigma G'_T = H_T$ kWh mon.$^{-1}$ m^{-2}	Q_{Coll} kWh mon.$^{-1}$ m^{-2}	G_{TC} W m^{-2}	Q_u kWh mon.$^{-1}$ m^{-2}	$\overline{\Phi}$ -	$\overline{T}_{amb}$ °C	$\overline{T}^*_{BHX,avg}$ °C	$\overline{T}^*_{Coll,avg}$ °C
Mar-09	82	25	1	33	0.7	6.2	13.5	6.2
Apr-09	155	59	58	52	0.6	14.1	17.5	16.2
May-09	163	60	54	54	0.6	15.9	19.1	17.9
Jun-09	165	61	55	55	0.6	17.2	20.3	19.3
Jul-09	166	66	33	60	0.7	20.0	22.0	21.2
Aug-09	165	69	40	59	0.7	20.7	22.7	22.2
Sep-09	117	40	84	34	0.5	16.2	20.0	19.4
Oct-09	62	20	28	24	0.7	9.8	11.6	10.8
Nov-09	23	17	-0	14	1.1	8.6	5.9	5.6
Dec-09	21	6	355	0	0.0	2.0	3.8	17.5
Jan-10	16	1	14	5	0.6	-2.0	1.2	1.2
Fep-10	40	15	-0	15	0.7	1.8	3.7	2.4
Mar-10	96	33	32	34	0.6	6.5	9.0	8.0
Apr-10	163	52	89	51	0.6	11.2	16.1	14.5
May-10	125	47	23	45	0.7	12.2	15.4	13.1
Jun-10	190	77	49	66	0.6	18.9	21.5	20.8
Jul-10	179	81	19	68	0.7	22.2	23.8	22.9
Aug-10	126	50	21	46	0.7	18.3	20.3	19.1
Sep-10	108	38	50	36	0.6	13.8	17.3	15.7
Oct-10	84	26	57	26	0.6	9.2	13.4	11.3
Nov-10	23	18	-0	15	1.2	6.6	4.5	3.6
Dec-10	13	8	-0	11	1.6	-2.0	-3.7	-4.4
Jan-11	31	14	5	12	0.7	2.4	3.8	3.2
Fep-11	45	16	-0	18	0.7	2.9	4.2	3.4
Mar-11	124	38	85	38	0.6	7.5	11.8	10.7
Apr-11	163	57	86	51	0.6	13.9	18.0	17.2
May-11	198	68	97	61	0.6	16.5	20.7	20.2
Jun-11	153	57	39	54	0.6	18.5	20.9	19.9
Mar-09	82	25	1	33	0.7	6.2	13.5	6.2

Appendix E Parameters in TRNSYS Ground Heat Exchanger Model

Table F.4: Applied parameters for the vertical ground heat exchanger model 557

	Parameter	Unit	Value
1	Storage volume	m^{-3}	Pi*GHX_no* GHX_Depth * (0.525 * GHX_distance)^2
2	Borehole depth	m	Free Parameter
3	Header depth	m	1
4	Number of boreholes	-	1
5	Borehole radius	m	
6	No. of boreholes in series	-	1
7	Number of radial regions	-	1
8	Number of vertical regions	-	10
9	Storage thermal conductivity	W $m^{-1}K^{-1}$	2
10	Storage heat capacity	kJ m^{-3} K^{-1}	2000
11	Negative of u-tubes/pore	-	-2
12	Outer radius of u-tube pipe	m	0.016
13	Inner radius of u-tube pipe	m	0.0131
14	Center-to-center half distance	m	0.04
15	Fill thermal conductivity	W $m^{-1}K^{-1}$	2
16	Pipe thermal conductivity	W $m^{-1}K^{-1}$	0.43
17	Gap thermal conductivity	W $m^{-1}K^{-1}$	1.75
18	Gap thickness	m	0
19	Reference borehole flow rate	string	1900
20	Reference temperature	C	10
21	Pipe to pipe heat transfer	-	-1
22	Fluid specific heat	kJ $kg^{-1}K^{-1}$	3.81
23	Fluid density	kg m^{-3}	1048
24	Insulation indicator	-	0
25	Insulation height fraction	-	0.5
26	Insulation thickness	m	0.0254
27	Insulation thermal conductivity	kJ $h^{-1}m^{-1}K^{-1}$	1
28	Number of simulation years	-	STOP
29	Maximum storage temperature	C	100
30	Initial surface temperature of storage volume	C	11
31	Initial thermal gradient of storage volume	any	0.025
32	Number of preheating years	-	0
33	Maximum preheat temperature	C	12
34	Minimum preheat temperature	C	4
35	Preheat phase delay	day	90

36	Average air temperature - preheat years	C	9.5
37	Amplitude of air temperature - preheat years	deltaC	15
38	Air temperature phase delay - preheat years	day	240
39	Number of ground layers	-	1
40	Thermal conductivity of layer -1	$Wm^{-1} K^{-1-}$	2
41	Heat capacity of layer -1	kJ $m^{-3} K^{-1}$	2000
42	Thickness of layer-1	m	160

Appendix F Seasonal Temperature Response Matrix

The seasonal temperature response matrix calculates the dimensionless, seasonal temperature response for any fully regenerated vertical ground heat exchanger field.

$$\boldsymbol{\Delta T'} = \begin{pmatrix} \Delta T'_{pulse} & \Delta T'_{cov,11} & \Delta T'_{cov,10} & \cdots & \Delta T'_{cov,1} \\ \Delta T'_{cov,1} & \Delta T'_{pulse} & \Delta T'_{cov,11} & \cdots & \Delta T'_{cov,2} \\ \Delta T'_{cov,2} & \Delta T'_{cov,1} & \Delta T'_{pulse} & \cdots & \Delta T'_{cov,3} \\ \cdots & \cdots & \cdots & \cdots & \cdots \\ \Delta T'_{cov,11} & \Delta T'_{cov,10} & \Delta T'_{cov,9} & \cdots & \Delta T'_{pulse} \end{pmatrix}$$

With

$$\Delta T'_{pulse} = \ln\left(4\frac{\alpha_g t_{pulse}}{r_{GHX}^2}\right) - \gamma$$

α_g	*Temperature diffusivity in* m²/s
r_{GHX}	*Borehole radius in* m
t_{pulse}	*Duration of the pulse in* s
γ	*Euler constant ~0.5772*
$\Delta T'_{pulse}$	*Dimensionless temperature drop due to pulse*

$\Delta T'_{cov,1} = 0.69315$

$\Delta T'_{cov,2} = 0.40547$

$\Delta T'_{cov,3} = 0.28768$

$\Delta T'_{cov,4} = 0.22314$

$\Delta T'_{cov,5} = 0.18232$

$\Delta T'_{cov,6} = 0.15415$

$\Delta T'_{cov,7} = 0.13353$

$\Delta T'_{cov,8} = 0.11778$

$\Delta T'_{cov,9} = 0.10536$

$\Delta T'_{cov,10} = 0.09531$

$\Delta T'_{cov,11} = 0.08701$

References

[1] UNFCC, “Report of the Conference of the Parties on its 16th session,” United Nations Framework Convention on Climate Change, Cancun, FCCC/CP/2010/7/Add.1, Mar. 2011.

[2] H.-H. Rogner, D. Zhou, R. Bradley, P. Crabbé, O. Edenhofer, B. (Australia) Hare, K. Kuijpers, and M. Yamaguchi, *Introduction. In Climate Change 2007: Mitigation. Contribution of Working Group III to the Fourth Assessment Report of the Intergovernmental Panel on Climate Change*. Cambridge, United Kingdom and New York, NY, USA: Cambridge University Press, 2007.

[3] IEA, “KEY WORLD ENERGY STATISTICS 2012,” International Energy Agency, Paris, France, 2012.

[4] IEA, “Co-generation and Renewables Solutions for a low-carbon energy future,” International Energy Agency, Paris, France, 2011.

[5] H. Nishihata, R. Kempener, G. Simbolotti, and G. Tosato, “Heat Pumps Technology Brief,” International Renewable Energy Agency (IRENA) and Energy Technology Systems Analysis Programme (ETSAP), Technology Brief E12, 2013.

[6] E. Bertram, J. Glembin, and J. Scheuren, “Unverglaste Metalldach-Sonnekollektoren in Wärmeversorgungssystemen: Systemkonzepte und Auslegung,” Deutsche Bundesstiftung Umwelt (DBU), Osnabrück, Final scientific report 21098, 2008.

[7] E. Bertram, M. Stegmann, and G. Rockendorf, “Solare Gebäudewärmeversorgung mit unverglasten photovoltaisch-thermischen Kollektoren, Erdsonden und Wärmepumpen für 100% Deckungsanteil, Teilprojekt B: Wissenschaftliche Begleitung: Kurzbezeichnung: BiSolar-WP,” Institut für Solarenergieforschung Hameln, Emmerthal, Abschlussbericht zum Vorhaben ; BMU 0325952B, 2011.

[8] B. Sibbitt, D. McClenahan, R. Djebbar, J. Thornton, B. Wong, J. Carriere, and J. Kokko, “The Performance of a High Solar Fraction Seasonal Storage District Heating System–Five Years of Operation,” *Energy Procedia*, vol. 30, pp. 856–865, 2012.

[9] D. Bauer, R. Marx, J. Nußbicker-Lux, F. Ochs, W. Heidemann, and H. Müller-Steinhagen, “German central solar heating plants with seasonal heat storage,” *Solar Energy*, vol. 84, no. 4, pp. 612–623, Apr. 2010.

[10] H. D. Baehr and S. Kabelac, *Thermodynamik: Grundlagen und technische Anwendungen*, 14., aktualisierte Auflage. Springer, Berlin, 2009.

[11] P. Pärisch, O. Mercker, J. Warmuth, R. Tepe, E. Bertram, and G. Rockendorf, “Investigations and model validation of a ground-coupled heat pump for the combination with solar collectors,” *Applied Thermal Engineering*, vol. 62, no. 2, pp. 375–381, Jan. 2014.

[12] WPZ Buchs, “Informationsblatt des Wärmepumpen-Testzentrums Buch s - Information sheet of the Heat Pump Test Center WPZ in Buchs Switzerland,” Interstaatliche Hochschule für Technik, Buchs, Switzerland, WPZ - Bulletin 01 - 2013, 2013.

[13] R. Buss, “Wärmepumpen barometer – EUROBSERV’ER,” Renac Renewables Academy, 2013.

[14] T. Afjei and M. Wettter, *Type 401,Compressor heat pump including frost and cycle losses*. Zürich/Luzern, Switzerland: Zentralschweizerisches Technikum Luzern, Ingenieurschule HTL, 1997.

[15] EN 14511-3, “Air conditioners, liquid chilling packages and heat pumps with electrically driven compressors for space heating and cooling — Part 3: Test methods; Deutsche Fassung EN 14511-3:2011,” CEN - EUROPEAN COMMITTEE FOR STANDARDIZATION, Brüssel, European Standard Ref. Nr. EN 14511-3:2011 D, 2011.

[16] O. Mercker, “Untersuchung des dynamischen Verhaltens von Erdsonden und Wärmepumpen in TRNSYS,” Masterthesis (M.Eng.), University of Applied Science - Nordhausen, Nordhausen, 2012.

[17] Verein Deutscher Ingenieure, “VDI 4640 Blatt 2 Thermische Nutzung des Untergrunds Erdgekoppelte Wärmepumpenanlagen.” VDI-Gesellschaft Energie und Umwelt, Sep-2001.

[18] F. Ochs, M. Haller, D. Carbonell, P. Pärisch, and D. Pahud, “Models of Sub - Components and Validation for the IEA SHC Task 44 / HPP Annex 38 Part D : Ground Heat Exchanger s,” IEA SHC / HP Programme, Innsbruck, Final Draft Revised A technical report of subtask C Report C2 Part D, 2013.

[19] B. Sanner, C. Karytsas, D. Mendrinos, and L. Rybach, “Current status of ground source heat pumps and underground thermal energy storage in Europe,” *Geothermics*, vol. 32, no. 4–6, pp. 579–588, Aug. 2003.

[20] J. Claesson and P. Eskilson, “Conductive heat extraction to a deep borehole: Thermal analysis and dimensioning rules,” *Energy*, vol. 13, no. 6, pp. 509–527, 1988.

[21] P. Platell, “Developing work on ground heat exchangers,” in *ECOSTOCK 2006 Conference Proceedings. New Jersey: ECOSTOCK*, 2006.

[22] C. Steins, F. Al-Sibai, and R. Kneer, “Der Einfluss großformatiger Koaxial-Erdwärmesonden (Speichersonden) auf den Wärmeübergang und -entzug,” in *Proceedings of “Geothermiekongress 2012,”* Karlsruhe, 2012.

[23] R. Koenigsdorff, *Oberflächennahe Geothermie für Gebäude: Grundlagen und Anwendungen zukunftsfähiger Heizung und Kühlung*. Fraunhofer Irb Verlag, 2011.

[24] M. Miara, D. Günter, T. Oltersdorf, and J. Wapler, “Wärmepumpen Effizienz,” Bundesministerium für Wirtschaft und Technologie, Abschlussbericht, Langfassung 0327401A, Apr. 2011.

[25] A. Huber and D. Pahud, “Untiefe Geothermie: Woher kommt die Energie,” *Forschungsprogramm Geothermie. Bundesamt für Energie (BFE), Bern*, 1999.

[26] “Leitfaden zur Erdwärmenutzung in Hamburg, Wärmegewinnung aus Erdwärmesonden und -kollektoren mit einer Heizleistung von max. 30 kW Ein Leitfaden für Planer, Ingenieure und Bauherren.,” Freie und Hansestadt Hamburg Behörde für Stadtentwicklung und Umwelt, Hamburg, Germany, 2011.

[27] “Erdwärmesonden - Leitfaden zur Nutzung von Erdwärme mit Erdwärmesonden,” Sächsisches Landesamt für Umwelt und Geologie, Referat 54 - Rohstoffgeologie, Dresden, L VII-4/1, 2007.

[28] H. Spliethoff, A. Hauer, and M. Reuß, *Qualitätssicherung bei Erdwärmesonden und Erdreichkollektoren: Abschlussbericht ; [Laufzeit: 01.11.07 bis 31.08.11*. [Garching b. München], 2012.

[29] “Leitlinien Qualitätssicherung Erdwärmesonden (LQS EWS,” Ministerium für Umwelt, Klima und Energiewirtschaft, Stuttgart, Germany, LQS EWS, 2011.

[30] H. D., Stephan, Karl Baehr, *Heat and mass transfer: with many worked examples and exercises*. Berlin [u.a.: Springer, 2011.

[31] P. Oberdorfer, “Heat Transport Phenomena in Shallow Geothermal Boreholes - Development of a Numerical Model and a Novel Extension for the Thermal Response Test Method by Applying Oscillating Excitations,” Dissertation, Georg-August-Universität Göttingen, Göttingen, 2014.

[32] P. Eskilson, *Superposition Borehole Model (SBM). Manual for Computer Code*. Lund, Sweden: University of Lund, 1986.

[33] M. Wetter and A. Huber, *TRNSYS Type 451 - Vertical Borehole heat exchanger - EWS Model - Model description and implementing into TRNSYS*. Zürich/Luzern, Switzerland: Huber Energietechnik AG, 1997.

[34] G. Hellström and J. W. Thonton, *Type 557, Vertical ground heat exchanger based on Duct Ground heat storage model*. Madison: Tess Thermal Energy System Specialists, 2004.

[35] G. Hellström and B. Sanner, *Earth Energy Designer - User Manual 2.0*. 2000.

[36] R. Koenigsdorff, A. Köhler, and C. Kirschmann, *GEO-HANDlight Programm zum Handrechenverfahren für Erdwärmesonden*. Biberach a.d. Riß, Germany: Hochschule Biberach, 2006.

[37] A. Huber, *Benutzerhandbuch zum Programm Programm EWS Version 4.7 Berechnung von Erdwärmesonden*. Switzerland: Huber Energietechnik AG, 2011.

[38] P. Eskilson, "Thermal Analysis of Heat extraction boreholes," Dissertation, 222 pages, University of Lund, Sweden, Lund, 1987.

[39] L. Lamarche and B. Beauchamp, "A new contribution to the finite line-source model for geothermal boreholes," *Energy and Buildings*, vol. 39, no. 2, pp. 188–198, Feb. 2007.

[40] Arthur Huber and D. Pahud, "Erweiterung des Programms EWS für Erdwärmesondenfelder," Bundesamtes für Energiewirtschaft, Bundesamtes für Energiewirtschaft, Schlussbericht, Sep. 1999.

[41] P. Loose, *Erdwärmenutzung versorgungstechnische Planung und Berechnung*. Heidelberg: Müller, 2009.

[42] L. Lamarche, S. Kajl, and B. Beauchamp, "A review of methods to evaluate borehole thermal resistances in geothermal heat-pump systems," *Geothermics*, vol. 39, no. 2, pp. 187–200, Jun. 2010.

[43] Elisabeth Kjellsson, "Solar Collectors Combined with Ground-Source Heat Pumps in Dwellings - Analyses of System Performance," Dissertation, Lund University, Lund, 2009.

[44] M. A. Bernier, "Closed-loop ground-coupled heat pump systems," *Ashrae Journal*, vol. 48, no. 9, pp. 12–25, 2006.

[45] M. Philippe, M. Bernier, and M. Dominique, "Sizing Calculation Spreadsheet - Vertical Geothermal Borefields," *ASHRAE Journal*, vol. July 2010, 2010.

[46] P. Pärisch, P. Oberdorfer, E. Bertam, R. Tepe, and G. Rockendorf, "Experimente und Modellvalidierung für die Erdsondenregeneration mit Solarwärme," in *Proceedings 12. Internationales Anwenderforum Oberflächennahe Geothermie*, Neumarkt i. d. Oberpfalz, Germany, 2013.

[47] G. Hellström, J. Claesson, Eftring, Johansson, L. Mazzarella, and D. Pahud, *Type 557, VERTICAL GROUND HEAT EXCHANGER (Duct Ground Heat Storage Model, Manual for Computer Code)*. Lund, Sweden: Department of mathematical physics Lund Institut of technology, 1981.

[48] Tess libraries, *TESS COMPONENT LIBRARIES General Descriptions*. Madison, Wisconsin, USA: Tess Thermal Energy System Specialists, 2011.

[49] E. Frank, "Modellierung und Auslegungsoptimierung unabgedeckter Solarkollektoren für die Vorerwärmung offener Fernwärmenetze," Dissertation, Kassel University Press, Kassel, 2007.

[50] G. Rockendorf, R. Sillmann, T. Bethe, and H. Köln, *Solare Freibadbeheizung - Absorberpfrüfung und Testergebnisse Anlagen Planung und Betrieb*, vol. 1. Auflage. Kandern: ist - Energieplan, 2001.

[51] MEFA, "Catalogue MEFA Energy systems," MEFA Befestigungs- und Montagesysteme GmbH, Kupferzell, Germany, 2013.

[52] UMASolar, "Spec Data Swimming pool Plumbing systems," Altamonte Springs, Florida, U.S.A., 22 51 00.

[53] RHEINZINK GmbH & Co. KG, "QUICK STEP® Das RHEINZINK Treppendach PLANUNG UND ANWENDUNG," Datteln, Germany, RZ-D-02-04-100.528-2, 2004.

[54] BEMO SYSTEMS and Bemo Systems GmbH, “PRODUKT UND LEISTUNG - BEMO Produktbroschuere,” lshofen-Eckartshausen, Germany, 05101083-3 2/04/13, 2013.

[55] Nelskamp, “SolarPowerPack® Heizen mit der Energie vom Dach,” Nelskamp, Schermbeck, Product broschure.

[56] I.-F. Primus, *Massivabsorber: die Wärmequelle für die Wärmepumpe*. Düsseldorf: Beton-Verl., 1995.

[57] M. D’Antoni and O. Saro, “Massive Solar-Thermal Collectors: A critical literature review,” *Renewable and Sustainable Energy Reviews*, vol. 16, no. 6, pp. 3666–3679, Aug. 2012.

[58] Allgäuer Solarzentrum, “WioSun Systemhaus für Photovoltaik Combined module PVT-Series EN,” WIOSUN GmbH & Co. KG, Product data sheet EN-PVT-DS-20120601, 2012.

[59] Solimpeks, “VOLTHER hybrid collectors data sheet,” Solimpeks Solar Energy Corp, PowerVolt & PowerTherm, Product data sheet.

[60] Energie Solaire, “Solar Collector Factsheet Energie Solaire Kollektor AS - Prüfbericht SPF,” Institut für Solartechnik SPF, Hochschule für Technik Rapperswil HSR, Rapperswil, Switzerland, Measurement data SCFv3.0fr, 2012.

[61] E. Bertram, D. Carbonell, B. Perers, M. Haller, M. Bunea, and S. Eicher, “Models of Sub-Components and Validation for the IEA SHC Task 44 / HPP Annex 38 Part B: Collector Models (Final Draft),” International Energy Agency, A technical report of subtask C Report C2 Part B, 2012.

[62] J. A. Duffie and W. A. Beckman, *Solar Engineering of Thermal Processes*, 3rd ed. Wiley, 2006.

[63] H. Soltau, “Testing the thermal performance of uncovered solar collectors,” *Solar energy*, vol. 49, no. 4, pp. 263–272, 1992.

[64] “EN 12975-2 Kollektoren - Teil 2 Prüfverfahren.” Beuth, 2006.

[65] “ISO/DIS 9806,” *Solar Energy — Solar thermal collectors — Test methods*, vol. 5695, 2011.

[66] M. Stegmann, E. Bertram, G. Rockendorf, and S. Janßen, “Model of an unglazed photovoltaic thermal collector based on standard test procedures,” in *Proceedings of ISES Solar World Congress*, Kassel, Germany, 2011.

[67] R. Pitz-Paal, “Kondensation an unabgedeckten Sonnenkollektoren, Diplomarbeit,” Diplomarbeit Ludwigs Maximillians Universität, München, Diplomarbeit, 1988.

[68] H. Soltau, *Das thermische Verhalten offener Kollektoren*. Düsseldorf: VDI-Verl., 1989.

[69] B. Perers, “VALIDATION OF A DYNAMIC MODEL FOR UNGLAZED COLLECTORS INCLUDING CONDENSATION. APPLICATION FOR STANDARDISED TESTING AND SIMULATION IN TRNSYS AND IDA,” *Proceedings of ISES Solar World Congress 2011, Kassel*, 2011.

[70] W. Eisenmann, O. Müller, F. Pujiula, and G. Zienterra, “Metal Roofs as Unglazed Solar Collectors, Coupled with Heat Pump and Ground Storage: Gains from Condensation, Basics for System Concepts,” *Proceedings of Eurosun 2006, Glasgow, Scotland*, 2006.

[71] M. Bunea, S. Eicher, C. Hildbrand, J. Bony, B. Perers, and S. Citherlet, “PERFORMANCE OF SOLAR COLLECTORS UNDER LOW TEMPERATURE CONDITIONS: Measurements and simulations results,” *Proceedings of Eurosun 2012, Rijeka Croatia*, vol. pdf-ID 040, 2012.

[72] E. Bertram, M. Stegmann, J. Scheuren, and G. Rockendorf, “CONDENSATION HEAT GAINS ON UNGLAZED SOLAR COLLECTORS IN HEAT PUMP SYSTEMS,” in *Proceedings of EuroSun 2010 International Conference on Solar Heating, Cooling and Buildings*, Graz, Austria, 2010.

[73] A. Wagner, *Photovoltaik Engineering : Handbuch für Planung, Entwicklung und Anwendung*, 2., bearb. Aufl. Berlin: Springer, 2006.

[74] I. Malenkovich, S. Eicher, and J. Bony, “Definition of Main System Boundaries and Performance Figures for Reporting on SHP Systems,” A technical report of Subtask B Deliverable B1.1, Final Document, 2012.

[75] P. Pärisch, I. Malenkovich, M. Hartl, E. Bertram, R. Tepe, and G. Rockendorf, “Effizienz oder Effektivität? Kennzahlen für die Bewertung von Solar-Wärmepumpensystemen,” in *Proceedings 23. Symposium Thermische Solarenergie*, Bad Staffelstein, Germany, 2013.

[76] T. L. Freeman, J. W. Mitchell, and T. E. Audit, “Performance of combined solar-heat pump systems,” *Solar Energy*, vol. 22, no. 2, pp. 125–135, 1979.

[77] T. L. Freeman, J. W. Mitchell, and T. E. Audit, “Performance of combined solar-heat pump systems,” *Solar Energy*, vol. 22, no. 2, pp. 125–135, 1979.

[78] K. J. Chua, S. K. Chou, and W. M. Yang, “Advances in heat pump systems: A review,” *Applied Energy*, vol. 87, no. 12, pp. 3611–3624, Dec. 2010.

[79] W. Sparber, K. Vajen, S. Herkel, J. Ruschenberg, A. Thür, R. Fedrizzi, and M. D´Antoni, “OVERVIEW ON SOLAR THERMAL PLUS HEAT PUMP SYSTEMS AND REVIEW OF MONITORING RESULTS,” International Energy Agency, IEA Task 44/ Annex 38 publication / outcome, Aug. 2011.

[80] A. M. Shahed and S. J. Harrison, “Preliminary review of geothermal as-sisted heat pumps.” Solar Calorimetry Laboratory, Department of Mechanical and Materials Engineering, 2006.

[81] A. R. Day and T. G. Karayiannis, “Review Paper: Solar-assisted heat pump research and development,” *Building Services Engineering Research and Technology*, vol. 15, no. 2, pp. 71–80, Jan. 1994.

[82] M. Haller, D. Carbonell, and E. Bertram, “Report C4 Synthesis of System Simulation Results for the IEA SHC Task 44 / HPP Annex 38 (Draft 9th Dec. 2013),” IEA SHC / HP Programme, Technical report of Subtask C Simulations Report C4, 2014.

[83] J. Ruschenburg, S. Herkel, and H.-M. Henning, “A statistical analysis on market-available solar thermal heat pump systems,” *Solar Energy*, vol. 95, pp. 79–89, Sep. 2013.

[84] J. V. Anderson, J. W. Mitchell, and W. A. Beckman, “A design method for parallel solar-heat pump systems,” *Solar Energy*, vol. 25, no. 2, pp. 155–163, 1980.

[85] M. Y. Haller, D. Carbonell, I. Mojic, C. Winteler, E. Bertam, B. Mircea, W. Lerch, and F. Ochs, “Solar and Heat Pump Systems - Summary of simulation results of the IEA SHC Task 44 / HPP Annex (submitted),” in *Proceedings*, Montreal, Canada, 2014.

[86] D. Carbonell, M. Haller, D. Philippen, and F. Elimar, “Simulations of combined solar thermal and heat pump Systems for domestic hot water and space heating,” *Energy Procedia*, vol. Volume 48, pp. 524–534, 2014.

[87] L. Spante, B. Bylander, and M. Larsson, “Bergvärmesystem för småhus. Resultat och erfarenheter från fältmätningar (‘Ground-Source Heat Pumps in Dwellings. Results and Experiences from Field Measurements’),” Vattenfall Älvkarlebylaboratoriet, UL-FUD-B 86:14, 1986.

[88] E. Bertram, J. Glembin, and G. Rockendorf, “Unglazed PVT collectors as additional heat source in heat pump systems with borehole heat exchanger,” *Energy Procedia*, vol. Volume 30, pp. 414–423, 2012.

[89] R. Tepe, M. Rönnelid, and B. Perers, “Swedish Solar Systems in Combination with Heat Pumps,” presented at the ISES Solar World Congress 2003, Göteborg, Oxford, 2004.

[90] E. Bertram, J. Glembin, J. Scheuren, and G. Zienterra, “Soil regeneration by unglazed solar collectors in heat pump systems,” presented at the ISES Solar World Congress 2009 renewable energy shaping our future, Johannesburg, South Africa, 2009.

[91] W. Hube, G. Burkhardt, S. Dölfel, and C. Wittwer, “Modellbasierte Untersuchung von Wärmepumpensystemen mit Solaranlage – Potentialabschätzung der solaren Quellenanhebung

für Elektrowärmepumpen," presented at the 19. Symposium Thermische Solarenergie, Regensburg, 2009.

[92] D. Pahud and B. Lachal, "Mesure des performances thermiques d'une pompe à chaleur couplée sur les sondes géothermiques à Lugano (TI)," Bundesamt für Energie, Bern, Abschlussbericht 40430 / 80266, Dec. 2004.

[93] V. Trillat-Berdal, B. Souyri, and G. Achard, "Numerical simulations of ground–coupled heat pumps combined with thermal solar collectors," presented at the PLEA2006 - The 23rd Conference on Passive and Low Energy Architecture, Geneva, Switzerland, 2006.

[94] R. M. Lazzarin, "Dual source heat pump systems: Operation and performance," *Energy and Buildings*, vol. 52, pp. 77–85, Sep. 2012.

[95] P. Pärisch, O. Arnold, E. Bertam, R. Tepe, and G. Rockendorf, "5 Regelungskonzepte für die parallel/serielle Einbindung von Solarkollektoren in erdgekoppelte Wärmepumpensysteme," in *24. Symposium Thermische Solarenergie*, Bad Staffelstein, Germany, 2014.

[96] M. Ménard, L. Mattei, F. Sprecher, R. Wolfensberger, M. Kriegers, and E. Christian, "Erhöhung der Quellentemperatur von Wärmepumpen - Auswirkungen auf Jahresarbeitszahl und Wirtschaftlichkeit -Schlussbericht," Stadt Zürich - Amt für Hochbauten, Fachstelle Energie und Gebäudetechnik, Zürich, Switzerland, Schlusssbericht 09-2011, 2011.

[97] A. D. Chiasson, C. Yavuzturk, and W. J. Talbert, "Design of School Building HVAC Retrofit with Hybrid Geothermal Heat-Pump System," *J. Arch. Engrg.*, vol. 10, no. 3, p. 103, 2004.

[98] P. Eslami-nejad, A. Langlois, S. Chapuis, M. Bernier, and W. Faraj, "Solar heat injection into boreholes," in *Canadian solar buildings conference. Toronto, Canada*, 2009.

[99] B. Perers, P. Kovacs, M. Olsson, M. Persson, and P. Ulrik, "A NEW TOOL FOR STANDARDIZED COLLECTOR PERFORMANCE CALCULATIONS," *Proceedings of ISES Solar World Congress 2011, Kassel*, 2011.

[100] M. D'Antoni and O. Saro, "Energy potential of a Massive Solar-Thermal Collector design in European climates," *Solar Energy*, vol. 93, pp. 195–208, Jul. 2013.

[101] M. Haller, R. Dott, J. Ruschenberg, F. Ochs, and J. Bony, "The Reference Framework for System Simulations of the IEA SHC Task 44 / HPP Annex 38 Part A: General Simulation Boundary Conditions," International Energy Agency, A technical report of subtask C Report C1 Part A, 2012.

[102] METEOTEST, J. Remund, and S. Kunz, *Meteonorm Data (Worldwide)*. Bern, Switzerland: METEOTEST.

[103] R. Dott, M. Haller, J. Ruschenberg, F. Ochs, and J. Bony, "The Reference Framework for System Simulations of the IEA SHC Task 44 / HPP Annex 38 Part B: Buildings and Space Heat Load," International Energy Agency, A technical report of subtask C Report C1 Part B, 2012.

[104] "IEA SHC || Task 44." [Online]. Available: http://task44.iea-shc.org/. [Accessed: 29-Dec-2013].

[105] E. Bertram, "Annex F to Report C3 of the IEA SHC Task 44 / HPP Annex 38 - Platform independence checks reported for T44A38," Report of Subtask C Adaption for the IEA SHC & HPP T44/A38 Boundary Conditions of ISFH Simulations in TRNSYS, Dec. 2013.

[106] E. Bertram, "Solar assisted heat pump systems with ground heat exchanger –simulation studies," *Energy Procedia*, vol. 48, pp. 505–515, 2014.

[107] CEN/TC113N380, "EN/TC 113 N 380 Mandate to CEN and CENELEC for the Elaboration and Adoption of Measurement Standards for Household Appliances: Water - Heaters, Hot Water Storage Appliances and Water Heating Systems," Brussels, Belgium, CEN/TC113N380, 2003.

[108] FprEN 16147, “FprEN 16147 Heat pumps with electrically driven compressors - Testing and requirements for marking for domestic hot water units,” 2010.

[109] A. Zottl and R. Niederbrucker, “Analyse und Betriebsverhalten und Optimierung von Wärmepumpenanlagen mit Erdwärmesonden,” presented at the Internationales Anwenderforum Oberflächennahe Geothermie, Neumarkt i. d. Oberpfalz, Germany, 2013.

[110] H. R. Gabathuler, H. Mayer, A. G. Gabathuler, and B. Ingenieure, “Wärmepumpenanlage mit Heizkörperheizung ohne Speicher,” Bundesamt für Energie, Bern, Switzerland, Schlussbericht, 2004.

[111] H. Recknagel, E.-R. Schramek, and E. Sprenger, *Taschenbuch für Heizung + Klimatechnik 07/08 Buch und CD-ROM (als SET)*. 2006.

[112] VDZ, “VdZ Information Nr.1 Energieeinsparung in Gebäuden Die richtige Dimensionierung von Wärmeerzeugern bei der Modernisierung,” Vereinigung der Deutschen Zentralheizungswirtschaft, Köln, 2003.

[113] VDI 4708-1, “VDI 4708-1 Central heat-water-installations; terms and calculation-basis,” Beuth Verlag, 1994.

[114] Viessmann, *Technical information Heat pumps*, vol. 05/2009. Allendorf (Eder): Viessmann Werke, 2009.

[115] K. Ochsner, *Wärmepumpen in der Heizungstechnik: Praxishandbuch für Installateure und Planer*. Heidelberg: Müller, 2007.

[116] F. Hartmann, *Systemtechnik für Wärmepumpen Solar- und Umweltwärme für Wohngebäude*. München;Heidelberg: Hüthig & Pflaum, 2009.

[117] M. Haller, R. Haberl, I. Mojic, and F. Elimar, “Hydraulic integration and control of heat pump and combi-storage: Same components, big differences,” in press 2014.

[118] Viessmann, *Technical guide Solar thermal systems*, vol. 05/2009. Allendorf (Eder): Viessmann Werke, 2009.

[119] R. Heimrath and M. Haller, “Project Report A2 of Subtask A, the Reference Heating System, the Template Solar System,” *A Report of the IEA-SHC Task32*, 2007.

[120] O. Arnold, “Simulationsstudie zur Optimierung von solarthermisch unterstützten Wärmepumpensystemen,” Hochschule Hannover, Hannover, Bachelor Thesis, 2013.

[121] E. Bertram, P. Pärisch, and R. Tepe, “Impact of solar heat pump system concepts on seasonal performance - Simulation studies,” *Proceedings of Eurosun 2012, International Solar Energy Society (ISES)-Europe Solar Conference, Rijeka Croatia*, p. ID 37, 2012.

[122] M. Haller and E. Frank, “ON THE POTENTIAL OF USING HEAT FROM SOLAR THERMAL COLLECTORS FOR HEAT PUMP EVAPORATORS,” *Proceedings of ISES Solar World Congress 2011, Kassel*, 2011.

[123] H. Drück, *Type 340, MULTIPORT Store - Model for TRNSYS*. Stuttgard, Germany: Institut für Thermodynamik und Wärmetechnik (ITW) Universität Stuttgart, 2006.

[124] P. Pärisch, O. Mercker, P. Oberdorfer, R. Tepe, and G. Rockendorf, “Experimente und Modellvalidierung für die Erdsondenregeneration mit Solarwärme,” in *Proceedings of Symposium Thermische Solarenergie*, Bad Staffelstein, Germany, 2013.

[125] S. A. Klein, W. A. Beckmann, J. W. Mitchell, J. A. Duffie, and T. A. Freeman, *TRNSYS 17, A Transient System Simulation Program, Solar Energy Laboratory University of Wisconsin, Madision*. Stuttgard, Germany, 2009.

[126] R. Dott, T. Afjei, A. Dalibard, D. Carbonell, A. Heinz, M. Haller, and A. Witzig, “Models of Sub-Components and Validation for the IEA SHC Task 44 / HPP Annex 38 Part C: Heat Pump Models,” International Energy Agency, A technical report of subtask C Deliverable C2.1 Part C, 2012.

[127] W. Keilholz, P. Sette, and E.-H. Soussi, *The W programming language User & Reference Manual*. Paris, France: Centre Scientifique et Technique du Bâtiment, 2009.

[128] M. Haller and B. Perers, *Type 832, „Dynamic Collector Model by Bengt Perers“*. Zürich, Switzerland: Institut für Solartechnik, Hochschule für Technik Rapperswil, 2012.

[129] S. Holst, *Type 362 Dynamic radiator model with pipes (Type 162)*. München, Germany: Bayerisches Zentrum für angewandte Energieforschung e.V., 2010.

[130] H.-J. Bungartz, M. Buchholz, D. Pflüger, and S. Zimmer, *Modellbildung und Simulation: eine anwendungsorientierte Einführung*. Berlin, Heidelberg: Springer Berlin Heidelberg, 2009.

[131] W. P. Keilholz, P. Riederer, and V. Ducreux, “SOLVING DIFFERENTIAL EQUATIONS IN TRNSYS WITHOUT PROGRAMMING,” 2009.

[132] Verein Deutscher Ingenieure, “VDI 4640 Blatt 1 Thermische Nutzung des Untergrunds Grundlagen, Genehmigungen, Umweltaspekte.” VDI-Gesellschaft Energie und Umwelt, Jun-2010.

[133] P. Pärisch, P. Oberdorfer, O. Mercker, R. Tepe, and G. Rockendorf, “USB_Pärisch_Experimente_web.pdf,” in *Proceedings 23. Symposium Thermische Solarenergie,* Bad Staffelstein, 2013.

[134] M. Ast, H. Eckl, J. Elbracht, K. Fischer, J. Fritz, S. Henke-Jelit, H. Jensen, S. Pester, and J. Sbresny, “Leitfaden Erdwärmenutzung in Niedersachsen - Rechtliche und technische Grundlagen,” Landesamt für Bergbau, Energie und Geologie, Niedersachsen, Hannover, GeoBerichte 24, 2012.

[135] M. Tholen and S. Walker-Hertkorn, *Arbeitshilfen Geothermie: Grundlagen für oberflächennahe Erdwärmesondenbohrungen*. Bonn: wvgw Wirtschafts- und Verlagsgesellschaft Gas und Wasser mbH, 2008.

[136] C. Ihle, R. Bader, and M. Golla, *Tabellenbuch Sanitär, Heizung, Lüftung. Anlagentechnik SHK Ausbildung und Praxis*, 8. ed. Bildungsverlag EINS, 2011.

[137] Rehau, “RAUGEO SYSTEMTECHNIK ZUR ERDWÄRMENUTZUNG,” Rehau AG, Rehau, Germany, Technical product information 827600, 2007.

[138] J. W. Thornton, *type 952 Buried Noded Pipe*. Madison: Tess Thermal Energy System Specialists, 2010.

[139] F. Besana, “Heat Rejection Problematic in SolarCombi+ System - Dissertation,” University of Bergamo, Bergamo, 2009.

[140] D. Bettoni and M. D´Antoni, *Type 880 – Dry cooler Mathematical description*. Bolzano, Italy: EURAC, European Research Academy, 2012.

[141] F. Auer and H. Schote, “Schlussbericht - Wärme aus der Umwelt auch gut für die Umwelt? Ergebnisse einer siebenjährigen Praxisuntersuchung: Erdgekoppelte Wärmepumpen sparen deutlich Primärenergie ein Kritische Bewertung von Luft-Wärmepumpen,” Lokale Agenda 21 – Gruppe Energie Lahr, Lahr, Schwarzwald, Germany, 2014.

[142] M. Miara and C. Russ, “Feldmessungen von Wärmepumpen in Wohngebäuden mit aktuellem Baustandard und in Bestandgebäuden,” presented at the 9. Internationales Anwenderforum Oberflächennahe Geothermie, 2009.

[143] W. Eisenmann, *Untersuchungen zu Leistungsfähigkeit und Materialaufwand von Sonnenkollektoren mit serpentinen- und harfenartiger Rohrverlegung - Dissertation*, vol. Verein Deutscher Ingenieure. Düsseldorf: VDI-Verlag, 2003.

[144] J. Christoffer, T. Deutschländer, and M. Webs, *Testreferenzjahre*. Offenbach am Main: Deutscher Wetterdienst www.dwd.de, 2004.

[145] M. Kübert and S. Walker-Hertkorn, “Grenzabstände bei Erdwärmesondenbohrungen,” presented at the Internationales Anwenderforum Oberflächennahe Geothermie, Bad Staffelstein, Regensburg, 2008.

[146] D. Bohne, G. Harhausen, and M. Wohlfahrt, “Thermisches Monitoring an Nichtwohngebäuden mit Einsatz von oberflächennaher Geothermie und Validierung von Wärmeeintrag und Entzug in den Untergrund.,” Leibniz Universität Hannover, Hannover, Inhaltlicher Abschlussbericht 0327364B, 2013.

[147] J. W. Thornton, *type 586 Pipe Pressure Drop Calculator*. Madison: Tess Thermal Energy System Specialists, 2004.

[148] H.-J. Kech, “Neue energiesparende Pumpenantriebe für Solaranlagen und Heizungstechnik, Phase B Abschlussbericht über das Forschungs- und Entwicklungsvorhaben,” WILO AG, Dortmund, BMWi Abschlussbericht - Kurzfassung 0329715 B, 2002.

[149] M. Baur, “Effizienz von Solaranlagen verbessern - Auch die Pumpe ist wichtig,” *SBZ - Sanitär Heizung Klima*, vol. 11/2007, pp. 54–55, 2007.

[150] Stiebel, *Planung und Installation. Wärmepumpen*. Holzminden, Germany: STIEBEL ELTRON, 2010.

[151] Strawa, “2013_Preisliste_strawa_S01-S92_Umschlagseiten.cdr - strawa_preisliste_hydraulische_weiche.pdf,” Strawa Wärmetechnik GmbH, Technical data sheet, 2013.

[152] STIWA, “Sparen beim Pumpen - Heizungspumpen,” *Stiftung Warentest*, vol. 9/2007, pp. 76–79, 2007.